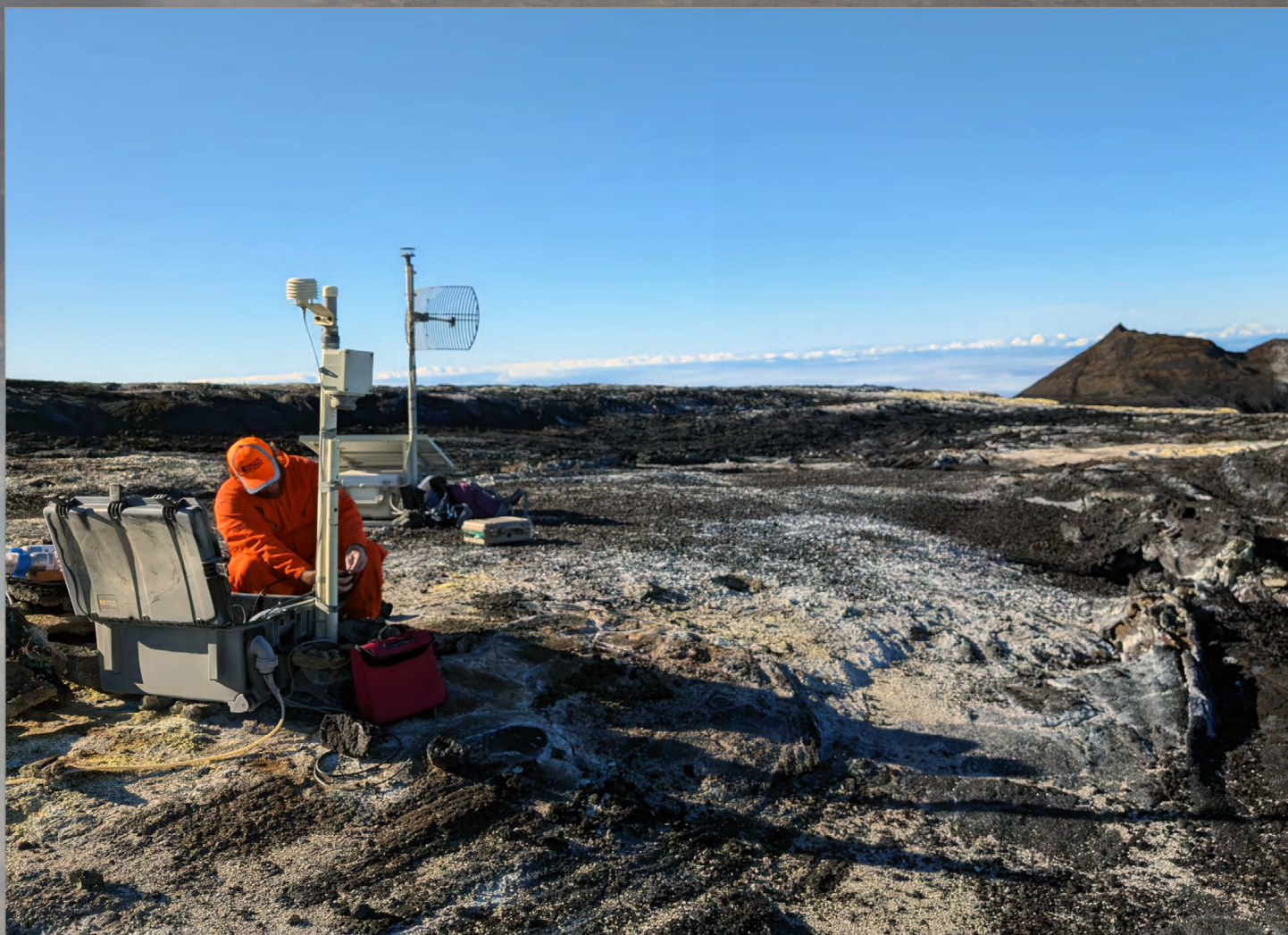


Recommended Capabilities and Instrumentation for Volcano Monitoring in the United States



Scientific Investigations Report 2024–5062

Cover. U.S. Geological Survey Hawaiian Volcano Observatory gas scientist M. Cappos installs a newly calibrated multicomponent gas analyzer system (multi-GAS) at the Sulfur Cone volcano monitoring station on Mauna Loa's Southwest Rift Zone, Hawai'i. The station is located at an elevation of 11,250 feet (3,430 meters) above sea level; work in these high-elevation environments necessitates extreme caution and diligence. Multi-GAS instruments provide continuous real-time monitoring of major volcanic gas species (water, carbon dioxide, sulfur dioxide, and hydrogen sulfide) and meteorological conditions (wind speed and direction, air temperature, and humidity) and must be replaced every 2 years on average. Monitoring the ratios of different volcanic gases here can help to identify changes to the magmatic system beneath the volcano. The surrounding ground is covered in elemental sulfur that is deposited by the constant degassing of volcanic sulfur gases. Photograph by C. Sealing, U.S. Geological Survey, August 2, 2024. Background image shows a typical view of the 2008–2018 lava lake in the Overlook crater within Halema'uma'u, Kīlauea. Photograph taken from a helicopter by Tim Orr, U.S. Geological Survey, on August 16, 2013.

Title page. Alaska Volcano Observatory field technician D. Ketner performing maintenance at volcano monitoring station GSIG on Igitkin Island in the western Aleutian Islands, Alaska. The station monitors volcanic activity from Great Sitkin Volcano (in the background). In May 2021, a volcanic explosion occurred at Great Sitkin Volcano, followed in July 2021 by an ongoing eruption of lava that now fills most of the summit crater. Photograph by W. Mayo, June 20, 2019; used with permission.

Recommended Capabilities and Instrumentation for Volcano Monitoring in the United States

Edited by Ashton F. Flinders, Jacob B. Lowenstern, Michelle L. Coombs, and
Michael P. Poland



Scientific Investigations Report 2024–5062

U.S. Department of the Interior
U.S. Geological Survey

U.S. Geological Survey, Reston, Virginia: 2024

For more information on the USGS—the Federal source for science about the Earth, its natural and living resources, natural hazards, and the environment—visit <https://www.usgs.gov> or call 1–888–ASK–USGS.

For an overview of USGS information products, including maps, imagery, and publications, visit <https://store.usgs.gov>.

Any use of trade, firm, or product names is for descriptive purposes only and does not imply endorsement by the U.S. Government.

Although this information product, for the most part, is in the public domain, it also may contain copyrighted materials as noted in the text. Permission to reproduce copyrighted items must be secured from the copyright owner.

Suggested citation:

Flinders, A.F., Lowenstern, J.B., Coombs, M.L., and Poland, M.P., eds., 2024, Recommended capabilities and instrumentation for volcano monitoring in the United States: U.S. Geological Survey Scientific Investigations Report 2024–5062, 124 p., <https://doi.org/10.3133/sir20245062>.

ISSN 2328-031X (print)

ISSN 2328-0328 (online)

Acknowledgments

We thank Heather Wright and Ninfa Bennington for their reviews of this volume and their many useful suggestions for reorganization, clarification, and consistency. We thank the following others for their valuable input on individual chapters: Sonja Behnke (Los Alamos National Laboratory), Deb Bergfeld (U.S. Geological Survey [USGS]), DelWayne Bohnenstiehl (North Carolina State University), Jackie Caplan-Auerbach (Western Washington University), William Chadwick Jr. (National Oceanic and Atmospheric Administration [NOAA]), David Damby (USGS), Robert Dziak (NOAA), John Eichelberger (University of Alaska Fairbanks), Bill Evans (USGS), Kristen Fauria (Vanderbilt University), Ronni Grapenthin (University of Alaska Fairbanks), Matthew Haney (USGS), James Kauahikaua (USGS), Taryn Lopez (University of Alaska Fairbanks), Larry Mastin (USGS), Michael Manga (University of California, Berkeley), Christina Neal (USGS), John Paskievitch (USGS), Matthew Patrick (USGS), Sara Peek (USGS), Cheryl Searcy (USGS), Brian Shiro (USGS), Tom Sisson (USGS), Cassandra Smith (USGS), Johan Varekamp (Wesleyan University), and Michael Zoeller (USGS). Tom Murray provided the initial request to create this update of the original Moran and others (2008) report. Charlie Mandeville, Wendy Stovall, Jon Major, Andy Calvert, Ken Hon, and Christina Neal (all USGS) reviewed previous versions and influenced the final implementation as a multichapter volume.

Contents

Chapter A

Introduction to Recommended Capabilities and Instrumentation for
Volcano Monitoring in the United States

By Ashton F. Flinders, Jacob B. Lowenstern, Michelle L. Coombs, and Michael P. Poland

Introduction.....1

How to Use This Report2

Summary of Recommendations2

References Cited.....8

Chapter B

Seismic Techniques and Suggested Instrumentation to
Monitor Volcanoes

By Weston A. Thelen, John J. Lyons, Aaron G. Wech, Seth C. Moran, Matthew M. Haney,
and Ashton F. Flinders

Introduction.....11

Recommended Capabilities11

General Recommendations and Considerations15

Summary—Recommendations for Volcano Levels 1–4 Seismic Networks16

References Cited.....16

Chapter C

Infrasound for Volcano Monitoring

By John J. Lyons, David Fee, Weston A. Thelen, Alexandra M. Iezzi, and Aaron G. Wech

Introduction.....21

Recommended Capabilities21

Overall Recommendations and Considerations27

Summary—Recommendations for Volcano Levels 1–4 Infrasound Networks27

References Cited.....28

Chapter D

Ground Deformation and Gravity for Volcano Monitoring

By Emily K. Montgomery-Brown, Kyle R. Anderson, Ingrid A. Johanson, Michael P. Poland,
and Ashton F. Flinders

Introduction.....	33
Recommended Capabilities	36
Summary—Recommendations for Level 1–4 Networks	41
References Cited.....	41

Chapter E

Volcanic Gas Monitoring

By Jennifer L. Lewicki, Christoph Kern, Peter J. Kelly, Patricia A. Nadeau, Tamar Elias, and
Laura E. Clor

Introduction.....	45
Instrumentation and Techniques.....	46
Recommended Capabilities	49
Summary—Recommendations for Levels 1–4 Volcanoes.....	50
References Cited.....	50

Chapter F

Streams, Springs, and Volcanic Lakes for Volcano Monitoring

By Steven E. Ingebritsen and Shaul Hurwitz

Introduction.....	57
Instrumentation Relevant to Streams, Springs, and Lakes.....	59
Recommended Capabilities	60
General Recommendations and Considerations	62
References Cited.....	62

Chapter G

Tracking Surface Changes Caused by Volcanic Activity

By Tim R. Orr, Hannah R. Dietterich, and Michael P. Poland

Introduction.....67

Instrumentation67

Recommended Capabilities69

Summary—Recommendations for Levels 1–4 Networks74

References Cited.....74

Chapter H

Monitoring Lahars

By Weston A. Thelen, John J. Lyons, Alexandra M. Iezzi, and Seth C. Moran

Introduction.....79

Recommended Capability.....80

References Cited.....82

Chapter I

Monitoring Marine Eruptions

By Gabrielle Tepp

Introduction.....87

Recommended Capabilities88

Summary and Other Considerations.....91

References Cited.....91

Chapter J

Special Topic—Eruption Plumes and Clouds

By David J. Schneider and Alexa R. Van Eaton

Introduction.....	95
Instrumentation.....	96
Recommended Capabilities	102
References Cited.....	103

Chapter K

Special Topic—Boreholes

By Shaul Hurwitz and Jacob B. Lowenstern

Introduction.....	109
Capabilities Provided.....	109
General Recommendations and Considerations	111
References Cited.....	111

Chapter L

Special Topic—Unoccupied Aircraft Systems

By Angela K. Diefenbach

Introduction.....	115
Capabilities Provided.....	115
General Recommendations and Considerations	116
References Cited.....	118

Chapter M

Special Topic—Rapid-Response Instrumentation

By Ashton F. Flinders

Introduction.....121

Recommended Instrumentation121

Additional Considerations123

Marine Eruptions.....123

References Cited.....124

Conversion Factors

International System of Units to U.S. customary units

Multiply	By	To obtain
Area		
square kilometer (km²)	247.1	acre
square kilometer (km²)	0.3861	square mile (mi²)
Length		
meter (m)	3.281	foot (ft)
meter (m)	1.094	yard (yd)
micrometer (µm)	0.0000394	inch (in.)
millimeter	0.03937	inch (in.)
kilometer (km)	0.6214	mile (mi)
Mass		
kilogram (kg)	2.205	pound, avoirdupois (lb)
Velocity		
meter per second (m/s)	3.281	foot per second (ft/s)

Temperature in degrees Celsius (°C) may be converted to degrees Fahrenheit (°F) as °F = (1.8 × °C) + 32.

Abbreviations

AFM	acoustic flow monitor
AIRS	Atmospheric Infrared Sounder
ANSS	Advanced National Seismic System
ASTER	Advanced Spaceborne Thermal Emission and Reflection Radiometer
AVHRR	Advanced Very High Resolution Radiometer
BTD	brightness temperature difference
CALIPSO	Caribbean Andesite Lava Island-volcano Precision Seismo-geodetic Observatory
COSMO-SkyMed	Constellation of Small Satellites for Mediterranean basin Observation
CTD	conductivity, temperature, and depth
DEM	digital elevation model
DOAS	differential optical absorption spectroscopy
EDM	electronic distance measurement

FLIR	forward-looking infrared
FTIR	Fourier transform infrared spectroscopy
GLISTIN-A	Airborne Glacier and Land Ice Surface Topography Interferometer
GNSS	Global Navigation Satellite System
GOES	Geostationary Operational Environmental Satellite
GOME-2	Global Ozone Monitoring Experiment 2
GPS	Global Positioning System
HD-YLAKE	Hydrothermal Dynamics of Yellowstone Lake
Hz	hertz
IASI	Infrared Atmospheric Sounding Interferometer
IMS	International Monitoring System
InSAR	interferometric synthetic aperture radar
IR	infrared
IRIS	Incorporated Research Institutions for Seismology
lidar	light detection and ranging
LVEW	Long Valley Exploratory Well
<i>M</i>	magnitude
MODIS	Moderate Resolution Imaging Spectroradiometer
multi-GAS	multicomponent gas analyzer system
NASA	National Aeronautics and Space Administration
NEXRAD	next-generation radar
NOAA	National Oceanic and Atmospheric Administration
NTIA	National Telecommunications and Information Administration
NVEWS	National Volcano Early Warning System
NWIS	National Water Information System
OBS	ocean-bottom seismometer
OMI	Ozone Mapping Instrument
OMPS	Ozone Mapping and Profiling Suite
PASSCAL	Portable Array Seismic Studies of the Continental Lithosphere
PBO	Plate Boundary Observatory
PIV	particle image velocimetry
POES	Polar Operational Environmental Satellite
ROV	remotely operated vehicle
RSAM	Real-Time Seismic Amplitude Measurement
RSP	Polynesian Seismic Network
RV	research vessel
SAR	synthetic aperture radar
SfM	structure from motion
SNPP	Suomi National Polar-Orbiting Operational Environmental Satellite System Preparatory Project
SOFAR	Sound Fixing and Ranging
sUAS	small class unoccupied aircraft system
SWIR	short-wave infrared
TropOMI	Tropospheric Monitoring Instrument
UAS	unoccupied aircraft system
USGS	U.S. Geological Survey
UTC	coordinated universal time
UV	ultraviolet
VAAC	Volcanic Ash Advisory Center
VHF	very high frequency
VHP	U.S. Geological Survey Volcano Hazards Program
VIIRS	Visible Infrared Imaging Radiometer Suite
VLP	very long period
VOLCAT	Volcanic Cloud Analysis Tool
VSC	U.S. Geological Survey Volcano Science Center
USD	U.S. dollar

Chapter A



U.S. Geological Survey Hawaiian Volcano Observatory gas scientist M. Capps installs a newly calibrated multicomponent gas analyzer system (multi-GAS) at the Sulfur Cone volcano monitoring station on Mauna Loa's Southwest Rift Zone, Hawai'i. The station is located at an elevation of 11,250 feet (3,430 meters) above sea level; work in these high-elevation environments necessitates extreme caution and diligence. Multi-GAS instruments provide continuous real-time monitoring of major volcanic gas species (water, carbon dioxide, sulfur dioxide, and hydrogen sulfide) and meteorological conditions (wind speed and direction, air temperature, and humidity) and must be replaced every 2 years on average. Monitoring the ratios of different volcanic gases here can help to identify changes to the magmatic system beneath the volcano. The surrounding ground is covered in elemental sulfur that is deposited by the constant degassing of volcanic sulfur gases. Photograph by C. Sealing, U.S. Geological Survey, August 2, 2024.

Chapter A

Introduction to Recommended Capabilities and Instrumentation for Volcano Monitoring in the United States

By Ashton F. Flinders, Jacob B. Lowenstern, Michelle L. Coombs, and Michael P. Poland

Introduction

The National Volcano Early Warning System (NVEWS) was authorized and partially funded by the U.S. Government in 2019. In response, the U.S. Geological Survey (USGS) Volcano Hazards Program asked its scientists to reflect on and summarize their views of best practices for volcano monitoring. The goal was to review and update the recommendations of a previous report (Moran and others, 2008) and to provide a more detailed analysis of capabilities and instrumentation for monitoring networks for U.S. volcanoes. This Scientific Investigations Report and its chapters reflect those USGS scientists' views and summaries and will serve as a guide for future network upgrades funded through NVEWS.

Given the well-documented hazards posed by volcanoes to population centers and aviation (for example, Blong, 1984; Scott, 1989; Neal and others, 1997, 2019; Guffanti and others, 2010; Shroder and Papale, 2014; Prata and Rose, 2015; Palmer, 2020), volcano monitoring is critical for ensuring public safety and for mitigating the impacts of volcanic activity. Accurate and timely forecasts are facilitated by well-designed monitoring networks that are in place long enough to allow for background behavior to be recognized and understood. Because precursory signals may be limited and unrest may progress rapidly to an eruption, our goal is to deploy monitoring systems that enable detection of the reactivation of dormant volcanoes as early as possible, allowing for public safety and risk mitigation. NVEWS planning is also informed by the results of Ewert and others (2005, 2018), whereby 161 U.S. volcanoes are currently categorized and ranked commensurate with their relative threat.

In each chapter, author(s) considered the need for some redundancy of instrumentation and telemetry, given the likelihood of occasional equipment failure, particularly in extreme and remote environments. Establishing digital telemetry networks requires advanced planning, sighting, radio-shot testing, and, inevitably, troubleshooting in the field. This is harder to achieve rapidly during a crisis; thus, an important goal for monitoring U.S. volcanoes is to establish digital telemetry backbones with redundancy and extra capacity to absorb additional instruments should a volcano begin to exhibit signs of unrest (fig. A1). The National Telecommunications and Information Administration (NTIA) imposed new regulations in the United States, eliminating the use of older analog radios for many purposes, which had been one previous means for redundant data delivery. However, the resulting conversion from analog to digital systems usefully

enables stations to accommodate new and multivariate real-time data streams (for example, Global Navigation Satellite System [GNSS] receivers, infrasound arrays, gas spectrometers, visible and infrared cameras, and broadband seismometers).

We note that other USGS and broader national and international hazard programs can leverage NVEWS instrumentation plans. Examples of this include the following:

1. Improved seismic coverage of volcanoes will increase the capability of the USGS Earthquake Hazards Program to detect and locate earthquakes, estimate ground shaking, and provide timely early warnings through the ShakeAlert Earthquake Early Warning System (Given and others, 2018).
2. The National Oceanic and Atmospheric Administration's Tsunami Program will benefit from additional seismic stations, particularly within the sparsely instrumented Aleutian Islands, Northern Mariana Islands, and American Samoa.
3. Infrasound stations can detect signals from landslides, debris flows and lahars, floods, and weather events, providing benefits to the National Weather Service and the USGS Landslide Hazards Program.



Figure A1. Photograph of a U.S. Geological Survey Alaska Volcano Observatory geophysicist orienting a radio antenna toward a monitoring station near Shishaldin Volcano, Alaska. View from southeast at seismic station BRPK. Shishaldin Volcano emits a gas plume, and the edifice is covered with debris from a 2019–20 eruption. Photograph by Allan Lerner, U.S. Geological Survey, August 20, 2020.

How to Use This Report

Magma moving toward the surface interacts with anything in its path, including hydrothermal systems, cooling magma bodies from previous intrusions, and surrounding host rock. These interactions lead to various geophysical and geochemical phenomena that volcano monitoring networks can detect. A primary goal of volcano monitoring is to detect and correctly interpret such phenomena to provide early and accurate warnings of impending eruptions and to forecast ongoing eruptions, which can last days, months, or years.

Effective monitoring of volcanoes is an interdisciplinary endeavor. Varied techniques are useful for tracking different aspects of preeruption unrest, an eruption itself, and its aftermath, all of which contribute to ensuring public safety. In this report, we first describe a core group of monitoring techniques—seismology, infrasound, ground deformation and gravity (geodesy), gas analysis, and hydrology—that have collectively proven effective for detecting precursory and syneruptive signals and for forecasting eruption timing and style. We then present sections on how these traditional technologies can be combined with other approaches to, for example, track surface changes with satellites and deployed cameras (fig. A2), detect lahars with infrasound and seismometers, and detect and track ash clouds and related lightning with satellite- and ground-based systems. Other chapters describe monitoring marine eruptions, the use of unoccupied aircraft systems, and monitoring from boreholes. Each section contains subsections describing specific capabilities and recommended instrumentation and techniques needed to attain those capabilities.

Aside from the practical, logistical, and financial considerations that may interfere with compliance to the recommendations herein, we also stress that there are scientific caveats. We specifically caution against compliance to our recommendations regarding the number of instruments. These numbers are estimated for a generic stratovolcano similar to Mount St. Helens, but significant variation in the

characteristics of U.S. volcanoes makes a one-size-fits-all approach impractical. In terms of spatial scale, 5 kilometers from the volcanic center has one meaning for isolated stratovolcanoes with a central vent, such as Augustine Volcano in Alaska, but quite a different meaning for much larger caldera systems, such as Yellowstone Caldera in Wyoming; shield volcanoes and their associated rift zones, such as Mauna Loa in Hawai‘i; and volcanic fields, such as the Clear Lake volcanic field in California.

Desired capabilities should be evaluated on a volcano-by-volcano basis. Not every potential capability is relevant at all volcanoes—for example, there is no need for a capability related to lahar detection at Mauna Loa. Similarly, several volcanoes in the Aleutian Islands are ranked as high threat predominantly because of their hazard to aviation (for example, Semisopochnoi Island and Great Sitkin Volcano; Ewert and others, 2018). The absence of permanent populations near these volcanoes can mean that advanced early warnings are not crucial for evacuation, but timely and accurate detection and notification of explosive eruptions are essential for aviation. Users of this report can determine those capabilities that are considered necessary for a given volcano of interest.

Summary of Recommendations

Summaries of our recommendations for instrumentation are listed in tables A1 (recommended instruments for volcano monitoring), A2 (recommended instruments for special topics), and A3 (recommended instrument cache for rapid response). In table A1, we summarize the recommendations of the chapters in this volume by monitoring levels. As originally defined by Ewert and others (2005), monitoring levels were directly linked to the volcanic-threat rankings. For example, level 1 networks were recommended to monitor very low-threat volcanoes, such as the Golden Trout Creek volcanic field, California; level 2

Figure A2. Photograph of U.S. Geological Survey Hawaiian Volcano Observatory geophysicist A. Flinders (left), volunteer C. Ruggles (middle), and geologist M. Zoeller (right) monitoring the resumption of volcanic activity within Halema‘uma‘u, the crater associated with Kīlauea, Hawai‘i, on January 5, 2023, using digital cameras and a laser rangefinder. Tracking and documenting surface changes during ongoing eruptions with rapidly deployed cameras is a long-standing technique that has greatly benefited from advances in technology. Photograph by U.S. Geological Survey, January 5, 2023.



Table A1. Recommended instrumentation for volcano monitoring in the United States by monitoring level.

[DEM, digital elevation model; GNSS, Global Navigation Satellite System; InSAR, interferometric synthetic aperture radar; km, kilometer; m, meter; SWIR, short-wave infrared]

Monitoring category	Monitoring level (monitoring need and volcano threat level)			
	1 (Minimal monitoring; very low threat)	2 (Limited monitoring for change detection; low threat)	3 (Basic real-time monitoring; moderate to high threat)	4 (Well monitored in real time; high to very high threat)
Seismic	Five seismic stations within 200 km of the volcanic center, including two stations within 50 km	Five seismic stations within 50 km of the volcanic center, including two stations within 10 km	Seven or more broadband seismic stations within 20 km of the volcanic center, including at least two stations within 5 km	Twelve to 25 broadband seismic stations within 20 km of the volcanic center, including at least eight stations within 10 km and four or more stations within 5 km; at least one broadband or strong-motion station within 10 km of the volcanic center. Small-aperture seismic array in places where logistics preclude placing stations high on the edifice
Infrasound	One array with four or more elements within 200–300 km of the volcanic center	At least one broadband infrasound sensor co-located with a three-component seismic sensor within 10 km of the volcanic center, and one array with four or more elements within 200–300 km	At least four broadband infrasound sensors co-located with three-component seismic sensors within 10 km of the volcanic center or 15 km of summit vents (for example, Mauna Loa and Kīlauea summits). At least one array with four or more elements within 15 km of the volcanic center or two arrays within 20 km of volcanic centers and main fissure systems with good azimuthal coverage along the trend of fissures. At least two arrays with six or more elements within 200–300 km of sources and with significantly different back-azimuths to sources	At least four broadband infrasound sensors co-located with three-component seismic sensors within 10 km of the volcanic center. At least two arrays with four or more elements each within 15 km of the volcanic center
Ground deformation and gravity	Baseline deformation measurements using InSAR; establish baseline GNSS and gravity survey networks and repeat surveys occasionally in case future unrest should warrant additional data collection	InSAR images acquired annually or every few years incorporated into automated processing and analysis; GNSS and gravity surveys repeated every several years (depending on logistics); a single, continuous-mode GNSS station within 5–10 km of the deforming source	Five to 10 telemetered continuous-mode GNSS stations, of which four are within 5–10 km of the deforming source and one is outside the area of expected deformation; if conditions permit, two to four borehole tiltmeters within 5–10 km of the deforming source. InSAR processing on at least an annual basis, and GNSS and microgravity surveys (as appropriate) every several years to supplement data collected from continuously operating stations	Sixteen or more continuous-mode GNSS stations, of which at least eight are within 5–10 km of the deforming source and two are outside the area of expected deformation; if conditions are appropriate, four to six borehole tiltmeters within 5–10 km of the deforming source, and one continuous gravimeter. Regular InSAR acquisition and processing, including multi-temporal approaches as conditions warrant. GNSS and microgravity surveys every year to every several years (as appropriate) to supplement data collected from continuously operating stations

Table A1. Recommended instrumentation for volcano monitoring in the United States by monitoring level.—Continued

Monitoring category	Monitoring level (monitoring need and volcano threat level)			
	1 (Minimal monitoring; very low threat)	2 (Limited monitoring for change detection; low threat)	3 (Basic real-time monitoring; moderate to high threat)	4 (Well monitored in real time; high to very high threat)
Gas	Automated daily satellite-based alerts of SO ₂ emissions. Ensure existence of gas geochemical data on any existing fumaroles or geothermal springs	Establish a satellite-based SO ₂ emission-rates catalog and characterize baseline gas geochemistry and emission rates using airborne and (or) ground-based sampling techniques on a 5- to 10-year schedule	Establish a satellite-based SO ₂ emission-rate time series at any volcano with an adequate level of degassing. Characterize baseline gas geochemistry and emission rates using airborne and (or) ground-based sampling techniques on a 3- to 5-year schedule. Conduct continuous monitoring and (or) survey measurements of gas emission rates as appropriate at any volcano with an adequate level of degassing	In addition to level 3 recommendations, characterize baseline gas geochemistry and emissions on a 1- to 2-year schedule
Springs, streams, and volcanic lakes	Compile an inventory of spring, stream, and well sites to identify those with indications of ongoing magmatic influence, such as elevated ³ He/ ⁴ He ratios, large fluxes of magmatic CO ₂ , or anomalous heat fluxes. This inventory would ideally include a field visit with sampling, basic measurements (temperature, pH, and specific conductance), and subsequent laboratory analysis for major-element chemistry and isotope ratios, potentially including those of C, O, H, and He	Same as for level 1	Same as for levels 1 and 2, with resampling every 5 to 10 years to gradually define baseline conditions and develop rating curves. Those springs and streams with clear magmatic signals and accessible sites may be targeted for longer term studies with deployed commercial off-the-shelf technology and conductivity, temperature, and depth sensors and autosamplers. Bathymetric and heat-flow mapping, identification of hydrothermal vents, and, in some cases, mapping the three-dimensional distribution of temperature, salinity, and dissolved gas	Where appropriate, characterize variability caused by factors such as tectonic earthquakes and semi-diurnal-seasonal influences (for example, barometric and tidal), including regular sampling surveys along all major drainages. Install instrumentation for multiyear (3–5 year) periods to collect hourly (or better) information on heat flux and magmatically derived solutes. At select volcanoes, continuous real-time monitoring of hydrologic parameters, targeting springs, and (or) streams that are known or likely to be influenced by magmatic processes, including periodic sampling and streamgaging to calibrate sensors and establish rating curves
Tracking surface changes caused by volcanic activity	Collect moderate-resolution baseline imagery and at least 10-m-resolution DEMs to provide a synoptic overview of volcanic landforms, deposits, and thermal features for later comparison. Implement automated hot spot detection and alerting	Same as for level 1	Collect and regularly update high-resolution baseline optical and thermal imagery; acquire a 5-m minimum-resolution DEM and high-spatial-resolution satellite images (<1-m resolution) or stereopair aerial imagery for detailed geologic and hazard mapping; deploy one telemetered ground-based optical camera	Same as for level 3, except baseline DEMs should be at least 1-m-resolution to improve hazards modeling; deploy two telemetered ground-based cameras, and a thermal camera where appropriate; regularly acquire high-resolution stereopairs and orthorectified optical and SWIR satellite and (or) aerial imagery

Table A1. Recommended instrumentation for volcano monitoring in the United States by monitoring level.—Continued

Monitoring category	Monitoring level (monitoring need and volcano threat level)			
	1 (Minimal monitoring; very low threat)	2 (Limited monitoring for change detection; low threat)	3 (Basic real-time monitoring; moderate to high threat)	4 (Well monitored in real time; high to very high threat)
Lahars	None	None	At least one four- to six-element infrasound array with sensitivity to multiple drainages sited to minimize topographic barriers to potentially active drainages and to provide azimuthal separation between drainages. Two seismometers in or near each drainage of interest, with one in the potential source area and the other in a downstream location but upstream from any population center or infrastructure that could be threatened. The infrasound array could be co-located with one of the seismic stations if conditions are acceptable	Three or more three- to six-element infrasound arrays along each potential flow channel that has high lahar hazard. Include at least one array with four to six elements that has sensitivity to multiple drainages to minimize topographic shielding and to provide azimuthal separation between drainages. At least one seismometer in the source area of each drainage, with additional sensors along each drainage at 1–5 km intervals. Some of these stations may already exist as part of a volcano monitoring network. Web cameras, where possible, to verify surface flow occurrence
Marine eruptions	Minimum of one to three land-based seismic stations optimized for T-phase detection, with distribution determined by the number and location of submarine volcanoes. Short-term (6–12 months) deployments of two to three non-real-time hydrophones for regions with higher risk, more volcanoes, and (or) sparser or more distant land-based networks. Weekly to daily regional satellite monitoring for signs of volcanic activity dependent on risk in the region	Same as for level 1 as well as bathymetric mapping of submarine volcanoes when possible	Same as for level 2 as well as one to two cabled small-aperture hydrophone arrays with four moorings. Additional optimized T-phase stations and short-term hydrophone deployments, dependent on regional situation and activity levels. Additional monitoring with satellites and other methods as needed for understanding eruption hazards. At least one real-time, marine-based instrument site with a broadband seismometer, hydrophone, and other sensors. Bathymetric mapping of submarine volcanoes every 5–10 years and after periods of volcanic activity	Same as for level 3 as well as at least four real-time marine-based instrument sites with a broadband seismometer, hydrophone, and other sensors. One to two infrasound sensors or arrays on the nearest islands. Bathymetric mapping every 1–5 years and after periods of volcanic activity

Table A2. Recommendations for volcano-threat-level-independent special topics for volcano monitoring in the United States.

[ENTLN, Earth Networks Total Lightning Network; GLD360, Global Lightning Detection Network; GOES, Geostationary Operational Environmental Satellite; km, kilometer; m, meter; NEXRAD, Next Generation Weather Radar; NLDN, National Lightning Detection Network; NOAA, National Oceanic and Atmospheric Administration; UAS, unoccupied aircraft system; USGS, U.S. Geological Survey; WWLLN, World Wide Lightning Location Network]

Monitoring category	Summary of recommendations
Eruption plumes and clouds	<p>Low-latency access to geostationary satellite image products from the GOES and Himawari platforms. Ideally, 5 minutes or less from image collection to USGS availability</p> <p>Access to polar-orbiting satellite image products from NOAA platforms. Ideally, a latency of 30 minutes or less from image collection to USGS availability</p> <p>Real-time data subscriptions and alarms from commercial and academic long-range lightning detection networks. Volcanoes in Alaska, Hawai‘i, and the Commonwealth of the Northern Mariana Islands are covered by the GLD360, ENTLN, and WWLLN networks, as well as moderate coverage from GOES Global Lightning Mapper. Volcanoes in the contiguous United States are additionally covered by the NLDN</p> <p>Deployment of a telemetered, short-range electrical sensor (very high frequency sensor, field mill, or similar) to capture small-scale vent discharges associated with the earliest stages of volcanic plume development</p> <p>Collaboration with National Weather Service and academic partners at the National Severe Storms Laboratory on volcanic cloud product development for the NEXRAD system and for portable radar systems</p> <p>Deployment of a radar system for rapid evaluation of eruptions with potential for ashfall on populated areas and substantial impacts to infrastructure</p> <p>Deployment of ash sensor and collection systems in targeted areas near an erupting volcano (within approximately 10–100 km depending on eruption dynamics and wind field)</p>
Boreholes	<p>Where feasible and appropriate, boreholes would be at least 200 to 300 m deep but also can include shallower boreholes where acquired data could yield important information</p> <p>Any borehole installation would include core recovery to better characterize the volcano’s subsurface structure and eruptive history</p> <p>After borehole installation, boreholes would ideally be fit with appropriate instrumentation, which could include some combination of seismometers, tiltmeters, strainmeters, pore-pressure sensors, temperature sensors, and geochemical sensors</p> <p>Given the substantially higher cost of drilling and installing instrumentation in deeper boreholes (for example, more than 1 km), partnerships with academic and government agencies (for example, the U.S. Department of Energy and the National Science Foundation) would be beneficial</p>
Unoccupied aircraft systems (UAS)	<p>Ideally, at least two accredited UAS remote pilots would be operational at each volcano observatory</p> <p>Ideally, each observatory would have a fleet of UAS platforms and sensors capable of a broad array of volcano monitoring techniques</p> <p>Long-term investment by the Volcano Hazards Program, to encourage expansion of UAS monitoring capabilities, including remote pilot training, procurement, development of platforms and sensors, and field campaign support, would benefit volcano threat preparedness</p>

Table A3. Recommended rapid-response instrument cache for volcano monitoring in the United States.

[In addition to the instrumentation listed below, the caches should include all associated station infrastructure and equipment to provide power and telemetry for ground-based instruments, including batteries, solar panels, radios, cabling, housing, and mounting equipment, as well as radio repeaters and (or) satellite uplinks to ensure continuous data streams for stations installed in remote areas. DOAS, differential optical absorption spectroscopy; FLIR, forward-looking infrared; FTIR, Fourier-transform infrared spectroscopy; GNSS, Global Navigation Satellite System; Hz, hertz; NOAA, National Oceanic and Atmospheric Administration; ppb, part per billion; ppm, part per million; UAS, unoccupied aircraft system; USGS, U.S. Geological Survey]

Monitoring category	Instrumentation
Seismic	Twelve broadband seismometers; 50–100 node-type seismometers
Infrasound	Twelve infrasound sensors and two four-element infrasound arrays
Ground deformation and gravity	Twelve GNSS receivers
Gas	Three scanning spectrometer systems, one SO ₂ camera, and one multicomponent gas analyzer system (multi-GAS) station. Instrumentation for performing periodic field surveys, including one mobile DOAS system, one portable SO ₂ camera, one portable multi-GAS system, one field FTIR system, one portable soil-CO ₂ fluxmeter, and equipment for direct sampling of fumaroles and springs. For airborne gas monitoring from fixed-wing and helicopter-borne missions, the cache would include one highly sensitive, temperature-stabilized DOAS spectrometer and dedicated in situ instruments that have the capability to measure CO ₂ at <1 ppm accuracy and precision and major sulfur gases (SO ₂ and H ₂ S) at <5 ppb accuracy and precision at a 1 Hz sampling rate. In addition, one UAS equipped with multi-GAS and DOAS systems would be available
Springs, streams, and volcanic lakes	No specific instrument recommendations
Tracking surface changes caused by volcanic activity	If deemed appropriate by the observatory; one handheld FLIR camera and (or) one airborne (gimble mount) FLIR. Four telemetered cameras with zoom (two with low-light capabilities)
Eruption plumes and clouds	If deemed appropriate by the observatory; one ground-based Doppler radar system and one or more short range very high-frequency sensors (or broadband) or field mill
Lahars	Eight broadband seismometers and two four-element infrasound arrays
Marine eruptions	Observatories responsible for monitoring volcanoes in marine environments (Aleutian Islands, Northern Mariana Islands, and American Samoa) would ideally pursue partnerships with internal and (or) external partners (for example, USGS Pacific Coastal and Marine Science Center, NOAA, and others), for developing a marine rapid-response instrument cache. Ideally, this cache would include ocean-bottom seismometers, hydrophones, bottom-pressure recorders, and other sensors of opportunity. When possible and appropriate, rapidly deploying multiple land-based seismometers optimized for T-phases on the nearest islands could supplement ocean-bottom seismometers and hydrophones

networks were needed at low-threat volcanoes (for example, Craters of the Moon, Idaho); level 3 networks were designed for moderate-threat volcanoes (for example, Bogoslof Island, Alaska); and level 4 networks were designed for monitoring both high-threat (Yellowstone Caldera, Wyoming) and very high-threat volcanoes, such as Mount Rainier, Washington. Moran and others (2008) opted not to stress a rigid tie between the volcanic-threat rankings and monitoring levels and to allow greater flexibility. In this volume, and in table A1, we also adopt a flexible approach whereby some high-threat volcanoes may warrant level 3, and others may warrant a level 4 monitoring network. USGS Volcanic Hazards Program staff will determine the specific monitoring level required at any particular volcano—a range of scientific, economic, and logistical parameters will be needed to design and implement the appropriate network.

References Cited

- Blong, R.J., 1984, *Volcanic hazards; a sourcebook on the effects of eruptions*: Orlando, Fla., Academic Press, 424 p.
- Ewert, J.W., Diefenbach, A.K., and Ramsey, D.W., 2018, 2018 update to the U.S. Geological Survey national volcanic threat assessment: U.S. Geological Survey Scientific Investigations Report 2018–5140, 40 p., <https://doi.org/10.3133/sir20185140>.
- Ewert, J.W., Guffanti, M., and Murray, T.L., 2005, An assessment of volcanic threat and monitoring capabilities in the United States—Framework for a National Volcano Early Warning System: U.S. Geological Survey Open-File Report 2005–1164, 62 p., <https://doi.org/10.3133/ofr20051164>.
- Given, D.D., Allen, R.M., Baltay, A.S., Bodin, P., Cochran, E.S., Creager, K., de Groot, R.M., Gee, L.S., Hauksson, E., Heaton, T.H., Hellweg, M., Murray, J.R., Thomas, V.I., Toomey, D., and Yelin, T.S., 2018, Revised technical implementation plan for the ShakeAlert system—An earthquake early warning system for the West Coast of the United States: U.S. Geological Survey Open-File Report 2018–1155, 42 p., <https://doi.org/10.3133/ofr20181155>.
- Guffanti, M., Schneider, D.J., Wallace, K.L., Hall, T., Bensimon, D.R., and Salinas, L.J., 2010, Aviation response to a widely dispersed volcanic ash and gas cloud from the August 2008 eruption of Kasatochi, Alaska, USA: *Journal of Geophysical Research, Atmospheres*, v. 115, no. D2, <https://doi.org/10.1029/2010JD013868>.
- Moran, S.C., Freymueller, J.T., LaHusen, R.G., McGee, K.A., Poland, M.P., Power, J.A., Schmidt, D.A., Schneider, D.J., Stephens, G., Werner, C.A., and White, R.A., 2008, Instrumentation recommendations for volcano monitoring at U.S. volcanoes under the National Volcano Early Warning System: U.S. Geological Survey Scientific Investigations Report 2008–5114, 47 p., <https://doi.org/10.3133/sir20085114>.
- Neal, C.A., Brantley, S.R., Antolik, L., Babb, J.L., Burgess, M., Calles, K., Cappos, M., Chang, J.C., Conway, S., Desmither, L., Dotray, P., Elias, T., Fukunaga, P., Fuke, S., Johanson, I.A., Kamibayashi, K., Kauahikaua, J., Lee, R.L., Pekalib, S., Miklius, A., Million, W., Moniz, C.J., Nadeau, P.A., Okubo, P., Parcheta, C., Patrick, M.R., Shiro, B., Swanson, D., Tollett, W., Trusdell, F., Zoeller, M.H., Montgomery-Brown, E.K., Anderson, K.R., Poland, M.P., Ball, J.L., Bard, J.A., Coombs, M., Dietterich, H.R., Kern, C., Thelen, W.A., Cervelli, P.F., Orr, T., Houghton, B.F., Gansecki, C., Hazlett, R., Lundgren, P., Diefenbach, A.K., Lerner, A., Waite, G., Kelly, P.J., Clor, L., Werner, C., Burgess, M., Mulliken, K., Fisher, G., and Damby, D., 2019, The 2018 rift eruption and summit collapse of Kīlauea Volcano: *Science*, v. 363, no. 6425, p. 367–374, <https://doi.org/10.1126/science.aav7046>.
- Neal, C.A., Casadevall, T.J., Miller, T.P., Hendley J.W., II, and Stauffer, P.H., 1997, Volcanic ash—Danger to aircraft in the North Pacific: U.S. Geological Survey Fact Sheet 030-97, 2 p.
- Palmer, J., 2020, The art of volcanic ash modeling 10 years after Eyjafjallajökull: *Eos*, v. 101, <https://doi.org/10.1029/2020EO142708>.
- Prata, F., and Rose, B., 2015, Volcanic ash hazards to aviation, chap. 52 of Sigurdsson, H., Houghton, B.F., McNutt, S.R., Rymer, H., and Stix, J., eds., *The Encyclopedia of Volcanoes*: San Diego, Academic Press, p. 911–934, <https://doi.org/10.1016/B978-0-12-385938-9.00052-3>.
- Scott, W.E., 1989, Volcanic and related hazards, chap. 2 of Tilling, R.I., ed., *Volcanic hazards (Short Course in Geology, v. 1)*: Washington, D.C., American Geophysical Union, p. 9–23.
- Shroder, J.F., and Papale, P., eds., 2014, *Volcanic hazards, risks, and disasters*: Amsterdam, Netherlands, Elsevier, 532 p.

Chapter B



Multidisciplinary monitoring site Sugar Bowl at Mount St. Helens, Washington. The steaming 2004–2008 volcanic dome is visible in the background. Photograph by T. Paladino, U.S. Geological Survey, February 13, 2024.

Chapter B

Seismic Techniques and Suggested Instrumentation to Monitor Volcanoes

By Weston A. Thelen, John J. Lyons, Aaron G. Wech, Seth C. Moran, Matthew M. Haney, and Ashton F. Flinders

Introduction

Changes in the pressure or location of magma can stress or break surrounding rocks and trigger flow of nearby waters and gases, causing seismic signals, such as discrete earthquakes and tremor. These phenomena are types of seismic unrest that commonly precede eruption and can be used to forecast volcanic activity. Mass movements at the surface, including avalanches, debris flows, and lahars, may also generate seismic signals that are specifically addressed in chapter H, this volume (Thelen and others, 2024). Our focus in this chapter is to determine the levels of instrumentation recommended to produce high-quality, well-constrained seismic observations important for early warning of impending eruptions, detecting changes in ongoing eruptions, and characterizing other hazardous volcanic events.

There are emerging techniques and new types of instrumentation, such as distributed acoustic sensing or rotational seismometers, that we do not consider here. These types of instrumentation show promise for monitoring but still require maturation before being considered more generally in volcano monitoring.

Most of the capabilities mentioned below are universal for all types of volcanic systems, although some are best applied to stratovolcanoes with an apical single vent. In some settings, such as calderas or shield volcanoes, we must broaden coverage to include multiple possible storage regions or vent locations. As an example, Thelen (2014) discretized the long rift zones of shield volcanoes in Hawai‘i as a set of evenly spaced “vents.” In this construct, each vent comes with recommendations, and several thousand network configurations were simulated to assess the effect on network quality levels and to determine the most efficient network design. The same process could be applied in a caldera setting or a volcanic field, where an evenly spaced grid of potential vents is considered. Localized recommendations for each unique system are beyond the scope of this report and left up to local experts to assess based on the conditions, restrictions, and requirements of each volcano.

Recommended Capabilities

Detect Changes in Earthquake Location, Seismic Energy Release, Event Type, and Source Properties

Marked increases in earthquake rates have been observed at erupting volcanoes as diverse in size, chemistry, and eruptive style as Kīlauea, Hawai‘i (Klein and others, 1987); Mount St. Helens, Washington (Malone and others, 1981; Moran and others, 2008a); and Mount Pinatubo, Philippines (Harlow and others, 1996). Depending on the volcano, precursory seismic sequences may be entirely composed of smaller magnitude ($M < 2$) earthquakes; for example, at Mount Spurr, Alaska, in 1992 (Power and others, 1995). Earthquake hypocenters have also been observed to migrate in advance of eruptions (for example, Klein and others, 1987; Harlow and others, 1996; Battaglia and others, 2005; Nakada and others, 2005). Finally, relocation of similar events (“multiplets”) has yielded precise relative locations, particularly when paired with matched filter techniques, which have proven useful for constraining magmatic processes in conduits (for example, Prejean and others, 2003; Shelly and others, 2013; Shelly and Thelen, 2019). Machine learning (ML) approaches are improving detection and location capabilities (for example, Wilding and others, 2022). Generally, the infrastructure requirements for ML approaches overlap entirely with the capabilities above. Most of the examples above are specific to volcano-tectonic earthquakes, and the ability to identify these types of events and assess changes in space and time are a critical capability for any volcano observatory.

In addition to volcano-tectonic earthquakes, volcanism is commonly associated with other types of seismicity, including seismic tremor, very long period (VLP) earthquakes, hybrid earthquakes, and low-frequency earthquakes. In a variety of unrest and eruption scenarios these non-standard types of earthquakes may dominate over volcano-tectonic seismicity, underscoring their importance in monitoring. Changes in seismicity have been observed before many eruptions, such as from dominantly volcano-tectonic to dominantly low-frequency

earthquakes in the hours, days, and weeks preceding the onset of eruptive activity at Mount St. Helens in 1980–86 and 2004 (Endo and others, 1981; Malone and others, 1983; Moran and others, 2008b), Mount Pinatubo in 1991 (Harlow and others, 1996), and Soufrière Hills in 1995 (Gardner and White, 2002). Automated techniques to differentiate between event types are especially important during unrest when high earthquake rates may overwhelm analysts. Some automated machine learning approaches are becoming more widely applied (for example, Bueno and others, 2020; Tan and others, 2023). It is also important to be able to characterize deep activity, such as deep long-period earthquakes, that may be precursors to eruptions (for example, White, 1996; Power and others, 2013; Frank and others, 2018).

Seismic tremor is commonly recognized during unrest and eruption. However, real-time analysis is typically limited to time series of amplitude and frequency content. In some eruptions, such as Pavlof Volcano in 2016 (Fee and others, 2017), seismicity was dominated by seismic tremor, with only a few discrete earthquakes identified and no precursory seismicity. Detection and tracking of seismic tremor have proven important at several volcanoes for accurate eruption forecasting and tracking of ongoing eruptions (for example, McNutt and others, 1995; Takagi and others, 2006; Hotovec and others, 2013). Locating seismic tremor using amplitude-based techniques (for example, Battaglia and Aki, 2003; Taisne and others, 2011) or network covariance (for example, Soubestre and others, 2019; Maher and others, 2023) is feasible in real time and important for monitoring dike intrusions and eruptions.

An additional recommended capability for seismic monitoring is on-scale recording of seismicity without clipping. Clipping of a seismic trace can occur during strong ground motion when the recording capabilities of the seismometer or digitizer are exceeded. Tracking long-term seismicity rates and energy release through techniques such as real-time seismic-amplitude measurement (Endo and Murray, 1991) at volcanoes has repeatedly proven to be an effective means of recognizing renewed volcanic activity. At some energetic volcanoes, however, seismicity before and (or) accompanying an eruption intensifies to the point where low-dynamic-range seismic systems within a few kilometers become saturated and cannot be used for tracking changes in seismicity and earthquake magnitudes (Endo and others, 1981; Malone and others, 1981; Moran and others, 2008b). This problem can be mostly solved by installing modern digitizers (24+ bit), thus greatly increasing the seismic-energy range over which on-scale recording can be obtained and ensuring the ability to track changes in seismic-energy release, event rate, and event type during the most energetic phases of a precursory or eruptive sequence. In cases where strong seismicity ($>M4$) has been observed or is expected, the dynamic range of a 24-bit digitizer-broadband combination may be exceeded within a few kilometers of the seismic source, and a strong-motion instrument co-located with a broadband seismometer within 10 kilometers (km) of an eruption site would ensure on-scale recording despite strong earthquakes and (or) tremor.

Instrumentation

In principle, a single seismic station can be used to track earthquake rate and record qualitative changes in seismic-energy release; however, at least two stations are required for robustly distinguishing between the signals produced by volcanic and nonvolcanic (for example, wind, anthropogenic noise, electronic interference) phenomena. For all location methods described above, at least four seismic observations are required to locate earthquakes and constrain the timing, but to optimize location quality, it is best to have eight or more observations. Fewer observations may be acceptable based on station distribution. Ideally, these sites would be clustered around areas of high seismicity to constrain the smallest events. But for deep long-period earthquakes, or earthquakes associated with offset magma transport systems, having a larger spread in stations is optimal, meaning more than eight sites are likely required for most systems. To track changes in depth, it is critical to have at least one station above the seismic source, which commonly means as close to the expected vent of the volcano as feasible (fig. B1). In many cases,



Figure B1. Photograph of monitoring station September Lobe (SEP) on the 1980–86 dome at Mount St. Helens, Washington. The site has co-located seismic, geodetic, tilt, and infrasound instruments. View is to the north; Spirit Lake is visible in the near-background and Mount Rainier is on the skyline. Photograph by Ben Pauk, U.S. Geological Survey, 2018.

logistical constraints such as glacier coverage, winter snow and ice conditions, volcanic hazard, telemetry, or land-use restrictions may preclude the installation of a station directly above the source of the earthquakes. In these cases, a small-aperture seismic array at the nearest practical site may offer the ability to track changes in depth very precisely through the calculation of an incidence angle (for example, Glasgow and others, 2018). Short-period, vertical-component instruments may be sufficient for some of the capabilities mentioned above; however, earthquake-location accuracy, especially in depth, is improved when S-wave arrival times are included, which are more reliably identified by using three-component seismometers. Moreover, adequate detection of all types of volcanic seismicity requires broadband sensitivity (120 seconds to 50 hertz). In the past decade, broadband seismometers have become more cost effective and require dramatically less power; thus, these instruments have become the preferred type of seismometer for volcano monitoring. If moderate earthquakes ($>M4$) or large explosions are expected at a given volcano, then at least one strong-motion sensor would ideally be co-located with a broadband seismometer within 10 km of an expected vent to provide on-scale recordings during unrest.

Recommendations

For level 1 volcanoes, the ideal network would be able to detect $>M1.5$ earthquakes and to locate (crudely) $>M3$ earthquakes. For level 2 volcanoes, the network would detect $>M1$ earthquakes, crudely locate $>M2$ earthquakes, and detect energetic seismic tremor. For level 3 volcanoes, the network would detect $>M0.5$ earthquakes and to accurately locate $>M1$ earthquakes while recording and distinguishing between all event types and detecting seismic tremor. For level 4 volcanoes, the network would detect and accurately locate $>M0$ earthquakes, determine event type, detect and locate seismic tremor, and provide on-scale recordings of energetic seismicity.

Detect Changes in Localized Stress Fields

Understanding the stress state within a volcano and how those stresses change over time is a key contribution of seismology to assessing volcanic hazards. Magma intrusions have been correlated with changes to the local stress field that overprint the background stress-field orientations. As such, they can provide some of the earliest clues of unrest related to magma intrusion, even during times when seismicity rates are near background. Stress-field changes have been detected during periods of quiescence, unrest, and eruption by (1) changes in fault-plane solutions (for example, Moran, 1994; Roman and others, 2004; Sánchez and others, 2004), (2) changes in b -value (the slope of the frequency-magnitude distribution) (Vinciguerra, 2002; Novelo-Casanova and others, 2006), and (3) changes in shear-wave-splitting directions (for example, Miller and Savage, 2001; Gerst and Savage, 2004; Johnson and Poland, 2013).

Stress rotations have been observed through analysis of fault-plane solutions in preeruptive sequences worldwide (Roman and Cashman, 2006). These stress rotations commonly differ from a background or regional direction prior to eruption and may be used to assess the likelihood of eruption (Roman and others, 2006). Further scrutiny of fault-plane solutions in space and time led to an estimation of viscosity during the 2018 eruption at Kīlauea (Roman and others, 2021). Automated fault-plane solutions can be calculated in near-real time (<5 minutes) if events are constrained by sufficient observations (see below).

Within an earthquake catalog, the rate of decrease of earthquake frequency with increasing size can be quantified by a b -value, which provides insight into the integration of cracks into longer fractures and faults that can fail as larger earthquakes. Vinciguerra (2002) used earthquake-catalog data to investigate temporal changes in b -values before and during the 1989 eruption of Mount Etna and reported precursory changes. Monitoring of temporal b -value changes requires real-time earthquake detection. Monitoring of spatial b -value changes requires real-time earthquake location, and thus multiple stations, and is difficult during vigorous seismic swarms.

When S-waves from regional earthquakes encounter anisotropy in the crust, they split into two new orthogonal waves that can be used to map out subsurface features (for example, underneath volcanoes). Changes in S-wave-splitting directions were reported by Miller and Savage (2001) and Gerst and Savage (2004) in association with the 1998 eruption of Mount Ruapehu; these authors inferred that the changes in S-wave-splitting direction were caused by intrusion of a 10-km-long dike. As with fault-plane solutions, S-wave-splitting directions can be calculated relatively rapidly if there are sufficient observations on a three-component network of seismometers.

Instrumentation

Fault-plane solutions, especially for volcano-tectonic earthquakes, are most commonly calculated from first-motion data. Source mechanisms also can be determined from P- to S- amplitude ratios (Julian and others, 1998; Pugh and others, 2016) or waveform modeling at long periods (for example, Chouet and others, 2003). Fault-plane solutions generally are poorly determined with fewer than 7 first motions and are most reliable with 10 or more first motions that are well distributed in azimuth and distance around the earthquake epicenter. Source mechanisms considering non-double couple sources, common in volcanic regions, require more data to constrain more unknowns. Amplitude ratios between P- and S-waves can also be used (Julian and others, 1998; Snoke, 2003; Pugh and others, 2016), but reliable S-wave picks require three-component sensors. Quality fault-plane solutions are also dependent on a quality velocity model and many non-double couple sources can be attributed to a poor velocity model or too few observations. To distinguish between temporal and spatial b -value changes, a seismic network must be able to locate events to within 1-km accuracy. Because b -values are more accurately determined over a wide range of

event magnitudes, on-scale recordings of earthquakes are essential for a quality magnitude calculation. S-wave splitting has been detected exclusively on broadband seismometers, although in principle S-wave splitting could be done with short-period, three-component sensors. Instruments must be deployed directly above the volume of interest. In addition, for a rapid S-wave splitting determination, S-waves must be timed on both horizontal channels, which is not commonplace for networks within the United States. S-wave picks can also be made using machine learning (for example, Zhu and Beroza, 2019).

Recommendations

For levels 1 and 2 volcanoes, this capability is not required. For level 3 volcanoes, it is advisable to quantify generalized stress fields near the volcanic center using fault-plane solutions and *b*-values for earthquakes $>M1$. For level 4 volcanoes, one can detect detailed stress-field changes, such as stress rotations, by constructing well-constrained fault-plane solutions and (or) moment tensors, non-double couple fault-plane solutions, mapping *b*-values at high spatial resolution, and detecting changes in S-wave-splitting directions over time.

Monitor Changes in Seismic Source and (or) Path Over Time

As magma intrudes into or beneath a volcanic edifice, it can compress pore spaces, open or close cracks, and otherwise affect the country rock surrounding the conduit. These changes will likely change the local bulk-rock properties (density, compressibility, and yield strength) of the subsurface and may produce observable changes in seismic velocity, attenuation, or source mechanism over time. Detection of these material changes in the subsurface can be important to understanding the causes of magma unrest and the potential for eruption.

Temporal changes in seismic velocity have been observed at several volcanic centers, most recently using ambient noise techniques (for example, Brenguier and others, 2008). At Piton de la Fournaise, decreases in seismic velocity occurred prior to several eruptions (Brenguier and others, 2008). At Kīlauea, changes in velocity were strongly correlated to changes in tilt, an exciting development at volcanoes without tiltmeters installed (Donaldson and others, 2017). Although the studies mentioned above use pairs of stations, Bennington and others (2018) used a single station at Mount Veniaminof, Alaska, to find precursory eruptive velocity changes and localize the depth of the velocity change.

Spatial and temporal changes in seismic velocity, sometimes referred to as four-dimensional tomography, could influence the assessment of volcanic hazard by combining emerging techniques. Knowing where magma is stored and transported assists in developing a conceptual model for understanding unrest. The utility of repeat travel time tomography has been demonstrated in some settings, where changes in the V_p/V_s ratio can be observed (Koulakov and others, 2013; Koulakov and Vargas, 2018). Using

catalogs improved through matched filtering or machine learning approaches may allow for more frequent and higher resolution tomography. Additionally, the length of continuous data records critical for ambient noise tomography is growing, allowing for repeated studies where an ambient noise model has already been calculated (for example, Brenguier and others, 2007; Flinders and Shen, 2017; Flinders and others, 2018).

Changes in country rock, such as fracturing or fluid injection, can also affect scattering properties of the medium, which influence the codas (tails) of individual earthquake seismograms. Recently, researchers have compared repeating earthquakes to show that variations occur only in the coda, a phenomenon that can be caused only by changes in country rock between the earthquake and the seismometer. Velocity changes were found in association with activity at Mount St. Helens (Hotovec-Ellis and others, 2014, 2015) and Kīlauea (Hotovec-Ellis and others, 2022).

Finally, changes in the properties of long-period events have been used to infer changes in magmatic systems over time. At Galeras volcano, Colombia, Gómez and Torres (1997) reported that coda durations increased and dominant frequencies decreased in long-period “tornillo”-type events before dome-damaging explosions. Kumagai and others (2001) showed that the characteristics of long-period seismic signals can change based on the proportion of gas, magma, and ash inside the resonating crack.

Instrumentation and Recommendations

For level 1 volcanoes, this capability is not required. For level 2 volcanoes, long-period events would ideally be detectable, as should event families for $>M1$ earthquakes. The network would be capable of detecting broad-scale changes in velocity over long periods of time. At level 3 volcanoes, the network would be able to detect long-period earthquakes and event families for $>M0.5$ earthquakes and to detect changes in travel time and broad-scale changes in seismic velocity over long periods of time. For level 4 volcanoes, the network would allow for determination of temporal source properties of long-period earthquakes, detection and location of event families for $>M0$ events, and construction of time-varying three-dimensional velocity models (provided local seismicity or seismic noise is sufficient).

Detect and Determine Source Mechanisms for Very Long Period and Long Period Events

As seismic networks have become denser and more sensitive to low frequencies, scientists have increasingly detected the occurrence of very long period (VLP) waves that may reflect the shallow movement of large volumes of magma or volcanic fluids related to intrusion and volcanic unrest. These VLP events manifest in discrete events (for example, Arciniega-Ceballos and others, 1999; Hidayat and others, 2000; Kumagai and others, 2001) and tremor (for example, De Lauro and others, 2005; Haney, 2010). VLP events or VLP tremor can be located using particle motions in a technique called radial semblance (Almendros and Chouet, 2003; Dawson and others, 2004). With the proper number and distribution

of broadband instrumentation, one can determine through the moment tensor the orientation and dimensions of the crack or sill that is generating the VLP and (or) long-period energy, providing critical information on the geometry of shallow parts of the magma plumbing system (Chouet and Dawson, 2011). Obtaining the moment tensor that helps define the plumbing system geometry is difficult in real time because of the complexity of volcanic topography and structure. In addition, calculating the moment tensor with waveform modeling is computationally intensive but potentially tractable in the near future (Auger and others, 2006). However, for multiyear eruptions or repeated eruptions that reuse shallow parts of the magma plumbing system, even results calculated weeks after an event can be useful for monitoring.

Instrumentation

VLP events can be detected with just two broadband sensors, although the sensors should be placed within a few wavelengths of the source epicenter (<5 km typically). Locating these events requires at least three broadband stations (preferably more to reduce errors) located within 5 km of the source epicenter (Dawson and others, 2004). At least three broadband stations within 5 km of the vent are required to completely determine all elements of the moment-tensor matrix as well as the location and single force terms, but typically such calculations are done with more than 10 stations. Such a high number of stations so close to an eruptive vent is only possible at a few volcanoes or for a limited temporary deployment. Where the geography allows and VLP activity has been documented, a dense network of broadband stations within 5 km would ideally be the goal. VLP earthquakes correlated with caldera collapse (Kumagai and others, 2001; Fontaine and others, 2019; Flinders and others, 2020) and large step-like inflations and (or) deflations can be substantially biased by band-limited seismometer response and are best interpreted with near station or co-located Global Navigation Satellite System (GNSS) data (Flinders and others, 2021).



Recommendations

For levels 1 and 2 volcanoes, this capability is not required. For level 3 volcanoes, the network would be able to detect VLP signals. For level 4 volcanoes, the network would detect and locate VLP events and track relative movement of the VLP source if the geography and land-use restrictions are permissive.

General Recommendations and Considerations

Broadband seismometers would ideally be prioritized over short-period seismometers because of the added sensitivity at low frequencies and added capabilities for volcano research purposes (for example, receiver functions and moment tensor inversions). There are several volcanic processes (described above) that generate low frequency seismic signals that benefit from observations only made possible through broadband instrumentation. With the added sensitivity comes added requirements for vaults that minimize thermal fluctuations and electronic noise. There have been substantial advances in vault testing and design with Transportable Array and ShakeAlert system buildouts, and future installations would follow as many of those design criteria as is feasible given the accessibility of the site and land-use restrictions (fig. B2). Broadband instruments also have a demonstrated sensitivity to tilt that could be useful during unrest if the sensor is sufficiently close to the source and inside a thermally stable vault (Lyons and others, 2012). The minimum sample rate for new installations is 50 samples per second, but 100 samples per second would be an ideal goal. This higher sample rate allows for more precise determination of P- and S-wave arrivals, higher precision lag estimates (good for relocations), earthquake waveform modeling, and more accurate polarities for focal mechanisms. Continuous low-latency seismic data are required, and efforts would ideally be made to comply with the U.S. Geological Survey's Earthquake Hazards Program Advanced National Seismic System (ANSS) performance standards where and when appropriate (U.S. Geological Survey, 2017; U.S. Geological Survey Earthquake Hazards Program, 2019).

Figure B2. Photograph of a U.S. Geological Survey field technician performing site maintenance on seismic station ISLZ on Unimak Island, central Aleutian Islands, Alaska. Photograph by Dane Ketner, U.S. Geological Survey, August 15, 2020.

Summary—Recommendations for Volcano Levels 1–4 Seismic Networks

Level 1.—Five seismic stations within 200 km of the volcanic center, including two stations within 50 km.

Level 2.—Five seismic stations within 50 km of the volcanic center, including two stations within 10 km.

Level 3.—Seven or more broadband seismic stations within 20 km of the volcanic center, including at least two stations within 5 km.

Level 4.—Twelve to 25 broadband seismic stations within 20 km of the volcanic center, including at least 8 stations within 10 km and 4 or more within 5 km; at least one broadband or strong-motion station within 10 km. Small-aperture seismic array in places where logistics preclude placing stations high on the edifice.

References Cited

- Almendros, J., and Chouet, B., 2003, Performance of the radial semblance method for the location of very long period volcanic signals: *Bulletin of the Seismological Society of America*, v. 93, no. 5, p. 1890–1903, <https://doi.org/10.1785/0120020143>.
- Arciniega-Ceballos, A., Chouet, B.A., and Dawson, P.B., 1999, Very long-period signals associated with Vulcanian explosions at Popocatepetl Volcano, Mexico: *Geophysical Research Letters*, v. 26, no. 19, p. 3013–3016, <https://doi.org/10.1029/1999GL005390>.
- Auger, E., D’Auria, L., Martini, M., Chouet, B., and Dawson, P., 2006, Real-time monitoring and massive inversion of source parameters of very long period seismic signals—An application to Stromboli Volcano, Italy: *Geophysical Research Letters*, *Solid Earth*, v. 33, no. 4, 5 p., <https://doi.org/10.1029/2005GL024703>.
- Battaglia, J., and Aki, K., 2003, Location of seismic events and eruptive fissures on the Piton de la Fournaise volcano using seismic amplitudes: *Journal of Geophysical Research Solid Earth*, v. 108, no. B8, article no. 2364.
- Battaglia, J., Ferrazzini, V., Staudacher, T., Aki, K., and Cheminée, J.L., 2005, Pre-eruptive migration of earthquakes at the Piton de la Fournaise volcano (Réunion Island): *Geophysical Journal International*, v. 161, no. 2, p. 549–558, <https://doi.org/10.1111/j.1365-246X.2005.02606.x>.
- Bennington, N., Haney, M., Thurber, C., and Zeng, X., 2018, Inferring magma dynamics at Veniaminof volcano via application of ambient noise: *Geophysical Research Letters*, v. 45, no. 21, p. 11,650–11,658, <https://doi.org/10.1029/2018GL079909>.
- Brenguier, F., Shapiro, N.M., Campillo, M., Ferrazzini, V., Duputel, Z., Coutant, O., and Nercessian, A., 2008, Towards forecasting volcanic eruptions using seismic noise: *Nature Geoscience*, v. 1, no. 2, p. 126–130, <https://doi.org/10.1038/ngeo104>.
- Brenguier, F., Shapiro, N.M., Campillo, M., Nercessian, A., and Ferrazzini, V., 2007, 3-D surface wave tomography of the Piton de la Fournaise Volcano using seismic noise correlations: *Geophysical Research Letters*, *Solid Earth*, v. 34, no. 2, <https://doi.org/10.1029/2006GL028586>.
- Bueno, A., Zuccarello, L., Díaz-Moreno, A., Woollam, J., Titos, M., Benítez, C., Álvarez, I., Prudencio, J., and de Angelis, S., 2020, PICOSS—Python interface for the classification of seismic signals: *Computers and Geosciences*, v. 142, no. 104531, <https://doi.org/10.1016/j.cageo.2020.104531>.
- Chouet, B., and Dawson, P., 2011, Shallow conduit system at Kilauea Volcano, Hawaii, revealed by seismic signals associated with degassing bursts: *Journal of Geophysical Research, Solid Earth*, v. 116, no. B12, <https://doi.org/10.1029/2011JB008677>.
- Chouet, B., Dawson, P., Ohminato, T., Martini, M., Saccorotti, G., Giudicepietro, F., De Luca, G., Milana, G., and Scarpa, R., 2003, Source mechanisms of explosions at Stromboli Volcano, Italy, determined from moment-tensor inversions of very-long-period data: *Journal of Geophysical Research, Solid Earth*, v. 108, no. B1, p. ESE 7-1–ESE 7-25, <https://doi.org/10.1029/2002JB001919>.
- Dawson, P., Whildin, D., and Chouet, B., 2004, Application of near real-time radial semblance to locate the shallow magmatic conduit at Kilauea Volcano, Hawaii: *Geophysical Research Letters*, *Solid Earth*, v. 31, no. 21, 4 p., <https://doi.org/10.1029/2004GL021163>.
- De Lauro, E., De Martino, S., Falanga, M., Palo, M., and Scarpa, R., 2005, Evidence of VLP volcanic tremor in the band [0.2–0.5] Hz at Stromboli Volcano, Italy: *Geophysical Research Letters*, *Solid Earth*, v. 32, no. 17, 4 p., <https://doi.org/10.1029/2005GL023466>.
- Donaldson, C., Caudron, C., Green, R.G., Thelen, W.A., and White, R.S., 2017, Relative seismic velocity variations correlate with deformation at Kilauea volcano: *Science Advances*, v. 3, no. 6, <https://doi.org/10.1126/sciadv.1700219>.
- Endo, E.T., Malone, S.D., Noson, L.L., and Weaver, C.S., 1981, Locations, magnitudes, and statistics of the March 20–May 18 earthquake sequence, in Lipman, P.W., and Mullineaux, D.R., eds., *The 1980 eruptions of Mount St. Helens: U.S. Geological Survey Professional Paper 1250*, p. 93–107, <https://doi.org/10.3133/pp1250>.
- Endo, E.T., and Murray, T., 1991, Real-time seismic amplitude measurement (RSAM): a volcano monitoring and prediction tool: *Bulletin of Volcanology*, v. 53, p. 533–545, <https://doi.org/10.1007/BF00298154>.

- Fee, D., Haney, M.M., Matoza, R.S., Van Eaton, A.R., Cervelli, P., Schneider, D.J., and Iezzi, A.M., 2017, Volcanic tremor and plume height hysteresis from Pavlof Volcano, Alaska: *Science* v. 355, p. 45–48, <https://doi.org/10.1126/science.aah6108>.
- Flinders, A.F., Johanson, I.A., Dawson, P.B., Anderson, K.R., Haney, M.M., and Shiro, B.R., 2020, Very-long-period (VLP) seismic artifacts during the 2018 caldera collapse at Kīlauea, Hawai‘i: *Seismological Research Letters*, v. 91, no. 6, p. 3417–3432, <https://doi.org/10.1785/02202000083>.
- Flinders, A.F., Kauahikaua, J.P., Hsieh, P.A., and Ingebritsen, S.E., 2021, Post audit of simulated groundwater flow to the short-lived (2019 to 2020) crater lake at Kīlauea volcano, Hawai‘i: *Groundwater*, v. 60, no. 1, p. 2–155, <https://doi.org/10.1111/gwat.13133>.
- Flinders, A.F., Shelly, D.R., Dawson, P.B., Hill, D.P., Tripoli, B., and Shen, Y., 2018, Seismic evidence for significant melt beneath the Long Valley Caldera, California, USA: *Geology*, v. 46, p. 799–802, <https://doi.org/10.1130/G45094.1>.
- Flinders, A.F., and Shen, Y., 2017, Seismic evidence for a possible deep crustal hot zone beneath southwest Washington: *Scientific Reports*, v. 7, article no. 7400, <https://doi.org/10.1038/s41598-017-07123-w>.
- Fontaine, F.R., Roult, G., Hejrani, B., Michon, L., Ferrazzini, V., Barruol, G., Tkalčić, H., Di Muro, A., Peltier, A., Reymond, D., Staudacher, T., and Massin, F., 2019, Very- and ultra-long-period seismic signals prior to and during caldera formation on La Réunion Island: *Scientific Reports*, v. 9, article no. 8068, <https://doi.org/10.1038/s41598-019-44439-1>.
- Frank, W.B., Shapiro, N.M., and Gusev, A.A., 2018, Progressive reactivation of the volcanic plumbing system beneath Tolbachik Volcano (Kamchatka, Russia) revealed by long-period seismicity: *Earth and Planetary Science Letters*, v. 493, p. 47–56, <https://doi.org/10.1016/j.epsl.2018.04.018>.
- Gardner, C.A., and White, R.A., 2002, Seismicity, gas emission and deformation from 18 July to 25 September 1995 during the initial phreatic phase of the eruption of Soufrière Hills Volcano, Montserrat, *in* Druitt, T.H., and Kokelaar, B.P., eds., *The eruption of Soufrière Hills Volcano, Montserrat, from 1995 to 1999*: Geological Society of London *Memoirs*, v. 21, p. 567–581, <https://doi.org/10.1144/GSL.MEM.2002.021.01.26>.
- Gerst, A., and Savage, M.K., 2004, Seismic anisotropy beneath Ruapehu Volcano—A possible eruption forecasting tool: *Science*, v. 306, no. 5701, p. 1543–1547, <https://doi.org/10.1126/science.1103445>.
- Glasgow, M.E., Schmandt, B., and Hansen, S.M., 2018, Upper crustal low-frequency seismicity at Mount St. Helens detected with a dense geophone array: *Journal of Volcanology and Geothermal Research*, v. 358, p. 329–341, <https://doi.org/10.1016/j.jvolgeores.2018.06.006>.
- Gómez, D.M., and Torres C., R.A., 1997, Unusual low-frequency volcanic seismic events with slowly decaying coda waves observed at Galeras and other volcanoes: *Journal of Volcanology and Geothermal Research*, v. 77, no. 1–4, p. 173–193, [https://doi.org/10.1016/S0377-0273\(96\)00093-5](https://doi.org/10.1016/S0377-0273(96)00093-5).
- Haney, M.M., 2010, Location and mechanism of very long period tremor during the 2008 eruption of Okmok Volcano from interstation arrival times: *Journal of Geophysical Research*, v. 115, no. B10, <https://doi.org/10.1029/2010JB007440>.
- Harlow, D.H., Power, J.A., Laguerre, E.P., Ambubuyog, G., White, R.A., and Hoblitt, R.H., 1996, Precursory seismicity and forecasting of the June 15, 1991, eruption of Mount Pinatubo, *in* Newhall, C.S., and Punongbayan, S., *Fire and mud—Eruptions and lahars of Mount Pinatubo, Philippines*: Seattle, University of Washington Press, p. 285–305.
- Hidayat, D., Voight, B., Langston, C., Ratdomopurbo, A., and Ebeling, C., 2000, Broadband seismic experiment at Merapi Volcano, Java, Indonesia—Very-long-period pulses embedded in multiphase earthquakes: *Journal of Volcanology and Geothermal Research*, v. 100, no. 1–4, p. 215–231, [https://doi.org/10.1016/S0377-0273\(00\)00138-4](https://doi.org/10.1016/S0377-0273(00)00138-4).
- Hotovec, A.J., Prejean, S.G., Vidale, J.E., and Gomberg, J., 2013, Strongly gliding harmonic tremor during the 2009 eruption of Redoubt Volcano: *Journal of Volcanology and Geothermal Research*, v. 259, p. 89–99, <https://doi.org/10.1016/j.jvolgeores.2012.01.001>.
- Hotovec-Ellis, A.J., Gomberg, J., Vidale, J.E., and Creager, K.C., 2014, A continuous record of intereruption velocity change at Mount St. Helens from coda wave interferometry: *Journal of Geophysical Research, Solid Earth*, v. 119, no. 3, p. 2199–2214, <https://doi.org/10.1002/2013JB010742>.
- Hotovec-Ellis, A.J., Shiro, B.R., Shelly, D.R., Anderson, K.R., Haney, M.M., Thelen, W.A., Montgomery-Brown, E.K., and Johanson, I.A., 2022, Earthquake-derived seismic velocity changes during the 2018 caldera collapse of Kīlauea volcano: *Journal of Geophysical Research Solid Earth*, v. 127, no. 2, <https://doi.org/10.1029/2021JB023324>.
- Hotovec-Ellis, A.J., Vidale, J.E., Gomberg, J., Thelen, W., and Moran, S.C., 2015, Changes in seismic velocity during the first 14 months of the 2004–2008 eruption of Mount St. Helens, Washington: *Journal of Geophysical Research, Solid Earth*, v. 120, no. 9, p. 6226–6240, <https://doi.org/10.1002/2015JB012101>.
- Johnson, J.H., and Poland, M.P., 2013, Seismic detection of increased degassing before Kīlauea’s 2008 summit explosion: *Nature Communications*, v. 4, no. 1668, <https://doi.org/10.1038/ncomms2703>.
- Julian, B., Miller, A.D., and Foulger, G.R., 1998, Non-double-couple earthquakes—I. Theory: *Reviews of Geophysics*, v. 36, no. 4, p. 525–549, <https://doi.org/10.1029/98RG00716>.

- Klein, F.W., Koyanagi, Y., Nakata, J.S., and Tanigawa, W.R., 1987, The seismicity of Kīlauea's magma system, *in* Decker, R.W., Wright, T.L., Stauffer, P.H., eds., *Volcanism in Hawaii*: U.S. Geological Survey Professional Paper 1350, p. 1019–1185, <https://doi.org/10.3133/pp1350>.
- Koulakov, I., and Vargas, C.A., 2018, Evolution of the magma conduit beneath the Galeras Volcano inferred from repeated seismic tomography: *Geophysical Research Letters*, v. 45, no. 15, p. 7514–7522, <https://doi.org/10.1029/2018GL078850>.
- Koulakov, I., West, M., and Izbekov, P., 2013, Fluid ascent during the 2004–2005 unrest at Mt. Spurr inferred from seismic tomography: *Geophysical Research Letters*, v. 40, no. 17, p. 4579–4582, <https://doi.org/10.1002/grl.50674>.
- Kumagai, H., Ohminato, T., Nakano, M., Ooi, M., Kubo, A., Inoue, H., and Oikawa, J., 2001, Very-long-period seismic signals and caldera formation at Miyake Island, Japan: *Science*, v. 293, no. 5530, p. 687–690, <https://doi.org/10.1126/science.1062136>.
- Lyons, J.J., Waite, G.P., Ichihara, M., and Lees, J.M., 2012, Tilt prior to explosions and the effect of topography on ultra-long-period seismic records at Fuego volcano, Guatemala: *Geophysical Research Letters*, v. 39, no. 8, p. L08305.
- Maher, S.P., Dawson, P., Hotovec-Ellis, A., Thelen, W.A., Jolly, A., Bennington, N., Chang, J.C., and Dotray, P., 2023, Characterizing and locating seismic tremor during the 2022 eruption of Mauna Loa volcano, Hawai'i, with network covariance: *The Seismic Record*, v. 3, no. 3, p. 228–238, <https://doi.org/10.1785/0320230020>.
- Malone, S.D., Boyko, C., and Weaver, C.S., 1983, Seismic precursors to the Mount St. Helens eruptions in 1981 and 1982: *Science*, v. 221, no. 4618, p. 1376–1378, <https://doi.org/10.1126/science.221.4618.1376>.
- Malone, S.D., Endo, E.T., Weaver, C.S., and Ramey, J.W., 1981, Seismic monitoring for eruption prediction, *in* Lipman, P.W., and Mullineaux, D.R., eds., *The 1980 eruptions of Mount St. Helens*: U.S. Geological Survey Professional Paper 1250, p. 803–813, <https://doi.org/10.3133/pp1250>.
- McNutt, S.R., Tytgat, G.C., and Power, J.A., 1995, Preliminary analyses of volcanic tremor associated with 1992 eruptions of Crater Peak, Mount Spurr Volcano, Alaska, *in* Keith, T.E.C., ed., *The 1992 eruptions of Crater Peak vent, Mount Spurr Volcano, Alaska*: U.S. Geological Survey Bulletin 2139, p. 161–178, <https://doi.org/10.3133/b2139>.
- Miller, V., and Savage, M., 2001, Changes in seismic anisotropy after volcanic eruptions—Evidence from Mount Ruapehu: *Science*, v. 293, no. 5538, p. 2231–2233, <https://doi.org/10.1126/science.1063463>.
- Moran, S.C., 1994, Seismicity at Mount St. Helens, 1987–1992—Evidence for repressurization of an active magmatic system: *Journal of Geophysical Research, Solid Earth*, v. 99, no. B3, p. 4341–4354, <https://doi.org/10.1029/93JB02993>.
- Moran, S.C., Malone, S.D., Qamar, A.I., Thelen, W.A., Wright, A.K., and Caplan-Auerbach, J., 2008a, Seismicity associated with renewed dome-building at Mount St. Helens, 2004–2005, *in* Sherrod, D.R., Scott, W.E., and Stauffer, P.H., eds., *A volcano rekindled—The renewed eruption of Mount St. Helens, 2004–2006*: U.S. Geological Survey Professional Paper 1750, p. 27–60, <https://doi.org/10.3133/pp1750>.
- Moran, S.C., McChesney, P.J., and Lockhart, A.B., 2008b, Seismicity and infrasound associated with explosions at Mount Saint Helens, 2004–2005, *in* Sherrod, D.R., Scott, W.E., and Stauffer, P.H., eds., *A volcano rekindled—The renewed eruption of Mount St. Helens, 2004–2006*: U.S. Geological Survey Professional Paper 1750, p. 111–127, <https://doi.org/10.3133/pp1750>.
- Nakada, S., Uto, K., Sakuma, S., Eichelberger, J.C., and Shimizu, H., 2005, Scientific results of conduit drilling in the Unzen Scientific Drilling Project (USDP): *Scientific Drilling*, v. 1, p. 18–22, <https://doi.org/10.2204/iodp.sd.3.01.2006>.
- Novelo-Casanova, D.A., Martínez-Bringas, A., and Valdés-González, C., 2006, Temporal variations of Q_c^{-1} and b -values associated to the December 2000–January 2001 volcanic activity at the Popocatepetl Volcano, Mexico: *Journal of Volcanology and Geothermal Research*, v. 152, no. 3–4, p. 347–358, <https://doi.org/10.1016/j.jvolgeores.2005.10.003>.
- Power, J.A., Jolly, A.D., Page, R.A., and McNutt, S.R., 1995, Seismicity and forecasting of the 1992 Eruptions of Crater Peak vent, Mount Spurr Volcano, Alaska—An overview, *in* *The 1992 Eruptions of Crater Peak vent, Mount Spurr Volcano, Alaska*: U.S. Geological Survey Bulletin 2139, p. 149–159, <https://doi.org/10.3133/b2139>.
- Power, J.A., Stihler, S.D., Chouet, B.A., Haney, M.M., and Ketner, D.M., 2013, Seismic observations of redoubt volcano, Alaska—1989–2010 and a conceptual model of the redoubt magmatic system: *Journal of Volcanology and Geothermal Research*, v. 259, p. 31–44.
- Prejean, S., Stork, A., Ellsworth, W., Hill, D., and Julian, B., 2003, High precision earthquake locations reveal seismogenic structure beneath Mammoth Mountain, California: *Geophysical Research Letters, Solid Earth*, v. 30, no. 24, <https://doi.org/10.1029/2003GL018334>.
- Pugh, D.J., White, R.S., and Christie, P.A.F., 2016, A Bayesian method for microseismic source inversion: *Geophysical Journal International*, v. 206, no. 2, p. 1009–1038, <https://doi.org/10.1093/gji/ggw186>.
- Roman, D.C., and Cashman, K.V., 2006, The origin of volcano-tectonic earthquake swarms: *Geology*, v. 34, no. 6, p. 457–460, <https://doi.org/10.1130/G22269.1>.
- Roman, D.C., Moran, S.C., Power, J.A., and Cashman, K.V., 2004, Temporal and spatial variation of local stress fields before and after the 1992 eruptions of Crater Peak vent, Mount Spurr volcano, Alaska: *Bulletin of the Seismological Society of America*, v. 94, no. 6, p. 2366–2379, <https://doi.org/10.1785/0120030259>.

- Roman, D.C., Neuberg, J., and Lockett, R.R., 2006, Assessing the likelihood of volcanic eruption through analysis of volcano-tectonic earthquake fault-plane solutions: *Earth and Planetary Science Letters*, v. 248, no. 1–2, p. 244–252, <https://doi.org/10.1016/j.epsl.2006.05.029>.
- Roman, D.C., Soldati, A., Dingwell, D.B., Houghton, B.F., and Shiro, B.R., 2021, Earthquakes indicated magma viscosity during Kīlauea’s 2018 eruption: *Nature*, v. 592, p. 237–241, <https://doi.org/10.1038/s41586-021-03400-x>.
- Sánchez, J.J., Wyss, M., and McNutt, S.R., 2004, Temporal-spatial variations of stress at Redoubt Volcano, Alaska, inferred from inversion of fault plane solutions: *Journal of Volcanology and Geothermal Research*, v. 130, no. 1–2, p. 1–30, [https://doi.org/10.1016/S0377-0273\(03\)00224-5](https://doi.org/10.1016/S0377-0273(03)00224-5).
- Shelly, D.R., Hill, D.P., Massin, F., Farrell, J., Smith, R.B., and Taira, T., 2013, A fluid-driven earthquake swarm on the margin of the Yellowstone caldera: *Journal of Geophysical Research, Solid Earth*, v. 118, no. 9, p. 4872–4886, <https://doi.org/10.1002/jgrb.50362>.
- Shelly, D.R., and Thelen, W.A., 2019, Anatomy of a caldera collapse—Kīlauea 2018 summit seismicity sequence in high resolution: *Geophysical Research Letters*, v. 46, no. 24, p. 14395–14403, <https://doi.org/10.1029/2019GL085636>.
- Snoke, J.A., 2003, FOMEC—FOCal MECHANism determinations: *International Geophysics*, v. 81, no. B, p. 1629–1630, [https://doi.org/10.1016/S0074-6142\(03\)80291-7](https://doi.org/10.1016/S0074-6142(03)80291-7).
- Soubestre, J., Seydoux, L., Shapiro, N.M., de Rosny, J., Droznin, D.V., Droznina, S.Y., Senyukov, S.L., and Gordeev, E.I., 2019, Depth migration of seismovolcanic tremor sources below the Klyuchevskoy volcanic group (Kamchatka) determined from a network-based analysis: *Geophysical Research Letters*, v. 46, no. 14, p. 8018–8030, <https://doi.org/10.1029/2019GL083465>.
- Taisne, B., Brenguier, F., Shapiro, N.M., and Ferrazzini, V., 2011, Imaging the dynamics of magma propagation using radiated seismic intensity: *Geophysical Research Letters*, *Solid Earth*, v. 38, no. 4, <https://doi.org/10.1029/2010GL046068>.
- Takagi, N., Kaneshima, S., Kawakatsu, H., Yamamoto, M., Sudo, Y., Ohkura, T., Yoshikawa, S., and Mori, T., 2006, Apparent migration of tremor source synchronized with the change in the tremor amplitude observed at Aso Volcano, Japan: *Journal of Volcanology and Geothermal Research*, v. 154, no. 3–4, p. 181–200, <https://doi.org/10.1016/j.jvolgeores.2006.02.001>.
- Tan, D., Fee, D., Hotovec-Ellis, A.J., Pesicek, J.D., Haney, M.M., Power, J.A., and Girona, T., 2023, Volcanic earthquake catalog enhancement using integrated detection, matched-filtering, and relocation tools: *Frontiers in Earth Science*, v. 11, article no. 1158442, <https://doi.org/10.3389/feart.2023.1158442>.
- Thelen, W.A., 2014, Seismic instrumentation plan for the Hawaiian Volcano Observatory: U.S. Geological Survey Scientific Investigations Report 2014–5179, 43 p., <https://doi.org/10.3133/sir20145179>.
- Thelen, W.A., Lyons, J.J., Iezzi, A.M., and Moran, S.C., 2024, Monitoring lahars and debris flows, chap. H of Flinders, A.F., Lowenstern, J.B., Coombs, M.L., and Poland, M.P., eds., *Recommended capabilities and instrumentation for volcano monitoring in the United States*: U.S. Geological Survey Scientific Investigations Report 2024–5062–H, 6 p., <https://doi.org/10.3133/sir20245062H>.
- U.S. Geological Survey, 2017, Advanced National Seismic System—Current status, development opportunities, and priorities for 2017–2027 (ver.1.1, July 2017): U.S. Geological Survey Circular 1429, 32 p., <https://doi.org/10.3133/cir1429>.
- U.S. Geological Survey Earthquake Hazards Program, 2019, Advanced National Seismic System Implementation Standards and Procedures (ver. 2.0): U.S. Geological Survey web page, accessed April 26, 2024, at <https://www.usgs.gov/media/files/anss-implementation-standards>.
- Vinciguerra, S., 2002, Damage mechanics preceding the September–October 1989 flank eruption at Mount Etna Volcano inferred by seismic scaling exponents: *Journal of Volcanology and Geothermal Research*, v. 113, no. 3–4, p. 391–397, [https://doi.org/10.1016/S0377-0273\(01\)00274-8](https://doi.org/10.1016/S0377-0273(01)00274-8).
- White, R., 1996, Precursory deep long-period earthquakes at Mount Pinatubo—Spatio-temporal link to a basalt trigger, in Newhall, C.S., and Punongbayan, S., eds., *Fire and mud—Eruptions and lahars of Mount Pinatubo*, Philippines: Seattle, University of Washington Press, p. 307–327.
- Wilding, J.D., Zhu, W., Ross, Z.E., and Jackson, J.M., 2022, The magmatic web beneath Hawai‘i: *Science*, v. 379, no. 6631, p. 462–468, <https://doi.org/10.1126/science.ade5755>.
- Zhu, W., and Beroza, G.C., 2019, PhaseNet—A deep-neural-network-based seismic arrival-time picking method: *Geophysical Journal International*, v. 216, no. 1, p. 261–273, <https://doi.org/10.1093/gji/ggy423>.

Chapter C



A windscreen covers a single infrasound sensor, co-located with a seismometer, as part of the U.S. Geological Survey Alaska Volcano Observatory volcano-monitoring network at Korovin Volcano on Atka Island, Alaska. Photograph by L. Toney, U.S. Geological Survey, July 27, 2019.

Chapter C

Infrasound for Volcano Monitoring

By John J. Lyons,¹ David Fee,² Weston A. Thelen,¹ Alexandra M. Iezzi,¹ and Aaron G. Wech¹

Introduction

Volcanic eruptions produce acoustic waves when volcanic gases and hot material rapidly expand in the atmosphere. Volcanic activity can produce acoustic signals with a wide range of frequencies, from very long period (>10 seconds) to audible (>20 hertz [Hz]), but the most energetic band is typically in the infrasound from 0.5 to 20 Hz. Studies of volcanic infrasound and the deployment of infrasound for volcano monitoring have increased rapidly in the past two decades as sensors have improved and as analytical tools have become more widely available. Improved sensors and tools have led to a growing diversity of eruptive activity being recorded and characterized, from Hawaiian to Plinian eruption styles at scales from local to global (Johnson and Ripepe, 2011; Fee and Matoza, 2013). Infrasound sensors on volcanoes are most commonly deployed locally with seismic stations, and the combination of co-located seismic and infrasound is more useful for characterizing unrest and detecting changes in activity than either data stream alone (for example, Lyons and others, 2016; Fee and others, 2017a; Matoza and others, 2018). At local (<15 kilometers [km]) to regional (15–250 km) distances from volcanoes, arrays of infrasound sensors are commonly deployed to detect coherent signals, constrain the direction to the source, and provide information on eruption dynamics; thus, infrasound is well suited to regional monitoring of volcanoes when local sensor networks are not feasible. A common usage of infrasound data in an observatory is to provide rapid confirmation that an explosion has occurred (for example, Coombs and others, 2018), although near-real-time eruption intensity quantification is also possible (Fee and others, 2010a; Ripepe and others, 2018; fig. C1). Infrasound is well suited to this task because it is not affected by clouds or precipitation and can propagate long distances with little attenuation. However, wind and ocean noise also produce infrasound, and spatiotemporal variability in the atmosphere can affect the propagation of infrasound, so care must be taken when deploying, analyzing, and interpreting the data. In addition to detecting and monitoring explosive activity, investigations of infrasound records from eruptions help constrain source processes, which in turn enhance syneruptive forecasting capabilities (for example, Fee and others, 2017b; Lyons and others, 2019).

The following is a description of the capabilities recommended for real-time monitoring of eruptive phenomena with infrasound. Infrasound is also beginning to be used for tracking hazardous surface flows that occur on volcanoes, including pyroclastic density currents (Ripepe and others, 2010), lahars (Johnson and Palma, 2015), debris flows (Marchetti and others, 2019), snow avalanches (Havens and others, 2014), and lava flows (Patrick and others, 2019). Please refer to the chapter on lahars (this volume; Thelen and others, 2024a) for more information on this application.

Recommended Capabilities

Detect, Characterize, and Monitor the Onset and Changes in Eruption Style for Local Eruptions

The most common usage of infrasound data in a volcano observatory is to rapidly detect explosive activity. Explosion energy does not always couple efficiently into the solid Earth, and seismic signals of explosions can be ambiguous or masked by noneruptive seismicity. This ambiguity can make explosion detection and characterization difficult using seismicity alone. The impulsive, high-amplitude infrasound signals typically associated with energetic explosions are easily identified and provide confirmation of explosive activity (for example, Mori and others, 1989; Johnson and Aster, 2005; Moran and others, 2008). Infrasound arrays (typically four or more sensors spaced 20 to 150 meters [m] apart; fig. C2 deployed within about 15 km of active vents provide real-time explosion detection monitoring by providing a back-azimuth to a coherent sound source (Ripepe and Marchetti, 2002; Matoza and others, 2007). Assuming an average speed of sound of 343 meters per second at 20 degrees Celsius, an explosion signal will arrive at the local (<15 km) array in 45 seconds or less, thus allowing for an automated notification within a minute. Local arrays also provide the ability to distinguish activity from multiple sources, which is important for systems that have multiple vents (Ripepe and Marchetti, 2002; Johnson, 2005) or have the potential for concurrent summit and flank activity (Marchetti and others, 2009; Cannata and others, 2011; Fee and others, 2011). At Mount Etna, Italy, years of repeated lava fountain episodes allowed Ripepe and others (2018) to develop an infrasound early warning system based on the number of array detections and the average signal amplitude in 1-minute windows (fig. C1). A similar approach may

¹U.S. Geological Survey.

²University of Alaska Fairbanks.

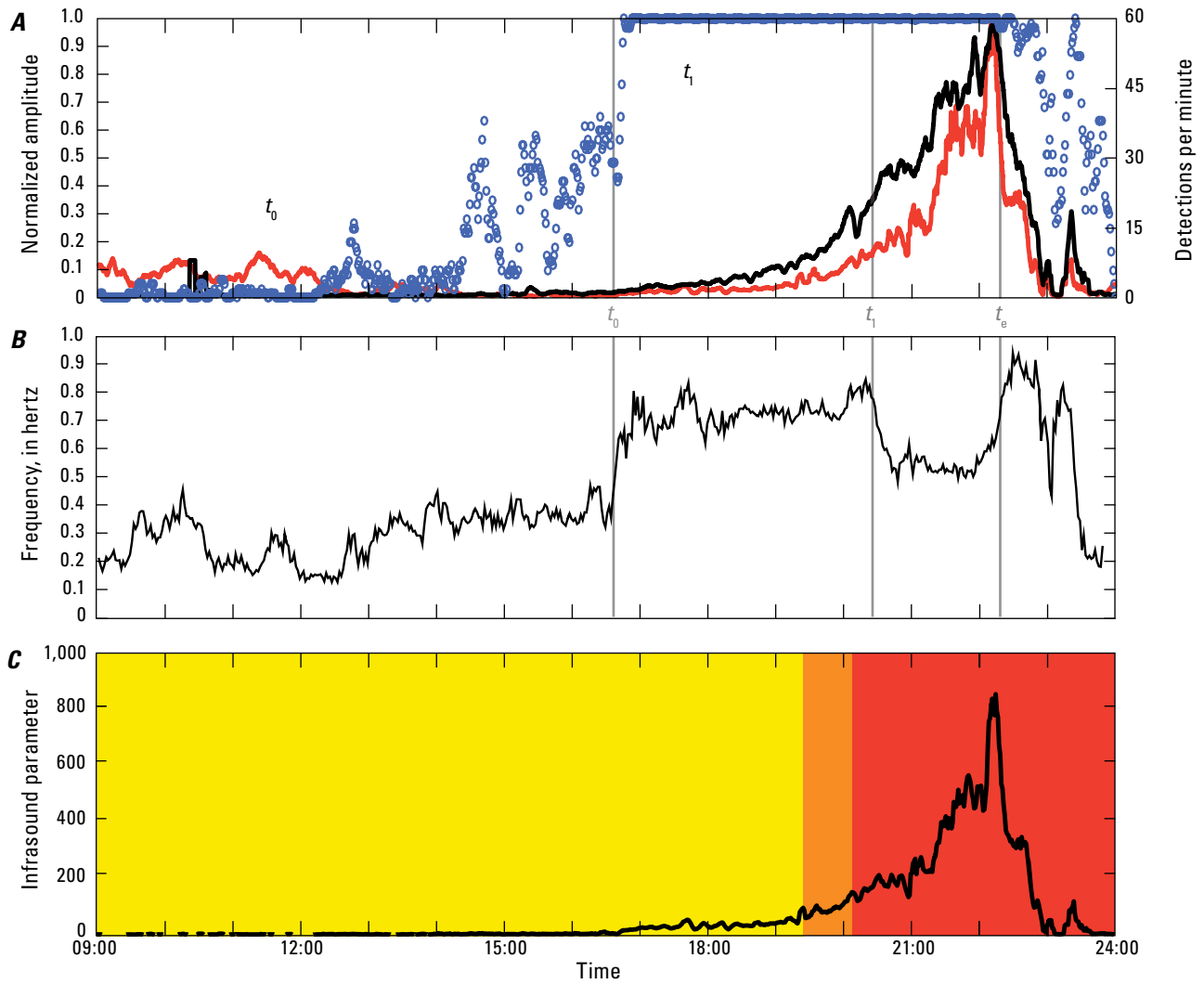
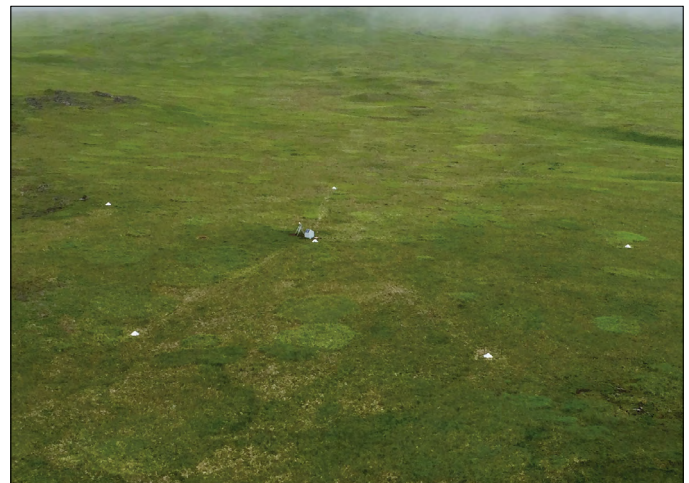


Figure C1. Example plots of eruption early warning from infrasound monitoring at Mount Etna, Italy. *A*, Normalized infrasound amplitude (red line), seismic amplitude (black line), and array detections per minute using a 5-second-long processing window shifted by 1 second (blue circles). Vent activity observed during this sequence include no activity (t_0), violent Strombolian activity (t_1), and ash-producing lava fountain activity (t_e). *B*, Fundamental frequency of infrasound. *C*, Infrasound parameter defined as the product of the mean amplitude and number of array detections per minute. When infrasound parameter levels reach threshold values for a sustained duration, alert levels are changed (colors) and messages are automatically sent to civil protection agencies. Modified from Ripepe and others (2018).

Figure C2. Aerial photograph of the Mount Okmok infrasound array (station OKIF) located on the eastern flank of Mount Okmok, Alaska. The six-element array is equipped with wind-noise-reduction filters and hosts a web camera. Infrasound element spacing ranges from 54 to 142 meters. This array provides both local and regional infrasound monitoring of volcanic activity. Photograph by J. Lyons, U.S. Geological Survey, 2018.



provide advanced notification of an increase in activity at other open-vent volcanoes.

In addition to arrays, distributed networks of infrasound sensors are also capable of detecting explosive eruptions using techniques like semblance (Johnson and others, 2011) and reverse time migration or back projection (Walker and others, 2010). Network infrasound for eruption detection has not been used as extensively as arrays to date but has the advantage that it can be deployed more easily than arrays when co-located with existing seismic stations. The other advantage of network infrasound over array infrasound is that it provides a two- or three-dimensional source location, rather than just a back azimuth to the source. However, unlike array infrasound, network infrasound is unable to take advantage of waveform stacking techniques to enhance signal-to-noise levels. An additional methodology to get a back-azimuth from a single infrasound sensor co-located with a three-component seismometer also shows promise for detecting and monitoring explosive activity (McKee and others, 2018). This approach is useful when arrays or networks are not feasible, or it could be used in a sparse seismic-acoustic network to constrain a source location.

Monitoring ongoing activity following initial detection requires that local stations can continue operating during eruptive activity, record on-scale, and can capture as wide a range of frequencies as possible. No substantial improvement in monitoring explosive signals is gained by installing sensors very close to potential vents, thus we prefer sites at distances of several kilometers or more to protect the sensors during eruptions and to provide continuous data. Modern broadband sensors with large dynamic ranges, low noise floors, and low power consumption are capable of recording most volcanic signals on-scale.

Beyond detecting explosive events and constraining their sources, the ability to further characterize infrasound signals in terms of amplitude, frequency content, and source mechanism can provide critical information on how an eruption is evolving. For example, infrasound signals have captured the subtle swelling of a lava plug prior to Vulcanian explosions (Yokoo and others, 2009) and aided in understanding the source of sound generation in Strombolian explosions (Vergnolle and Brandeis, 1996; Gerst and others, 2013). Infrasound has been used to help constrain some of the source parameters needed to model ash-cloud rise and transport (Mastin and others, 2009), including acoustic source velocities, volume flux, and mass eruption rate (Caplan-Auerbach and others, 2010; Ripepe and others, 2013; Lamb and others, 2015). More recently, numerical methods have allowed for accurate accounting of wavefield distortion from topography, permitting full-waveform inversion of infrasound signals to estimate eruption mass flow rate and total eruption mass (Kim and Lees, 2011; Kim and others, 2015; Fee and others, 2017b). This is a powerful method of quantifying source characteristics but requires high-resolution digital elevation models to accurately account for the influence of topography on the wavefield.

Variations in baseline degassing can signal a change in activity before an eruption begins, both on short (Fischer and others, 2002; Nadeau and others, 2011) and long (Edmonds and others, 2003; Aiuppa and others, 2017) timescales, but gas monitoring sensors are currently limited by daylight or

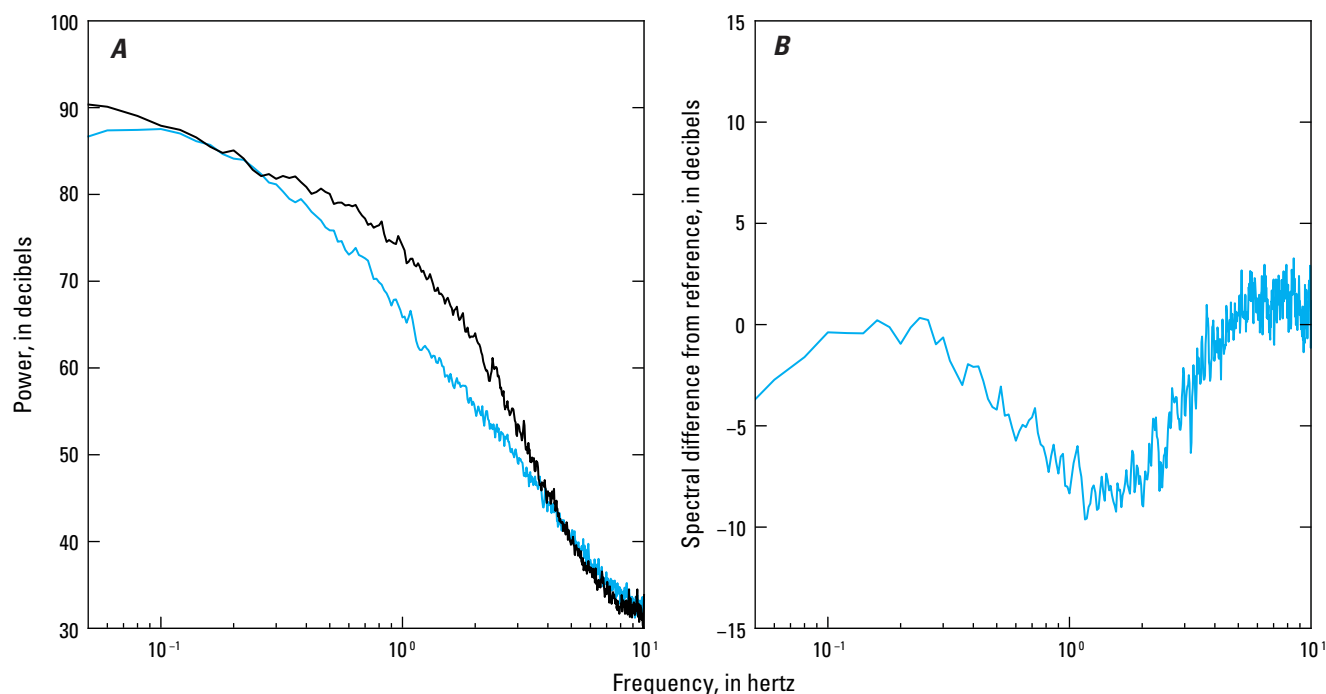
clear weather requirements and depend on the wind direction. Infrasound can monitor baseline degassing if it is sufficiently energetic to generate detectable pressure perturbations in the atmosphere (Garcés and others, 2003; Johnson and others, 2018).

Instrumentation

A single infrasound sensor co-located with a three-component seismometer can detect explosive activity. However, to detect low-level and potentially precursory activity, at least one array of four or more infrasound sensors within 15 km of the source region is recommended. A network of four or more single infrasound sensors can detect and locate energetic explosions and would ideally be co-located with seismometers. To constrain source locations and monitor continuous activity, possibly from multiple vents, at least two arrays at different azimuths from the source region are needed. Dominant wind direction and infrasound propagation in different seasons should be considered when siting a station. To fully characterize the infrasound wavefield and model source mechanisms, a network of four or more single infrasound sensors and two arrays are needed. This configuration also provides monitoring redundancy in case sensors or telemetry paths are damaged during an eruption. Sensors should have a high dynamic range and low noise floor. Local stations on volcanoes are commonly in exposed, wind-prone sites. Because wind is the primary source of noise in infrasound data, site selection should consider the elevation and exposure to wind. Preferred sites are typically in dense vegetation or forest and lack major topographic barriers between source and receiver. Wind-noise-reducing filters should also be used at all sites to improve signal-to-noise ratios (Walker and Hedlin, 2009), and recent advancements have produced wind screens that are easy to deploy, do not affect the acoustic response, and can increase the signal-to-noise ratio by as much as 8 decibels (fig. C3). Sampling rate also affects array estimates of source back-azimuth and trace velocity (Szuberla and Olson, 2004), and although sample rates will be constrained by digitizer specifications and telemetry limitations, it is recommended that the sampling frequency be 100 to 400 Hz to decrease uncertainty in these parameters. In the case that real-time data cannot be streamed at 100 Hz, onboard storage should be utilized for near-real-time or post-event analysis.

Recommendations for Local Monitoring of Stratovolcanoes

Infrasound instrumentation is not required for level 1 volcanoes. For level 2, it is important to be able to detect explosions (on-scale) and characterize their signals. We recommend at least one broadband infrasound sensor to be co-located with a three-component seismic sensor within 10 km of the volcanic center. For level 3 volcanoes, explosions would ideally be detected on-scale and automatically, permitting source location determination, explosion characterization, and resolution of low signal-to-noise events. At least four broadband infrasound sensors would ideally be co-located with three-component seismic



EXPLANATION

- Station ADKI, with windscreen
- Reference, no windscreen

Figure C3. Example of infrasound noise reduction using a windscreen. *A*, Power spectra for a sensor under a windscreen (blue) and a reference sensor not under a windscreen (black). *B*, Difference in spectral power between the reference sensor and the sensor covered by the windscreen. A reduction of about 8 decibels in wind noise is achieved at 2 hertz. *C*, Photograph shows the 1.2-meter-diameter aluminum windscreen installed over the infrasound sensor on Adak Island, Alaska (infrasound array ADKI). Photograph by J. Lyons, U.S. Geological Survey, June 12, 2017.

sensors within 10 km of the volcanic center and at least one array with four or more elements would be placed within 15 km of the volcanic center. For level 4 volcanoes, explosive eruptions would ideally be detected on-scale and automatically with the potential to locate multiple different sources. The system would be able to characterize explosion signals, to resolve low signal-to-noise events and to monitor baseline degassing. We recommend at least four broadband infrasound sensors co-located with three-component seismic sensors within 10 km of the volcanic center. At least two arrays with four or more elements each would ideally be placed within 15 km of the volcanic center.

Detect Local Fissure Eruptions and Track Vent Migration

Basaltic shield volcanoes pose eruption hazards that are sufficiently different than most stratovolcanoes to warrant separate consideration for infrasound monitoring. The 2018 eruption of Kīlauea (Neal and others, 2019) and the 2014 eruption of

Bárðarbunga, Iceland (Sigmundsson and others, 2014), are recent examples of the effect and complexity of fast-moving, fissure eruptions. Monitoring these systems present major challenges; eruptions can occur along fissure systems that are tens of kilometers long and vent locations can migrate rapidly. During the 2018 Kīlauea activity, there were concurrent eruptions from the summit caldera and 40 km downrift from the summit in the lower East Rift Zone, each with unique hazards (Neal and others, 2019; Thelen and others, 2022). Although the eruptive vent location at a stratovolcano can shift (Fee and others, 2016), shield volcanoes are typically larger than stratovolcanoes and may host multiple vents or fissure systems. Mauna Loa, Hawai‘i, the world’s largest volcano, has erupted lava flows as long as 50 km from the summit, the Northeast Rift Zone, and the Southwest Rift Zone, which means most major population centers on the Island of Hawai‘i face lava flow hazards (Trusdell, 1995).

Infrasound observations of fissure and lava flow eruptions are limited, but multiple arrays are currently the best way to detect and locate sources potentially distributed over a large area. Energetic lava fountaining activity from Kīlauea’s 2018 Ahu‘aīlā‘au vent

produced continuous, broadband infrasound energy peaking at 1.5 Hz. The spillway lava flow signals had spectra similar to the fountaining, but with much lower amplitudes (Lyons and others, 2021). In addition to the four-element campaign array 500 m from Ahu‘ailā‘au, a six-element permanent array was installed during the eruption 3.7 km north of Ahu‘ailā‘au. Both arrays recorded amplitude variations as the effusion rate increased and decreased, but only the proximal array was able to resolve the changes in back-azimuth accompanying the amplitude variations. This indicates that permanent monitoring arrays may be sufficient to detect effusion rate variability at vents distributed along fissure zones, but that details of how and where changes in effusion rate are occurring in vent areas may not be resolvable. Campaign arrays could fill these gaps once vent locations have stabilized. Large volcanic systems with extensive rift zones, like Mauna Loa, would require two or more arrays to detect and monitor activity.

Recommendations for Monitoring Rift Eruptions

No instrumentation is recommended for levels 1 and 2 volcanoes. For levels 3 and 4, it is important to rapidly detect the onset of lava fountaining and activity associated with fissure opening, track multiple vent source locations, and monitor infrasound energy levels as a proxy for effusion rate. We recommend at least four broadband infrasound sensors co-located with three-component seismic sensors within 15 km of summit vents (for example, Mauna Loa and Kīlauea summits). At least two arrays would ideally be placed within 20 km of volcanic centers and main fissure systems, and with good azimuthal coverage along the trend of fissures. Once fissure activity stabilizes, efforts should be made to install at least one additional array as close as possible, but ideally within a few kilometers, from the fissure location. Arrays would ideally be equipped with four or more elements, following the station spacing, wind noise reduction, and sample rate suggestions above.

Detect and Constrain Source of Regional Explosive Eruptions

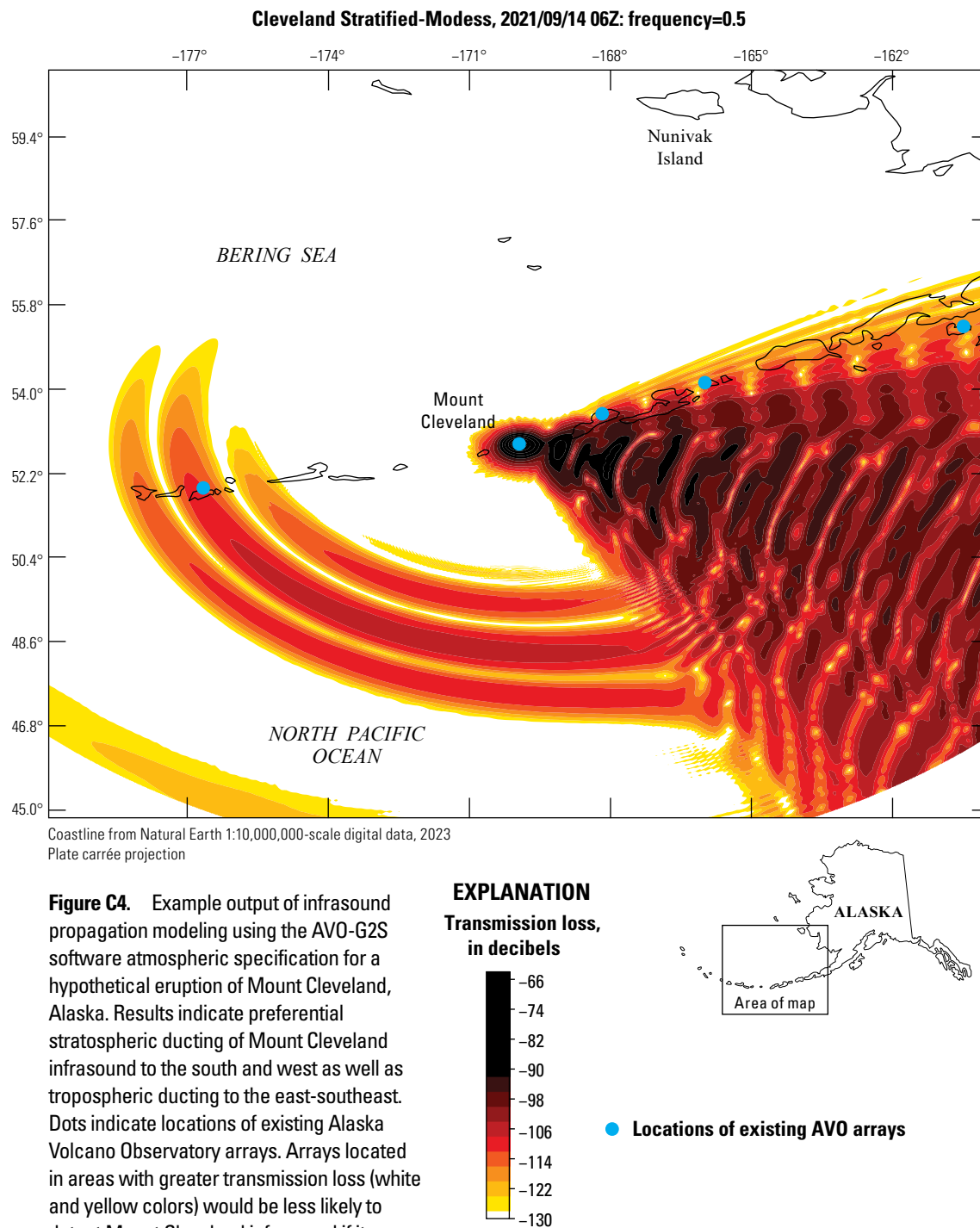
Infrasound arrays at regional (15–250 km) and global (>250 km) distances from active volcanoes can be an effective eruption detection and monitoring tool, particularly at volcanoes lacking in situ instrumentation (De Angelis and others, 2012; Lyons and others, 2020). Because of the temperature structure of the atmosphere and prevailing winds, infrasound is commonly ducted into one of the three main atmospheric waveguides in the troposphere, stratosphere, and thermosphere (Drob and others, 2003). The tropospheric and stratospheric ducts are most important for detecting and monitoring regional volcanic activity and will be discussed here. Atmospheric ducts are a result of vertical temperature gradients and winds, and thus sound speed, in the atmosphere. As sound propagates away from a source on the ground, it generally is refracted upward until the sound speed at height exceeds that at the source, resulting in a downward refraction. The refraction at height plus surface reflections

produce ducts that allow for distal propagation of infrasound. The initial upward refraction of sound can result in acoustic shadow zones outside of about 15 km from the source (Fairfield, 1980); however, combined effects of ducting, volcanic elevations above the surface, and the relatively low attenuation of infrasound in the troposphere and stratosphere allows signals from eruptions to be detected in great detail hundreds of kilometers from volcanic sources. Examples include eruptions at Kasatochi Island and Mount Okmok, Alaska, in 2008 (Fee and others, 2010b), Redoubt Volcano, Alaska, in 2009 (Fee and others, 2013), Bogoslof Island, Alaska, in 2016–17 (Lyons and others, 2019), and Sarychev Peak, Kuril Islands, Russia, in 2009 (Matoza and others, 2011).

Wind speed and direction also affect infrasound propagation at regional distances. Tropospheric ducts typically form when winds are in the direction of the receivers and are highly dependent on local weather conditions and thus temporally unstable (Drob and others, 2003; Le Pichon and others, 2006; Ceranna and others, 2009). Stratospheric ducts are predominantly controlled by zonal (east-west) stratospheric winds that vary more seasonally, resulting in larger and longer-lived ducts than in the troposphere (Drob and others, 2003; Le Pichon and others, 2006). The dependence of regional detections on atmospheric conditions has motivated improvements toward real-time characterization of atmospheric conditions and infrasound propagation modeling to predict the type of infrasonic arrivals for given sources and receivers (Drob and others, 2003; Schwaiger and others, 2019). Open-source software, AVO-G2S (available at <https://code.usgs.gov/vsc/volcano-avog2s>), allows users to model the effects of atmospheric conditions on infrasound propagation (Schwaiger and others, 2019). These and other infrasound propagation models can be used to anticipate propagation paths, atmospheric ducts, and infrasound shadow zones from hypothetical eruptions (fig. C4).

Owing to their more direct path and low energy loss, tropospheric infrasound arrivals are crucial to regional volcano monitoring; however, we prefer to deploy regional arrays at a source distance where both tropospheric and stratospheric waves can be detected. This crossover distance is typically in the 200–300 km range, which also allows for timely notifications of volcanic activity (about 12.5 minutes at 250 km). At these source-receiver ranges, low signal amplitudes can be even smaller than background noise; thus, it is critical that regional arrays are equipped with wind noise reduction devices and are installed in low-noise environments (Walker and Hedlin, 2009). All regional infrasound arrays installed by the Alaska Volcano Observatory since 2017 have been equipped with 1.2-m-diameter aluminum mesh windscreens (Lyons and others, 2020; figs. C2 and C3).

The seasonality of stratospheric winds in much of the northern hemisphere results in different directions of preferential atmospheric propagation between summer and winter (Iezzi and others, 2018; Schwaiger and others, 2020). Having at least two arrays in the 200–300 km range of potential sources and at sufficiently different azimuths so that at least one is downwind during summer and winter will help ensure year-round detection capability. Multiple regional arrays at various azimuths from sources also allows for source location using the intersection of the back-azimuths from all available arrays (Matoza and others, 2017).



The relatively low attenuation of infrasound propagating in the troposphere and stratosphere means source characteristics are preserved even when signals have traveled hundreds of kilometers. At remote volcanoes without local networks, regional infrasound can be a primary data source for determining explosion origin times and durations, as was the case for the 2008 Kasatochi Island and Mount Okmok

eruptions in Alaska (Fee and others, 2010a), the 2009 Sarychev Peak eruption (Matoza and others, 2011), and the 2016–17 eruption of Bogoslof Island (Coombs and others, 2018; Lyons and others, 2020). Infrasound recorded regionally can also be used to infer changing eruption intensity. For example, acoustic power from eruptions of Tungurahua in Ecuador were compared to ash-cloud heights from satellite data and show

good correlations between increasing acoustic power and cloud height as eruptions intensified (Fee and others, 2010a). Detailed observations of infrasound and seismic amplitudes in concert with cloud height are increasingly used to track eruption progress and can be used to assess hazards (Fee and others, 2017a).

Instrumentation

A minimum recommendation for detecting eruption signals with infrasound at regional distances is a four-element array with 30–100 m irregular spacing between elements. More ideally, multiple four- to six-element arrays at 200–300 km spacing are suggested for regional monitoring of multiple sources and may provide the ability to locate sources in addition to resolving a source back-azimuth. Multiple regional arrays also allow for eruption detections despite seasonally variable atmospheric conditions. Most modern, field-ready digitizers have a maximum of six channels; however, arrays could be expanded to include more elements if channels are available. More array elements with a range of irregular spacing between elements improves the azimuthal resolution of the array, broadens the frequency response capability of the array, and reduces spatial aliasing. As mentioned in the chapter on seismic monitoring (this volume; Thelen and others, 2024b), it is recommended to sample at 100 to 400 Hz to decrease uncertainty in array estimates of source back-azimuth and trace velocity (Szuberla and Olson, 2004).

Recommendations for Regional Monitoring

For levels 1 and 2 volcanoes, regional arrays are ideal to detect major explosive eruptions, to constrain source back-azimuth, and to characterize eruption signals. We recommend one array with four or more elements within 200–300 km. For levels 3 and 4 volcanoes, we recommend at least two arrays with six or more elements within 200–300 km of potential sources and with substantially different back-azimuths to sources. The goal is to detect moderate-sized explosive eruptions, to constrain source location, and to characterize explosion signals.

Overall Recommendations and Considerations

The instrument guidance outlined here provides a framework for infrasound monitoring of a wide spectrum of volcanic activity in diverse tectonic and geographic regions. Major gains in infrasound sensor technology and the algorithms needed to automatically process the data have occurred in the past decade. Infrasound is now a primary monitoring tool for detecting volcanic activity in Alaska and is being used more widely at other U.S. volcano observatories.

The ability of infrasound to rapidly confirm the onset of eruptive activity from a distance regardless of most weather conditions or time of day make it an invaluable observatory tool and a necessity at levels 3 and 4 volcanoes. As analog stations are upgraded to digital, more infrasound is being deployed alongside seismic and other instrumentation. This allows more, more varied, and subtle volcanic phenomenon to be recorded and fuels the development of improved tools for real-time analysis and display of infrasound data. Exciting advances are being made in real-time source location and characterization using networks of sensors, as well as getting a source back-azimuth using a single co-located seismic and infrasound sensor. Infrasound is also showing promise for detecting, locating, and tracking moving sources like fissure eruptions, lahars, lava flows, and landslides. As with most monitoring data, infrasound provides the most useful information when combined with other geophysical and remote sensing data.

Summary—Recommendations for Volcano Levels 1–4 Infrasound Networks

All instrument recommendations are based on following the station spacing, wind noise reduction, and sample rate recommendations provided in the “Detect, Characterize, and Monitor the Onset and Changes in Eruption Style for Local Eruptions” section.

Level 1.—One array with four or more elements within 200–300 km of the volcanic center.

Level 2.—At least one broadband infrasound sensor co-located with a three-component seismic sensor within 10 km of the volcanic center, and one array with four or more elements within 200–300 km of the volcanic center.

Level 3.—At least four broadband infrasound sensors co-located with three-component seismic sensors within 10 km of the volcanic center or 15 km of summit vents (for example, Mauna Loa and Kilauea summits). At least one array with four or more elements within 15 km of the volcanic center or two arrays within 20 km of volcanic centers and main fissure systems with good azimuthal coverage along the trend of fissures. At least two arrays with six or more elements within 200–300 km of sources and with substantially different back-azimuths to sources.

Level 4.—At least four broadband infrasound sensors co-located with three-component seismic sensors within 10 km of the volcanic center. At least two arrays with four or more elements each within 15 km of the volcanic center.

References Cited

- Aiuppa, A., Bitetto, M., Francofonte, V., Velasquez, G., Bucarey Parra, C., Guidice, G., Liuzzo, M., Moretti, R., Moussallam, Y., Peters, N., Tamburello, G., Valderrama, O., and Curtis, A., 2017, A CO₂-gas precursor to the March 2015 Villarica volcano eruption: *Geochemistry, Geophysics, Geosystems*, v. 18, no. 6, p. 2120–2132, <https://doi.org/10.1002/2017GC006892>.
- Cannata, A., Sciotto, M., Spampinato, L., and Spina, L., 2011, Insights into explosive activity at closely-spaced eruptive vents using infrasound signals—Example of Mount Etna 2008 eruption: *Journal of Volcanology and Geothermal Research*, v. 208, no. 1–2, p. 1–11, <https://doi.org/10.1016/j.jvolgeores.2011.09.003>.
- Caplan-Auerbach, J., Bellesiles, A., and Fernandes, J.K., 2010, Estimates of eruption velocity and plume height from infrasonic recordings of the 2006 eruption of Augustine Volcano, Alaska: *Journal of Volcanology and Geothermal Research*, v. 189, no. 1–2, p. 12–18, <https://doi.org/10.1016/j.jvolgeores.2009.10.002>.
- Ceranna, L., Le Pichon, A., Green, D.N., and Mialle, P., 2009, The Buncefield explosion—A benchmark for infrasound analysis across Central Europe: *Geophysical Journal International*, v. 177, no. 2, p. 491–508, <https://doi.org/10.1111/j.1365-246X.2008.03998.x>.
- Coombs, M.L., Wech, A.G., Haney, M.M., Lyons, J.J., Schneider, D.J., Schwaiger, H.F., Wallace, K.L., Fee, D., Freymueller, J.T., Schaefer, J.R., and Tepp, G., 2018, Short-term forecasting and detection of explosions during the 2016–2017 eruption of Bogoslof Volcano, Alaska: *Frontiers in Earth Science*, v. 6, no. 122, <https://doi.org/10.3389/feart.2018.00122>.
- De Angelis, S., Fee, D., Haney, M., and Schneider, D., 2012, Detecting hidden volcanic explosions from Mt. Cleveland Volcano, Alaska with infrasound and ground-coupled airwaves: *Geophysical Research Letters*, v. 39, no. 21, <https://doi.org/10.1029/2012GL053635>.
- Drob, D.P., Picone, J.M., and Garcés, M., 2003, Global morphology of infrasound propagation: *Journal of Geophysical Research*, v. 108, no. D21, 13 p., <https://doi.org/10.1029/2002JD003307>.
- Edmonds, M., Herd, R.A., Galle, B., and Oppenheimer, C.M., 2003, Automated, high time-resolution measurements of SO₂ flux at Soufrière Hills Volcano, Montserrat: *Bulletin of Volcanology*, v. 65, no. 8, p. 578–586, <https://doi.org/10.1007/s00445-003-0286-x>.
- Fairfield, C., 1980, OMSI sound project—The acoustic effects of the Mount St. Helens eruption on May 18 1980: *Oregon Geology*, v. 42, no. 12, p. 200–202, <https://doi.org/10.5860/choice.50-6197>.
- Fee, D., Garcés, M., Orr, T., and Poland, M., 2011, Infrasound from the 2007 fissure eruptions of Kīlauea Volcano, Hawai'i: *Geophysical Research Letters*, v. 38, no. 6, p. 1–5, <https://doi.org/10.1029/2010GL046422>.
- Fee, D., Garcés, M., and Steffke, A., 2010a, Infrasound from Tungurahua Volcano 2006–2008—Strombolian to Plinian eruptive activity: *Journal of Volcanology and Geothermal Research*, v. 193, no. 1–2, p. 67–81, <https://doi.org/10.1016/j.jvolgeores.2010.03.006>.
- Fee, D., Haney, M., Matoza, R., Szuberla, C., Lyons, J., and Waythomas, C., 2016, Seismic envelope-based detection and location of ground-coupled airwaves from volcanoes in Alaska: *Bulletin of the Seismological Society of America*, v. 106, no. 3, p. 1024–1035, <https://doi.org/10.1785/0120150244>.
- Fee, D., Haney, M.M., Matoza, R.S., Van Eaton, A.R., Cervelli, P., Schneider, D.J., and Iezzi, A.M., 2017a, Volcanic tremor and plume height hysteresis from Pavlof Volcano, Alaska: *Science* v. 355, p. 45–48., <https://doi.org/10.1126/science.aah6108>.
- Fee, D., Izbekov, P., Kim, K., Yokoo, A., Lopez, T., Prata, F., Kazahaya, R., Nakamichi, H. and Iguchi, M., 2017b, Eruption mass estimation using infrasound waveform inversion and ash and gas measurements—Evaluation at Sakurajima Volcano, Japan: *Earth and Planetary Science Letters*, v. 480, p. 42–52, <https://doi.org/10.1016/J.EPSL.2017.09.043>.
- Fee, D., and Matoza, R.S., 2013, An overview of volcano infrasound: From hawaiian to plinian, local to global: *Journal of Volcanology and Geothermal Research*, v. 249, p. 123–139, <https://doi.org/10.1016/j.jvolgeores.2012.09.002>.
- Fee, D., McNutt, S.R., Lopez, T.M., Arnoult, K.M., Szuberla, C.A.L., and Olson, J.V., 2013, Combining local and remote infrasound recordings from the 2009 Redoubt Volcano eruption: *Journal of Volcanology and Geothermal Research*, v. 259, p. 100–114, <https://doi.org/10.1016/j.jvolgeores.2011.09.012>.
- Fee, D., Steffke, A., and Garcés, M., 2010b, Characterization of the 2008 Kasatochi and Okmok eruptions using remote infrasound arrays: *Journal of Geophysical Research*, v. 115, no. D2, <https://doi.org/10.1029/2009jd013621>.
- Fischer, T.P., Roggensack, K., and Kyle, P.R., 2002, Open and almost shut case for explosive eruptions—Vent processes determined by SO₂ emission rates at Karymsky volcano, Kamchatka: *Geology*, v. 30, no. 12, p. 1059–1062, [https://doi.org/10.1130/0091-7613\(2002\)030<1059:OAASCF>2.0.CO;2](https://doi.org/10.1130/0091-7613(2002)030<1059:OAASCF>2.0.CO;2).
- Garcés, M., Harris, A., Hetzer, C., Johnson, J., Rowland, S., Marchetti, E., and Okubo, P., 2003, Infrasonic tremor observed at Kīlauea Volcano, Hawai'i: *Geophysical Research Letters*, v. 30, no. 20, <https://doi.org/10.1029/2003GL018038>.

- Gerst, A., Hort, M., Aster, R.C., Johnson, J.B., and Kyle, P.R., 2013, The first second of volcanic eruptions from the Erebus volcano lava lake, Antarctica—Energies, pressures, seismology, and infrasound: *Journal of Geophysical Research, Solid Earth*, v. 118, no. 7, p. 3318–3340, <https://doi.org/10.1002/jgrb.50234>.
- Havens, S., Marshall, H.P., Johnson, J.B., and Nicholson, B., 2014, Calculating the velocity of a fast-moving snow avalanche using an infrasound array: *Geophysical Research Letters*, v. 41, no. 17, p. 6191–6198, <https://doi.org/10.1002/2014GL061254>.
- Iezzi, A.M., Schwaiger, H.F., Fee, D., and Haney, M.M., 2018, Application of an updated atmospheric model to explore volcano infrasound propagation and detection in Alaska: *Journal of Volcanology and Geothermal Research*, v. 371, p. 192–205, <https://doi.org/10.1016/j.jvolgeores.2018.03.009>.
- Johnson, J.B., 2005, Source location variability and volcanic vent mapping with a small-aperture infrasound array at Stromboli Volcano, Italy: *Bulletin of Volcanology*, v. 67, no. 1–14, <https://doi.org/10.1007/s00445-004-0356-8>.
- Johnson, J.B., and Aster, R.C., 2005, Relative partitioning of acoustic and seismic energy during Strombolian eruptions: *Journal of Volcanology and Geothermal Research*, v. 148, no. 3–4, p. 334–354, <https://doi.org/10.1016/j.jvolgeores.2005.05.002>.
- Johnson, J.B., and Palma, J.L., 2015, Lahar infrasound associated with Volcán Villarrica's 3 March 2015 eruption: *Geophysical Research Letters*, v. 42, no. 15, p. 6324–6331, <https://doi.org/10.1002/2015GL065024>.
- Johnson, J.B., and Ripepe, M., 2011, Volcano infrasound—A review: *Journal of Volcanology and Geothermal Research*, v. 206, no. 3–4, p. 61–69, <https://doi.org/10.1016/j.jvolgeores.2011.06.006>.
- Johnson, J.B., Watson, L.M., Palma, J.L., Dunham, E.M., and Anderson, J.F., 2018, Forecasting the eruption of an open-vent volcano using resonant infrasound tones: *Geophysical Research Letters*, v. 45, no. 5, p. 2213–2220, <https://doi.org/10.1002/2017GL076506>.
- Johnson, J.H., Savage, M.K., and Townend, J., 2011, Distinguishing between stress-induced and structural anisotropy at Mount Ruapehu volcano, New Zealand: *Journal of Geophysical Research*, v. 116, no. B12, 18 p., <https://doi.org/10.1029/2011JB008308>.
- Kim, K., Fee, D., Yokoo, A., and Lees, J.M., 2015, Acoustic source inversion to estimate volume flux from volcanic explosions: *Geophysical Research Letters*, v. 42, no. 13, p. 5243–5249, <https://doi.org/10.1002/2015GL064466>.
- Kim, K., and Lees, J.M., 2011, Finite-difference time-domain modeling of transient infrasonic wavefields excited by volcanic explosions: *Geophysical Research Letters*, v. 38, no. 6, <https://doi.org/10.1029/2010GL046615>.
- Lamb, O.D., De Angelis, S., and Lavallée, Y., 2015, Using infrasound to constrain ash plume rise: *Journal of Applied Volcanology*, v. 4, no. 20, <https://doi.org/10.1186/s13617-015-0038-6>.
- Le Pichon, A., Ceranna, L., Garcés, M., Drob, D., and Millet, C., 2006, On using infrasound from interacting ocean swells for global continuous measurements of winds and temperature in the stratosphere: *Journal of Geophysical Research Atmospheres*, v. 111, no. D11, p. 1–7, <https://doi.org/10.1029/2005JD006690>.
- Lyons, J.J., Dietterich, H.R., Patrick, M.P., and Fee, D., 2021, High-speed lava flow infrasound from Kīlauea's fissure 8 and its utility in monitoring effusion rate: *Bulletin of Volcanology*, v. 83, no. 66, <https://doi.org/10.1007/s00445-021-01488-7>.
- Lyons, J.J., Haney, M.M., Fee, D., Wech, A.G., and Waythomas, C.F., 2019, Infrasound from giant bubbles during explosive submarine eruptions: *Nature Geoscience*, v. 12, no. 11, p. 952–958, <https://doi.org/10.1038/s41561-019-0461-0>.
- Lyons, J.J., Haney, M.M., Werner, C., Kelly, P., Patrick, M., Kern, C., and Trusdell, F., 2016, Long period seismicity and very long period infrasound driven by shallow magmatic degassing at Mount Pagan, Mariana Islands: *Journal of Geophysical Research, Solid Earth*, v. 121, no. 1, p. 188–209, <https://doi.org/10.1002/2015JB012490>.
- Lyons, J.J., Iezzi, A.M., Fee, D., Schwaiger, H.F., Wech, A.G., and Haney, M.M., 2020, Infrasound generated by the 2016–2017 shallow submarine eruption of Bogoslof volcano, Alaska: *Bulletin of Volcanology*, v. 82, no. 19, <https://doi.org/10.1007/s00445-019-1355-0>.
- Marchetti, E., Ripepe, M., Olivieri, G., Caffo, S., and Privitera, E., 2009, Infrasonic evidences for branched conduit dynamics at Mount Etna volcano, Italy: *Geophysical Research Letters, Solid Earth*, v. 36, no. 19, <https://doi.org/10.1029/2009gl040070>.
- Marchetti, E., Walter, F., Barfucci, G., Genco, R., Wenner, M., Ripepe, M., McArdell, B., and Price, C., 2019, Infrasound array analysis of debris flow activity and implication for early warning: *Journal of Geophysical Research, Earth Surface*, v. 124, no. 2, p. 567–587, <https://doi.org/10.1029/2018JF004785>.
- Mastin, L.G., Guffanti, M., Servranckx, R., Webley, P., Barsotti, S., Dean, K., Durant, A., Ewert, J.W., Neri, A., Rose, W.I., Schneider, D., Siebert, L., Stunder, B., Swanson, G., Tupper, A., Volentik, A., and Waythomas, C.F., 2009, A multidisciplinary effort to assign realistic source parameters to models of volcanic ash-cloud transport and dispersion during eruptions: *Journal of Volcanology and Geothermal Research*, v. 186, no. 1–2, p. 10–21, <https://doi.org/10.1016/j.jvolgeores.2009.01.008>.

- Matoza, R.S., Fee, D., Green, D.N., Le Pichon, A., Vergoz, J., Haney, M.M., Mikesell, T.D., Franco, L., Valderrama, A., Kelley, M.R., McKee, K., and Ceranna, L., 2018, Local, regional, and remote seismo-acoustic observations of the April 2015 VEI 4 eruption of Calbuco Volcano, Chile: *Journal of Geophysical Research, Solid Earth*, v. 123, no. 5, p. 3814–3827, <https://doi.org/10.1002/2017JB015182>.
- Matoza, R.S., Green, D.N., Le Pichon, A., Shearer, P.M., Fee, D., Mialle, P., and Ceranna, L., 2017, Automated detection and cataloging of global explosive volcanism using the International Monitoring System infrasound network: *Journal of Geophysical Research, Solid Earth*, v. 122, no. 4, p. 2946–2971, <https://doi.org/10.1002/2016JB013356>.
- Matoza, R.S., Hedlin, M.A.H., and Garcés, M.A., 2007, An infrasound array study of Mount St. Helens: *Journal of Volcanology and Geothermal Research*, v. 160, no. 3–4, p. 249–262, <https://doi.org/10.1016/j.jvolgeores.2006.10.006>.
- Matoza, R.S., Le Pichon, A., Vergoz, J., Herry, P., Lalande, J.-M., Lee, H., Che, I.-Y., and Rybin, A., 2011, Infrasonic observations of the June 2009 Sarychev Peak eruption, Kuril Islands—Implications for infrasonic monitoring of remote explosive volcanism: *Journal of Volcanology and Geothermal Research*, v. 200, no. 1–2, p. 35–48, <https://doi.org/10.1016/j.jvolgeores.2010.11.022>.
- McKee, K., Fee, D., Haney, M., Matoza, R.S., and Lyons, J., 2018, Infrasound signal detection and back azimuth estimation using ground-coupled airwaves on a seismo-acoustic sensor pair: *Journal of Geophysical Research, Solid Earth*, v. 123, no. 8, p. 6826–6844, <https://doi.org/10.1029/2017JB015132>.
- Moran, S.C., Malone, S.D., Qamar, A.I., Thelen, W.A., Wright, A.K., and Caplan-Auerbach, J., 2008, Seismicity associated with renewed dome-building at Mount St. Helens, 2004–2005, chap. 2 of Sherrod, D.R., Scott, W.E., and Stauffer, P.H., eds., *A volcano rekindled—The renewed eruption of Mount St. Helens, 2004–2006*: U.S. Geological Survey Professional Paper 1750, p. 27–60, <https://doi.org/10.3133/pp1750>.
- Mori, J., Patia, H., McKee, C., Itikarai, I., Lowenstein, P., De Saint Ours, P., and Talai, B., 1989, Seismicity associated with eruptive activity at Langila volcano, Papua New Guinea: *Journal of Volcanology and Geothermal Research*, v. 38, no. 3–4, p. 243–255, [https://doi.org/10.1016/0377-0273\(89\)90040-1](https://doi.org/10.1016/0377-0273(89)90040-1).
- Nadeau, P.A., Palma, J.L., and Waite, G.P., 2011, Linking volcanic tremor, degassing, and eruption dynamics via SO₂ imaging: *Geophysical Research Letters, Solid Earth*, v. 38, no. 1, <https://doi.org/10.1029/2010GL045820>.
- Neal, C.A., Brantley, S.R., Antolik, L., Babb, J.L., Burgess, M., Calles, K., Cappos, M., Chang, J.C., Conway, S., Desmither, L., Dotray, P., Elias, T., Fukunaga, P., Fuke, S., Johanson, I.A., Kamibayashi, K., Kauahikaua, J., Lee, R.L., Pekalib, S., Miklius, A., Million, W., Moniz, C.J., Nadeau, P.A., Okubo, P., Parcheta, C., Patrick, M.R., Shiro, B., Swanson, D., Tollett, W., Trusdell, F., Zoeller, M.H., Montgomery-Brown, E.K., Anderson, K.R., Poland, M.P., Ball, J.L., Bard, J.A., Coombs, M., Dietterich, H.R., Kern, C., Thelen, W.A., Cervelli, P.F., Orr, T., Houghton, B.F., Gansecki, C., Hazlett, R., Lundgren, P., Diefenbach, A.K., Lerner, A., Waite, G., Kelly, P.J., Clor, L., Werner, C., Burgess, M., Mulliken, K., Fisher, G., and Damby, D., 2019, The 2018 rift eruption and summit collapse of Kīlauea Volcano: *Science*, v. 363, no. 6425, p. 367–374, <https://doi.org/10.1126/science.aav7046>.
- Patrick, M.R., Dietterich, H.R., Lyons, J.J., Diefenbach, A.K., Parcheta, C., Anderson, K.R., Namiki, A., Sumita, I., Shiro, B., and Kauahikaua, J.P., 2019, Cyclic lava effusion during the 2018 eruption of Kīlauea Volcano: *Science*, v. 366, no. 6470, <https://doi.org/10.1126/science.aay9070>.
- Ripepe, M., Bonadonna, C., Folch, A., Delle Donne, D., Lacanna, G., Marchetti, E., and Höskuldsson, A., 2013, Ash-plume dynamics and eruption source parameters by infrasound and thermal imagery—The 2010 Eyjafjallajökull eruption: *Earth and Planetary Science Letters*, v. 366, p. 112–121, <https://doi.org/10.1016/j.epsl.2013.02.005>.
- Ripepe, M., De Angelis, S., Lacanna, G., and Voight, B., 2010, Observation of infrasonic and gravity waves at Soufrière Hills Volcano, Montserrat: *Geophysical Research Letters, Solid Earth*, v. 37, no. 19, 5 p., <https://doi.org/10.1029/2010GL042557>.
- Ripepe, M., and Marchetti, E., 2002, Array tracking of infrasonic sources at Stromboli volcano: *Geophysical Research Letters*, v. 29, no. 22, p. 33-1–33-4, <https://doi.org/10.1029/2002GL015452>.
- Ripepe, M., Marchetti, E., Delle Donne, D., Genco, R., Innocenti, L., Lacanna, G., and Valade, S., 2018, Infrasonic early warning system for explosive eruptions: *Journal of Geophysical Research, Solid Earth*, v. 123, no. 11, p. 9570–9585, <https://doi.org/10.1029/2018JB015561>.
- Schwaiger, H.F., Iezzi, A.M., and Fee, D., 2019, AVO-G2S—A modified, open-source Ground-to-Space atmospheric specification for infrasound modeling: *Computers and Geosciences*, v. 125, p. 90–97, <https://doi.org/10.1016/j.cageo.2018.12.013>.
- Schwaiger, H.F., Lyons, J.J., Iezzi, A.M., Fee, D., and Haney, M.M., 2020, Evolving infrasound detections from Bogoslof volcano, Alaska—Insights from atmospheric propagation modeling: *Bulletin of Volcanology*, v. 82, no. 27, <https://doi.org/10.1007/s00445-020-1360-3>.

- Sigmundsson, F., Hooper, A., Hreinsdóttir, S., Vogfjörð, K.S., Ófeigsson, B.G., Heimisson, E.R., Dumont, S., Parks, M., Spaans, K., Gudmundsson, G.B., Drouin, V., Árnadóttir, T., Jónsdóttir, K., Gudmundsson, M.T., Högnadóttir, T., Fridriksdóttir, H.M., Hensch, M., Einarsson, P., Magnússon, E., Samsonov, S., Brandsdóttir, B., White, R.S., Ágústsdóttir, T., Greenfield, T., Green, R.G., Hjartardóttir, A.R., Pedersen, R., Bennett, R.A., Geirsson, H., La Femina, P.C., Björnsson, H., Pálsson, F., Sturkell, E., Bean, C.J., Möllhoff, M., Braidon, A.K., and Eibl, E.P.S., 2014, Segmented lateral dyke growth in a rifting event at Bárðarbunga volcanic system, Iceland: *Nature*, v. 517, p. 191–195, <https://doi.org/10.1038/nature14111>.
- Szuberla, C.A.L., and Olson, J.V., 2004, Uncertainties associated with parameter estimation in atmospheric infrasound arrays: *The Journal of the Acoustical Society of America*, v. 115, no. 1, p. 253–258, <https://doi.org/10.1121/1.1635407>.
- Thelen, W.A., Lyons, J.J., Iezzi, A.M., and Moran, S.C., 2024a, Monitoring lahars and debris flows, chap. H of Flinders, A.F., Lowenstern, J.B., Coombs, M.L., and Poland, M.P., eds., Recommended capabilities and instrumentation for volcano monitoring in the United States: U.S. Geological Survey Scientific Investigations Report 2024–5062–H, 6 p., <https://doi.org/10.3133/sir20245062H>.
- Thelen, W.A., Lyons, J.J., Wech, A.G., Moran, S.C., Haney, M.M., and Flinders, A.F., 2024b, Seismic techniques and suggested instrumentation to monitor volcanoes, chap. B of Flinders, A.F., Lowenstern, J.B., Coombs, M.L., and Poland, M.P., eds., Recommended capabilities and instrumentation for volcano monitoring in the United States: U.S. Geological Survey Scientific Investigations Report 2024–5062–B, 9 p., <https://doi.org/10.3133/sir20245062B>.
- Thelen, W., Waite, G., Lyons, J., and Fee, D., 2022, Infrasound observations and constraints on the 2018 eruption of Kīlauea Volcano, Hawaii: *Bulletin of Volcanology*, v. 84, no. 76, <https://doi.org/10.1007/s00445-022-01583-3>.
- Trusdell, F.A., 1995, Lava flow hazards and risk assessment on Mauna Loa Volcano, Hawaii, in Rhodes, J., and Lockwood, J., eds., *Mauna Loa revealed—Structure, composition, history, and hazards*, v. 92, p. 327–336, <https://doi.org/10.1029/GM092p0327>.
- Vergnolle, S., and Brandeis, G., 1996, Strombolian explosions—I. A large bubble breaking at the surface of a lava column as a source of sound: *Journal of Geophysical Research, Solid Earth*, v. 101, no. B9, p. 20433–20447, <https://doi.org/10.1029/96JB01178>.
- Walker, K.T., and Hedlin, M.A.H., 2009, A review of wind-noise reduction methodologies, in Le Pichon, A., Blanc, E., and Hauchecorne, A., eds., *Infrasound monitoring for atmospheric studies*: Springer, Dordrecht, Netherlands, p. 141–182, https://doi.org/10.1007/978-1-4020-9508-5_5.
- Walker, K.T., Hedlin, M.A.H., de Groot-Hedlin, C., Vergoz, J., Le Pichon, A., and Drob, D.P., 2010, Source location of the 19 February 2008 Oregon bolide using seismic networks and infrasound arrays: *Journal of Geophysical Research, Solid Earth*, v. 115, no. B12, p. 1–17, <https://doi.org/10.1029/2010JB007863>.
- Yokoo, A., Tameguri, T., and Iguchi, M., 2009, Swelling of a lava plug associated with a Vulcanian eruption at Sakurajima Volcano, Japan, as revealed by infrasound record—Case study of the eruption on January 2, 2007: *Bulletin of Volcanology*, v. 72, no. 6, p. 619–630, <https://doi.org/10.1007/s00445-008-0247-5>.

Chapter D



U.S. Geological Survey scientist A. Ellis installing a temporary Global Navigation Satellite System station south of the summit of Kilauea, Hawai'i. This station is part of a network of stations measured annually. The long profile of Mauna Loa is prominent in the background. Photograph by D. Phillips, U.S. Geological Survey, May 2024.

Chapter D

Ground Deformation and Gravity for Volcano Monitoring

By Emily K. Montgomery-Brown, Kyle R. Anderson, Ingrid A. Johanson, Michael P. Poland, and Ashton F. Flinders

Introduction

When magma accumulates or migrates, it can cause pressurization and related ground deformation. Characterization of surface deformation provides important constraints on the potential for future volcanic activity, especially in combination with seismic activity, gas emissions, and other indicators. A wide variety of techniques and instrument types have been applied to the study of ground deformation at volcanoes (sidebar ,p. 2; Dzurisin, 2000, 2003, 2007). Geodetic instruments include continuously recording Global Navigation Satellite System (GNSS; of which the United States' Global Positioning System is one example) stations (fig. D1), borehole tiltmeters, and interferometric synthetic aperture radar (InSAR) measurements (from satellites, occupied and

unoccupied aircraft systems, and ground-based sensors). Additional geodetic measurements like continuous- and survey-mode gravity (fig. D2) can contribute substantially to interpreting these data. Borehole strainmeters (see chapter K, this volume, by Hurwitz and Lowenstern, 2024) also have outstanding utility for monitoring deformation, although because of cost and permitting challenges, we do not include them as part of standard volcano monitoring networks for U.S. volcanoes. Still other techniques like light detection and ranging (lidar), structure from motion, and optical satellite data can be used to derive gross topographic changes, which can be used to map volcanic deposits, infer eruption rates, and gain insights into the source processes associated with eruptive activity (see chapter G, this volume, on tracking surface changes caused by volcanic activity; Orr and others, 2024).



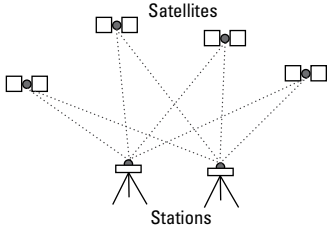
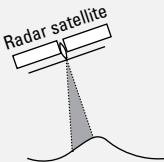
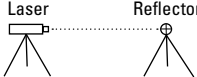
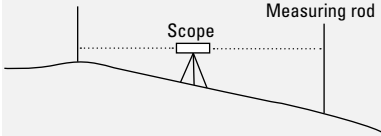

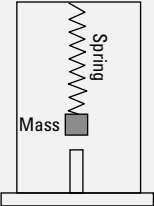
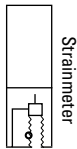
Figure D1. Photograph showing a U.S. Geological Survey Hawaiian Volcano Observatory geophysicist downloading data from the Global Navigation Satellite System (GNSS) station PUL2 along the middle East Rift Zone of Kilauea, Hawai'i. This semi-permanent station was deployed during the 2018 eruption to help monitor ongoing deformation from Kilauea's East Rift Zone and from a magnitude 6.9 earthquake. Photograph by P. Dotray, U.S. Geological Survey, September 10, 2019.

Figure D2. Photograph showing U.S. Geological Survey geophysicist measuring gravity at a station on the rim of Mount St. Helens, Washington. This station, NWDO, is northwest of the 2004–08 lava dome and part of the Mount St. Helens campaign gravity network. Positive residual gravity anomalies from this and five other stations indicated a net subsurface mass increase on the 2004–08 lava dome from 2010 to 2016. Spirit Lake can be seen in the middle ground, and Mount Rainier, Washington, in the background. Photograph by M. Poland, U.S. Geological Survey, August 17, 2010.



Sidebar—Description of geodetic techniques

[km, kilometer; m, meter]

Geodetic Technique	Description	Utility
Global Navigation Satellite Systems (GNSS) 	Antenna and receiver packages are installed permanently or temporarily over ground markers to record orbiting satellite messages that are used to compute precise positions.	Good temporal resolution, three-dimensional motions, and potential for real-time monitoring. Spatial coverage may be limited by permitting and financial considerations.
Interferometric synthetic aperture radar (InSAR) 	Interference between paired images from a radar satellite taken at different times from slightly different places is used to determine the deformation that occurred between image acquisitions.	Good spatial coverage over light vegetation. Data availability depends on satellite orbital parameters and space agency priorities.
Electronic distance measurement (EDM) 	Horizontal laser distance measurements are compared to determine horizontal deformation changes. Measurements are commonly made at two optical frequencies to correct for atmospheric interference.	Labor- and time-intensive measurement practices, meaning that EDM is commonly limited to smaller networks and infrequent data collection.
Leveling 	Measurements of vertical elevation along profile lines that can be compared to determine vertical deformation changes.	Highly accurate. Labor- and time-intensive measurement practices, meaning that leveling is commonly limited to smaller networks and infrequent data collection.
Tiltmeter 	Electronic measurement of ground tilt (like a carpenter's level).	Capable of high-frequency (~1 minute) temporal sampling, making it useful for real-time monitoring; particularly sensitive to shallow magma sources. Lowest noise data require expensive boreholes; platform installations offer a noisier alternative. Can be subject to anomalous signals caused by daily thermal signals, rainfall effects, and so on.
Microgravity changes 	A highly accurate gravimeter measures changes in gravity caused by subsurface mass changes.	Instruments are expensive and surveys are time intensive. Measurements are most sensitive to shallow (<3 km) gravity sources.
Borehole strainmeter 	An instrument coupled to rock inside a relatively deep (200–250 m) borehole; measures crustal strain.	Capable of high-frequency temporal sampling (1–2 minutes). Sensitive to small changes. Expensive to drill a borehole.

Experience has shown that no single geodetic monitoring technique is adequate to detect and track the entire range of ground-motion patterns that occur at volcanoes, primarily because of the temporal and spatial diversity of volcano deformation (fig. D3). Similarly, the magnitude of surface deformation varies widely. Geodetic monitoring strategies should therefore include multiple techniques and instrument types to cover a wide range of spatial and temporal scales.

In identifying recommendations for geodetic instrumentation for volcano monitoring networks, we attempted to maximize the diversity of instrument types to measure the full range of deformation signals and minimize their expense and number; thus, we do not include several well-known deformation-monitoring techniques in our recommendations. Extensometers, for example, measure strains over distances of a few meters and have an excellent record of success in detecting changes in preeruptive localized ground motion across existing cracks, including at Mount St. Helens, Washington (Iwatsubo and others, 1992), and Piton de la Fournaise, Réunion Island (Peltier and others, 2006). Despite being relatively inexpensive, extensometers are best used primarily when localized ground displacements (for example, ground cracks) need to be tracked, and are not necessary at all volcanoes.

In considering volcano deformation monitoring strategies, two complicating factors are deserving of special attention. First, not all deformation is driven by subsurface magmatic activity—for example, at many large stratovolcanoes (for example, Mount Rainier), flank collapses and landslides are significant geologic hazards (Reid and others, 2001) that may

occur even in the absence of magmatic activity. Monitoring the stability of volcanoes is thus another critical application of geodetic monitoring networks to inform hazard assessment. One of the most famous examples of edifice instability is the large flank collapse that initiated the May 18, 1980, eruption of Mount St. Helens. Deformation monitoring had detected a bulge on the north flank of the mountain in April 1980 that was expanding by several meters per day (Lipman and others, 1981). Given that flank collapses can happen at any time during a period of volcanic unrest (or even outside a period of unrest), the capability to assess edifice stability is critical.

Second, although volcanoes are commonly treated as idealized structures that erupt from single points, like central-vent stratovolcanoes, many are characterized by long rift zones from which eruptions may originate, and distributed volcanic fields are characterized by broadly spaced vents. For example, linear dikes are common at Kīlauea, Mauna Loa, and between Mount Shasta and Medicine Lake in California. At Kīlauea, one of these linear dikes emerged more than 40 kilometers (km) away from the summit of the volcano during the lower East Rift Zone eruption in 2018. Other volcanic fields, like Lassen volcanic center, California, or the San Francisco Volcanic Field, Arizona, have many small vents spread over a wide area. Although the instrumentation guidelines presented in this chapter remain phrased for central-vent volcanoes, they should be modified as needed in the context of the eruptive characteristics of each individual volcanic system.

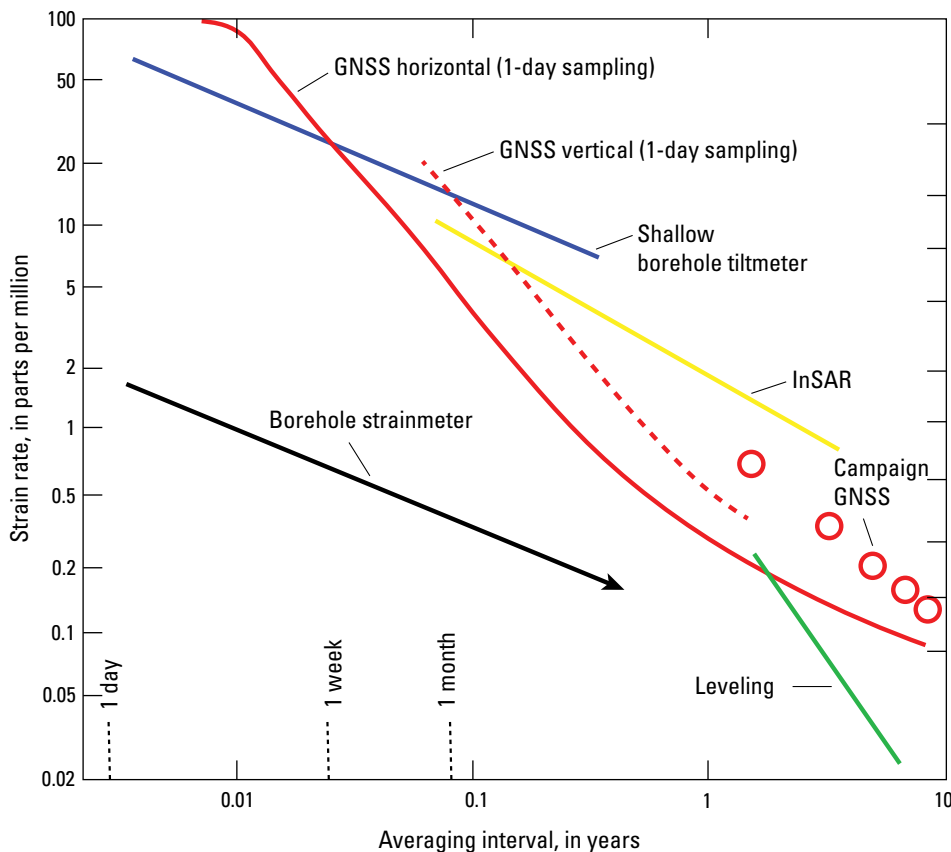


Figure D3. Graph showing strain rate detection limits versus averaging interval for typical volcano geodetic monitoring techniques. Strains for permanent Global Navigation Satellite System (GNSS) stations and interferometric synthetic aperture radar (InSAR) pixels are calculated assuming stations are 8 kilometers apart. Circles represent campaign GNSS measurements at longer time intervals. Note that borehole strainmeters provide the best measurements over timescales of minutes to days, whereas campaign GNSS, leveling, and InSAR provide the best measurements over months to years. Thus, multiple types of instrumentation are recommended to provide optimal geodetic observations over both space and time. Modified from Dzurisin (2007).

Spatial analysis of geodetic network coverage could help to ensure adequate instrumentation in areas where volcanism can occur over a broad area as opposed to a central vent. As an example, consider the adjacent volcanoes Mount Shasta and Medicine Lake. If station locations are chosen based only on the distance from the centers of the volcanoes, then any geodetic anomalies between the two volcanoes—an area of potential volcanism as indicated by the presence of volcanic features—may remain undetected by ground-based instrumentation. The spatial analysis is accomplished via a grid of pressure point sources (Mogi, 1958) evenly distributed across the map area, at a depth of 5 km in this example (fig. D4). Each source is inflated until predicted deformations exceed the GNSS white noise uncertainty estimates at one site (Langbein, 2017; Murray and Svarc, 2017). This volume of detectable magma provides a measure of the quality of the coverage (fig. D4). The results indicate that, as of 2022, there is a large area between Mount Shasta and Medicine Lake volcano with existing mapped dikes in which a substantial amount of magma could intrude without being detected geodetically. Applying this style of analysis to individual volcanic systems can provide a guide for designing network geometry given the expected locations of future eruptions.

Recommended Capabilities

The three capabilities, increasingly relevant at higher threat volcanoes, recommended here for deformation monitoring networks are (1) detection of changes in deformation patterns, potentially in near-real time, (2) if deformation is detected, then localization of subsurface source(s) of deformation in three dimensions and estimation of its (their) magnitude and geometry, and (3) if deformation is detected, recognition of magmatic versus nonmagmatic deformation. Capabilities 2 and 3 are intimately linked because the volume and depth of a source must first be estimated to infer its origin, but we describe these capabilities separately for clarity and provide justification based on examples from volcanoes around the world.

We make recommendations for specific numbers of instruments to enable each capability. The GNSS instrumentation recommendations are partly based on numerical simulations of hypothetical surface-deformation patterns. Given the diversity of volcano type, size, eruptive behavior, local geography, accessibility, and environment, the instrument mix and deployment strategy should be customized to each volcano. Accordingly, we give ranges of instrument numbers but, as

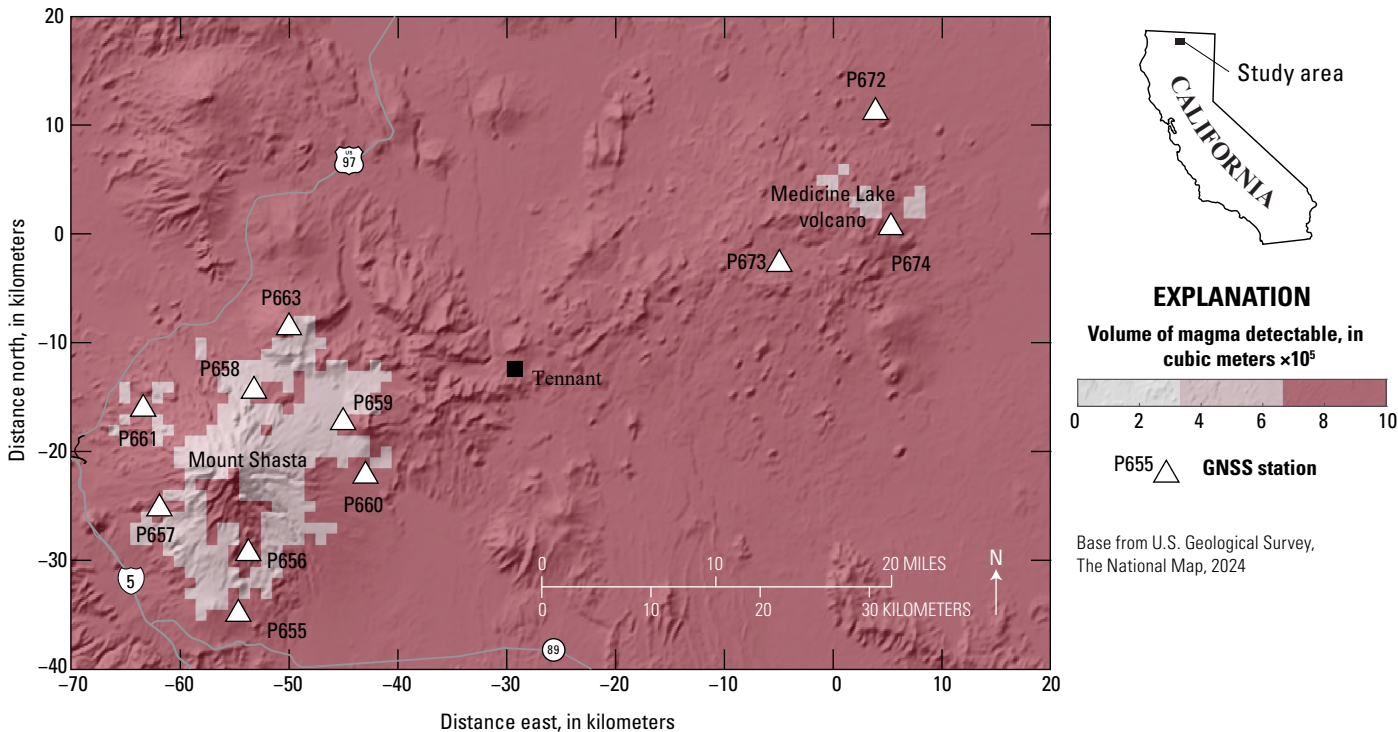


Figure D4. Map showing the amount of magma detectable by the current Global Navigation Satellite System (GNSS) networks at Mount Shasta and Medicine Lake volcano, California. Acceptable coverage is observed at the volcanic centers; however, minimal coverage is present in the area between them where evidence of past eruptions exists. The darkest areas indicate regions where more than 0.001 cubic kilometer (1×10^6 cubic meters) of magma could intrude undetected by the GNSS network.

discussed in this volume's introduction (Flinders and others, 2024), there are financial, practical, and scientific considerations that will ultimately govern the monitoring strategies that can be deployed at any specific volcano.

Detect Changes in Surface Deformation Patterns

Although detecting spatial and temporal changes in surface deformation may be the most important capability of a geodetic monitoring network, it is challenging because of the wide range of time and length scales over which these changes can take place. In terms of timing, precursory deformation was detected only 30 minutes before the eruption of Hekla in Iceland in 1991 (Linde and others, 1993), several hours before an eruption at Mount Etna in Italy in 2002 (Aloisi and others, 2003), and 7 minutes before the phreatic eruption at Ontake in Japan in 2016 (Yamaoka and others, 2016). Deformation measurements at Mount St. Helens contributed to successful predictions days to weeks before more than a dozen dome-building eruptions during 1980–86 (Swanson and others, 1983; Chadwick and others, 1988; Chadwick and Swanson, 1989). At the long end of the range, anomalous surface deformation can extend for months to years. For example, at Augustine Volcano, Alaska, deformation was recognized several months before the onset of eruptive activity there in 2006 (Cervelli and others, 2006), and InSAR-detected deformation at Three Sisters, Oregon (Wicks and others, 2002), could represent an example of decades-long intrusive deformation that may never result in an eruption. An eruption did occur at Rabaul, Papua New Guinea, after decades of deformation (Robertson and Kilburn, 2016). The capability to detect short- and long-term changes in the deformation field is therefore critical for characterizing stable magma systems and more rapid changes.

Spatial scales of deformation can be similarly diverse. Highly localized deformation has been detected prior to small phreatic explosions in Japan (Kobayashi, 2018), whereas surface displacements prior to the 2009 eruption of Redoubt Volcano, Alaska, were detected at a GNSS site nearly 30 km from the volcano (Grapenthin and others, 2013). Broad regions of gentle surface uplift—centimeters of ground motion spread over tens of kilometers—have been associated with magma accumulation in several locations, including multiple volcanoes in the central Andes of South America (Pritchard and Simons, 2004).

Instrumentation

GNSS receivers and borehole tiltmeters currently can provide the required near-real-time data but should have a latency of no more than a few minutes. Whereas GNSS can detect near-real-time deformation, real-time solutions can be subject to substantial noise sources. Tilt is especially sensitive for detecting changes over minutes to hours in shallow magma sources, and arrays of borehole tiltmeters have been used independently of other data types to model source depths and volume changes at Kīlauea (Miklius and Cervelli, 2003; Anderson and others, 2015). Continuous gravimeter and strainmeter stations can also provide

sensitive real-time ground-displacement measurements, although gravimeters must be co-located with a continuous-mode GNSS station for elevation control. High-rate GNSS should also be exploited as a tool for detecting rapid transient deformation and enabling measurements of three-dimensional position changes. These instruments complement each other, providing different sensitivities and capabilities (table D1) that can be used to measure a range of geodetic changes at volcanoes. For example, borehole tilt is well suited to detect short-term transient deformation, like dike intrusion, whereas GNSS is more stable over longer time periods and thus better for tracking signals like slow inflation. Episodic InSAR measurements and GNSS and gravity surveys would ideally be performed, if practical, to provide longer term measurements with higher spatial resolution than is possible with continuous-mode stations. InSAR is especially useful for detecting and characterizing flank stability (for example, Schaefer and others, 2019).

Recommendations

For level 1 volcanoes, we recommend establishing a baseline monitoring network with the purpose of understanding background deformation characteristics and tectonic influences. This baseline can then be used for comparison in the future if continuous geodetic monitoring becomes necessary. Baseline monitoring can be done primarily by InSAR with an annual or several-year cadence and prioritize development of automated processing and detection algorithms. Baseline GNSS and gravity survey networks would ideally be established and remeasured occasionally (5–10 years) with the goal of understanding background local and tectonic deformation.

At level 2 volcanoes, the goal is to detect long-term deformation changes. Thus, campaign GNSS data should be collected every 1–5 years to supplement automated InSAR monitoring and allow for repeat gravity surveys. One continuous-mode GNSS station is recommended within a few kilometers of the most likely vent location (distance dependent on the size of the volcano).

For level 3 volcanoes, spatial and temporal scales of deformation can vary widely, requiring both increased spatial density and real- or near-real-time data with a goal of detecting rapid changes in the deformation field detected within a few days (depending on the magnitude and style of the signal). Two or three continuous-mode GNSS stations within 5–10 km of the deforming source are recommended, and one or more stations farther afield are recommended to provide a stable reference outside the deforming region. A borehole tiltmeter is also recommended if the magma system is shallow and susceptible to signals in the detectable range of tiltmeters. Gravity surveys should be repeated as practical every few years. Automated InSAR processing and analysis should be scrutinized annually, or more often if deformation is detected.

Finally, at level 4 volcanoes, deformation changes would ideally be detected with a lower latency of no more than a few hours, depending on signal magnitude and pattern, and increased station density to cover the possible deforming regions. Five to

eight continuous-mode GNSS stations are recommended for detecting deformation changes. If conditions are appropriate, two to three borehole tiltmeters would be placed near the deformation source. One continuous gravimeter would be placed near the volcano, as close as possible to any likely sources of mass change (because the strength of any gravity signal will diminish rapidly with distance), co-located with a continuous-mode GNSS station for elevation control. The volcano would ideally receive regular tasking by InSAR-capable satellites, with interferograms generated across weeks to months as conditions warrant.

Locate Geodetic Sources and Estimate Source Magnitude and Geometry

Another primary goal of deformation monitoring at active volcanoes is to map the geometry, strength (generally expressed as change in volume), and three-dimensional position of magma bodies. Is an intrusion growing? Where (and how deep) is it? Can we map its movement over time? Source volume change and location cannot be uniquely determined if the spatial resolution of deformation measurements is too low. For example, Delaney and McTigue (1994) showed that volume-change estimates depend heavily on reservoir geometry, but campaign measurements at deforming volcanoes can commonly be fit equally well by multiple deformation source geometries (Dzurisin and others, 2002; Fournier and Freymueller, 2008)—such as point sources of volume change (Mogi, 1958) and horizontal opening-mode dislocations that approximate sills (Okada, 1985). Volume changes calculated from the different geometries can vary by 30 percent (Dzurisin and others, 2002). Source depth also depends on geometry, and this trade-off can result in uncertainty if data coverage is insufficient; for example, sources that are shallow and weak can produce deformation magnitudes that are similar to sources that are deep and strong. Because different source geometries produce different patterns of horizontal and vertical surface deformation (for example, Dieterich and Decker, 1975), any geodetic monitoring network would ideally have the capability of measuring different components and spatial scales of ground displacements to distinguish among competing models.

Estimates of source strength are important to assessments of future activity, especially at restless or active volcanoes. For example, at Soufrière Hills volcano, Montserrat, GNSS measurements detected time-varying behavior of a deformation source 5–6 km beneath the volcano (Wadge and others, 2006). During eruptive periods, they showed that the reservoir (source) contracted as magma withdrawal exceeded supply from deeper regions. During eruptive pauses, the reservoir inflated as magma accumulated. Rates of volume change are therefore useful as an indicator of the likely future course of an eruption. Magma accumulation beneath active volcanoes can be steady or episodic, and long-term records such as those at Kīlauea and Mauna Loa are especially useful. Xue and Freymueller (2020) constructed an approximately 25-year record of magma accumulation for three Aleutian Arc volcanoes using a fusion of campaign and continuous GNSS data with InSAR; they found a variety of timescales for episodic and near-continuous magma accumulation.

The ability to distinguish between one versus multiple deformation sources is also critical for inferring source location, depth, and strength. For example, surface deformation at Mauna Loa has been modeled as caused by a combination of two sources (a point source and a dike), resulting in a complex deformation field (Amelung and others, 2007; Varugu and Amelung, 2021). Separating these two sources was critical in assessing the unrest leading up to the 2022 eruption of Mauna Loa and seeing the shallowing of the dike. If the deformation-monitoring network contains too few stations or is not designed to distinguish between the effects of these two competing sources, interpretations of surface-deformation data would be unreliable and could lead to incorrect interpretations of volcanic unrest. At Mount Okmok, Alaska, for example, Xue and others (2020) found that InSAR and GNSS displacements gave different estimates of the magma system geometry owing to the different spatial sampling of the data, although both datasets could be satisfied by a combination of a point source and a shallow sill-like source.

Instrumentation

For the best sensitivity to source location, geometry, and strength, deformation should be measured over a range of distances from the source. These measurements can be done in near-real time with a network of continuous-mode GNSS instruments and borehole tiltmeters, or over longer time scales using InSAR and (or) GNSS surveys. Both strategies should be used because InSAR measurements and GNSS surveys provide the densest spatial resolution, whereas borehole tilt and continuous-mode GNSS provide the densest temporal resolution. InSAR and GNSS also have different sensitivities to nonvolcanic deformation sources (see following “Recommendations” section), which can bias estimates of source location and geometry.

To formalize a recommendation for numbers of near-real-time continuous-mode GNSS instruments, we performed numerical simulations of the sensitivity of the density of continuous-mode GNSS stations to a buried inflation source (fig. D5). In our hypothetical scenario, we assumed a source at 2.5-km depth, which is typical of the shallowest magma-accumulation zones at several volcanoes (Brandsdóttir and others, 1997; Iwashita and others, 2005; Pagli and others, 2006; Yun and others, 2006). Synthetic three-component surface displacements were forward-calculated for a point-source model (Mogi, 1958), assuming a modest volumetric inflation of 0.001 cubic kilometers. Gaussian random noise was added to the synthetic data by assuming a standard deviation of 2 millimeters (mm) in the horizontal components and of 6 mm in the vertical component (typical of continuous-mode GNSS data).

We used a Monte Carlo algorithm to run multiple simulations with different station distributions. A GNSS network was constructed by randomly locating stations around the volcanic edifice, with 95 percent of stations within 11 km of the volcano’s summit (beneath which the source is located) and a reference station 30 km away. A total of 1,000 simulations were performed for a given number of stations, with each simulation using a unique station distribution. The synthetic data were inverted

using a nonlinear minimization algorithm to solve for volumetric inflation, source depth, and location.

The uncertainty in model parameters (volume change and source depth) as a function of number of stations is plotted in figure D5. Resolution of source (the χ^2 parameter is a representation of the fitness of all combined model parameters—depth, location, and volume change) improves as the number of stations increases. For example, the uncertainty in source depth for a network of four stations is about ± 2.5 km, indicating that the source could statistically reside anywhere from 0 to 5 km of the surface (given an actual source depth of 2.5 km). However, the uncertainty decreases to about ± 1 km with a network of more than 15 stations. Volume-change uncertainty was similarly affected by the number of stations.

Recommendations

Given the relatively low threat level of levels 1 and 2 volcanoes, we do not recommend additional geodetic equipment for this capability in the absence of unrest. At level 3 volcanoes, it becomes more important to locate and estimate volume change within a subsurface deformation source. Five to 10 high-quality continuous-mode GNSS stations are recommended, of which four should be within 5 km of the deforming source and one outside the area of expected surface deformation (to provide a stable reference). In addition, two to four borehole tiltmeters placed within 5–10 km of the deforming source are recommended if the source is shallow and susceptible to deformation in the range measurable by tiltmeters. InSAR data would ideally be acquired and scrutinized at least on an annual

basis, augmented by GNSS surveys every several years to fill in gaps not covered by the continuous GNSS network. Finally, we recommend a baseline gravity survey for reference if a potential magmatic intrusion is identified. At level 4 volcanoes, we seek to provide robust constraints on the location of, and volume change within, any subsurface deformation source. To achieve that end, we recommend 16 to 20 continuous-mode GNSS stations, of which at least eight are within 5–10 km of the deforming source and two are outside the area of expected surface deformation (to provide a stable reference for high-rate positioning, and to help distinguish volcanic and nonvolcanic deformation). In addition, if the source is appropriate, between four to six borehole tiltmeters would be placed within 5–10 km of the deforming source. Annual (summer to summer) InSAR measurements would be complemented with frequent summertime views, dependent on satellite cadence, at volcanoes where snow interferes with data quality. At snow-free volcanoes, InSAR images would ideally be compiled as frequently as is practical. Campaign GNSS surveys would be repeated every few years (if practical), particularly at those volcanoes where InSAR measurements are challenged by environmental conditions and where continuous-mode GNSS stations have detected anomalous surface deformation. One continuous gravimeter would ideally be placed near the volcano if conditions are appropriate. It should be installed as close as possible to any likely sources of mass change (because the strength of any gravity signal diminishes rapidly with distance) and be co-located with a continuous-mode GNSS station for elevation control. Repeat gravity surveys should cover the deforming area.

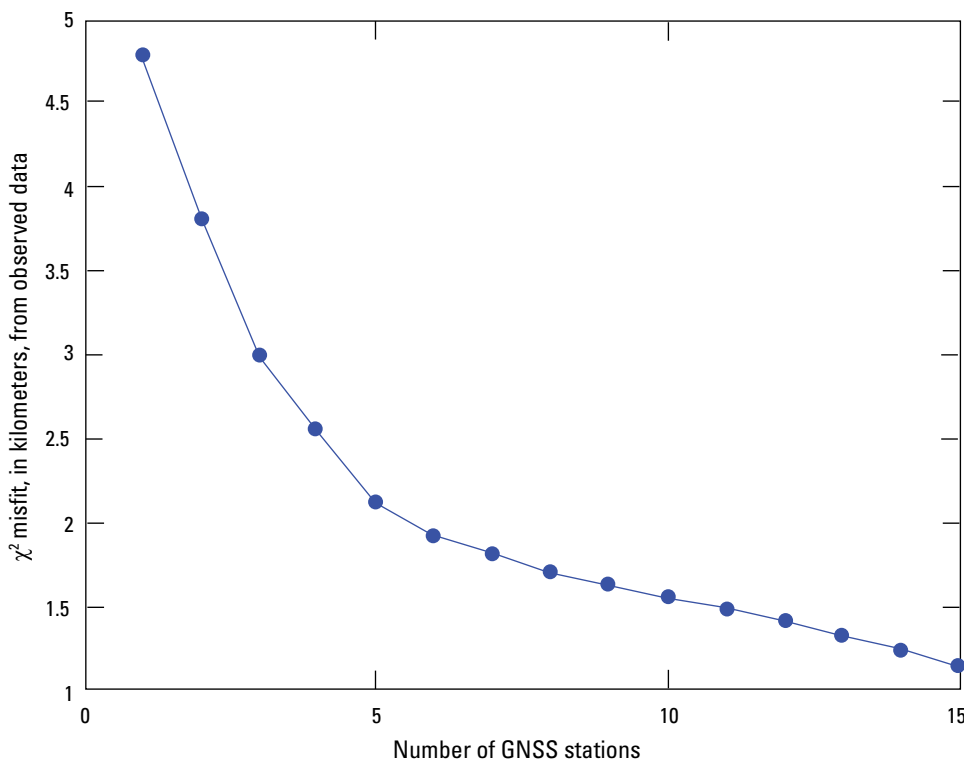


Figure D5. Plot showing the goodness of fit for a modeled magma reservoir determined from a variable number of Global Navigation Satellite System (GNSS) stations. More stations provide better constraints on model parameters (χ^2 represents the combined fitness of four model parameters: depth, two horizontal components of location, and volume change); misfit decreases substantially with more than 5 stations and further improves with 15 stations. The magma reservoir was modeled to be at 2.5 kilometers depth.

Differentiate between Volcanic and Nonvolcanic Ground Deformation

Differentiating volcanic from nonvolcanic (for example, tectonic or hydrologic) surface deformation is crucial to the interpretation of observed displacement patterns and their implications. For example, in 1998, anomalous ground displacements were detected in continuous- and survey-mode GNSS data from Popocatepetl, Mexico (Larson and others, 2004). The surface deformation was associated with transient tectonic slip on the subduction interface, more than 100 km away from the volcano, and therefore presented no significant volcanic hazard. In November 2000, continuous-mode GNSS stations south of Kīlauea's summit moved 2 centimeters closer to the ocean over a period of about 48 hours (Cervelli and others, 2002). The large GNSS network on the Island of Hawai'i enabled scientists to determine that the surface deformation was a result of aseismic fault slip (a small increment of flank collapse) that is sometimes, but not always, directly linked to the ongoing eruption of the volcano, and therefore not indicative of a likely change in the eruption or its impacts (Cervelli and others, 2002; Brooks and others, 2006; Segall and others, 2006; Montgomery-Brown and others, 2015).

At arc volcanoes and other volcanoes in tectonically active regions, significant nonvolcanic deformation is always likely. In addition to volcanic deformation, ground displacements at most volcanoes result from a combination of processes—motion of the volcanic region relative to the stable plate, motion along faults that can be both local and regional (for example, elastic strain resulting from the locked main thrust interface of a subduction zone), and other local processes like geothermal- or groundwater-induced displacements. The tectonic processes commonly can be accounted for by referencing the displacements of the volcano-monitoring stations to sites that are nearby but off the volcano. When no such reference sites are available or when reference sites have failed, plate motion models can be used, but may not be as precise. When the volcanic signal is exceptionally large, the reference sites may be displaced, which can complicate interpretation of the data; however, this situation can be accounted for by explicitly modeling the deformation as being relative to the reference sites. Deformation from local or regional fault motion generally can be compensated for by using data from periods of no volcanic signal or from other regional data. Elastic strain from a locked subduction zone is commonly manifested as approximately arc-normal contraction, can be comparable in magnitude to the volcanic signal, and varies widely in space (for example, Zweck and others, 2002; Dzurisin and others, 2015). Volcanoes commonly lie on or near active upper-crustal faults, motion on which can cause significant ground displacements that may or may not be related to volcanic sources. Numbers of deformation-monitoring instruments, particularly GNSS

stations, would ideally be increased for volcanoes on or near major faults to better distinguish magmatic and tectonic processes. Hydrologic signals are usually seasonal in nature and can be distinguished from volcanic signals based on their pattern of occurrence (Langbein, 2017).

Instrumentation

Far-field continuous-mode GNSS stations are needed at distances much farther than the expected depth of the volcanic reservoir to model and remove nonvolcanic deformation signals from local volcano-monitoring networks; the number of stations depends on the size of each volcanic center and the complexity of its tectonic environment. The high-spatial-resolution capability of InSAR can also be exploited to detect fault motion and other nonvolcanic deformation; thus, repeat InSAR analyses would also be performed.

Recommendations

No additional instruments are needed for levels 1 and 2 volcanoes in the absence of unrest. For level 3 volcanoes, it is worth adding additional instrumentation to confirm whether anomalous ground displacements are caused by magmatic phenomena. Five to ten continuous-mode GNSS stations are recommended, of which at least two would ideally be located outside the area of expected deformation (to provide a stable reference) and four within 5–10 km of the deforming source. InSAR measurements would ideally be acquired and analyzed every few years. GNSS surveys would be undertaken every several years to supplement InSAR measurements and data from continuous-mode GNSS stations.

Additional instruments are recommended for level 4 volcanoes to confirm whether anomalous ground displacements are caused by magmatic phenomena and, if it is not magmatic, to identify the cause of the anomalous displacement. We recommend 16 to 20 continuous-mode GNSS stations, of which at least five would be located within 5–10 km of the deforming source and two outside the area of expected deformation (to provide a stable reference). We recommend collecting InSAR measurements annually (summer to summer) or during the summer at volcanoes that are covered by snow during the winter and more frequently at snow-free volcanoes depending on satellite cadence. There would ideally be regular (every few years) GNSS surveys to supplement data from InSAR measurements and continuous-mode GNSS stations. One continuous gravimeter would be placed near the volcano if conditions are appropriate. It should be installed as close as possible to any likely sources of mass change (because the strength of any gravity signal diminishes rapidly with distance) and should be co-located with a continuous-mode GNSS station for elevation control. Repeat gravity surveys would ideally cover the deforming area.

Summary—Recommendations for Level 1–4 Networks

Level 1.—Baseline deformation measurements using InSAR. Establish baseline GNSS and gravity survey networks and repeat surveys occasionally in case future unrest warrants additional data collection.

Level 2.—InSAR images acquired annually or every few years and incorporated into automated processing and analysis. GNSS and gravity surveys repeated every several years (depending on logistics). A single, continuous-mode GNSS station within 5–10 km of the deforming source.

Level 3.—About 5–10 telemetered continuous-mode GNSS stations, of which four are within 5–10 km of the deforming source and one is outside the area of expected deformation. If conditions permit, two to four borehole tiltmeters within 5–10 km of the deforming source. InSAR processing on at least an annual basis, and GNSS and gravity surveys (as appropriate) every several years to supplement data collected from continuously operating stations.

Level 4.—At least 16 continuous-mode GNSS stations, of which at least eight are within 5–10 km of the deforming source and two are outside the area of expected deformation. If conditions are appropriate, four to six borehole tiltmeters within 5–10 km of the deforming source and one continuous gravimeter. Regular InSAR acquisition and processing, including multitemporal approaches as conditions warrant. GNSS and gravity surveys to supplement data collected from continuously operating stations.

References Cited

- Aloisi, M., Bonaccorso, A., Gambino, S., Mattia, M., and Puglisi, G., 2003, Etna 2002 eruption imaged from continuous tilt and GPS data: *Geophysical Research Letters*, v. 30, no. 23, 5 p., <https://doi.org/10.1029/2003GL018896>.
- Amelung, F., Yun, S.-H., Walter, T.R., Segall, P., and Kim, S.W., 2007, Stress control of deep rift intrusion at Mauna Loa volcano, Hawaii: *Science*, v. 316, no. 5827, p. 1026–1030, <https://doi.org/10.1126/science.1140035>.
- Anderson, K.R., Poland, M.P., Johnson, J.H., and Miklius, A., 2015, Episodic deflation-inflation events at Kīlauea Volcano and implications for the shallow magma system, *in* Carey, R., Cayol, V., Poland, M., and Weis, D., eds., *Hawaiian Volcanoes—From source to surface: American Geophysical Union Geophysical Monograph 208*, p. 229–250, <https://doi.org/10.1002/9781118872079.ch11>.
- Brandsdóttir, B., Menke, W., Einarsson, P., White, R.S., and Staples, R.K., 1997, Färoe-Iceland Ridge Experiment 2. Crustal structure of the Krafla central volcano: *Journal of Geophysical Research*, v. 102, no. B4, p. 7867–7886, <https://doi.org/10.1029/96JB03799>.
- Brooks, B.A., Foster, J.H., Bevis, M., Frazer, L.N., Wolfe, C.J., and Behn, M., 2006, Periodic slow earthquakes on the flank of Kīlauea volcano, Hawai‘i: *Earth and Planetary Science Letters*, v. 246, no. 3–4, p. 207–216.
- Cervelli, P., Segall, P., Johnson, K., Lisowski, M., and Miklius, A., 2002, Sudden aseismic fault slip on the south flank of Kīlauea Volcano: *Nature*, v. 415, no. 6875, p. 1014–1018, <https://doi.org/10.1038/4151014a>.
- Cervelli, P.F., Fournier, T., Freymueller, J., and Power, J.A., 2006, Ground deformation associated with the precursory unrest and early phases of the January 2006 eruption of Augustine Volcano, Alaska: *Geophysical Research Letters*, v. 33, no. 18, <https://doi.org/10.1029/2006GL027219>.
- Chadwick, W.W., Jr., Archuleta, R.J., and Swanson, D.A., 1988, The mechanics of ground deformation precursory to dome-building extrusions at Mount St. Helens, 1981–1982: *Journal of Geophysical Research*, v. 93, no. B5, p. 4351–4366, <https://doi.org/10.1029/JB093iB05p04351>.
- Chadwick, W.W., Jr., and Swanson, D.A., 1989, Thrust faults and related structures in the crater floor of Mount St. Helens volcano, Washington: *Geological Society of America Bulletin*, v. 101, no. 12, p. 1507–1519, [https://doi.org/10.1130/0016-7606\(1989\)101<1507:TFARSI>2.3.CO;2](https://doi.org/10.1130/0016-7606(1989)101<1507:TFARSI>2.3.CO;2).
- Delaney, P.T., and McTigue, D.F., 1994, Volume of magma accumulation or withdrawal estimated from surface uplift or subsidence, with application to the 1960 collapse of Kīlauea Volcano: *Bulletin of Volcanology*, v. 56, no. 6–7, p. 417–424, <https://doi.org/10.1007/BF00302823>.
- Dieterich, J.H., and Decker, R.W., 1975, Finite element modeling of surface deformation associated with volcanism: *Journal of Geophysical Research*, v. 80, no. 29, p. 4094–4102, <https://doi.org/10.1029/JB080i029p04094>.
- Dzurisin, D., 2000, Volcano geodesy—Challenges and opportunities for the 21st century: *Royal Society of London Philosophical Transactions*, ser. A, v. 358, no. 1770, p. 1547–1566, <https://doi.org/10.1098/rsta.2000.0603>.
- Dzurisin, D., 2003, A comprehensive approach to monitoring volcano deformation as a window on the eruption cycle: *Reviews of Geophysics*, v. 41, no. 1, <https://doi.org/10.1029/2001RG000107>.
- Dzurisin, D., 2007, Volcano deformation—New geodetic monitoring techniques: Berlin, Springer-Verlag, 441 p.

- Dzurisin, D., Poland, M.P., and Bürgmann, R., 2002, Steady subsidence of Medicine Lake volcano, northern California, revealed by repeated leveling surveys: *Journal of Geophysical Research Solid Earth*, v. 107, no. B12, <https://doi.org/10.1029/2001JB000893>.
- Dzurisin, D., Moran, S.C., Lisowski, M., Schilling, S.P., Anderson, K.R., and Werner, C., 2015, The 2004–2008 dome-building eruption at Mount St. Helens, Washington—Epilogue: *Bulletin of Volcanology*, v. 77, no. 10, p. 1–17, <https://doi.org/10.1007/s00445-015-0973-4>.
- Flinders, A.F., Lowenstern, J.B., Coombs, M.L., and Poland, M.P., 2024, Introduction to recommended capabilities and instrumentation for volcano monitoring in the United States, chap. A of Flinders, A.F., Lowenstern, J.B., Coombs, M.L., and Poland, M.P., eds., *Recommended capabilities and instrumentation for volcano monitoring in the United States: U.S. Geological Survey Scientific Investigations Report 2024–5062–A*, 8 p., <https://doi.org/10.3133/sir20245062A>.
- Fournier, T., and Freymueller, J., 2008, Inflation detected at Mount Veniaminof, Alaska, with campaign GPS: *Geophysical Research Letters*, v. 35, no. 20, <https://doi.org/10.1029/2008GL035503>.
- Grapenthin, R., Freymueller, J.T., and Kaufman, A.M., 2013, Geodetic observations during the 2009 eruption of Redoubt Volcano, Alaska: *Journal of Volcanology and Geothermal Research*, 259, p. 115–132, <https://doi.org/10.1016/j.jvolgeores.2012.04.021>.
- Hurwitz, S., and Lowenstern, J.B., 2024, Special topic—Boreholes, chap. K of Flinders, A.F., Lowenstern, J.B., Coombs, M.L., and Poland, M.P., eds., *Recommended capabilities and instrumentation for volcano monitoring in the United States: U.S. Geological Survey Scientific Investigations Report 2024–5062–K*, 5 p., <https://doi.org/10.3133/sir20245062K>.
- Iwashita, S., Takahashi, H., Okazaki, N., Miyamura, J., Kasahara, M., Ichiyangi, M., Takahashi, R., and Nakagawa, M., 2005, Volcanic inflation of Mount Hokkaido-Komagatake, Japan, determined from a dense GPS array: *Geophysical Research Letters*, v. 32, no. 20, 4 p., <https://doi.org/10.1029/2005GL023438>.
- Iwatsubo, E.Y., Ewert, J.W., and Murray, T.L., 1992, Monitoring radial crack deformation by displacement meters, in Ewert, J., and Swanson, D., eds., *Monitoring volcanoes—Techniques and strategies used by the staff of the Cascades Volcano Observatory, 1980–90: U.S. Geological Survey Bulletin 1966*, p. 95–101.
- Kobayashi, T., 2018, Locally distributed ground deformation in an area of potential phreatic eruption, Midagahara volcano, Japan, detected by single-look-based InSAR time series analysis: *Journal of Volcanology and Geothermal Research*, v. 357, p. 213–223 <https://doi.org/10.1016/j.jvolgeores.2018.04.023>.
- Langbein, J., 2017, Improved efficiency of maximum likelihood analysis of time series with temporally correlated errors: *Journal of Geodesy*, v. 91, p. 985–994, <https://doi.org/10.1007/s00190-017-1002-5>.
- Larson, K.M., Lowry, A.R., Kostoglodov, V., Hutton, W., Sánchez, O., Hudnut, K., and Suárez, G., 2004, Crustal deformation measurements in Guerrero, Mexico: *Journal of Geophysical Research, Solid Earth*, v. 109, no. B4, <https://doi.org/10.1029/2003JB002843>.
- Linde, A.T., Agustsson, K., Sacks, I.S., and Stefansson, R., 1993, Mechanism of the 1991 eruptions of Hekla from continuous borehole strain monitoring: *Nature*, v. 365, no. 6448, p. 737–740, <https://doi.org/10.1038/365737a0>.
- Lipman, P.W., Moore, J.G., and Swanson, D.A., 1981, Bulging of the north flank before the May 18 eruption—Ggeodetic data, in Lipman, P.W., and Mullineaux, D.R., eds., *The 1980 eruptions of Mount St. Helens, Washington: U.S. Geological Survey Professional Paper 1250*, p. 143–156, <https://doi.org/10.3133/pp1250>.
- Miklius, A., and Cervelli, P., 2003, Interaction between Kilauea and Mauna Loa: *Nature*, v. 421, no. 229, <https://doi.org/10.1038/421229a>.
- Mogi, K., 1958, Relations between the eruptions of various volcanoes and the deformations of the ground surfaces around them: *Earthquake Research Institute Bulletin*, v. 36, no. 2, p. 99–134.
- Montgomery-Brown, E.K., Poland, M.P., and Miklius, A., 2015, Delicate balance of magmatic-tectonic interaction at Kilauea Volcano, Hawai‘i, revealed from slow slip events, in Carey, R., Cayol, V., Poland, M., and Weis, D., eds., *Hawaiian Volcanoes—From source to surface: American Geophysical Union Geophysical Monograph 208*, p. 229–250, <https://doi.org/10.1002/9781118872079.ch13>.
- Murray, J.R., and Svarc, J., 2017, Global Positioning System data collection, processing, and analysis conducted by the U.S. Geological Survey Earthquake Hazards Program: *Seismological Research Letters*, v. 88, no. 3, p. 916–925, <https://doi.org/10.1785/0220160204>.
- Okada, Y., 1985, Surface deformation due to shear and tensile faults in a half-space: *Bulletin of the Seismological Society of America*, v. 75, no. 4, p. 1135–1154, <https://doi.org/10.1785/BSSA0750041135>.
- Orr, T.R., Dietterich, H.R., and Poland, M.P., 2024, Tracking surface changes caused by volcanic activity, chap. G of Flinders, A.F., Lowenstern, J.B., Coombs, M.L., and Poland, M.P., eds., *Recommended capabilities and instrumentation for volcano monitoring in the United States: U.S. Geological Survey Scientific Investigations Report 2024–5062–G*, 11 p., <https://doi.org/10.3133/sir20245062G>.

- Pagli, C., Sigmundsson, F., Árnadóttir, T., Einarsson, P., and Sturkell, E., 2006, Deflation of the Askja volcanic system—Constraints on the deformation source from combined inversion of satellite radar interferograms and GPS measurements: *Journal of Volcanology and Geothermal Research*, v. 152, no. 1–2, p. 97–108, <https://doi.org/10.1016/j.jvolgeores.2005.09.014>.
- Peltier, A., Staudacher, T., Catherine, P., Ricard, L.-P., Kowalski, P., and Bachelery, P., 2006, Subtle precursors of volcanic eruptions at Piton de la Fournaise detected by extensometers: *Geophysical Research Letters*, v. 33, no. 6, 5 p., <https://doi.org/10.1029/2005GL025495>.
- Pritchard, M.E., and Simons, M., 2004, An InSAR-based survey of volcanic deformation in the central Andes: *Geochemistry, Geophysics, Geosystems*, v. 5, no. 2, <https://doi.org/10.1029/2003GC000610>.
- Reid, M.E., Sisson, T.W., and Brien, D.L., 2001, Volcano collapse promoted by hydrothermal alteration and edifice shape, Mount Rainier, Washington: *Geology*, v. 29, no. 9, p. 779–782, [https://doi.org/10.1130/0091-7613\(2001\)029<0779:VCPBHA>2.0.CO;2](https://doi.org/10.1130/0091-7613(2001)029<0779:VCPBHA>2.0.CO;2).
- Robertson, R.M., and Kilburn, C.R., 2016, Deformation regime and long-term precursors to eruption at large calderas—Rabaul, Papua New Guinea: *Earth and Planetary Science Letters*, v. 438, p. 86–94, <https://doi.org/10.1016/j.epsl.2016.01.003>.
- Schaefer, L.N., Di Traglia, F., Chaussard, E., Lu, Z., Nolesini, T., and Casagli, N., 2019, Monitoring volcano slope instability with Synthetic Aperture Radar—A review and new data from Pacaya (Guatemala) and Stromboli (Italy) volcanoes: *Earth-Science Reviews*, v. 192, p. 236–257, <https://doi.org/10.1016/j.earscirev.2019.03.009>.
- Segall, P., Desmarais, E.K., Shelly, D., Miklius, A., and Cervelli, P., 2006, Earthquakes triggered by silent slip events on Kīlauea Volcano, Hawaii: *Nature*, v. 442, no. 7098, p. 71–74, <https://doi.org/10.1038/nature04938>.
- Swanson, D.A., Casadevall, T.J., Dzurisin, D., Malone, S.D., Newhall, C.G., and Weaver, C.S., 1983, Predicting eruptions at Mount St. Helens, June 1980 through December 1982: *Science*, v. 221, no. 4618, p. 1369–1376, <https://doi.org/10.1126/science.221.4618.1369>.
- Varugu, B., and Amelung, F., 2021, Southward growth of Mauna Loa’s dike-like magma body driven by topographic stress: *Scientific Reports*, v. 11, article no. 9816, <https://doi.org/10.1038/s41598-021-89203-6>.
- Wadge, G., Mattioli, G.S., and Herd, R.A., 2006, Ground deformation at Soufrière Hills Volcano, Montserrat during 1998–2000 measured by radar interferometry and GPS: *Journal of Volcanology and Geothermal Research*, v. 152, no. 1–2, p. 157–173, <https://doi.org/10.1016/j.jvolgeores.2005.11.007>.
- Wicks, C.W., Dzurisin, D., Ingebritsen, S., Thatcher, W., Lu, Z., and Iverson, J., 2002, Magmatic activity beneath the quiescent Three Sisters volcanic center, central Oregon Cascade Range, USA: *Geophysical Research Letters*, v. 29, no. 7, p. 26-1–26-4, <https://doi.org/10.1029/2001GL014205>.
- Xue, X., and Freymueller, J.T., 2020, A 25-year history of volcano magma supply in the east central Aleutian arc, Alaska: *Geophysical Research Letters*, v. 47, no. 15, <https://doi.org/10.1029/2020GL088388>.
- Xue, X., Freymueller, J., and Lu, Z., 2020, Modeling the post-eruptive deformation at Okmok based on the GPS and InSAR time series—Changes in the shallow magma storage system: *Journal of Geophysical Research, Solid Earth*, v. 125, no. 2, <https://doi.org/10.1029/2019JB017801>.
- Yamaoka, K., Geshi, N., Hashimoto, T., Ingebritsen, S.E., and Oikawa, T., 2016, Special issue “The phreatic eruption of Mt. Ontake Volcano in 2014,” in Yamaoka, K., Ingebritsen, S., Oikawa, T., Hashimoto, T., and Geshi, N., eds., *The phreatic eruption of Mt. Ontake Volcano in 2014: Earth, Planets, and Space*, v. 68, no. 175, <https://doi.org/10.1186/s40623-016-0548-4>.
- Yun, S., Segall, P., and Zebker, H., 2006, Constraints on magma chamber geometry at Sierra Negra Volcano, Galápagos, based on InSAR observations: *Journal of Volcanology and Geothermal Research*, v. 150, no. 1–3, p. 232–243, <https://doi.org/10.1016/j.jvolgeores.2005.07.009>.
- Zweck, C., Freymueller, J.T., and Cohen, S.C., 2002, Three-dimensional elastic dislocation modeling of the postseismic response to the 1964 Alaska earthquake: *Journal of Geophysical Research, Solid Earth*, v. 107, no. B4, 12 p., <https://doi.org/10.1029/2001JB000409>.

Chapter E



Scanning Differential Optical Absorption Spectrometer (DOAS) instruments scan the sky looking for the characteristic absorption of sunlight by volcanic gases overhead. This scanning DOAS station is located on the east flank of Mount St. Helens, Washington, where it continuously checks for anomalous degassing behavior. Photograph by C. Kern, U.S. Geological Survey, 2021.

Chapter E

Volcanic Gas Monitoring

By Jennifer L. Lewicki, Christoph Kern, Peter J. Kelly, Patricia A. Nadeau, Tamar Elias, and Laura E. Clor

Introduction

As magma rises through the crust, decreasing pressure conditions allow volatiles to exsolve from the magma. These volatiles then migrate upward through the crust, where they can be stored at shallower levels or escape to the atmosphere. Rising magma also heats rock masses beneath volcanic centers, causing water in shallow aquifers and hydrothermal systems to boil and release additional gases and steam (see chapter F, this volume; Ingebritsen and Hurwitz, 2024). The chemistry and quantity of gases that reach the surface during periods of quiescence or volcanic unrest can reveal that gas-rich magma is ascending, crystallizing, or alternatively stalling, with important implications for volcanic hazard (for example, Sutton and others, 1992; Aiuppa and others, 2007, 2021; Werner and others, 2009, 2011, 2012; Moretti and others, 2013; de Moor and others, 2016; Lewicki and others, 2019; Edmonds and others, 2022; Kern and others, 2022; Kunrat and others, 2022).

Most volcanoes in Alaska and the western United States are characterized by weak degassing, with one or more low-temperature fumaroles (typically near the local boiling temperature of water) and connect to a deeper and sometimes extensive hydrothermal system (for example, McGee and others, 2001; Symonds and others, 2003a, b). Hydrothermal systems will affect the chemistry of rising gases exsolved from deeper magma (Symonds and others, 2001), including sulfur dioxide (SO_2), hydrogen chloride (HCl), and water vapor (for example, Doukas and Gerlach, 1995; Gerlach and others, 1998, 2008; Symonds and others, 2001; Werner and others, 2013). As an example, depending on factors such as temperature, pressure, and oxidation state, rising SO_2 will react with groundwater to form hydrogen sulfide (H_2S) gas, dissolved sulfate (SO_4^{2-}), or elemental sulfur (Christenson, 2000; Symonds and others, 2001; Werner and

others, 2008). The reaction and dissolution of SO_2 into shallow groundwater is commonly referred to as scrubbing, and can reduce the likelihood that ascending, degassing magma can be detected. Carbon dioxide, however, in addition to exsolving from magma early in the ascent process, is not easily removed by hydrothermal fluids (Lowenstern, 2001). As scrubbing and other processes take place, the $\text{SO}_2/\text{H}_2\text{S}$, CO_2/SO_2 , and $\text{CO}_2/\text{H}_2\text{S}$ ratios may change. High rates of SO_2 emission indicate that magma has moved to relatively shallow levels in the volcano and that the system has heated up enough to establish dry pathways from depth to the surface. Monitoring multiple gas species and the total output of those species is thereby useful for volcano monitoring during both periods of quiescence, to establish background degassing conditions, and during unrest, when gas geochemistry and emission rates can provide information on changing conditions, such as magma ascent.

To provide context for multidisciplinary volcano forecasts, we focus on the following two key required capabilities: (1) characterizing baseline geochemistry and gas discharge from volcanoes and volcanic regions and (2) monitoring changes in gas geochemistry and discharge to inform forecasts of volcanic eruptions and their effects. Sufficient baseline data must be collected to identify and interpret anomalous degassing associated with volcanic unrest (for example, Sorey and others, 1998; Rouwet and others, 2014). Differences in volcano type, baseline degassing rates, local hydrology, and geography (for example, high versus low latitude) will result in a different baseline for each volcano. Volcanoes of any threat level that exhibit one or more degassing phenomena would ideally be monitored by techniques needed to establish baseline degassing data, with the sampling frequency of baseline data dictated by the threat level (table E1). Additional monitoring techniques become necessary during periods of unrest.

Table E1. Estimated number of degassing volcanoes and types of degassing phenomena in the United States by volcano threat level.

Threat level	Total number of volcanoes	Number of degassing volcanoes	Number of volcanoes with detectable plumes using airborne capabilities	Number of volcanoes with accessible fumaroles	Number of volcanoes with accessible bubbling springs	Number of volcanoes with diffuse degassing
Very high	18	18	8	12	15	7
High	37	28	14	21	14	5
Moderate	48	26	6	14	13	4
Low	33	4	0	1	1	0
Very low	20	3	0	0	0	0

In general, three of the most important techniques for gas monitoring are (1) direct sampling of fumarole, spring, and soil gases for laboratory geochemical measurements, (2) measurements of the chemical composition of the volcanic plume and emission rates of major gas species (for example, H_2O , CO_2 , SO_2 , and H_2S) by satellite, airborne, or ground-based techniques, and (3) measurements of diffuse emissions of CO_2 and other gases through soils. Various methods and instruments may be useful both for baseline studies and during unrest.

Instrumentation and Techniques

Direct Sampling

Direct sampling with subsequent laboratory analyses (fig. E1) is currently the only way to fully characterize the concentrations and isotopic compositions of major, minor, and trace gas species discharging from volcanoes (for example, Giggenbach and Gougel, 1989; Chiodini and others, 1993; Giggenbach, 1996; Vaselli and others, 2006; Janik and Bergfeld, 2010; Bergfeld and others, 2014, 2019; Fischer and others, 2015). Direct sampling requires field collection of gases into empty evacuated flasks or evacuated caustic-solution-filled (“Giggenbach”) bottles and transport back to the laboratory. This process is laborious and time consuming but, when practical to carry out on a regular basis, can be a powerful volcano surveillance tool (for example, Chiodini and others, 2015; Paonita and others, 2016). The U.S. Geological Survey (USGS) typically carries out direct gas sampling at



Figure E1. Photograph showing U.S. Geological Survey Hawaiian Volcano Observatory scientists directly sampling volcanic gases from Kilauea, Hawai‘i. Direct sampling of gas emanating from Ha‘akulamanu (Sulphur Banks location) in Hawai‘i Volcanoes National Park is part of a routine quarterly gas-sampling schedule for monitoring changes in chemical and isotopic compositions and potential unrest. Photograph by P. Nadeau, U.S. Geological Survey, September 9, 2019.

most several times per year (for example, Mammoth Mountain, California) to once every several years (for example, Mount Shasta, California). However, because degassing features are not easily accessed, many volcanoes do not have gas-sampling plans in place and are sampled less frequently, if at all.

Volcanic Plume Measurements

UV Spectroscopy and SO_2 Cameras

Abundances and emission rates of gases in volcanic plumes can be monitored by ground, airborne, or satellite-based instruments (for example, Gerlach and others, 1997; Werner and others, 2011; Kelly and others, 2013; Mori and others, 2016; Stix and others, 2018). Plume SO_2 emission rates can be and typically are measured using spectrometers and cameras (for example, Edmonds and others, 2003; Elias and others, 2006; Galle and others, 2010; Kern and others, 2015a). Such devices operate remotely and need only a view of the plume to collect data, so they can be installed at low-elevation sites (fig. E2). The most common spectrometers belong to the differential optical absorption spectroscopy (DOAS) family and can either be used during campaign traverses beneath a plume or installed in seasonal and (or) permanent monitoring stations where they scan the sky from horizon to horizon to detect volcanic gases overhead. Upward-looking static spectrometers may also be useful in certain cases where scanning spectrometers are inappropriate, such as at Kilauea from 2008 to 2018 when the plume was too close to the ground to resolve with scanning spectrometers (Elias and others, 2018).

Sulfur dioxide (SO_2) cameras can identify otherwise transparent plumes and offer temporal resolutions on the order of a few seconds, allowing for interpretation of gas emissions alongside high-resolution geophysical data. The synoptic view of plumes provided by SO_2 cameras has allowed tracking of puffs and other features for derivation of plume speed, which has historically been a large source of error in spectrometer-based measurements of SO_2 emission rates. Studies using camera imagery of SO_2 plumes have already shed light on eruption dynamics and degassing behavior at multiple volcanoes around the world (for example, Mori and Burton, 2009; Nadeau and others, 2011; Stebel and others, 2015; Campion and others, 2018). These cameras, like spectrometers, mostly rely on ultraviolet (UV) radiation and cannot obtain measurements at night; however, some have been developed using infrared sensors, which make nighttime measurements of SO_2 possible (Prata and Bernardo, 2014; Gabrieli and others, 2016). Although SO_2 cameras have most commonly been deployed in campaign mode, they have also been installed at sites



Figure E2. Photograph showing an SO₂ camera measuring plume SO₂-emission rates at Shishaldin Volcano on Unimak Island in the Aleutian Islands, Alaska. Photograph by C. Kern, U.S. Geological Survey, 2015.

permanently (Burton and others, 2015; Kern and others, 2015b). The newest, and most accurate, iterations of SO₂ camera systems integrate the cameras with spectrometers.

As SO₂ spectrometers and cameras measure scattered solar radiation that has passed through the entire atmosphere before being detected, the measurements are mostly limited to gases with relatively low concentrations in the background atmosphere, such as SO₂. Other accessible volcanic gases include bromine monoxide and chlorine dioxide (Bobrowski and others, 2003; Lübcke and others, 2014; Kern and Lyons, 2018), and, in certain situations, water vapor (Kern and others, 2017).

FTIR Spectroscopy

Other plume gases can be measured remotely using an infrared spectrometer, or Fourier transform infrared spectrometer (FTIR). Specifically, remote FTIR can measure H₂O, CO₂, SO₂, HCl, HF, CO, and COS and typically uses an incandescent infrared (IR) source from a volcano itself, but an IR lamp can alternatively be used for specific volcano geometries (for example, Oppenheimer and others, 1998; Edmonds and Gerlach, 2007). These measurements can be used to calculate diagnostic gas ratios and relative compositions can be scaled by the SO₂ emission rate to obtain emission rates of other gas species.

Multi-GAS

Continuous monitoring of plume gas compositions in real time has been a long-standing goal within volcano science (for example, Sato and McGee, 1981; McGee and others, 1987; McGee and Sutton, 1994), and immense progress has been made with the introduction and proliferation of the multicomponent gas analyzer system (multi-GAS) technique (Aiuppa and others, 2005; Shinohara, 2005). Broadly, multi-GAS is a class of in-situ

instruments that simultaneously measure the abundances of major volcanic gas species, typically H₂O, CO₂, SO₂, and H₂S, in plumes for the purpose of calculating diagnostic gas ratios. In these instruments, plume gas is drawn (typically from close to a fumarole source) by a pump through miniature optical and electrochemical gas sensors that are arranged in series and integrated with a datalogger and other electronics into a compact, field-portable package. Multi-GAS has proven to be a practical, flexible, and valuable approach for obtaining measurements of volcanic gas compositions and has greatly contributed to the rapid evolution of volcanic gas monitoring over the past 15 years or so. Between about 2010 and 2021, the USGS built and deployed 48 multi-GAS instruments for ground-based monitoring, fixed-wing and helicopter-borne measurements, and (or) on unoccupied aircraft systems (UAS). Owing to the custom nature, many variations exist with some instruments able to measure additional species like hydrogen (H₂) (Aiuppa and others, 2011), HCl (Roberts and others, 2017), or methane (CH₄) (Salas-Navarro and others, 2022) or constructed as non-pumped, passive sampling systems (Roberts and others, 2012). Like remote FTIR, relative compositions measured by multi-GAS can be scaled by the SO₂ emission rate to obtain emission rates of other relevant gas species.

Field-Based Isotopic Measurements

Recent advances have been made in instrumentation for field-based isotopic measurements of volcanic gases, allowing for rapid tracking of their source. Portable cavity ring-down spectrometers have been used to make ground-based and airborne measurements of the carbon isotopic composition of CO₂ and oxygen and hydrogen isotopic compositions of H₂O in plumes (for example, Rizzo and others, 2014; Fischer and Lopez, 2016; Stix and others, 2017; Takahashi and others, 2019; D'Arcy and others, 2022). Progress has also been made in the development of

a field-portable mass spectrometer capable of sub-daily $^3\text{He}/^4\text{He}$ ratio measurements (Hurwitz and others, 2018; McMurtry and others, 2019) and a passive-diffusion-sampler suite to determine how helium concentrations and $^3\text{He}/^4\text{He}$ ratios vary with time (Dame and others, 2015). Neither the field-portable mass spectrometer nor the passive-diffusion-sampler suite is ready for operational deployment; they remain experimental.

Satellite Remote Sensing for SO_2

Of the three most abundant magmatic gases— H_2O , CO_2 , and SO_2 —only SO_2 can be reliably detected and measured by current satellite-based remote sensing techniques. Although airborne and (or) ground-based measurements of gas emissions are more sensitive and accurate than satellite-based methods, these measurements are logistically challenging at remote volcanoes, such as in the Aleutian or Mariana Islands. At these volcanoes, routine satellite analysis may provide early notice of volcanic unrest or the onset of an otherwise undetected low-level eruption. Satellite detection and measurement of SO_2 emissions is possible using data collected at both UV and thermal-IR wavelengths.

At UV wavelengths, the primary sensors are Ozone Mapping and Profiling Suite (OMPS), Ozone Mapping Instrument (OMI), Tropospheric Monitoring Instrument (TropOMI), and the Global Ozone Monitoring Experiment 2 (GOME-2). These instruments were primarily designed for measuring ozone and other nonvolcanic atmospheric gases and aerosols but include wavelength coverage that allows for the detection of SO_2 and are useful for monitoring volcanic sources (Carn and others, 2016). TropOMI has been shown to be especially capable in detecting passive (noneruptive) SO_2 emissions at remote volcanoes in Alaska; it has been incorporated into the Alaska Volcano Observatory's daily satellite monitoring checks and is used to monitor gas emissions in Hawai'i (Fioletov and others, 2020). The UV-based instruments that are the most sensitive to SO_2 detection are not able to detect gas at night or in low-light, high-latitude winter, but IR sensors such as the Infrared Atmospheric Sounding Interferometer (IASI) and the Atmospheric Infrared Sounder (AIRS) have been useful for detecting large SO_2 emissions from explosive eruptions.

Diffuse Degassing Measurements

Accumulation Chamber

Whereas an increase in CO_2 emissions can signal magma ascent, characterizing a change in a volcanic plume is challenging because of the relatively high background atmospheric concentrations of CO_2 . Similarly, some volcanoes have substantial diffuse CO_2 degassing but lack volcanic plumes (for example, Mammoth Mountain, California). The accumulation chamber approach can be used in these cases for either continuous CO_2 flux monitoring at a single location or surveys to map the spatial distribution and estimate the CO_2 emission rate of a defined area (for example, Chiodini and others, 1998; Cardellini and others,

2003; Lewicki and others, 2005; Werner and others, 2014). Two limitations of the continuous accumulation chamber instrument are that it typically cannot operate with substantial snow on the ground and it characterizes CO_2 fluxes on small spatial scales (square centimeters). Both continuous and survey-style accumulation chamber instruments have been modified to measure diffuse fluxes of other gas species, such as H_2S (for example, Bergfeld and others, 2012; Pérez and others, 2012) and CH_4 (for example, Cardellini and others, 2003). Because soil CO_2 flux surveys are commonly laborious and time consuming, the USGS typically carries them out annually at specific sites of known high CO_2 emissions (for example, Mammoth Mountain and Yellowstone Caldera).

Eddy Covariance

Eddy covariance is a micrometeorological technique (fig. E3) to continuously measure fluxes of CO_2 , H_2O , and heat (for example, Anderson and Farrar, 2001; Werner and others, 2000, 2003; Lewicki and others, 2008, 2017; Lewicki, 2021). Eddy covariance provides flux measurements that are averaged over time and space, with a spatial scale much larger (square

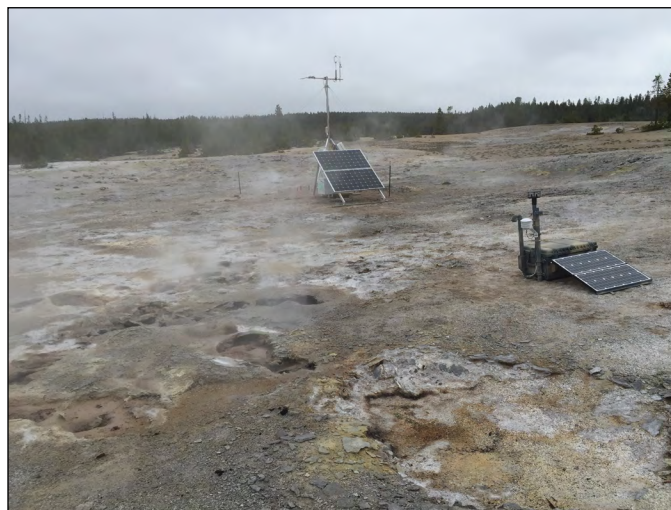


Figure E3. Photograph showing an eddy covariance station (background) and a multi-GAS station (foreground) in an area of Norris Geyser Basin, Yellowstone National Park, Wyoming. This is an elongated, northeast-southwest-oriented area north of Yellowstone Caldera characterized by bare, acid-altered, and steaming ground with fumaroles, frying pans (areas of sizzling ground), and small bubbling pools. Data collected during a campaign study in 2016 provided important information on baseline variations in gas and heat emissions against which future change can be assessed in the context of caldera unrest (Lewicki and others, 2017). The combined eddy covariance and multi-GAS approach provides a powerful tool for quasi-continuous measurements of gas and heat emissions and integration with other continuous geophysical observations for improved volcano-hydrothermal monitoring. The eddy covariance station was redeployed in this area from July 2018 to November 2020. Photograph by J. Lewicki, U.S. Geological Survey, 2016.

meter to square kilometer) than a single continuous accumulation chamber instrument. Additionally, these measurements can be made over snowpack and integrate gas and heat emissions from heterogeneous sources, such as soils, fumaroles, and pools. Eddy covariance flux measurements are only considered valid, however, if made over suitable terrain (flat to moderately complex) and during suitable atmospheric conditions, as determined by standard quality-control assessments.

UAS-Based Geochemical Monitoring

The development and miniaturization of gas sensors has led to substantial advances in the ability to utilize UAS technology for monitoring volcanic emissions at many restless volcanoes around the world (for example, D'Arcy and others, 2018; Syahbana and others, 2019; Liu and others, 2020; Galle and others, 2021). UAS are uniquely suited to provide transformative insight into the geochemistry of volcanic systems primarily because they offer new access for data collection. For example, volcanoes with low-level gas emissions undetectable by traditional airborne surveys or satellites can be surveyed by UAS, which can fly low and slow to detect and map subtle noneruptive gas fluxes and their variability over relatively large areas. Likewise, UAS can enter hazardous areas with lethal concentrations of gas emissions (for example, the Ahu'a'ilā'au vent during the 2018 eruption of Kīlauea) that are too dangerous for traditional aircraft and are inaccessible to field crews. In addition, UAS provide continuous, high-rate sampling that is more useful for mapping emissions than a single point-based measurement from ground surveys.

Recommended Capabilities

Characterize Baseline Gas Geochemistry and Discharge of Dormant Volcanoes

Periodic sampling and analysis of gases from existing fumaroles, springs, and (or) soils on quiescent volcanoes is critical to characterize and understand long-term geochemical trends and changes relevant to monitoring volcanic gas. Collection of high-quality gas and water samples (see chapter F, this volume; Ingebritsen and Hurwitz, 2024) and laboratory analysis is required to characterize the chemical and isotopic compositions of gases emitted from each volcano during noneruptive conditions. Supporting parameters, such as fumarole, spring, and (or) soil gas temperature and spring-water specific conductance and pH, are also typically measured. Such work is important as incipient changes in magmatic conditions may only be recognized through subtle variations in gas geochemistry (for example, helium isotope ratios).

Characterizing baseline gas-emission rates during periods of quiescence is critical to identify subsequent anomalous increases in the output of CO₂ and other volcanic gases. Emission rates can directly reflect the amount of magma degassing at depth; for

example, CO₂ reacts only minimally with hydrothermal systems and shallow ground water before being emitted at the surface (Lowenstern, 2001).

Recommendations

All accessible geothermal springs and fumaroles on U.S. volcanoes would ideally be sampled once, even those volcanoes considered to be level 1. Typically, ground-based, gas-flux measurements are unnecessary at level 1 volcanoes; however, automated satellite-based techniques can be alarmed to detect any unexpected SO₂ anomalies. Level 2 volcanoes would ideally receive periodic sampling and analysis of gases from fumaroles, springs, and (or) soils every 5 to 10 years to recharacterize geochemical baselines. We also recommend establishing a SO₂ emission-rate catalog using TropOMI data (or equivalent). Finally, it is important to conduct airborne and (or) ground-based emission-rate surveys for CO₂, SO₂, and H₂S on a 5- to 10-year schedule. For level 3 volcanoes, resampling of gas chemistry would ideally be on a 3- to 5-year schedule. Satellite-based SO₂ emission-rate time series and airborne and (or) similar ground-based surveys would be conducted on a 3- to 5-year schedule. Finally, at dormant level 4 volcanoes, we recommend resampling of springs and fumaroles and emission rate surveys for CO₂, SO₂, and H₂S on a 1- to 2-year schedule.

Monitor Changes in Gas Geochemistry and Discharge during Unrest and Eruption

The best way to detect changes in gas discharge and geochemistry during volcanic unrest is to have existing equipment in place that can provide key monitoring data to observatory scientists. We recommend installation of continuous networks or periodic to extended (days to months) deployments at U.S. volcanoes that either frequently erupt (for example, Kīlauea, Mount Cleveland, Pavlof Volcano, and Shishaldin Volcano) or are quiescent but display a substantial level of degassing (for example, Mount Baker, Yellowstone Caldera, and Mammoth Mountain). Off-the-shelf UV scanning technologies for SO₂, multi-GAS systems for fumarolic compositions, and automated measurement systems for diffuse CO₂ emissions could either be permanently installed or at least deployed at such volcanoes for periods of weeks to months each year when field conditions permit. In-situ gas sampling from fumaroles, springs, and (or) soils should be coordinated so that these datasets can be compared and detailed geochemical information can be obtained.

In conjunction with ground-based gas measurements, frequent airborne measurements (for example, from fixed-wing helicopter or UAS platforms) of volcanic plumes are needed to identify key changes in volcano degassing that signal various stages in the progression of a volcano from unrest to eruption (for example, Werner and others, 2012, 2013). Such measurements are particularly important at remote and (or) rugged volcanoes where ground access is difficult.

Recommendations

Airborne gas-emission rates would ideally be determined for any volcano showing signs of unrest or erupting. To provide greater context and improved temporal resolution, it is also important to deploy continuous monitoring instrumentation (or survey measurements) of gas emission rates and geochemical compositions at any volcano with measurable degassing. In-situ gas sampling from fumaroles, springs, and (or) soils would ideally be coordinated.

General Recommendations and Considerations

As shown in table E1, active degassing occurs at 100 percent of level 4 (very high threat) volcanoes, 76 percent of level 3 (high threat) volcanoes, and 54 percent of level 2 (moderate threat) volcanoes. Higher threat-level volcanoes commonly display multiple types of gas emission, whereas lower threat-level volcanoes exhibit few, if any, signs of degassing. Volcanic plumes may change in character over time and may or may not be detectable using airborne capabilities; thus, the number of volcanoes with detectable plumes noted in table E1 is an estimate based on observations over the last 10 years or so. We recommend that the gas-monitoring strategy be prioritized both by the threat level of the volcano and the type of gas emission demonstrated by the volcano. For example, Mount Shasta is a very high threat volcano with accessible fumaroles and springs, but the gas output by fumaroles is not measurable by airborne instruments, nor are areas of diffuse degassing known. The gas-monitoring strategy for Mount Shasta would therefore include regular fumarole and spring gas sampling and a yearly airborne survey (flyby for detection and measurement, if detected) to assess whether a CO₂ plume is being emitted in the absence of any thermal signature. At a lower threat volcano with the same types of gas emissions, the gas-monitoring strategy would be the same but with a longer lag time between repeat ground-based or airborne sampling.

We do not recommend that continuous gas-monitoring networks be established on dormant volcanoes without substantial degassing and (or) with low threat levels; however, baseline gas geochemistry and emission rates established for levels 2–4 volcanoes, would provide background data essential for interpreting the magmatic and hydrologic processes that might accompany unrest. Additional instrumentation would be deployed for continuous long-term monitoring on an individual basis at volcanoes with sufficient degassing.

If at any point a volcano becomes restless, all applicable techniques could be used to assess emerging volcanic activity. The degree of response will be dictated by the degree of unrest, logistics, and hazard level. For example, where logistically possible, emerging unrest might be best monitored by increasing measurement frequency to approximately monthly at high and very high threat volcanoes. If the degree of unrest further increases, so should the measurement frequency. For all degrees of unrest, newly evolving techniques could be sought and incorporated into the USGS gas-monitoring program as appropriate.

Summary—Recommendations for Levels 1–4 Volcanoes

Level 1.—Automate daily satellite-based alerts of SO₂ emissions. Ensure existence of gas geochemical data on any existing fumaroles or geothermal springs.

Level 2.—Establish a satellite-based SO₂ emission-rate catalog and characterize baseline gas geochemistry and emission rates using airborne and (or) ground-based sampling techniques on a 5- to 10-year schedule.

Level 3.—Establish a satellite-based SO₂ emission-rate time series at any volcano with an adequate level of degassing. Characterize baseline gas geochemistry and emission rates using airborne and (or) ground-based sampling techniques on a 3- to 5-year schedule. Conduct continuous monitoring and (or) survey measurements of gas emission rates as appropriate at any volcano with an adequate level of degassing.

Level 4.—In addition to level 3 recommendations, characterize baseline gas geochemistry and emissions on a 1- to 2-year schedule.

In the event of unrest at a volcano of any threat level, the most practical and effective existing and available techniques would ideally be used to assess evolving activity.

References Cited

- Aiuppa, A., Bitetto, M., Donne, D.D., LaMonica, F.P., Tamburello, G., Coppola, D., Della Schiava, M., Innocenti, L., Lacanna, G., Laiolo, M., Massimetti, F., Pistolesi, M., Silengo, M.C., and Ripepe, M., 2021, Volcanic CO₂ tracks the incubation period of basaltic paroxysms: *Science Advances*, v. 7, no. 38, <https://doi.org/10.1126/sciadv.abh0191>.
- Aiuppa, A., Federico, C., Guidice, G., and Gurrieri, S., 2005, Chemical mapping of a fumarolic field—La Fossa Crater, Vulcano Island (Aeolian Islands, Italy): *Geophysical Research Letters*, Solid Earth, v. 32, no. 13, <https://doi.org/10.1029/2005GL023207>.
- Aiuppa, A., Moretti, R., Federico, C., Giudice, G., Gurrieri, S., Liuzzo, M., Papale, P., Shinohara, H., and Valenza, M., 2007, Forecasting Etna eruptions by real-time observation of volcanic gas composition: *Geology*, v. 35, no. 12, p. 1115–1118, <https://doi.org/10.1130/G24149A.1>.
- Aiuppa, A., Shinohara, H., Tamburello, G., Guidice, G., Liuzzo, M., and Moretti, R., 2011, Hydrogen in the gas plume of an open-vent volcano, Mount Etna, Italy: *Journal of Geophysical Research*, Solid Earth, v. 116, no. B10, <https://doi.org/10.1029/2011JB008461>.

- Anderson, D.E., and Farrar, C.D., 2001, Eddy covariance measurement of CO₂ flux to the atmosphere from an area of high volcanogenic emissions, Mammoth Mountain, California: *Chemical Geology*, v. 177, no. 1–2, p. 31–42, [https://doi.org/10.1016/S0009-2541\(00\)00380-6](https://doi.org/10.1016/S0009-2541(00)00380-6).
- Bergfeld, D., Evans, W.C., Lowenstern, J.B., and Hurwitz, S., 2012, Carbon dioxide and hydrogen sulfide degassing and cryptic thermal input to Brimstone Basin, Yellowstone National Park, Wyoming: *Chemical Geology*, v. 330–331, p. 233–243, <https://doi.org/10.1016/j.chemgeo.2012.09.001>.
- Bergfeld, D., Lewicki, J.L., Evans, W.C., Hunt, A.G., Revesz, K., and Huebner, M., 2014, Geochemical investigation of the hydrothermal system on Akutan Island, Alaska, July 2012: U.S. Geological Survey Scientific Investigations Report 2013–5231, 20 p., <https://doi.org/10.3133/sir20135231>.
- Bergfeld, D., Lowenstern, J.B., Hunt, A.G., Hurwitz, S., McCleskey, B.R., and Peek, S.E., 2019, Chemical and isotopic data on gases and waters for thermal and non-thermal features across Yellowstone National Park (ver. 2.0, March 2019): U.S. Geological Survey data release, <https://doi.org/10.5066/F7H13105>.
- Bobrowski, N., Hönninger, G., Galle, B., and Platt, U., 2003, Detection of bromine monoxide in a volcanic plume: *Nature*, v. 423, p. 273–276, <https://doi.org/10.1038/nature01625>.
- Burton, M., Prata, F., and Platt, U., 2015, Volcanological applications of SO₂ cameras: *Journal of Volcanology and Geothermal Research*, v. 300, p. 2–6, <https://doi.org/10.1016/j.jvolgeores.2014.09.008>.
- Campion, R., Delgado-Granados, H., Legrand, D., Taquet, N., Boulesteix, T., Pedraza-Espitia, S., and Lecocq, T., 2018, Breathing and coughing—The extraordinarily high degassing of Popocatepetl Volcano investigated with an SO₂ camera: *Frontiers in Earth Science*, v. 6, <https://doi.org/10.3389/feart.2018.00163>.
- Cardellini, C., Chiodini, G., Frondini, F., Granieri, D., Lewicki, J., and Peruzzi, L., 2003, Accumulation chamber measurements of methane fluxes—Application to volcanic-geothermal areas and landfills: *Applied Geochemistry*, v. 18, p. 45–54, [https://doi.org/10.1016/S0883-2927\(02\)00091-4](https://doi.org/10.1016/S0883-2927(02)00091-4).
- Carn, S.A., Clarisse, L., and Prata, A.J., 2016, Multi-decadal satellite measurements of global volcanic degassing: *Journal of Volcanology and Geothermal Research*, v. 311, p. 99–134, <https://doi.org/10.1016/j.jvolgeores.2016.01.002>.
- Chiodini, G., Cioni, R., Guidi, M., Raco, B., and Marini, L., 1998, Soil CO₂ flux measurements in volcanic and geothermal areas: *Applied Geochemistry*, v. 13, p. 543–552, [https://doi.org/10.1016/S0883-2927\(97\)00076-0](https://doi.org/10.1016/S0883-2927(97)00076-0).
- Chiodini, G., Cioni, R., and Marini, L., 1993, Reactions governing the chemistry of crater fumaroles from Vulcano Island, Italy, and implications for volcanic surveillance: *Applied Geochemistry*, v. 8, no. 4, p. 357–371, [https://doi.org/10.1016/0883-2927\(93\)90004-Z](https://doi.org/10.1016/0883-2927(93)90004-Z).
- Chiodini, G., Vandemeulebrouck, J., Caliro, S., D’Auria, L., De Martino, P., Mangiacapra, A., and Petrillo, Z., 2015, Evidence of thermal-driven processes triggering the 2005–2014 unrest at Campi Flegrei caldera: *Earth and Planetary Science Letters*, v. 414, p. 58–67.
- Christenson, B.W., 2000, Geochemistry of fluids associated with the 1995–1996 eruption of Mount Ruapehu, New Zealand—Signatures and processes in the magmatic-hydrothermal system: *Journal of Volcanology and Geothermal Research*, v. 97, no. 1–4, p. 1–30, [https://doi.org/10.1016/S0377-0273\(99\)00167-5](https://doi.org/10.1016/S0377-0273(99)00167-5).
- Dame, B.E., Solomon, D.K., Evans, W.C., and Ingebritsen, S.E., 2015, Developing a new, passive diffusion sampler suite to detect helium anomalies associated with volcanic unrest: *Bulletin of Volcanology*, v. 77, no. 3, <https://doi.org/10.1007/s00445-015-0912-4>.
- D’Arcy, F., de Moor, J.M., Stix, J., Alan, A., Bogue, R., Corrales, E., Diaz, J.A., Mick, E., Salas-Navarro, J., and Lauzeral, R., 2022, New insights into carbon isotope systematics at Poás volcano, Costa Rica: *Journal of Volcanology and Geothermal Research*, v. 431, article no. 107639, <https://doi.org/10.1016/j.jvolgeores.2022.107639>.
- D’Arcy, F., Stix, J., de Moor, J., Rüdiger, J., Diaz, J., Alan, A., and Corrales, E., 2018, Drones swoop in to measure gas belched from volcanoes: *Eos*, v. 99, <https://doi.org/10.1029/2018eo102329>.
- de Moor, J.M., Aiuppa, A., Pacheco, J., Avard, G., Kern, C., Liuzzo, M., Martinez, M., Guidice, G., and Fischer, T.P., 2016, Short-period volcanic gas precursors to phreatic eruptions—Insights from Poás Volcano, Costa Rica: *Earth and Planetary Science Letters*, v. 442, p. 218–227, <https://doi.org/10.1016/j.epsl.2016.02.056>.
- Doukas, M.P., and Gerlach, T.M., 1995, Sulfur dioxide scrubbing during the 1992 eruptions of Crater Peak, Mount Spurr volcano, Alaska, in Keith, T.E.C., ed., *The 1992 eruptions of Crater Peak vent, Mount Spurr volcano, Alaska*: U.S. Geological Survey Bulletin 2139, p. 47–57, <https://doi.org/10.3133/b2139>.
- Edmonds, M., and Gerlach, T.M., 2007, Vapor segregation and loss in basaltic melts: *Geology*, v. 35, no. 8, p. 751–754, <https://doi.org/10.1130/G23464A.1>.
- Edmonds, M., Herd, R.A., Galle, B., and Oppenheimer, C.M., 2003, Automated, high time-resolution measurements of SO₂ flux at Soufrière Hills Volcano, Montserrat: *Bulletin of Volcanology*, v. 65, p. 578–586, <https://doi.org/10.1007/s00445-003-0286-x>.

- Edmonds, M., Liu, E., and Cashman, K., 2022, Open-vent volcanoes fueled by depth-integrated magma degassing: *Bulletin of Volcanology*, v. 84, no. 28, <https://doi.org/10.1007/s00445-021-01522-8>.
- Elias, T., Kern, C., Horton, K.A., Sutton, A.J., and Garbeil, H., 2018, Measuring SO₂ emission rates at Kīlauea Volcano, Hawaii, using an array of upward-looking UV spectrometers, 2014–2017: *Frontiers in Earth Science*, v. 6, no. 214, <https://doi.org/10.3389/feart.2018.00214>.
- Elias, T., Sutton, A.J., Oppenheimer, C., Horton, K.A., Garbeil, H., Tsanev, V., McGonigle, A.J.S., and Williams-Jones, G., 2006, Comparison of COSPEC and two miniature ultraviolet spectrometer systems for SO₂ measurements using scattered sunlight: *Bulletin of Volcanology*, v. 68, p. 313–322, <https://doi.org/10.1007/s00445-005-0026-5>.
- Fioletov, V., McLinden, C.A., Griffin, D., Theys, N., Loyola, D.G., Hedelt, P., Krotkov, N.A., and Li, C., 2020, Anthropogenic and volcanic point source SO₂ emissions derived from TROPOMI on board Sentinel-5 Precursor—First results: *Atmospheric Chemistry and Physics*, v. 20, no. 9, p. 5591–5607, <https://doi.org/10.5194/acp-20-5591-2020>.
- Fischer, T.P., and Lopez, T.M., 2016, First airborne samples of a volcanic plume for $\delta^{13}\text{C}$ of CO₂ determinations: *Geophysical Research Letters*, v. 43, no. 7, p. 3272–3279, <https://doi.org/10.1002/2016GL068499>.
- Fischer, T.P., Ramírez, C., Mora-Amador, R.A., Hilton, D.R., Barnes, J.D., Sharp, Z.D., Le Brun, M., De Moor, J.M., Barry, P.H., Füre, E., and Shaw, A.M., 2015, Temporal variations in fumarole gas chemistry at Poás volcano, Costa Rica: *Journal of Volcanology and Geothermal Research*, v. 294, p. 56–70, <https://doi.org/10.1016/j.jvolgeores.2015.02.002>.
- Gabrieli, A., Wright, R., Lucey, P.G., Porter, J.N., Garbeil, H., Pilger, E., and Wood, M., 2016, Characterization and initial field test of an 8–14 μm thermal infrared hyperspectral imager for measuring SO₂ in volcanic plumes: *Bulletin of Volcanology*, v. 78, no. 73, <https://doi.org/10.1007/s00445-016-1068-6>.
- Galle, B., Johansson, M., Rivera, C., Zhang, Y., Kihlman, M., Kern, C., Lehmann, T., Platt, U., Arellano S., and Hidalgo, S., 2010, Network for Observation of Volcanic and Atmospheric Change (NOVAC)—A global network for volcanic gas monitoring: Network layout and instrument description: *Journal of Geophysical Research, Atmospheres*, v. 115, no. D5, <https://doi.org/10.1029/2009JD011823>.
- Galle, B., Arellano, S., Bobrowski, N., Conde, V., Fischer, T.P., Gerdes, G., Gutmann, A., Hoffmann, T., Itikarai, I., Krejci, T., Liu, E.J., Mulina, K., Nowicki, S., Richardson, T., Rüdiger, J., Wood, K., and Xu, J., 2021, A multi-purpose, multi-rotor drone system for long-range and high-altitude volcanic gas plume measurements: *Atmospheric Measurement Techniques*, v. 14, p. 4255–4277, <https://doi.org/10.5194/amt-14-4255-2021>.
- Gerlach, T.M., Delgado, H., McGee, K.A., Doukas, M.P., Venegas, J.J., and Cárdenas, L., 1997, Application of the LI-COR CO₂ analyzer to volcanic plumes—A case study, Volcán Popocatepetl, Mexico, June 7 and 10, 1995: *Journal of Geophysical Research*, v. 102, no. B4, p. 8005–8019, <https://doi.org/10.1029/96JB03887>.
- Gerlach, T.M., McGee, K.A., and Doukas, M.P., 2008, Emission rates of CO₂, SO₂, and H₂S, scrubbing, and preeruption excess volatiles at Mount St. Helens, 2004–2005, chap. 26 of Sherrod, D.R., Scott, W.E., and Stauffer, P.H., eds., *A volcano rekindled—The renewed eruption of Mount St. Helens, 2004–2006*: U.S. Geological Survey Professional Paper 1750, p. 543–571, <https://doi.org/10.3133/pp175026>.
- Gerlach, T.M., McGee, K.A., Sutton, A.J., and Elias, T., 1998, Rates of volcanic CO₂ degassing from airborne determinations of SO₂ emission rates and plume CO₂/SO₂—Test study at Pu‘u ‘O‘o cone, Kīlauea Volcano, Hawaii: *Geophysical Research Letters*, v. 25, no. 14, p. 2675–2678, <https://doi.org/10.1029/98GL02030>.
- Giggenbach, W.F., 1996, Chemical composition of volcanic gases, in Scarpa R., and Tilling, R., eds., *Monitoring and Mitigation of Volcano Hazards*: Berlin, Springer Verlag, p. 221–256.
- Giggenbach, W.F., and Gougel, R.L., 1989, Collection and analysis of geothermal and volcanic water and gas discharges: New Zealand, Institute of Geological and Nuclear Sciences Report CD2401, p. 36–53.
- Hurwitz, S., Peek, S., Kelly, P.J., Lewicki, J.L., Bergfeld, D., Evans, W., Wilkinson, S.K., Hunt, A.G., McMurtry, G.M., Jolly, J., Deluze, J., Horn, E., Lucic, G., Oze, C., and Horton T.W., 2018, New technologies to measure temporal variations of magmatic helium and CO₂ emissions at Mammoth Mountain California [abs.]: American Geophysical Union, 2018 Fall Meeting, Washington D.C., abstract V43I-0251.
- Ingebritsen, S.E. and Hurwitz, S., 2024, Streams, springs, and volcanic lakes for volcano monitoring, chap. F of Flinders, A.F., Lowenstern, J.B., Coombs, M.L., and Poland, M.P., eds., *Recommended capabilities and instrumentation for volcano monitoring in the United States*: U.S. Geological Survey Scientific Investigations Report 2024–5062–F, 9 p., <https://doi.org/10.3133/sir20245062F>.
- Janik, C.J., and Bergfeld, D., 2010, Analyses of gas, steam and water samples collected in and around Lassen Volcanic National Park, California, 1975–2002: U.S. Geological Survey Open-File Report 2010–1036, 13 p., <https://doi.org/10.3133/ofr20101036>.
- Kelly, P.J., Kern, C., Roberts, T.J., Lopez, T., Werner, C., and Aiuppa, A., 2013, Rapid chemical evolution of tropospheric volcanic emissions from Redoubt Volcano, Alaska, based on observations of ozone and halogen-containing gases: *Journal of Volcanology and Geothermal Research*, v. 259, p. 317–333, <https://doi.org/10.1016/j.jvolgeores.2012.04.023>.

- Kern, C., Aiuppa, A., and de Moor, J.M., 2022, A golden era for volcanic gas geochemistry?: *Bulletin of Volcanology*, v. 84, no. 43, <https://doi.org/10.1007/s00445-022-01556-6>.
- Kern, C., Lübcke, P., Bobrowski, N., Campion, R., Mori, T., Smekens, J.-F., Stebel, K., Tamburello, G., Burton, M., Platt, U., and Prata, F., 2015a, Intercomparison of SO₂ camera systems for imaging volcanic gas plumes: *Journal of Volcanology and Geothermal Research*, v. 300, p. 22–36, <https://doi.org/10.1016/j.jvolgeores.2014.08.026>.
- Kern, C., and Lyons, J.J., 2018, Spatial distribution of halogen oxides in the plume of Mount Pagan Volcano, Mariana Islands: *Geophysical Research Letters*, v. 45, no. 18, p. 9588–9596, <https://doi.org/10.1029/2018GL079245>.
- Kern, C., Masias, P., Apaza, F., Reath, K.A., and Platt, U., 2017, Remote measurement of high preeruptive water vapor emissions at Sabancaya volcano by passive differential optical absorption spectroscopy: *Journal of Geophysical Research, Solid Earth*, v. 122, no. 5, p. 3540–3564, <https://doi.org/10.1002/2017JB014020>.
- Kern, C., Sutton, A.J., Elias, T., Lee, R.L., Kamibayashi, K.P., Antolik, L., and Werner, C.A., 2015b, An automated SO₂ camera system for continuous, real-time monitoring of gas emissions from Kilauea Volcano's summit Overlook Crater: *Journal of Volcanology and Geothermal Research*, v. 300, p. 81–94, <https://doi.org/10.1016/j.jvolgeores.2014.12.004>.
- Kunrat, S., Kern, C., Alfianti, H., and Lerner, A.H., 2022, Forecasting explosions at Sinabung Volcano, Indonesia, based on SO₂ emission rates: *Frontiers in Earth Science*, v. 10, <https://doi.org/10.3389/feart.2022.976928>.
- Lewicki, J.L., 2021, Long-term year-round observations of magmatic CO₂ emissions on Mammoth Mountain, California, USA: *Journal of Volcanology and Geothermal Research*, v. 418, article no. 107347, <https://doi.org/10.1016/j.jvolgeores.2021.107347>.
- Lewicki, J.L., Bergfeld, D., Cardellini, C., Chiodini, G., Granieri, D., Varley, N., and Werner, C., 2005, Comparative soil CO₂ flux measurements and geostatistical estimation methods on Masaya volcano, Nicaragua: *Bulletin of Volcanology*, v. 68, p. 76–90, <https://doi.org/10.1007/s00445-005-0423-9>.
- Lewicki, J.L., Evans, W.C., Montgomery-Brown, E.K., Mangan, M.T., King, J.C., and Hunt, A.G., 2019, Rate of magma supply beneath Mammoth Mountain, California, based on helium isotopes and CO₂ emissions: *Geophysical Research Letters*, v. 46, p. 4636–4644, <https://doi.org/10.1029/2019GL082487>.
- Lewicki, J.L., Fischer, M.L., and Hilley, G.E., 2008, Six-week time series of eddy covariance CO₂ flux at Mammoth Mountain, California—Performance evaluation and role of meteorological forcing: *Journal of Volcanology and Geothermal Research*, v. 171, p. 178–190, <https://doi.org/10.1016/j.jvolgeores.2007.11.029>.
- Lewicki, J.L., Kelly, P.J., Bergfeld, D., Vaughan, R.G., and Lowenstern, J.B., 2017, Monitoring gas and heat emissions at Norris Geyser Basin, Yellowstone National Park, USA based on a combined eddy covariance and Multi-GAS approach: *Journal of Volcanology and Geothermal Research*, v. 347, p. 312–326, <https://doi.org/10.1016/j.jvolgeores.2017.10.001>.
- Liu, E.J., Aiuppa, A., Alan, A., Arellano, S., Bitetto, M., Bobrowski, N., Carn, S., Clarke, R., Corrales, E., de Moor, J.M., Diaz, J.A., Edmonds, M., Fischer, T.P., Freer, J., Fricke, G.M., Galle, B., Gerdes, G., Giudice, G., Gutmann, A., Hayer, C., Itikarai, I., Jones, J., Mason, E., McCormick Kilbride, B.T., Mulina, K., Nowicki, S., Rahilly, K., Richardson, T., Rüdiger, J., Schipper, C.I., Watson, I.M., and Wood, K., 2020, Aerial strategies advance volcanic gas measurements at inaccessible, strongly degassing volcanoes: *Science Advances*, v. 6, no. 44, <https://doi.org/10.1126/sciadv.abb9103>.
- Lowenstern, J.B., 2001, Carbon dioxide in magmas and implications for hydrothermal systems: *Mineralium Deposita*, v. 36, no. 6, p. 490–502, <https://doi.org/10.1007/s001260100185>.
- Lübcke, P., Bobrowski, N., Arellano, S., Galle, B., Garzón, G., Vogel, L., and Platt, U., 2014, BrO/SO₂ molar ratios from scanning DOAS measurements in the NOVAC network: *Solid Earth*, v. 5, no. 1, p. 409–424, <https://doi.org/10.5194/se-5-409-2014>.
- McGee, K.A., Sutton, J., and Sato, M., 1987, Use of satellite telemetry for monitoring active volcanoes, with a case study of a gas-emission event at Kilauea volcano, December 1982, in Decker, R.W., Wright, T.L., and Stauffer, H., eds., *Volcanism in Hawaii*. U.S. Geological Survey Professional Paper 1350, p. 821–825.
- McGee, K.A., Doukas, M.P., and Gerlach, T.M., 2001, Quiescent hydrogen sulfide and carbon dioxide degassing from Mount Baker, Washington: *Geophysical Research Letters*, v. 28, no. 23, p. 4479–4483, <https://doi.org/10.1029/2001GL013250>.
- McGee, K.A., and Sutton, A.J., 1994, Eruptive activity at Mount St. Helens, Washington, USA, 1984–1988—A gas geochemistry perspective: *Bulletin of Volcanology*, v. 56, p. 435–446, <https://doi.org/10.1007/BF00302825>.
- McMurtry, G.M., Dasilveira, L.A., Horn, E.L., DeLuze, J.R., and Blessing, J.E., 2019, High ³He/⁴He ratios in lower East Rift Zone steaming vents precede a new phase of Kilauea 2018 eruption by 8 months: *Scientific Reports*, v. 9, no. 11860, <https://doi.org/10.1038/s41598-019-48268-0>.
- Moretti, R., Arienzo, I., Civetta, L., Orsi, G., and Papale, P., 2013, Multiple magma degassing sources at an explosive volcano: *Earth and Planetary Science Letters*, v. 367, p. 95–104, <https://doi.org/10.1016/j.epsl.2013.02.013>.
- Mori, T., and Burton, M., 2009, Quantification of the gas mass emitted during single explosions on Stromboli with the SO₂ imaging camera: *Journal of Volcanology and Geothermal Research*, v. 188, no. 4, p. 395–400, <https://doi.org/10.1016/j.jvolgeores.2009.10.005>.

- Mori, T., Hashimoto, T., Terada, A., Yoshimoto, M., Kazahaya, R., Shinohara, H., and Tanaka, R., 2016, Volcanic plume measurements using a UAV for the 2014 Mt. Ontake eruption: *Earth, Planets and Space*, v. 68, no. 49., <https://doi.org/10.1186/s40623-016-0418-0>.
- Nadeau, P.A., Palma, J.L., and Waite, G.P., 2011, Linking volcanic tremor, degassing, and eruption dynamics via SO_2 imaging: *Geophysical Research Letters*, v. 38, no. 1, <https://doi.org/10.1029/2010GL045820>.
- Oppenheimer, C., Francis, P., Burton, M., Maciejewski, A.J.H., and Boardman, L., 1998, Remote measurements of volcanic gases by Fourier transform infrared spectroscopy: *Applied Physics B*, v. 67, p. 505–515, <https://doi.org/10.1007/s003400050536>.
- Paonita, A., Caracausi, A., Martelli, M., and Rizzo, A.L., 2016, Temporal variations of helium isotopes in volcanic gases quantify pre-eruptive refill and pressurization in magma reservoirs—The Mount Etna case: *Geology*, v. 44, no. 7, p. 499–502, <https://doi.org/10.1130/G37807.1>.
- Pérez, N.M., Padilla, G.D., Padrón, E., Hernández, P.A., Melián, G.V., Barrancos, J., Dionis, S., Nolasco, D., Rodriguez, F., Calvo, D., and Hernández, Í., 2012, Precursory diffuse CO_2 and H_2S emission signatures of the 2011–2012 El Hierro submarine eruption, Canary Islands: *Geophysical Research Letters*, v. 39, no. 16, <https://doi.org/10.1029/2012GL052410>.
- Prata, A.J. and Bernardo, C., 2014, Retrieval of sulfur dioxide from a ground-based thermal-infrared imaging camera: *Atmospheric Measurement Techniques Discussions*, v. 7, no. 9, p. 2807–2828, <https://doi.org/10.5194/amt-7-2807-2014>.
- Rizzo, A., Jost, H., Caracausi, A., Paonita, A., Liotta, M., and Martelli, M., 2014, Real-time measurements of the concentration and isotope composition of atmospheric and volcanic CO_2 at Mount Etna (Italy): *Geophysical Research Letters*, v. 41, no. 7, p. 2382–2389, <https://doi.org/10.1002/2014GL059722>.
- Roberts, T.J., Braban, C.F., Oppenheimer, C., Martin, R.S., Freshwater, R.A., Dawson, D.H., Griffiths, P.T., Cox, R.A., Saffell, J.R., and Jones, R.L., 2012, Electrochemical sensing of volcanic plumes: *Chemical Geology*, v. 332–333, p. 74–91, <https://doi.org/10.1016/j.chemgeo.2012.08.027>.
- Roberts, T.J., Lurton, T., Giudice, G., Liuzzo, M., Aiuppa, A., Coltelli, M., Vignelles, D., Salerno, G., Couté, B., Chartier, M., Baron, R., Saffell, J.R., and Scaillet, B., 2017, Validation of a novel Multi-Gas sensor for volcanic HCl alongside H_2S and SO_2 at Mt. Etna: *Bulletin of Volcanology*, v. 79, no. 36, <https://doi.org/10.1007/s00445-017-1114-z>.
- Rouwet, D., Sandri, L., Marzocchi, W., Gottsmann, J., Selva, J., Tonini, R., and Papale, P., 2014, Recognizing and tracking volcanic hazards related to non-magmatic unrest—A review: *Journal of Applied Volcanology*, v. 3, no. 17, <https://doi.org/10.1186/s13617-014-0017-3>.
- Salas-Navarro, J., Stix, J., and de Moor, J.M., 2022, A new multi-GAS system for continuous monitoring of CO_2/CH_4 ratios at active volcanoes: *Journal of Volcanology and Geothermal Research*, v. 426, <https://doi.org/10.1016/j.jvolgeores.2022.107533>.
- Sato, M., and McGee, K.A., 1981, Continuous monitoring of hydrogen on the south flank of Mount St. Helens, *in* Lipman, P.W., and Mullineaux, D.R., eds., *The 1980 eruptions of Mount St. Helens*, Washington: U.S. Geological Survey Professional Paper 1250, p. 209–219, <https://doi.org/10.3133/pp1250>.
- Shinohara, H., 2005, A new technique to estimate volcanic gas composition—Plume measurements with a portable multi-sensor system: *Journal of Volcanology and Geothermal Research*, v. 143, p. 319–333, <https://doi.org/10.1016/j.jvolgeores.2004.12.004>.
- Sorey, M.L., Evans, W.C., Kennedy, B.M., Farrar, C.D., Hainsworth, L.J., and Hausback, B., 1998, Carbon dioxide and helium emissions from a reservoir of magmatic gas beneath Mammoth Mountain, California: *Journal of Geophysical Research, Solid Earth*, v. 103, no. B7, p. 15303–15323, <https://doi.org/10.1029/98JB01389>.
- Stebel, K., Amigo, A., Thomas, H., and Prata, A.J., 2015, First estimates of fumarolic SO_2 fluxes from Putana volcano, Chile, using an ultraviolet imaging camera: *Journal of Volcanology and Geothermal Research*, v. 300, p. 112–120, <https://doi.org/10.1016/j.jvolgeores.2014.12.021>.
- Stix, J., de Moor, J.M., Rüdiger, J., Alan, A., Corrales, E., D'Arcy, F., Diaz, J.A., and Liotta, M., 2018, Using drones and miniaturized instrumentation to study degassing at Turrialba and Masaya volcanoes, Central America: *Journal of Geophysical Research, Solid Earth*, v. 123, no. 8, p. 6501–6520, <https://doi.org/10.1029/2018JB015655>.
- Stix, J., Lucic, G., and Malowany, K., 2017, Near real-time field measurements of $\delta^{13}\text{C}$ in CO_2 from volcanoes: *Bulletin of Volcanology*, v. 79, no. 62, <https://doi.org/10.1007/s00445-017-1144-6>.
- Sutton, A.J., McGee, K.A., Casadevall, T.J., and Stokes, J.B., 1992, Fundamental volcanic-gas-study techniques; an integrated approach to monitoring, *in* Ewert, J.W., and Swanson, D.A., eds., *Monitoring volcanoes; techniques and strategies used by the staff of the Cascades Volcano Observatory, 1980–90*: U.S. Geological Survey Bulletin 1966, p. 181–188, https://doi.org/10.3133/b1966_1992.

- Syahbana, D.K., Kasbani, K., Suantika, G., Prambada, O., Andreas, A.S., Saing, U.B., Kunrat, S.L., Andreastuti, S., Martanto, M., Kriswati, E., Suparman, Y., Humaida, H., Ogburn, S., Kelly, P.J., Wellik, J., Wright, H.M.N., Pesicek, J.D., Wessels, R., Kern C., Lisowski, M., Diefenbach, A., Poland, M., Beauducel, F., Pallister, J., Vaughan, R.G., and Lowenstern, J.B., 2019, The 2017–19 activity at Mount Agung in Bali (Indonesia)—Intense unrest, monitoring, crisis response, evacuation, and eruption: *Scientific Reports*, v. 9, no. 8848, <https://doi.org/10.1038/s41598-019-45295-9>.
- Symonds, R.B., Gerlach, T.M. and Reed, M.H., 2001, Magmatic gas scrubbing—Implications for volcano monitoring: *Journal of Volcanology and Geothermal Research*, v. 108, no. 1–4, p. 303–341, [https://doi.org/10.1016/S0377-0273\(00\)00292-4](https://doi.org/10.1016/S0377-0273(00)00292-4).
- Symonds, R.B., Janik, C.J., Evans, W.C., Ritchie, B.E., Counce, D., Poreda, R.J., and Iven, M., 2003a, Scrubbing masks magmatic degassing during repose at Cascade-Range and Aleutian-Arc volcanoes: U.S. Geological Survey Open-File Report 2003–435, 22 p., <https://doi.org/10.3133/ofr03435>.
- Symonds, R.B., Poreda, R.J., Evans, W.C., Janik, C.J., and Ritchie, B.E., 2003b, Mantle and crustal sources of carbon, nitrogen, and noble gases in Cascade-Range and Aleutian-Arc volcanic gases: U.S. Geological Survey Open-File Report 2003–436, 26 p., <https://doi.org/10.3133/ofr03436>.
- Takahashi, K.U., Tsunogai, U., Nakagawa, F., and Sukigara, C., 2019, Stable hydrogen and oxygen isotopic compositions of water vapor in volcanic plumes sampled in glass bottles using cavity ring-down spectroscopy: *Journal of Volcanology and Geothermal Research*, v. 384, p. 232–240, <https://doi.org/10.1016/j.jvolgeores.2019.07.020>.
- Vaselli, O., Tassi, F., Montegrossi, G., Capaccioni, B., and Giannini, L., 2006, Sampling and analysis of volcanic gases: *Acta Vulcanologica*, v. 18, p. 65–76.
- Werner, C., Bergfeld, D., Farrar, C.D., Doukas, M.P., Kelly, P.J., and Kern, C., 2014, Decadal-scale variability of diffuse CO₂ emissions and seismicity revealed from long-term monitoring (1995–2013) at Mammoth Mountain, California, USA: *Journal of Volcanology and Geothermal Research*, v. 289, p. 51–63, <https://doi.org/10.1016/j.jvolgeores.2014.10.020>.
- Werner, C., Chiodini, G., Voigt, D., Caliro, S., Avino, R., Russo, M., Brombach, T., Wyngaard, J., and Brantley, S., 2003, Monitoring volcanic hazard using eddy covariance at Solfatara volcano, Naples, Italy: *Earth and Planetary Science Letters*, v. 210, no. 3–4, p. 561–577, [https://doi.org/10.1016/S0012-821X\(03\)00127-4](https://doi.org/10.1016/S0012-821X(03)00127-4).
- Werner, C.A., Doukas, M.P., and Kelly, P.J., 2011, Gas emissions from failed and actual eruptions from Cook Inlet Volcanoes, Alaska, 1989–2006: *Bulletin of Volcanology*, v. 73, no. 2, p. 155–173, <https://doi.org/10.1007/s00445-011-0453-4>.
- Werner, C., Evans, W.C., Kelly, P.J., McGimsey, R., Pfeffer, M., Doukas, M., and Neal, C., 2012, Deep magmatic degassing versus scrubbing—Elevated CO₂ emissions and C/S in the lead-up to the 2009 eruption of Redoubt Volcano, Alaska: *Geochemistry, Geophysics, Geosystems*, v. 13, no. 3, <https://doi.org/10.1029/2011GC003794>.
- Werner, C., Evans, W.C., Poland, M., Tucker, D.S., and Doukas, M.P., 2009, Long-term changes in quiescent degassing at Mount Baker Volcano, Washington, USA; Evidence for a stalled intrusion in 1975 and connection to a deep magma source: *Journal of Volcanology and Geothermal Research*, v. 186, nos. 3–4, p. 379–386, <https://doi.org/10.1016/j.jvolgeores.2009.07.006>.
- Werner, C., Hurst, T., Scott, B., Sherburn, S., Christenson, B.W., Cole-Baker, J., and Mullan, B., 2008, Variability of passive gas emissions, seismicity, and deformation during crater lake growth at White Island Volcano, New Zealand, 2002–2006: *Journal of Geophysical Research, Solid Earth*, v. 113, no. B1, 15 p., <https://doi.org/10.1029/2007JB005094>.
- Werner, C., Kelly, P.J., Doukas, M., Lopez, T., Pfeffer, M., McGimsey, R., and Neal, C., 2013, Degassing of CO₂, SO₂, and H₂S associated with the 2009 eruption of Redoubt Volcano, Alaska: *Journal of Volcanology and Geothermal Research*, v. 259, p. 270–284, <https://doi.org/10.1016/j.jvolgeores.2012.04.012>.
- Werner, C., Wyngaard, J.C., and Brantley, S.L., 2000, Eddy-correlation measurement of hydrothermal gases: *Geophysical Research Letters*, v. 27, no. 18, p. 2925–2928, <https://doi.org/10.1029/2000GL011765>.

Chapter F



U.S. Geological Survey hydrologist recording data at an unnamed warm spring on the north flank of Mount St. Helens, Washington, where in-situ measurements of conductivity, temperature, and depth were obtained at hourly frequency from 2009 to 2017. Photograph by K. Spicer, U.S. Geological Survey, September 22, 2016.

Chapter F

Streams, Springs, and Volcanic Lakes for Volcano Monitoring

By Steven E. Ingebritsen and Shaul Hurwitz

Introduction

Volcanic unrest can trigger appreciable change to surface waters such as streams, springs, and volcanic lakes. Magma degassing produces gases and soluble salts that are absorbed into groundwater that feeds streams and lakes. As magma ascends, the amount of heat and degassing will increase, and so will any related geochemical and thermal signal. Subsurface magma movement can cause pressurization that alters hydrostatic head and may induce groundwater discharge. Fluid-pressure changes have been linked to distal volcano-tectonic earthquakes (White and McCausland, 2016; Coulon and others, 2017) and phreatic eruptions (for example, Yamaoka and others, 2016). Clearly, changes in groundwater and surface waters are both indicators of unrest and clues to how and where magma is rising toward the surface. Where possible, it is prudent to incorporate real-time hydrologic data into multiparameter monitoring of restless volcanoes. Hydrologic dynamics can also be tracked by changes in groundwater levels that are commonly measured in shallow boreholes (see chapter K, this volume, on boreholes; Hurwitz and Lowenstern, 2024).

Although inferred to be common, relatively few volcano-hydrology anomalies are well documented, and many are essentially anecdotal (Newhall and others, 2001), reflecting the fact that high-resolution time series remain rare. Extreme examples include the 2008 eruption of Nevado del Huila, Colombia, where relatively minor phreatomagmatic eruptions were accompanied by expulsion of as much as 300 million cubic meters of groundwater from fissures high on the volcano (Worni and others, 2011), generating large lahars. Substantial decreases in flow rate from springs about 8 kilometers from the summit of Mayon Volcano, Philippines, have been noted before most eruptions in the 20th century (Newhall and others, 2001). Stream monitoring at Redoubt Volcano in 2009 allowed Werner and others (2012) to recognize that groundwater was unable to absorb (or scrub) the high flux of volcanic gas and that a high CO_2/SO_2 precursor signal had been evident for 5 months prior to the eruption. A key to better interpreting hydrologic anomalies—or even identifying them—is therefore obtaining adequate baseline data.

Most hydrologic monitoring at U.S. volcanoes has been accomplished by intermittent sampling surveys with annual or less frequent sampling (for example, <https://hot.springchem.wr.usgs.gov/index.php>). More frequent sampling, however, generally is needed to establish reliable baselines. A recent hydrologic and hydrothermal monitoring experiment at 25 sites

and 10 of the 12 level 4 (very high threat) volcanoes in the U.S. portion of the Cascade Range demonstrated that there is sufficient temporal variability in hydrothermal fluxes, even during quiescent periods, that one-time measurements will commonly have limited interpretive value (Crankshaw and others, 2018). Thus, surveys are best augmented with data from streamgages (for example, Evans and others, 2004; Bergfeld and others, 2008). Streamflow (water discharge) data allow measured temperature and specific conductance to be converted to heat and solute mass fluxes, which could be insightful parameters for detecting anomalous activity (McCleskey and others, 2012). At the Yellowstone Caldera, long-term monitoring of river solutes has allowed calculation of the chloride flux, a proxy for heat discharge (Hurwitz and others, 2007; McCleskey and others, 2016) from the subsurface magma. This is readily accomplished because data from streamgages are continuously recorded and archived by the U.S. Geological Survey (USGS) National Water Information System (NWIS) (USGS, 2024).

Similar studies on stratovolcanoes or shield volcanoes would be scientifically useful, and yet are logistically challenging, requiring streamgages on numerous radial drainages complemented by either frequent manual sampling or numerous deployments of equipment to measure water temperature and specific conductance as a proxy for water chemistry. Another challenge is that some volcanic areas, especially shield volcanoes, are characterized by near-surface porous rocks and soils, such that surface streams are rare and replaced by distant, dilute large-volume springs with only a trace of any original volcanically sourced water (Manga, 2001; Hurwitz and others, 2021).

Volcanic lakes are worthy of special attention for monitoring efforts, as their temperature and composition can provide evidence of increased flux of volatile-rich fluids from below. Quantifying changes in volatile and heat release from magma can be simpler in lakes than for volcanoes with radial drainages and no major lakes. Moreover, volcanic lakes pose a range of hazards themselves, including phreatomagmatic eruptions, debris flows, flank collapse, tsunamis, and toxic gas release (Mastin and Witter, 2000; Delmelle and others, 2015; Manville, 2015; Rouwet and others, 2015)—hazards that have historically been responsible for substantial loss of life at many volcanoes worldwide (Manville, 2015). Catastrophic CO_2 release at Lake Nyos, Cameroon, in 1986 suffocated about 1,750 people and about 3,500 livestock and was probably triggered by a large landslide into the gas-saturated lake (Kling and others, 1987; Evans and others, 1993). Gas-charged springs in Soda Bay within Clear Lake (California) have caused

almost a dozen deaths to bathers in the past hundred years (ABC News, 2000). A 2005 example of lake overturn and abundant gas release was documented at Mount Chiginagak in Alaska (Schaefer and others, 2008) but did not result in any human casualties.

Although thermally stratified lakes, which promote trapping of exsolved magmatic gas, tend to develop in tropical regions, the phenomenon can also arise where salinity creates meromixis (a condition in which a lake does not mix completely), as occurs in Mono Lake, California (Jellison and Melack, 1993; Jellison and others, 1998).

If magma erupts or flows into a lake, the interaction between hot magma and cold water can be explosive (Mastin and others, 2004; Zimanowski and others, 2015) and substantially expand the area affected by the eruption. Another hazard is the breaching of crater rims by landslides triggered by volcanic and (or) seismic activity. Under some circumstances, substantial volumes of water can be displaced, leading to large floods and lahars. Late Holocene lake flooding from Aniakchak Crater in the Alaska Peninsula (Waythomas, 2022) and from Paulina Lake in Newberry Crater, Oregon (Chitwood and Jensen, 2000), caused by the failure of outlet sills, testify to the substantial hazards at lake-filled calderas.

Several volcanic systems in the United States host lakes known to receive heat and gas from underlying magma. These lakes vary widely in area, depth, and chemical composition. Lakes are present at level 4 volcanoes, including Crater Lake and Newberry Volcano in Oregon; Yellowstone Caldera in Wyoming; Long Valley Caldera, Clear Lake volcanic field, Medicine Lake, and Salton Buttes in California; and Aniakchak Crater, Mount Katmai, Fisher Caldera, Mount Okmok, and Kaguyak Crater, among others, in Alaska. A water lake was present in Halema'uma'u, the crater of Kīlauea, Hawai'i (fig. F1), from October 2019 to December 2020. Level 3 volcanoes with lakes include Mono Lake volcanic field (Calif.), Mount Bachelor (Ore.), Ukinrek Maars and Mount Chiginagak (Alaska), and Soda Lake

(Nevada). In addition, there are lakes at many levels 1 and 2 volcanoes. In the United States, there are no strongly acidic lakes that receive abundant input of magmatic gas, such as those found at Mount Ruapehu (New Zealand), Ijen and Kelud (Indonesia), and Poás (Costa Rica). Nevertheless, many contain fluids that provide clues to magmatic processes below.

Since publication of a previous report on recommended instrumentation for volcano monitoring (Moran and others, 2008), continuous hydrologic monitoring has become increasingly feasible. However, changes in water pressure, temperature, and chemistry remain, in general, poorly studied phenomena at volcanoes (Sparks, 2003; National Academies of Sciences, Engineering, and Medicine, 2017). Recent efforts by the USGS have included the temporary study of Cascade Range volcanoes, which included frequent (15 minute to hourly) temporal sampling of temperature, depth, and conductivity (Crankshaw and others, 2018; Ingebritsen and Evans, 2019). At Yellowstone Caldera, many streamgages have now added thermistors and specific conductance sensors, allowing estimation of time-dependent chloride flux as a proxy for variations in subsurface heat flux (McCleskey and others, 2012, 2016). Efforts to better understand lakes have also accelerated, with bathymetric mapping and sampling carried out at several locations in the United States. Especially thorough work was done at Yellowstone Lake thanks to the Hydrothermal Dynamics of Yellowstone Lake (HD-YLAKE, <https://hdylake.org>) project, funded primarily by the National Science Foundation. In addition to geophysical surveys and recovery of cores and other samples, HD-YLAKE investigations included remotely operated vehicle (ROV) investigations of hydrothermal vents on the lake floor (fig. F2). Data collected by the ROV provided a better understanding of the thermal and chemical influx from lake-bottom hydrothermal systems (Sohn and others, 2017).

Figure F1. Photograph showing U.S. Geological Survey Hawaiian Volcano Observatory geologist measuring lake-surface temperatures using a thermal camera at Kīlauea's short-lived crater lake. Flat areas of lava flow surfaces beyond and above the lake are former sections of the crater floor of Halema'uma'u that subsided hundreds of meters during the 2018 caldera collapse. Yellow areas are regions of substantial sulfur precipitation. Photograph by K. Mulliken, U.S. Geological Survey, December 18, 2019.





Figure F2. Photograph showing scientists aboard research vessel (RV) *Annie II* monitoring control room video of the remotely operated vehicle (ROV) *Yogi* being deployed in Yellowstone Lake, Wyoming, August 2017. The ROV made heat-flow measurements at a thermal field on the lake floor as part of the multiyear Hydrothermal Dynamics of Yellowstone Lake (HD-YLAKE) project (Sohn and others, 2017). Photograph by S. Hurwitz, U.S. Geological Survey.

In this chapter, we focus on detecting changes in the chemistry, temperature, discharge, or water levels of streams, springs, and lakes that can be caused by seismicity, volumetric strains, or increases in gas flux associated with ascending magma. There is unavoidable overlap with other chapters of this report. Samples of water and gas can also be obtained in boreholes (chapter K, this volume; Hurwitz and Lowenstern, 2024), both shallow and deep. Gas monitoring (chapter E, this volume; Lewicki and others, 2024) relies in part on samples from springs and wells, particularly where measurable gas plumes are absent. Water acts as a trigger and lubricant for landslides and sediment-rich floods, and so hydrology has obvious relevance for lahar monitoring, as discussed in chapter H (this volume; Thelen and others, 2024). Shared situational awareness among scientists engaged in geophysical, gas, and hydrologic monitoring will improve overall understanding of the volcanic hazard.

Instrumentation Relevant to Streams, Springs, and Lakes

Most continuous, long-term hydrologic monitoring to date has emphasized a subset of relatively easy-to-measure parameters, namely water level, temperature, and electrical conductivity. Commercial off-the-shelf instrumentation now includes devices that can measure conductivity, temperature, and depth (that is, CTD) within a stream, lake, or well. They typically contain a memory cache that can store several years of data collected at hourly intervals (or less time for more frequent sampling), and

data can be retrieved in the field without removing the sensor itself. When needed, these data can be telemetered in real time. Site conditions on volcanoes commonly pose severe challenges for continuous sensors, including high-temperature and corrosive waters and energetic and (or) sediment-laden streams. However, sensor technology and reliability continue to improve.

Water flow rates are measured through streamgaging techniques where the rate of water flow is measured at a standard depth above the streambed and combined with a survey of the stream's cross-sectional area. By performing similar measurements at different flow rates (usually at different times of the year), a rating curve can be developed to allow measurements of a stream's stage to be correlated with water discharge. A typical USGS NWIS installation at a streamgage measures flow rate but can also include sensors for air and water temperature, precipitation, and specific conductance (electrical conductivity). These parameters can be converted to heat or mass flux as well as ionic species of interest (McCleskey and others, 2012). Ion-specific probe technology continues to evolve, and it may soon be possible to directly sense and quantify concentrations of species of interest, such as dissolved inorganic carbon, chloride, sulfate, boron, arsenic, and mercury.

Another useful instrument for background or long-term studies is an autosampler that pumps water into a series of sample containers at a set interval (hourly, daily, weekly, and so on) for later manual retrieval and laboratory analysis of a time series (Ono and others, 2020). This automation greatly enhances the efficiency of baseline investigations to understand the dynamics of hydrothermal discharge that may be characterized by diurnal, seasonal, or climatic variations.

Recommended Capabilities

Detect Changes in Chemistry, Temperature, Discharge, or Water Levels of Streams and Springs

During unrest, information on hydrologic changes represents a key part of multiparameter monitoring. Such data can reveal important subsurface changes to the magmatic system, with relevance to eruption forecasts. Ideally, hydrologic data will be automatically collected and delivered to the observatory along with geophysical data. However, only rarely is this currently the case. Hydrologic monitoring, like gas monitoring, generally requires more human involvement than geophysical monitoring; only limited information can be obtained from unattended instrumentation. Safety factors can complicate rapid response during unrest, limiting where samples can be obtained and new instrumentation installed. Another persistent challenge is latency with respect to laboratory-based geochemical measurement of key constituents, such as isotope ratios.

To optimize sampling, and placement of appropriate instrumentation during unrest, it is important to develop an understanding of baseline hydrothermal activity in the volcanic system. This requires a consistent program of water sampling for chemical analysis and extended deployments of samplers. The relation between geochemical and thermal anomalies in water and volcanic unrest may be difficult to assess without volcano-specific conceptual models and sufficient baseline data. Moreover, water sampling during unrest episodes at Mammoth Mountain, Calif. (Evans and others, 2002); Three Sisters, Ore. (Evans and others, 2004); and Mount St. Helens, Wash. (Bergfeld and others, 2008), has shown that not all springs and streams on a volcano will respond to unrest. This makes it difficult to determine in advance the optimal placement of monitoring sites.

Long (multiyear) and high-resolution (hourly or better) hydrologic time series are ideal for determining whether hydrologic anomalies are related to volcanic unrest, including residual effects of previous intrusions or eruptions, or to nonvolcanic phenomena such as changes in meteoric-water flux, tectonic earthquakes, and anthropogenic influences. Yet sampling logistics are highly variable. Although some sampling sites are within reach of roads (some locations at Yellowstone National Park and Clear Lake volcanic field), others are high on the slopes of remote volcanoes like Glacier Peak, Wash. Although sensor technology is fast evolving, there are still few commercial off-the-shelf instruments that can measure relevant parameters and sustain multiyear deployment in sometimes hot, chemically aggressive waters. For these and other reasons, hydrologic monitoring strategies are still evolving, and a generic standard has yet to be defined and agreed upon.

Recommendations

At levels 1 and 2 volcanoes, we recommend an inventory of spring, stream, and well sites to identify those with indications of ongoing magmatic influence such as elevated $^3\text{He}/^4\text{He}$ ratios, large fluxes of magmatic CO_2 , or anomalous heat fluxes. This would

require a field visit, sampling, basic measurements (temperature, pH, and specific conductance), and subsequent laboratory analysis for major element chemistry and isotope ratios, potentially including those of carbon, oxygen, hydrogen, and helium. Level 3 volcanoes would ideally have similar background studies, combined with resampling every 5 to 10 years to gradually define baseline conditions and develop rating curves. Those springs and streams with clear magmatic signals and accessible sites may be targeted for longer term studies with deployed commercial off-the-shelf CTD sensors and autosamplers. At level 4 volcanoes, appropriate sites would ideally be characterized such that baseline parameters allow quantitative assessment of variability caused by factors such as tectonic earthquakes and semidiurnal and seasonal (for example, barometric and tidal) influences. Regular sampling surveys along all major drainages will better define baseline characteristics and behavior. We recommend installation of instrumentation for multiyear (3–5 year) periods to collect hourly (or better) information on heat flux and magmatically derived solutes. Sampling surveys should include water chemistry and temperature. Combined with measurements of spring- and streamflow, these surveys would permit calculation of the mass flow rate of magma-derived constituents. Moreover, at selected level 4 volcanoes, we encourage continuous real-time monitoring of hydrologic parameters, targeting springs, and (or) streams that are known or likely to be influenced by magmatic processes. The number and type of instruments would be tailored to site-specific considerations and reflect evolving technology. Periodic sampling and streamgaging would ideally be performed to calibrate sensors and establish rating curves for dissolved species of interest and streamflow, allowing mass flowrates of magma-derived constituents to be calculated continuously. Because many level 4 volcanoes are remote, observatories would need to prioritize work based on relative threat level, exposed population, logistical complexity, cost, and other factors.

Monitor and Characterize Geochemical and Geophysical Changes in Volcanic Lakes

Changes in volcanic lakes, for example deformation on the lake floor, are by nature less accessible than changes in springs and streams. The three-dimensional nature of volcanic lakes similarly requires different approaches, including geophysical techniques, to monitor and characterize changes. Baseline data would help guide future monitoring and hazard assessment. These include bathymetric and heat-flow mapping, characterization of hydrothermal vents and the three-dimensional distribution of temperature, salinity, and dissolved species of magmatic origin in lake waters. These measurements will enable quantification of heat and gas into, and out of, the lake—information that is required to assess the potential for lake overturns and release of toxic gases into the atmosphere.

Many of these basic studies and follow-up monitoring operations would build upon developments in oceanic research, including advances in seafloor geodesy (Bürgmann and Chadwell, 2014) and the establishment of a cabled observatory at Axial Seamount off the Pacific Northwest coast (Kelley and others, 2014). Lessons can also be learned from the 1-year deployment

of lake-bottom seismometers in Yellowstone Lake (for example, Smalls and others, 2019) and from echo-sounder deployments at Kelud, Indonesia, which tracked changes in gas discharge into the crater lake several months before volcanic eruptions (Vandemeulebrouck and others, 2000; Caudron and others, 2012). Echo sounding takes advantage of the large acoustic impedance contrast between water and gas bubbles. All these technological developments should help to establish monitoring systems unique to volcanic lakes and will likely be best accomplished with collaborators from the ocean-sciences community.

Volcanic and (or) magmatic heat and gas inputs into active volcanic lakes are either focused through hydrothermal vents or are more diffuse throughout most of the lakebed (for example, Pasternack and Varekamp, 1997; Varekamp, 2015). Lakes that are hydrothermally active and deemed to pose a threat to communities and infrastructure should be monitored by continuous instruments. Fundamental data needed to monitor volcanic lakes include temperature, water level, water depth, and visual observations of color and physical state. The temperatures of volcanic lakes are determined primarily by the magnitude of the volcanic heat influx relative to the surface area of the lake; other factors include the temperature and influx rate of groundwater or surface water. Smaller lakes exhibit rapid temperature increases with only small heat inputs, whereas large lakes are buffered against variations in heat input (Pasternack and Varekamp, 1997). Changes in heat and gas discharge into lakes can be early indicators of ascending magma. Total emission rates can be substantially underestimated, and the chemical and isotopic composition of the gas altered, when gases exsolved from magma are dissolved into lake water instead of escaping directly into the atmosphere (for example, Varekamp, 2015). Lake-floor deformation stations and chemical sensors that can track changes in the composition of thermal water flowing into lakes would also provide valuable information.

Because lake levels are influenced by climate and weather, meteorological stations are also needed near monitored lakes. Geophysical surveys (primarily seismic reflection and magnetics) can provide additional information on the location of hydrothermal vents and deposits (for example, Johnson and others, 2003; Brothers and others, 2009).

Instrumentation

Cameras are essential for real-time visual monitoring of changes in volcanic lakes; they provide valuable context for evaluating changes in other monitoring data (see chapter G, this volume, on tracking surface changes; Orr and others, 2024). Image acquisition rates must be tailored to the possible timescales of activity. Quiescent baseline activity could be tracked with low image rates (images every few minutes to tens of minutes), but more dynamic activity, such as lake agitation or small explosions, requires higher rates (one or more images every second) and higher resolution. A hybrid approach in bandwidth-limited scenarios involves low image rates transmitted over a network coupled with high image rates stored locally at the camera site and collected manually for later analysis.

Quantitatively tracking lake color can be accomplished with a handheld colorimeter. Objective measurements of color

may presage future hazards, as lake color can reflect water chemistry (Ohsawa and others, 2010). The USGS Hawaiian Volcano Observatory used a Konica-Minolta CS-160 colorimeter to measure color at Kīlauea's short-lived summit lake during field campaigns in 2019. Such colorimeters might be modified to operate in a continuous mode with data transmitted to the observatory.

Thermal cameras offer a tool for remote temperature monitoring if the lake is not approachable. Thermal cameras transmitting images in real time to the observatory provide continuous monitoring (Patrick and others, 2014). One benefit of thermal imaging is that the data can be collected at night. Thermal data can also be obtained via satellite; for example, Advanced Spaceborne Thermal Emission and Reflection Radiometer (ASTER) data were used to reconstruct temperatures at Copahue crater lake (on the border of Argentina and Chile) during a quiescent period between eruptions in 2000 and 2012 (Candela-Becerra and others, 2020). The analysis revealed surface temperature variations of as high as 15 degrees Celsius in two different periods and a substantial temperature decrease prior to the December 2012 eruption.

Gas flux from lakes can be monitored by techniques outlined in chapter E on gas monitoring (this volume; Lewicki and others, 2024), including multicomponent gas analyzer systems, accumulation chambers (fig. F3), and eddy covariance. Gas flow near vents could also be monitored by hydroacoustic and echo-sounding methods (for example, Rouwet and others, 2014, and references therein).



Figure F3. Photograph showing U.S. Geological Survey California Volcano Observatory geologist measuring CO₂ flux on the surface of East Lake, Newberry Crater, Oregon. Photograph by L. Clor, U.S. Geological Survey, July 29, 2020.

Unoccupied aircraft systems (UAS) (discussed in chapter L, this volume; Diefenbach, 2024) offer a new means of monitoring hydrologic activity at volcanic lakes through direct water sampling. Thermal cameras onboard UAS can provide near-field remote measurements of water temperature, and repeat surveys can be flown for temperature-change detection. UAS also facilitate direct sampling to support geochemical monitoring of volcanic lakes (for example, Terada and others, 2018; Nadeau and others, 2020).

Recommendations

Lake monitoring is not required at every volcano; relatively few volcanoes have lakes, and some of those are in remote areas and pose little risk. There are, however, some volcanic lakes where the hazards could affect society. Monitoring of those lakes would ideally be done at a level commensurate with the associated risk.

No continuous monitoring is recommended for lakes on levels 1 and 2 volcanoes, but background data would ideally be collected consistent with the goals for detecting changes in streams and springs. At lakes on level 3 volcanoes, we recommend characterizing baseline geochemical and geophysical properties to guide future monitoring. Baseline surveys would ideally include bathymetric and heat-flow mapping, identification of hydrothermal vents, and, in some cases, mapping the three-dimensional distribution of temperature, salinity, and dissolved gas. For lakes at level 4 volcanoes, we recommend the same background surveys as for lakes on level 3 volcanoes but increasing the degree to which continuous real-time data are collected. The number and type of instruments should be tailored to site-specific considerations and reflect evolving technology, but would ideally include temperature, surface activity, gas emissions, and chemistry, supplemented by regular surveys and sampling as appropriate. At lakes with active hydrothermal vents, campaign and (or) real-time measurements of vent temperature, discharge, and chemistry would be made to quantitatively assess variability caused by factors such as magmatic activity, tectonic earthquakes, and semidiurnal and seasonal (for example, barometric pressure and tidal) influences.

General Recommendations and Considerations

In this chapter, we make suggestions for background studies, temporary deployments, and potential real-time data from hydrologic features to inform volcano monitoring. There will be inevitable overlap with the strategies and goals outlined in chapter E of this volume on monitoring gas (Lewicki and others, 2024), as water and gases can reflect geothermal and magma-sourced components. Moreover, hydrologic monitoring might include looking at dissolved gases, and gas monitoring would need to consider the effects of gas-water-rock interaction, thus requiring careful coordination for acquisition of the optimal parameters. One difference between monitoring gases and water is that the latter may require a more regional approach, recognizing that water and springs may discharge miles away from volcanic centers, whereas

gas flow is generally more vertically directed in the crust and studies would be focused higher on the volcanic edifice.

References Cited

- ABC News, 2000, Hot spring may have claimed another victim: ABC News, September 25, 2000, accessed April 15, 2024, at <https://abcnews.go.com/Technology/story?id=119923&page=1>.
- Bergfeld, D., Evans, W.C., McGee, K.A., and Spicer, K.R., 2008, Pre- and post-eruptive investigations of gas and water samples from Mount St. Helens, Washington, 2002 to 2005, *in* Sherrod, D.R., Scott, W.E., and Stauffer, P.H., eds., *A volcano rekindled—The renewed eruption of Mount St. Helens, 2004–2006*: U.S. Geological Survey Professional Paper 1750, p. 523–542, <https://doi.org/10.3133/pp175025>.
- Brothers, D.S., Driscoll, N.W., Kent, G.M., Harding, A.J., Babcock, J.M., and Baskin, R.L., 2009, Tectonic evolution of the Salton Sea inferred from seismic reflection data: *Nature Geoscience*, v. 2, p. 581–584, <https://doi.org/10.1038/ngeo590>.
- Bürgmann, R., and Chadwell, D., 2014, Seafloor geodesy: *Annual Review of Earth and Planetary Sciences*, v. 42, p. 509–534, <https://doi.org/10.1146/annurev-earth-060313-054953>.
- Candela-Becerra, L.J., Toyos, G., Suárez-Herrera, C.A., Castro-Godoy, S., and Agosto, M., 2020, Thermal evolution of the Crater Lake of Copahue Volcano with ASTER during the last quiescence period between 2000 and 2012 eruptions: *Journal of Volcanology and Geothermal Research*, v. 392, article no. 106752, <https://doi.org/10.1016/j.jvolgeores.2019.106752>.
- Caudron, C., Mazot, A., and Bernard, A., 2012, Carbon dioxide dynamics in Kelud volcanic lake: *Journal of Geophysical Research, Solid Earth*, v. 117, no. B5, <https://doi.org/10.1029/2011JB008806>.
- Chitwood, L.A., and Jensen, R.A., 2000, Large prehistoric flood along Paulina Creek, Newberry Volcano, Oregon—What's New at Newberry Volcano, Oregon: *Guidebook for the Friends of the Pleistocene Eighth Annual Pacific Northwest Cell Field Trip*, p. 31–40.
- Coulon, C.A., Hsieh, P.A., White, R., Lowenstern, J.B., and Ingebritsen, S.E., 2017, Causes of distal volcano-tectonic seismicity inferred from hydrothermal modeling: *Journal of Volcanology and Geothermal Research*, v. 345, p. 98–108, <https://doi.org/10.1016/j.jvolgeores.2017.07.011>.
- Crankshaw, I.M., Archfield, S.A., Newman, A.C., Bergfeld, D., Clor, L.E., Spicer, K.R., Kelly, P.J., Evans, W.C., and Ingebritsen, S.E., 2018, Multi-year high-frequency hydrothermal monitoring of selected high-threat Cascade Range volcanoes: *Journal of Volcanology and Geothermal Research*, v. 356, p. 24–35, <https://doi.org/10.1016/j.jvolgeores.2018.02.014>.

- Diefenbach, A.K., 2024, Special topic—Unoccupied aircraft systems, chap. L of Flinders, A.F., Lowenstern, J.B., Coombs, M.L., and Poland, M.P., eds., Recommended capabilities and instrumentation for volcano monitoring in the United States: U.S. Geological Survey Scientific Investigations Report 2024–5062–L, 5 p., <https://doi.org/10.3133/sir20245062L>.
- Delmelle, P., Henley, R.W., and Bernard, A., 2015, Volcano-related lakes, chap. 48 of Sigurdsson, H., Houghton, B.F., McNutt, S.R., Rymer, H., and Stix, J., eds., *The Encyclopedia of Volcanoes* (2d ed.): San Diego, Academic Press, p. 851–864, <https://doi.org/10.1016/B978-0-12-385938-9.00048-1>.
- Evans, W.C., Kling, G.W., Tuttle, M.L., Tanyileke, G., and White, L.D., 1993, Gas buildup in Lake Nyos, Cameroon—The recharge process and its consequences: *Applied Geochemistry*, v. 8, no. 3, p. 207–221, [https://doi.org/10.1016/0883-2927\(93\)90036-G](https://doi.org/10.1016/0883-2927(93)90036-G).
- Evans, W.C., Sorey, M.L., Cook, A.C., Kennedy, B.M., Shuster, D.L., Colvard, E.M., White, L.D., and Huebner, M.A., 2002, Tracing and quantifying magmatic carbon discharge in cold groundwaters—Lessons learned from Mammoth Mountain, USA: *Journal of Volcanology and Geothermal Research*, v. 114, nos. 3–4, p. 291–312, [https://doi.org/10.1016/S0377-0273\(01\)00268-2](https://doi.org/10.1016/S0377-0273(01)00268-2).
- Evans, W.C., van Soest, M.C., Mariner, R.H., Hurwitz, S., Ingebritsen, S.E., Wicks, C.W., Jr., and Schmidt, M.E., 2004, Magmatic intrusion west of Three Sisters, central Oregon, USA—The perspective from spring geochemistry: *Geology*, v. 32, p. 69–72, <https://doi.org/10.1130/G19974.1>.
- Hurwitz, S., and Lowenstern, J.B., 2024, Special topic—Boreholes, chap. K of Flinders, A.F., Lowenstern, J.B., Coombs, M.L., and Poland, M.P., eds., Recommended capabilities and instrumentation for volcano monitoring in the United States: U.S. Geological Survey Scientific Investigations Report 2024–5062–K, 5 p., <https://doi.org/10.3133/sir20245062K>.
- Hurwitz, S., Lowenstern, J.B., and Heasler, H., 2007, Spatial and temporal geochemical trends in the hydrothermal system of Yellowstone National Park—Inferences from river solute fluxes: *Journal of Volcanology and Geothermal Research*, v. 162, nos. 3–4, p. 149–171, <https://doi.org/10.1016/j.jvolgeores.2007.01.003>.
- Hurwitz, S., Peek, S.E., Scholl, M.A., Bergfeld, D., Evans, W.C., Kauahikaua, J.P., Gingerich, S.B., Hsieh, P.A., Lee, R.L., Younger, E.F., and Ingebritsen, S.E., 2021, Groundwater dynamics at Kīlauea Volcano and vicinity, Hawai‘i, chap. F of Patrick, M., Orr, T., Swanson, D., and Houghton, B., eds., *The 2008–2018 summit lava lake at Kīlauea Volcano, Hawai‘i*: U.S. Geological Survey Professional Paper 1867, 28 p., <https://doi.org/10.3133/pp1867F>.
- Ingebritsen, S.E., and Evans, W.C., 2019, Potential for increased hydrothermal arsenic flux during volcanic unrest—Implications for California water supply: *Applied Geochemistry*, v. 108, article no. 104384, <https://doi.org/10.1016/j.apgeochem.2019.104384>.
- Jellison, R., and Melack, J.M., 1993, Meromixis in hypersaline Mono Lake, California. 1. Stratification and vertical mixing during the onset, persistence, and breakdown of meromixis: *Limnology and Oceanography*, v. 38, p. 1008–1019, <https://doi.org/10.4319/lo.1993.38.5.1008>.
- Jellison, R., Romero, J., and Melack, J.M., 1998, The onset of meromixis during restoration of Mono Lake, California—Unintended consequences of reducing water diversions: *Limnology and Oceanography*, v. 43, p. 706–711, <https://doi.org/10.4319/lo.1998.43.4.0706>.
- Johnson, S.Y., Stephenson, W.J., Morgan, L.A., Shanks, W.C., III, and Pierce, K.L., 2003, Hydrothermal and tectonic activity in northern Yellowstone Lake, Wyoming: *Geological Society of America Bulletin*, v. 115, p. 954–971, <https://doi.org/10.1130/B25111.1>.
- Kelley, D.S., Delaney, J.R., and Juniper, S.K., 2014, Establishing a new era of submarine volcanic observatories—Cabling Axial Seamount and the Endeavour Segment of the Juan de Fuca Ridge: *Marine Geology*, v. 352, p. 426–450, <https://doi.org/10.1016/j.margeo.2014.03.010>.
- Kling, G.W., Clark, M.A., Wagner, G.N., Compton, H.R., Humphrey, A.M., Devine, J.D., Evans, W.C., Lockwood, J.P., Tuttle, M.L., and Koenigsberg, E.J., 1987, The 1986 Lake Nyos gas disaster in Cameroon, West Africa: *Science*, v. 236, no. 4798, <https://doi.org/10.1126/science.236.4798.169>.
- Lewicki, J.L., Kern, C., Kelly, P.J., Nadeau, P.A., Elias, T., and Clor, L.E., 2024, Volcanic gas monitoring, chap. E of Flinders, A.F., Lowenstern, J.B., Coombs, M.L., and Poland, M.P., eds., Recommended capabilities and instrumentation for volcano monitoring in the United States: U.S. Geological Survey Scientific Investigations Report 2024–5062–E, 11 p., <https://doi.org/10.3133/sir20245062E>.
- Manga, M., 2001, Using springs to study groundwater flow and active geologic processes: *Annual Review of Earth and Planetary Sciences*, v. 29, p. 201–228, <https://doi.org/10.1146/annurev.earth.29.1.201>.
- Manville, V., 2015, Volcano-hydrologic hazards from volcanic lakes, in *Volcanic Lakes*: Springer, Berlin, Heidelberg, p. 21–71, https://doi.org/10.1007/978-3-642-36833-2_2.
- Mastin, L.G., Christiansen, R.L., Thornber, C., Lowenstern, J., and Beeson, M., 2004, What makes hydromagmatic eruptions violent? Some insights from the Keanakāko‘i Ash, Kīlauea Volcano, Hawai‘i: *Journal of Volcanology and Geothermal Research*, v. 137, p. 15–31.

- Mastin, L.G., and Witter, J.B., 2000, The hazards of eruptions through lakes and seawater: *Journal of Volcanology and Geothermal Research*, v. 97, p. 195–214, [https://doi.org/10.1016/S0377-0273\(99\)00174-2](https://doi.org/10.1016/S0377-0273(99)00174-2).
- McCleskey, R.B., Clor, L.E., Lowenstern, J.B., Evans, W.C., Nordstrom, D.K., Heasler, H., and Huebner, M.A., 2012, Solute and geothermal flux monitoring using electrical conductivity in the Madison, Firehole, and Gibbon Rivers, Yellowstone National Park: *Applied Geochemistry*, v. 27, no. 12, p. 2370–2381, <https://doi.org/10.1016/j.apgeochem.2012.07.019>.
- McCleskey, R.B., Lowenstern, J.B., Schaper, J., Nordstrom, D.K., Heasler, H.P., and Mahony, D., 2016, Geothermal solute flux monitoring and the source and fate of solutes in the Snake River, Yellowstone National Park, WY: *Applied Geochemistry*, v. 73, p. 142–156, <https://doi.org/10.1016/j.apgeochem.2016.08.006>.
- Moran, S.C., Freymueller, J.T., LaHusen, R.G., McGee, K.A., Poland, M.P., Power, J.A., Schmidt, D.A., Schneider, D.J., Stephens, G., Werner, C.A., and White, R.A., 2008, Instrumentation recommendations for volcano monitoring at U.S. volcanoes under the National Volcano Early Warning System: U.S. Geological Survey Scientific Investigations Report 2008–5114, 47 p., <https://doi.org/10.3133/sir20085114>.
- Nadeau, P. A., Diefenbach, A.K., Hurwitz, S., and Swanson, D.A., 2020, From lava to water—A new era at Kīlauea: *Eos*, v. 101, <https://doi.org/10.1029/2020EO149557>.
- National Academies of Sciences, Engineering, and Medicine, 2017, Volcanic eruptions and their repose, unrest, precursors, and timing: The National Academies Press, Washington, D.C., 134 p., <https://doi.org/10.17226/24650>.
- Newhall, C.G., Albano, S.E., Matsumoto, N., and Sandoval, T., 2001, Roles of groundwater in volcanic unrest: *Journal of the Geological Society of the Philippines*, v. 56, p. 69–84.
- Ohsawa, S., Saito, T., Yoshikawa, S., Mawatari, H., Yamada, M., Amita, K., Takamatsu, N., Sudo, Y., and Kagiya, T., 2010, Color change of lake water at the active crater lake of Aso volcano, Yudamari, Japan—Is it in response to change in water quality induced by volcanic activity?: *Limnology*, v. 11, p. 207–215, <https://doi.org/10.1007/s10201-009-0304-6>.
- Ono, T., Mori, T., and Tsunomori, F., 2020, High-frequency field auto-sampling of volcanic waters discharged near craters of active volcanoes: *Bulletin of Volcanology*, v. 82, no. 2, p. 1–15, <https://doi.org/10.1007/s00445-020-1357-y>.
- Orr, T.R., Dietterich, H.R., and Poland, M.P., 2024, Tracking surface changes caused by volcanic activity, chap. G of Flinders, A.F., Lowenstern, J.B., Coombs, M.L., and Poland, M.P., eds., Recommended capabilities and instrumentation for volcano monitoring in the United States: U.S. Geological Survey Scientific Investigations Report 2024–5062–G, 11 p., <https://doi.org/10.3133/sir20245062G>.
- Pasternack, G.B., and Varekamp, J.C., 1997, Volcanic lake systematics—I. Physical constraints: *Bulletin of Volcanology*, v. 58, p. 528–538, <https://doi.org/10.1007/s004450050160>.
- Patrick, M.R., Orr, T., Antolik, L., Lee, L., and Kamibayashi, K., 2014, Continuous monitoring of Hawaiian volcanoes with thermal cameras: *Journal of Applied Volcanology*, v. 3, no. 1, p. 1–19, <https://doi.org/10.1186/2191-5040-3-1>.
- Rouwet, D., Christenson, B., Tassi, F., and Vandemeulebrouck, J., eds., 2015, Volcanic lakes: Springer-Verlag, Berlin, Heidelberg, 533 p., <https://doi.org/10.1007/978-3-642-36833-2>.
- Rouwet, D., Sandri, L., Marzocchi, W., Gottsmann, J., Selva, J., Tonini, R., and Papale, P., 2014, Recognizing and tracking volcanic hazards related to non-magmatic unrest—A review: *Journal of Applied Volcanology*, v. 3, no. 17, <https://doi.org/10.1186/s13617-014-0017-3>.
- Schaefer, J.R., Scott, W.E., Evans, W.C., Jorgenson, J., McGimsey, R.G., and Wang, B., 2008, The 2005 catastrophic acid crater lake drainage, lahar, and acidic aerosol formation at Mount Chiginagak volcano, Alaska, USA—Field observations and preliminary water and vegetation chemistry results: *Geochemistry, Geophysics, Geosystems*, v. 9, no. 7, <https://doi.org/10.1029/2007GC001900>.
- Smalls, P.T., Sohn, R.A., and Collins, J.A., 2019, Lake-bottom seismograph observations of microseisms in Yellowstone Lake: *Seismological Research Letters*, v. 90, p. 1200–1208, <https://doi.org/10.1785/0220180242>.
- Sohn, R., Harris, R., Linder, C., Luttrell, K., Lovalvo, D., Morgan, L., Seyfried, W., and Shanks, P., 2017, Exploring the restless floor of Yellowstone Lake: *Eos*, v. 98, <https://doi.org/10.1029/2017EO087035>.
- Sparks, R.S.J., 2003, Forecasting volcanic eruptions: *Earth and Planetary Science Letters*, v. 210, nos. 1–2, p. 1–15, [https://doi.org/10.1016/S0012-821X\(03\)00124-9](https://doi.org/10.1016/S0012-821X(03)00124-9).
- Terada, A., Morita, Y., Hashimoto, T., Mori, T., Ohba, T., Yaguchi, M., and Kanda, W., 2018, Water sampling using a drone at Yugama crater lake, Kusatsu-Shirane volcano, Japan: *Earth, Planets and Space*, v. 70, no. 64, <https://doi.org/10.1186/s40623-018-0835-3>.
- Thelen, W.A., Lyons, J.J., Iezzi, A.M., and Moran, S.C., 2024, Monitoring lahars and debris flows, chap. H of Flinders, A.F., Lowenstern, J.B., Coombs, M.L., and Poland, M.P., eds., Recommended capabilities and instrumentation for volcano monitoring in the United States: U.S. Geological Survey Scientific Investigations Report 2024–5062–H, 6 p., <https://doi.org/10.3133/sir20245062H>.
- U.S. Geological Survey [USGS], 2024, USGS water data for the Nation: U.S. Geological Survey National Water Information System database, accessed April 15, 2024, at <https://doi.org/10.5066/F7P55KJN>.

- Vandemeulebrouck, J., Sabroux, J.C., Halbwachs, M., Poussielgue, N., Grangeon, J., and Tabbagh, J., 2000, Hydroacoustic noise precursors of the 1990 eruption of Kelut Volcano, Indonesia: *Journal of Volcanology and Geothermal Research*, v. 97, nos. 1–4, p. 443–456, [https://doi.org/10.1016/S0377-0273\(99\)00176-6](https://doi.org/10.1016/S0377-0273(99)00176-6).
- Varekamp, J.C., 2015, The chemical composition and evolution of volcanic lakes, *in* Rouwet, D., Christenson, B., Tassi, F., Vandemeulebrouck, J., eds., *Volcanic Lakes*: Springer, Berlin, Heidelberg, p. 93–123, https://doi.org/10.1007/978-3-642-36833-2_4.
- Waythomas, C.F., 2022, Selected crater and small caldera lakes in Alaska—Characteristics and hazards: *Frontiers in Earth Science*, v. 9, <https://doi.org/10.3389/feart.2021.751216>.
- Werner, C., Evans, W.C., Kelly, P.J., McGimsey, R., Pfeffer, M., Doukas, M., and Neal, C., 2012, Deep magmatic degassing versus scrubbing—Elevated CO₂ emissions and C/S in the lead-up to the 2009 eruption of Redoubt Volcano, Alaska: *Geochemistry, Geophysics, Geosystems*, v. 13, no. 3, <https://doi.org/10.1029/2011GC003794>.
- White, R., and McCausland, W., 2016, Volcano-tectonic earthquakes—A new tool for estimating intrusive volumes and forecasting eruptions: *Journal of Volcanology and Geothermal Research*, v. 309, p. 139–155, <https://doi.org/10.1016/j.jvolgeores.2015.10.020>.
- Worni, R., Huggel, C., Stoffel, M., and Pulgarin, B., 2011, Challenges of modeling current very large lahars at Nevado del Huila Volcano, Colombia: *Bulletin of Volcanology*, v. 74, p. 309–324, <https://doi.org/10.1007/s00445-011-0522-8>.
- Yamaoka, K., Geshi, N., Hashimoto, T., Ingebritsen, S.E., and Oikawa, T., 2016, Special issue “The phreatic eruption of Mt. Ontake volcano in 2014”: *Earth, Planets and Space*, v. 68, no. 175, <https://doi.org/10.1186/s40623-016-0548-4>.
- Zimanowski, B., Büttner, R., Dellino, P., White, J.D.L., and Wohletz, K.H., 2015, Magma-water interaction and phreatomagmatic fragmentation, chap. 26 *of* Sigurdsson, H., Houghton, B.F., McNutt, S.R., Rymer, H., and Stix, J., eds, *The Encyclopedia of Volcanoes*: San Diego, Academic Press, p. 473–484, <https://doi.org/10.1016/B978-0-12-385938-9.00026-2>.

Chapter G



Photograph from the northwest rim of Kīlauea, Hawai'i, of the resumption of lava lake activity within Halema'uma'u following a new eruption on September 29, 2021. The photograph was taken shortly after the eruption began and shows two web cameras and volcanic fissures producing lava that is accumulating within the crater. This was the second summit eruption after the devastating 2018 caldera collapse and lasted over a year, until December 9, 2022. Photograph by L. Gallant, U.S. Geological Survey, September 30, 2021.

Chapter G

Tracking Surface Changes Caused by Volcanic Activity

By Tim R. Orr, Hannah R. Dietterich, and Michael P. Poland

Introduction

Dynamic volcanic landscapes produce various changes at the surface of volcanic edifices. For example, rising magma can induce thermal emissions, formation of ground cracks, and variations in glacier and edifice morphology; volcanic deposits from eruptions can transform the land surface with tephra fall, pyroclastic flows, lava flows and domes, and lahars; and geomorphic changes from landslides and lahars can occur in the absence of unrest or eruption.

The best way to detect these changes is with imagery obtained via satellite, aircraft (including unoccupied aircraft systems, or UAS), and ground-based imaging. Rapid advances in imaging technologies have been leveraged by the U.S. Geological Survey (USGS) Volcano Hazards Program to improve the ability to monitor volcanoes. To this end, the guidance outlined here provides a framework for tracking volcanic unrest and the emplacement and evolution of volcanic deposits, further elucidating the processes associated with volcanic eruptions. The techniques currently used include (1) various telemetered and non-telemetered cameras, (2) high-resolution ground-based optical (visible to short-wave infrared wavelengths) and thermal infrared photography, (3) satellite and airborne thermal, optical, and synthetic aperture radar (SAR) imagery, and (4) light detection and ranging (lidar) surveys from airborne and ground-based platforms. Given that similar or overlapping techniques are applied to meet the capabilities listed in this chapter, we first provide an overview of remote sensing techniques. The use of UAS in monitoring surface change is briefly mentioned in this chapter and described in more detail in the dedicated UAS chapter (chapter L, this volume; Diefenbach, 2024).

Instrumentation

Space-Based Sensors

Satellite remote sensing provides synoptic views of a volcanic edifice and the surface changes and emplacement of deposits through time before, during, and after an eruption. High-resolution satellite imaging with visible, infrared, and SAR sensors is critical for mapping and characterization of volcanic vents and deposits over large areas and inaccessible or dangerous terrain (Patrick and others, 2016; Waythomas and

others, 2020). Satellite data sources vary widely with respect to spectral coverage (wavelengths of 300 nanometers to 300 millimeters; that is, ultraviolet, visible, middle infrared, thermal infrared, and microwave), spatial resolution (submeter to tens of kilometers), and temporal resolution (as often as 1 minute to several weeks between repeat acquisitions). In contrast to airborne and ground-based remote sensing, space-based remote sensing imagery can capture local (tens of kilometers) to regional (thousands of kilometers) scales, typically with global coverage. New satellite sensors and constellations of satellites with multiple platforms operating the same sensor, like the Constellation of Small Satellites for Mediterranean basin Observation (COSMO-SkyMed) and Sentinel-2 A and B, offer greater spatial, spectral (additional channels and increased sensitivity), and temporal resolution. This allows for observations of steam, ash, and high-temperature thermal emissions, as well as surficial change from deformation and eruption deposits. Advances in lower spatial resolution meteorological satellites, including the launch of Visible Infrared Imaging Radiometer Suite (VIIRS) instruments on a constellation of satellites starting in 2011 and new Geostationary Operational Environmental Satellite (GOES) satellites, are providing visible and infrared views at higher temporal (as short as 1-minute for GOES mesoscale) and spatial resolution (as high as 375 meters [m] VIIRS imagery bands) than ever before to capture large-scale volcanic activity in near-real time. Other developments include faster transfer of large datasets, cloud-based data storage and processing, and automated processing of near-real-time data that can be programmed to provide alerts when noteworthy changes are detected.

Collaboration among the USGS, the National Aeronautics and Space Administration (NASA), and other agencies and research groups worldwide have helped bring research and experimental operational products into use by the USGS for volcano monitoring. For example, with the launch of Landsat 8 in 2013 and the launch of Landsat 9 in 2021, the USGS Landsat program provides routine observations of the Earth's surface. The Landsat 8 and 9 sensors provide better spatial and spectral resolution than their predecessors, with bands covering 0.43–12.51 micrometer, spatial resolution as high as 15 m, and a repeat time of 16 days. Complementary sensors aboard the European Space Agency Sentinel-2 satellite constellation are also operational (repeat interval of 5 days), and together these instruments provide regular multispectral imaging of volcanoes, eruption deposits, high-temperature thermal features, vegetation changes, and other phenomena.

Although traditionally used in volcanology for deformation monitoring (and highlighted in chapter D, this volume, on ground deformation and gravity change; Montgomery-Brown and others, 2024), SAR data provide the unique capability to view the surfaces of volcanoes through clouds, steam, and ash emissions, revealing new eruption deposits (for example, lava flows, dome growth, ash fallout, and lahars) and other surficial changes (such as ground cracking), and are also used to generate digital elevation models (DEMs). The USGS has used various SAR data from cooperating agencies such as the European Space Agency (Sentinel), Canadian Space Agency (Radarsat), German Aerospace Center (TerraSAR-X and TanDEM-X), Japan Aerospace Exploration Agency (Advanced Land Observing Satellite), and Italian Space Agency (COSMO-SkyMed). These datasets offer resolutions less than 1 m and repeat cycles of days to weeks. The joint NASA-Indian Space Research Organization Synthetic Aperture Radar Mission, with a planned launch date in 2024, will mark the first satellite-based SAR mission by the United States and will provide routine data for volcano monitoring.

Airborne Sensors

Technological developments in camera systems, UAS platforms, and image-processing software have revolutionized the resolution and quality of airborne remote sensing data products. The data generated may include visible images, thermal infrared images acquired with forward-looking infrared (FLIR) cameras, topographic data produced by lidar and structure from motion (SfM) methods, and airborne SAR. On-demand overflights with crewed and unoccupied aircraft can provide regular observations of activity to track eruption evolution and detect changes, thereby improving eruption forecasts (Poland and others, 2016; Neal and others, 2019; Dietterich and others, 2021). Optical and thermal imagery and video are used for observations and characterization of eruptive activity, such as eruptive style, deposit extents, eruption rates, and lava temperature. Data acquired from airborne surveys can be processed with SfM photogrammetric methods to construct DEMs at centimeter resolution (for example, Dietterich and others, 2021) and high-resolution orthoimagery, including visible wavelengths for mapping and thermal infrared wavelengths for tracking surface temperatures (for example, Patrick and others, 2017).

Airborne SAR has been widely used to acquire high-resolution DEMs at U.S. volcanoes (for example, the USGS Alaska Mapping Initiative) and has been deployed in eruption response to document topographic change during eruptions. NASA's Airborne Glacier and Land Ice Surface Topography Interferometer (GLISTIN-A) SAR instrument flies on a crewed aircraft and utilizes single-pass interferometric synthetic aperture radar (InSAR) to construct DEMs on demand (for example, Lundgren and others, 2019). Similarly, airborne lidar is deployed to collect high-resolution, high-precision terrain data at volcanoes before, during, and after eruptions. Lidar data, particularly acquired from low-altitude aircraft, offer centimeter-scale resolution and the ability to filter results to obtain bare-earth

topographic data in vegetated regions. Unlike space-based remote sensing, acquisition of airborne remote sensing data is, in most cases, spatially limited to individual volcanoes.

Ground-Based Sensors

Ground-based optical and thermal cameras, including both telemetered and non-telemetered systems, are a proven means of detecting eruption onset, tracking and documenting eruptive activity, and monitoring morphological and temperature changes at volcanoes (for example, Major and others, 2008). Their use depends on adequate visibility and lighting (for optical systems), both of which can be limited by weather conditions, viewing geometry, and darkness, such as during winter eruptions at high-latitude volcanoes in Alaska. Low-light (near-infrared) and thermal infrared cameras can readily capture warm features and work overnight and through minor steam and gas emissions. Current web cameras (fig. G1) can capture images with as high as 4,000-pixel resolution with high dynamic range, representing a vast improvement in imaging quality compared to web cameras from the early 2000s. Some camera systems offer remote control of pan, tilt, and zoom functions to change their field of view, streaming or time-lapse video acquisition, and (or) capture and storage of video on-board for later retrieval. Many readily available modern camera systems even use cellular telemetry and thus permit rapid deployment outside of an existing telemetry network if there is cell reception.

Individual cameras, including high-speed cameras, have provided quantitative information on lava fountain heights (Wolfe and others, 1988; Orr and others, 2015), the elevations of lava lakes (Orr and Rea, 2012; Patrick and others, 2014),



Figure G1. Photograph showing the Mount Cleveland web camera at Concord Point, Chuginadak Island, Islands of Four Mountains, Aleutian Islands, Alaska. The station also hosts the CLCO seismic station and an array of infrasound sensors. The south flank of little-studied Tana Anguna (Tana) volcano rises in the background. Photograph by M. Kaufman, University of Alaska Fairbanks, July 19, 2018; used with permission.

lava lake surface motion (Patrick and Orr, 2018), spattering dynamics (Mintz and others, 2021), and explosion particle tracking (Taddeucci and others, 2012; Vanderkluysen and others, 2012). Ground-based cameras deployed in combination can be used to quantify topographic changes (for example, Major and others, 2009). Other types of ground-based remote sensing instrumentation, such as SAR and automated laser rangefinders, have also been used to characterize surface change (for example, Di Traglia and others, 2014; Patrick and others, 2019), but require favorable viewing conditions for deployment.

Recommended Capabilities

Collect Baseline Imagery and Topography

Volcano observatories assess volcanic hazards to support land-use planning, emergency-response, and public awareness. This requires studies to determine the style and frequency of past eruptions and the potential effects of future activity. Fundamental to such studies are aerial and satellite images to identify past eruptive products and accurately map their distribution. In addition, DEMs are required for hazard assessment and modeling because many volcanic hazards are controlled by topography. For example, assessing the regions that are most at risk from inundation by lahars, pyroclastic density currents, and lava flows requires accurate and up-to-date DEMs. Similarly, terrain is a fundamental control on edifice stability, and DEMs are therefore needed for slope-stability assessment. Finally, preeruptive imagery and DEMs are key baseline data for comparing with syneruptive or posteruptive data to detect and characterize eruptive activity and volcanic unrest.

Instrumentation

The most used image sources for geologic and hazard mapping include high-resolution aerial and satellite images. High-spatial-resolution (submeter), cloud-free visible and near-infrared imagery of quiescent volcanoes is widely available. These data are supplemented by lower resolution (tens of meters) Landsat or Sentinel data for additional spectral information, such as for identifying the extent of hydrothermal alteration. Airborne SAR instruments, like NASA's GLISTIN-A, and airborne lidar have been deployed to collect high-resolution and high-precision terrain data at volcanoes before, during, and after eruptions (Lundgren and others, 2019; Mosbrucker and others, 2020).

Recommendations

We suggest acquisition of moderate-resolution baseline imagery (for example, Landsat 8 or 9 or Sentinel-2) and 10-meter minimum resolution DEMs at all levels 1 and 2 volcanoes. For level 3 volcanoes, we suggest acquisition of a 5-meter minimum resolution DEM and high-spatial-resolution satellite images

(WorldView or equivalent; 1 meter or better resolution) or stereo aerial imagery to allow for detailed geologic and hazard mapping. The same procedures would ideally be followed for level 4 volcanoes except that the DEMs should have a 1-meter minimum resolution to improve hazards modeling of lahars, pyroclastic density currents, lava flows, and other phenomena. A high-spatial-resolution orthoimage would ideally be re-collected for levels 3 and 4 volcanoes at least every year, and DEMs would be re-collected at least every 10 years. High-resolution imagery and DEMs would ideally be collected regularly during and following eruptions for volcanoes of all levels. The frequency of acquisitions are typically tailored to the hazards, eruptive style, timescales, weather, and remoteness of eruptions. All DEMs should be bare earth, representing the topography with vegetation and structures removed, and all imagery should be georeferenced and orthorectified.

Track Unrest and Eruptive Activity

Restless and higher threat volcanoes require routine observational monitoring to maintain awareness. When these volcanoes enter a state of unrest or erupt, there is then a constant need to observe and document activity, map deposits, and measure eruption rates. Various techniques have been developed and utilized that are cost effective and provide increased viewing potential, as well as increased safety for scientific field crews. These techniques include (1) telemetered and non-telemetered ground-based cameras (including time-lapse, low-light, and infrared), (2) aerial observation and imaging using crewed aircraft and UAS, (3) high-resolution satellite optical and thermal images, (4) airborne and satellite SAR, and (5) ground and airborne lidar. Owing to the many variables regarding access, logistics, eruption style, and climate, the use of these techniques needs to be tailored to the individual volcano. For example, radar (and, in the case of hot targets, infrared) techniques are particularly useful where visual observations are limited by steam, clouds, or fog, which can complicate interpretations of other monitoring data.

Instrumentation

Imagery from all sensors at all spatial and temporal scales is critical to detecting changes associated with volcanic unrest and the deposits and dynamics of eruptions. These images can be analyzed qualitatively to detect and describe changes in surface features (for example, appearance or disappearance of a lake, a new lahar, or an ash deposit). High-resolution imagery for ground, airborne, and satellite platforms can also be orthorectified and analyzed for mapping and measuring these features (for example, mapping the extent of a lava flow through time). Analysis uses spectral characteristics, feature tracking, and change detection to identify, trace, and quantify surface deposits and changes at volcanoes. During the 2019–20 Shishaldin Volcano eruption, for example, thermal, optical, and SAR satellite imagery were jointly analyzed to document the changes in the summit crater, lava flows, and plumes associated with eruption to inform assessment of current activity and potential hazards (fig. G2).

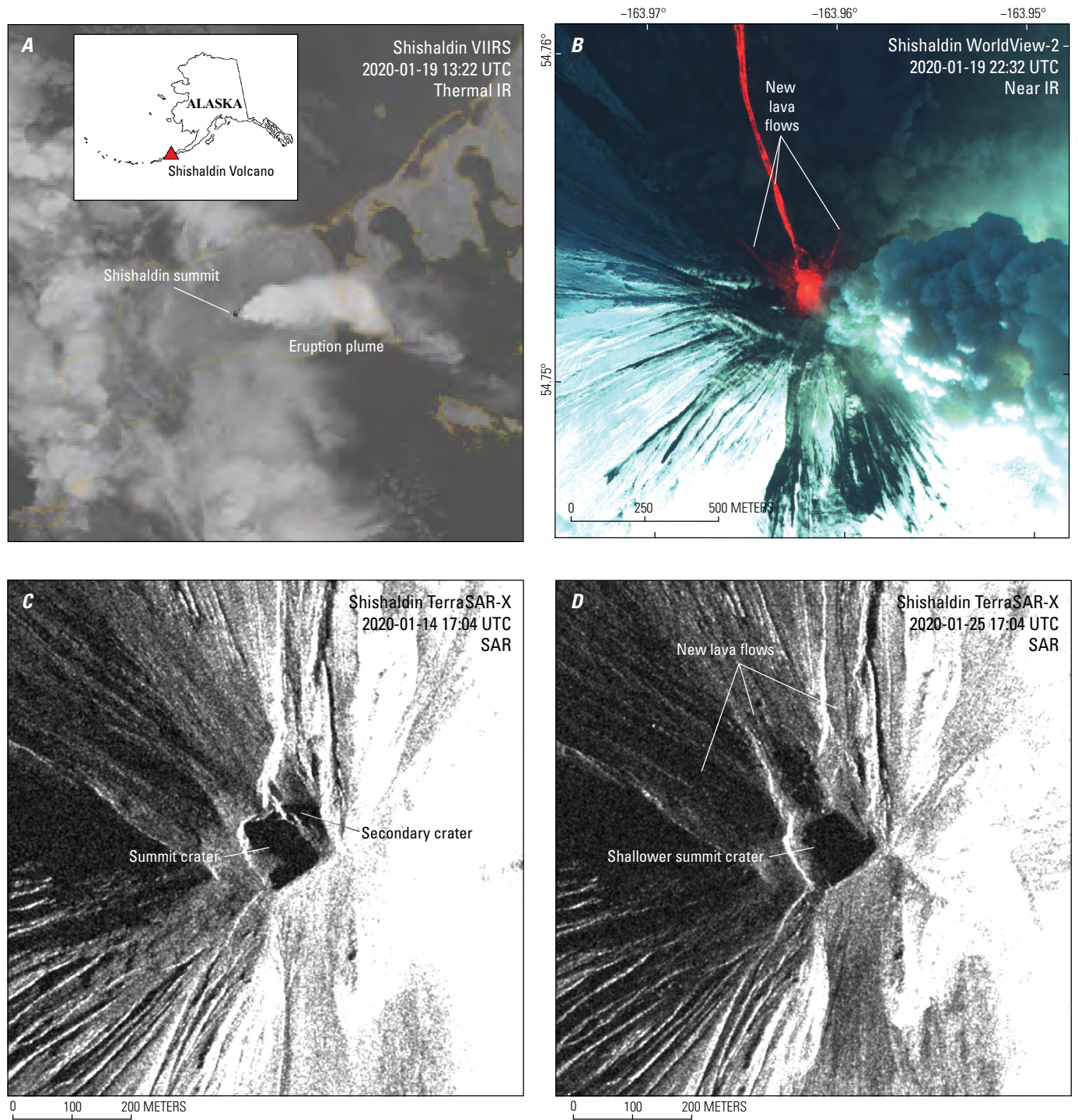


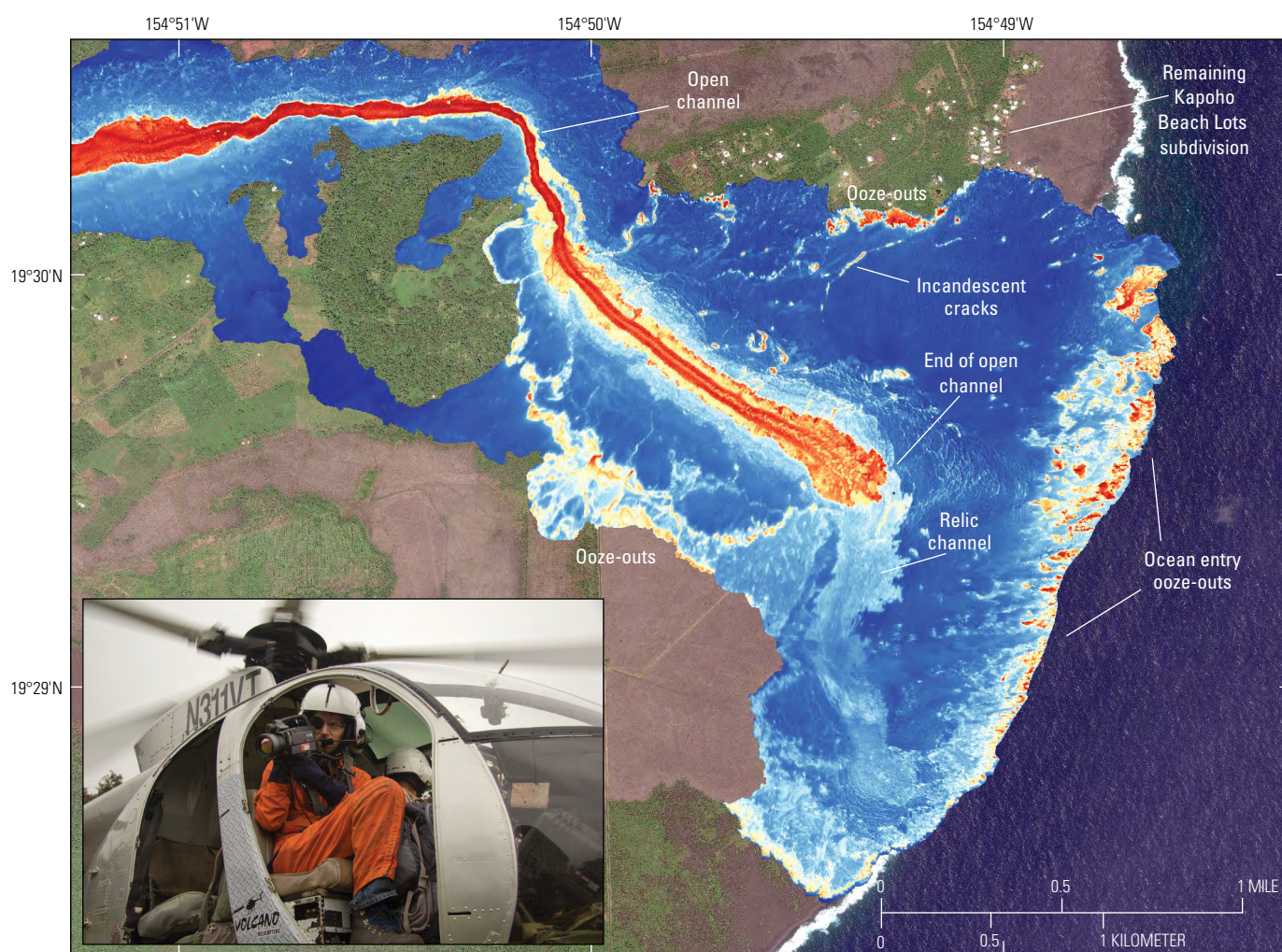
Figure G2. Satellite imagery of the January 19–20, 2020, explosive event of Shishaldin Volcano, Alaska. *A*, Thermal infrared (IR) image (Visible Infrared Imaging Radiometer Suite [VIIRS] on January 19 at 13:22 coordinated universal time [UTC]) of the diffuse ash and gas plume produced by lava fountaining. *B*, Off-nadir near-infrared false color image (WorldView-2 on January 19 at 22:33 UTC) of lava flows to the north, northwest, and northeast being fed from a central scoria cone that is actively fountaining and producing a vertical column of steam and minor ash. *C*, Preeruptive (January 14) high-resolution TerraSAR-X synthetic aperture radar (SAR) backscatter image showing the summit region of Shishaldin Volcano (illumination from the southeast), including a deep summit crater with a secondary crater to the northeast. *D*, Posteruptive (January 25) high-resolution TerraSAR-X backscatter image showing the summit region of Shishaldin Volcano (illumination from the southeast), including new lava flows visible in part *B* and a single, shallower summit crater. WorldView-2 imagery, Maxar, copyright 2024, U.S. Government Plus license. TerraSAR-X copyright 2019 German Aerospace Center (DLR); courtesy of Simon Plank, DLR.

Using airborne and satellite remote sensing to rapidly construct DEMs is critical for measuring topographic changes caused by deposition of newly erupted material at an erupting volcano. Satellite stereophotogrammetry (WorldView) and SAR (TanDEM-X) can capture high-resolution (<5 m) terrain data, which have been used for such applications as tracking island growth during the 2016–17 eruption of Bogoslof Island (Coombs and others, 2019) and measuring lava effusion rates at Kīlauea (Poland, 2014). SfM software permits in-house construction of submeter resolution DEMs from aerial images captured during routine overflights, including FLIR imagery where volcanic plumes can obscure visible imagery or where eruptive activity is difficult to discern optically (for example, Patrick and others, 2017).

Aerial surveys using visible and infrared photogrammetry and single-pass InSAR (NASA's GLISTIN-A) offer higher

resolution (<5 m) and on-demand DEM generation capabilities. Additionally, overflights with crewed aircraft and UAS provide airborne video and imagery surveys that can be integrated with image processing techniques for quantifying eruption dynamics and constructing orthorectified visible and thermal maps at submeter resolution (Patrick and others, 2017; Neal and others, 2019; Dietterich and others, 2021). The USGS Hawaiian Volcano Observatory has routinely acquired repeat thermal imagery from aircraft overflights to provide situational awareness to the National Park Service, county, State, and Federal emergency response managers, and the public. This technique was critical to mapping lava flow development and associated hazards during Kīlauea's 2018 lower East Rift Zone eruption (fig. G3).

Eruption rates can be determined by comparison of topography over time, which can be derived from both optical



Base image from Worldview 2, May 23, 2018
Maxar, copyright 2024, U.S. Government Plus license

Figure G3. Flow field thermal imagery from June 27, 2018, overlain on a preeruptive image of the 2018 lower East Rift Zone eruption of Kīlauea, Hawaiʻi, acquired on May 23, 2018. Photograph shows a U.S. Geological Survey Hawaiian Volcano Observatory geologist using a forward looking infrared camera from a helicopter to thermally image a lava flow at Kīlauea, Hawaiʻi. Photograph by T. Orr, U.S. Geological Survey, March 4, 2016.



(for example, Bagnardi and others, 2016) and SAR (for example, Poland, 2014) satellite data, but even simple morphological changes detected qualitatively in remote sensing imagery can provide important hazards information. The successful forecast of hazardous eruptive activity at Merapi, Indonesia, in 2010, for instance, was based on SAR amplitude imagery that was used to characterize lava dome growth patterns over time (Pallister and others, 2013). Effusion rates calculated using airborne thermal-imaging cameras can be more accurate than those determined from satellite because of the higher dynamic range and spatial resolution of the aerial observations (Patrick and others, 2017). SAR and photogrammetric techniques both produce digital surface models that may not represent the bare-earth topography in vegetated areas; therefore, airborne lidar data are essential for capturing topographic change with high accuracy and resolution within vegetated areas. Ground-based multiview stereo imagery, InSAR, and lidar can similarly track local topographic change, such as from lava flow emplacement, mass movements, and crater floor and lava lake level changes.

Recommendations

Baseline observational monitoring of levels 1 and 2 volcanoes is met by collecting satellite imagery (see “Collect Baseline Imagery and Topography” section). For baseline observational monitoring of level 3 volcanoes, we suggest deployment of at least one telemetered optical camera. For level 4 volcanoes, we suggest at least two telemetered cameras with different views of the volcano. At level 4 and frequently restless volcanoes, we also suggest regular (about monthly) acquisition of high-spatial-resolution, georeferenced and orthorectified visible, short-wave infrared (SWIR), and radar satellite images or aerial imagery.

During periods of unrest or eruption, imagery and DEMs would be acquired more frequently from satellite or aerial platforms, satellite or airborne SAR, or lidar surveys. Visual and (or) thermal orthomosaics could be constructed from airborne imagery surveys using SfM techniques. Additional telemetered and (or) time-lapse or video and video-lapse camera capabilities could be deployed if practical to document lava extrusion, pyroclastic flows, and other eruptive phenomena. Acquisition intervals of ground-based cameras could be adjusted to capture rapidly changing activity.

Detect and Characterize Thermal Emissions Through Time

Prior to eruption, as magma intrudes a volcano, surface heat flow may increase, resulting in the development of, or changes to existing, fumarolic activity, fractures, hot springs, crater lakes, and snow and ice fields. Detection and tracking of these changes relative to the volcano’s background state can play an important role in understanding the processes involved in volcanic unrest. Regular monitoring of thermal emissions can therefore offer a valuable tool to detect unrest at an early stage, and likely well

before an eruption occurs. For example, long-term temperature changes have been tracked prior to eruptions using ground-based radiometers (Harris and others, 2005b), satellite imagery (Reath and others, 2019; Girona and others, 2021), and airborne thermal data (Schneider and others, 2008; Wessels and others, 2013).

During eruptions, characterization of volcanic radiative power is an important parameter that can be used to evaluate the magnitude and evolution of volcanic activity. Tracking total volcanic radiative power through time can reveal precursory thermal signals and how eruptive activity is evolving through time (for example, Wright and others, 2002; Coppola and others, 2016). Radiative power can be estimated from low-spatial-resolution data but requires knowledge of the subpixel fraction of the hot feature—information obtainable from higher resolution satellite data or thermal-imaging radiometric data. The volcanic radiative power can be further refined into estimates of effusion rate (Harris and others, 1997) and total eruption volume, which are important for understanding magma supply and producing lava flow hazard assessments. Although effusion rate can be calculated by using low-spatial-resolution satellite data (Harris and others, 1997; Patrick and others, 2016), more accurate estimates are obtainable by using data from thermal-imaging cameras, which have a much higher dynamic range and spatial resolution (Harris and others, 2005a; Patrick and others, 2017; fig. G3). These higher resolution data collected from the ground or from aircraft can be combined with the synoptic, repetitive view that satellite data provide to produce a time series of lava effusion over the course of an eruption.

Instrumentation

Infrared data track changes in the locations, sizes, and strengths of thermal signals through time and can be used to detect unrest and measure eruption rates. Imagery can be acquired at various spatial and temporal resolutions—meteorological satellites capture low spatial but high temporal resolution with Advanced Very High Resolution Radiometer (AVHRR), GOES, Moderate Resolution Imaging Spectroradiometer (MODIS), and VIIRS for hot objects (Harris and others, 1997; Dehn and others, 2002; Wright and others, 2002, 2004); less frequent medium-resolution imagery from the Advanced Spaceborne Thermal Emission and Reflection Radiometer (ASTER) and Landsat (Flynn and others, 2001; Ramsey and Dehn, 2004); and very high spatial and temporal resolution from infrared cameras in aircraft- and ground-based applications (Harris and others, 2005b; Vaughan and others, 2005; Patrick and others, 2014, 2017). These sensors also vary in spectral bands and resolution. Hot surfaces can also be detected and characterized in the near-infrared and SWIR wavelengths by more sensors and at higher spatial resolution than thermal infrared at all scales (for example, Landsat 8 and 9 thermal infrared resolution is 100 m, but its SWIR resolution is 30 m).

Automated hot spot detection and processing of thermal emissions from frequent low- and moderate-resolution satellite data, as well as infrared web cameras, can provide critical early detection and characterization of volcanic unrest and eruption. Algorithms for automated thermal time series processing of

satellite imagery detect thermal signals above background at volcanoes and may be used to generate alerts of new activity and quantify thermal output through time during an eruption at the spatial and temporal resolutions of the satellite data (for example, MODVOLC or MIROVA; Wright and others, 2004; Coppola and others, 2016). Quantitative thermal flux (volcanic radiative power; fig. G4) can importantly be used to estimate lava effusion rates through time (for example, Harris and others, 2005a; Loewen and others, 2021). Similarly, automated processing of thermal web camera imagery allows detection of sudden increases in temperature indicative of eruption onset, as well as tracking and characterization of thermal features (for example, Patrick and others, 2014). These and other algorithms may also detect weaker thermal emissions prior to eruption (Dehn and others, 2000; Girona and others, 2021).

Detection, precise mapping, and analysis of subtle changes in thermal features must utilize higher resolution airborne and satellite imagery. Signs of unrest may be expressed in moderate- to high-resolution thermal imagery, such as changes in geothermal areas (for example, Vaughan and others, 2020). During eruption, high-resolution thermal imagery can track activity in detail, such as lava lake level or lava flow or dome extents, lava transport systems such as channels and tubes, surface temperatures, and flow dynamics (for example, Wessels and others 2013; Patrick and others, 2014, 2017; figs. G2 and G3). Telemetered thermal infrared camera data

can provide the most frequent views, whereas high-resolution airborne and satellite imagery have lower temporal resolution.

Recommendations

Any available low-spatial-resolution satellite data may be used to establish baseline thermal features and for automated hot spot detection and alerting for anomalous significant thermal activity for levels 1 and 2 volcanoes (for example, Coppola and others, 2016).

For levels 3 and 4 volcanoes, it is important to frequently characterize volcanic thermal flux (for example, radiative power) to detect eruption precursors and to track changes in thermal features over time. We suggest acquiring baseline knowledge of the distribution and temperature of thermal features. Mapping and temporal comparisons can be made at moderate to high resolution with ASTER and Landsat 8 or 9, tasking WorldView-3 SWIR and (or) nighttime Landsat 8 or 9, and thermal imagery captured during repeat airborne (both crewed and unoccupied) and ground-based missions (for example, Vaughan and others, 2012). We also suggest using high temporal, low spatial resolution meteorological satellite data for automated hot spot detection, tracking, and alerting for anomalous significant thermal activity (for example, Coppola and others, 2016). During eruptive activity, it is important to distinguish lava effusion from other thermal signals, such as

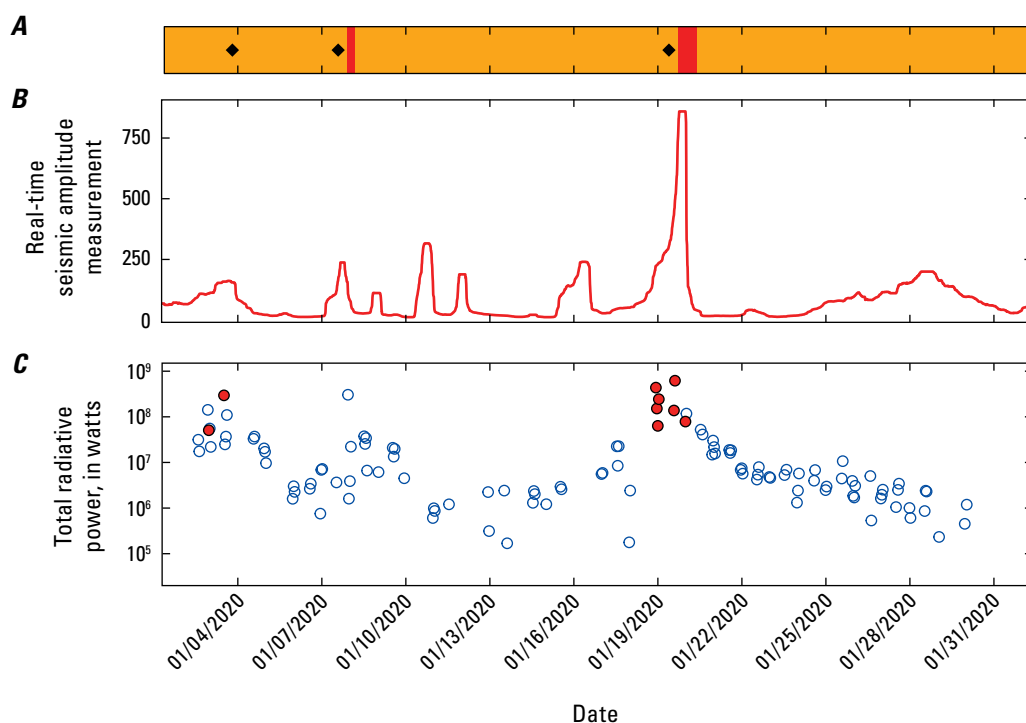


Figure G4. Plots showing the timeline of eruptive activity at Shishaldin Volcano, Alaska, in January 2020. *A*, Changes in aviation color code. Black diamonds indicate when ash-producing events occurred. *B*, Seismic tremor, shown as real-time seismic amplitude measurements (Endo and Murray, 1991) at station SSBA, plotted as a 12-hour average. *C*, Quantitative radiative power from the Visible Infrared Imaging Radiometer Suite (VIIRS) (following method described by Loewen and others, 2021). Open circles show when elevated surface temperatures were detected; filled circles show when those elevated temperatures exceeded the VIIRS sensor range and the pixels were saturated. The offset in ash events from color code changes is because of retrospective timing of the event starting date compared to when formal notifications or color code changes were issued. Dates shown as month/day/year.

pyroclastic flows and Strombolian activity, and to characterize a time series of thermal flux (and estimated eruption rate) from lava domes, flows, and other features. High-spatial-resolution georeferenced mapping of lava dome and flow extents, lava channel and lava tube systems, and thermal signatures that capture the style and level of activity through time can be done using commercial satellite SWIR, and (or) airborne or ground-based thermal cameras (for example, fig. G2).

At level 4 volcanoes, we additionally suggest using higher resolution airborne and ground-based thermal imagery for on-demand and high-temporal-resolution observations. We also suggest deployment of at least one telemetered thermal infrared camera, and (or) low-light camera, ideally co-located with an optical camera, where allowed by environmental conditions and viewing geometry, and additionally warranted by activity level (for example, areas of frequent eruptive activity, or where there is a history of thermal precursors prior to eruptions).

During periods of unrest and eruption, additional cameras (telemetered and [or] time-lapse or video or video-lapse) with low-light or thermal-infrared capabilities could be deployed to further document lava extrusion, fountaining and Strombolian activity, pyroclastic flows, and other phenomena that have thermal signatures. Throughout an eruption, it is important to distinguish between these phenomena and to characterize a time series of thermal flux (and estimated eruption rate) from lava domes, flows, and other features. High-spatial-resolution georeferenced mapping of lava dome and flow extents, channel and tube systems, and thermal signatures that capture the style and level of activity through time could be done using commercial satellite SWIR and ground-based and (or) airborne thermal cameras (for example, Patrick and others, 2017). A very high-temporal-resolution time series of volcanic radiative power can be based on GOES imagery acquired every 1 to 10 minutes to capture rapid changes in eruption dynamics.

Summary—Recommendations for Levels 1–4 Networks

Level 1.—Collect moderate-resolution baseline imagery and at least 10-m-resolution DEMs to provide a synoptic overview of volcanic landforms, deposits, and thermal features for later comparison. Implement automated hot spot detection and alerting.

Level 2.—Same as for level 1.

Level 3.—Collect and regularly update high-resolution baseline optical and thermal imagery and at least 5-m-resolution DEMs to provide a synoptic overview of volcanic landforms, deposits, and thermal features for later comparison and for detailed geologic and hazard mapping; deploy one telemetered ground-based optical camera. During periods of unrest or eruption, construct high-resolution visual and (or) thermal orthomosaics

and generate new DEMs as necessary, perform automated time-series processing and mapping of thermal features, and implement automated hot spot detection to generate alerts of anomalous thermal activity.

Level 4.—Same as level 3, except baseline DEMs would ideally be at least 1-m resolution to improve hazards modeling; deploy two telemetered ground-based cameras and a thermal camera where appropriate. Regularly acquire high-resolution stereopairs and orthorectified optical and SWIR satellite and (or) aerial imagery. During periods of unrest or eruption, frequently characterize thermal flux with satellite, airborne, and ground-based thermal imagery to track changes and estimate eruption rates, increase acquisition of imagery and DEMs, deploy additional telemetered and (or) time-lapse cameras with video, low-light, or thermal-infrared capabilities.

References Cited

- Bagnardi, M., González, P.J., and Hooper, A., 2016, High-resolution digital elevation model from tri-stereo Pleiades-1 satellite imagery for lava flow volume estimates at Fogo Volcano: *Geophysical Research Letters*, v. 43, no. 12, p. 6267–6275, <https://doi.org/10.1002/2016GL069457>.
- Coombs, M., Wallace, K., Cameron, C., Lyons, J., Wech, A., Angeli, K., and Cervelli, P., 2019, Overview, chronology, and impacts of the 2016–2017 eruption of Bogoslof volcano, Alaska: *Bulletin of Volcanology*, v. 81, no. 62, 23 p., <https://doi.org/10.1007/s00445-019-1322-9>.
- Coppola, D., Campion, R., Laiolo, M., Cuoco, E., Balagizi, C., Ripepe, M., Cigolini, C., and Tedesco, D., 2016, Birth of a lava lake—Nyamulagira volcano 2011–2015: *Bulletin of Volcanology*, v. 78, no. 20., 13 p., <https://doi.org/10.1007/s00445-016-1014-7>.
- Dehn, J., Dean, K., and Engle, K., 2000, Thermal monitoring of North Pacific volcanoes from space: *Geology*, v. 28, no. 8, p. 755–758, [https://doi.org/10.1130/0091-7613\(2000\)28<755:TMONPV>2.0.CO;2](https://doi.org/10.1130/0091-7613(2000)28<755:TMONPV>2.0.CO;2).
- Dehn, J., Dean, K.G., Engle, K., and Izbekov, P., 2002, Thermal precursors in satellite images of the 1999 eruption of Shishaldin Volcano: *Bulletin of Volcanology*, v. 64, no. 8, p. 525–534, <https://doi.org/10.1007/s00445-002-0227-0>.
- Diefenbach, A.K., 2024, Special topic—Unoccupied aircraft systems, chap. L of Flinders, A.F., Lowenstern, J.B., Coombs, M.L., and Poland, M.P., eds., Recommended capabilities and instrumentation for volcano monitoring in the United States: U.S. Geological Survey Scientific Investigations Report 2024–5062–L, 5 p., <https://doi.org/10.3133/sir20245062L>.

- Dietterich, H.R., Diefenbach, A.K., Soule, S.A., Zoeller, M.H., Patrick, M.P., Major, J.J., and Lundgren, P.R., 2021, Lava effusion rate evolution and erupted volume during the 2018 Kīlauea lower East Rift Zone eruption: *Bulletin of Volcanology*, v. 83, no. 25, 18 p., <https://doi.org/10.1007/s00445-021-01443-6>.
- Di Traglia, F., Nolesini, T., Intrieri, E., Mugnai, F., Leva, D., Rosi, M., and Casagli, N., 2014, Review of ten years of volcano deformations recorded by the ground-based InSAR monitoring system at Stromboli volcano—A tool to mitigate volcano flank dynamics and intense volcanic activity: *Earth-Science Reviews*, v. 139, p. 317–335, <https://doi.org/10.1016/j.earscirev.2014.09.011>.
- Endo, E.T., and Murray, T., 1991, Real-time seismic amplitude measurement (RSAM)—A volcano monitoring and prediction tool: *Bulletin of Volcanology*, v. 53, p. 533–545, <https://doi.org/10.1007/BF00298154>.
- Flynn, L.P., Harris, A.J.L., and Wright, R., 2001, Improved identification of volcanic features using Landsat 7 ETM+: *Remote Sensing of Environment*, v. 78, no. 1–2, p. 180–193, [https://doi.org/10.1016/S0034-4257\(01\)00258-9](https://doi.org/10.1016/S0034-4257(01)00258-9).
- Girona, T., Realmuto, V., and Lundgren, P., 2021, Large-scale thermal unrest of volcanoes for years prior to eruption: *Nature Geoscience*, v. 14, p. 238–241, <https://doi.org/10.1038/s41561-021-00705-4>.
- Harris, A.J.L., Keszthelyi, L., Flynn, L.P., Mougini-Mark, P.J., Thornber, C., Kauahikaua, J., Sherrod, D., Trusdell, F., Sawyer, M.W., and Flament, P., 1997, Chronology of the episode 54 eruption at Kīlauea Volcano, Hawaii, from GOES-9 satellite data: *Geophysical Research Letters*, v. 24, no. 24, p. 3281–3284, <https://doi.org/10.1029/97GL03165>.
- Harris, A., Dehn, J., Patrick, M., Calvari, S., Ripepe, M., and Lodato, L., 2005a, Lava effusion rates from hand-held thermal infrared imagery—An example from the June 2003 effusive activity at Stromboli: *Bulletin of Volcanology*, v. 68, no. 2, p. 107–117, <https://doi.org/10.1007/s00445-005-0425-7>.
- Harris, A., Pirie, D., Horton, K., Garbeil, H., Pilger, E., Ramm, H., Hoblitt, R., Thornber, C., Ripepe, M., Marchetti, E., and Poggi, P., 2005b, DUCKS—Low cost thermal monitoring units for near-vent deployment: *Journal of Volcanology and Geothermal Research*, v. 143, no. 4, p. 335–360, <https://doi.org/10.1016/j.jvolgeores.2004.12.007>.
- Loewen, M.W., Dietterich, H.R., Graham, N., and Izbekov, P., 2021, Evolution in eruptive style of the 2018 eruption of Veniaminof volcano, Alaska, reflected in groundmass textures and remote sensing: *Bulletin of Volcanology*, v. 83, no. 72, 19 p., <https://doi.org/10.1007/s00445-021-01489-6>.
- Lundgren, P.R., Bagnardi, M., and Dietterich, H., 2019, Topographic changes during the 2018 Kīlauea eruption from single-pass airborne InSAR: *Geophysical Research Letters*, v. 46, no. 16, p. 9554–9562, <https://doi.org/10.1029/2019GL083501>.
- Major, J.J., Kingsbury, C.G., Poland, M.P., and LaHusen, R.G., 2008, Extrusion rate of the Mount St. Helens lava dome estimated from terrestrial imagery, November 2004–December 2005, chap. 12 of Sherrod, D.R., Scott, W.E., and Stauffer, P.H., eds., *A volcano rekindled—The renewed eruption of Mount St. Helens, 2004–2006*: U.S. Geological Survey Professional Paper 1750-12, p. 237–255, <https://doi.org/10.3133/pp175012>.
- Mintz, B.G., Houghton, B.F., Llewellyn, E.W., Orr, T.R., Taddeucci, J., Carey, R.J., Kueppers, U., Gaudin, D., Patrick, M.R., Burton, M., Scarlato, P., and La Spina, A., 2021, Patterns of bubble bursting and weak explosive activity in an active lava lake—Halema‘ūma‘u, Kīlauea, 2015, chap. E of Patrick, M., Orr, T., Swanson, D., and Houghton, B., eds., *The 2008–2018 summit lava lake at Kīlauea Volcano, Hawai‘i*: U.S. Geological Survey Professional Paper 1867, 16 p., 6 videos, <https://doi.org/10.3133/pp1867E>.
- Montgomery-Brown, E.K., Anderson, K.R., Johanson, I., Poland, M.P., and Flinders, A.F., 2024, Ground deformation and gravity, chap. D of Flinders, A.F., Lowenstern, J.B., Coombs, M.L., and Poland, M.P., eds., *Recommended capabilities and instrumentation for volcano monitoring in the United States*: U.S. Geological Survey Scientific Investigations Report 2024–5062–D, 11 p., <https://doi.org/10.3133/sir20245062D>.
- Mosbrucker, A.R., Zoeller, M.H., and Ramsey, D.W., 2020, Digital elevation model of Kīlauea Volcano, Hawai‘i, based on July 2019 airborne lidar surveys: U.S. Geological Survey data release, <https://doi.org/10.5066/P9F1ZU8O>.
- Neal, C.A., Brantley, S.R., Antolik, L., Babb, J.L., Burgess, M., Calles, K., Capps, M., Chang, J.C., Conway, S., Desmither, L., Dotray, P., Elias, T., Fukunaga, P., Fuke, S., Johanson, I.A., Kamibayashi, K., Kauahikaua, J., Lee, R.L., Pekalib, S., Miklius, A., Million, W., Moniz, C.J., Nadeau, P.A., Okubo, P., Parcheta, C., Patrick, M.R., Shiro, B., Swanson, D., Tollett, W., Trusdell, F., Zoeller, M.H., Montgomery-Brown, E.K., Anderson, K.R., Poland, M.P., Ball, J.L., Bard, J.A., Coombs, M., Dietterich, H.R., Kern, C., Thelen, W.A., Cervelli, P.F., Orr, T., Houghton, B.F., Gansecki, C., Hazlett, R., Lundgren, P., Diefenbach, A.K., Lerner, A., Waite, G., Kelly, P.J., Clor, L., Werner, C., Burgess, M., Mulliken, K., Fisher, G., and Damby, D., 2019, The 2018 rift eruption and summit collapse of Kīlauea Volcano: *Science*, v. 363, no. 6425, p. 367–374, <https://doi.org/10.1126/science.aav7046>.

- Orr, T.R., Poland, M.P., Patrick, M.R., Thelen, W.A., Sutton, A.J., Elias, T., Thornber, C.R., Parcheta, C., and Wooten, K.M., 2015, Kīlauea's 5–9 March 2011 Kamoamoa fissure eruption and its relation to 30+ years of activity from Pu'u Ō'ō, chap. 18 of Carey, R., Cayol, V., Poland, M., and Weis, D., eds., *Hawaiian volcanoes—From source to surface*: Wiley, Hoboken, New Jersey, p. 393–420, <https://doi.org/10.1002/9781118872079.ch18>.
- Orr, T.R., and Rea, J.C., 2012, Time-lapse camera observations of gas piston activity at Pu'u Ō'ō, Kīlauea volcano, Hawai'i: *Bulletin of Volcanology*, v. 74, no. 10, p. 2353–2362, <https://doi.org/10.1007/s00445-012-0667-0>.
- Pallister, J.S., Schneider, D.J., Griswold, J.P., Keeler, R.H., Burton, W.C., Noyles, C., Newhall, C.G., and Ratdomopurbo, A., 2013, Merapi 2010 eruption—Chronology and extrusion rates monitored with satellite radar and used in eruption forecasting: *Journal of Volcanology and Geothermal Research*, v. 261, p. 144–152, <https://doi.org/10.1016/j.jvolgeores.2012.07.012>.
- Patrick, M.R., Kauahikaua, Orr, T., Davies, A., and Ramsey, M., 2016, Operational thermal remote sensing and lava flow monitoring at the Hawaiian Volcano Observatory: *Geological Society, London, Special Publications*, v. 426, no. 1, p. 489–503, <https://doi.org/10.1144/SP426.17>.
- Patrick, M.R., and Orr, T.R., 2018, Operational tracking of lava lake surface motion at Kīlauea Volcano, Hawai'i: *U.S. Geological Survey Techniques and Methods*, book 13, chap. A3, 12 p., <https://doi.org/10.3133/tm13A3>.
- Patrick, M.R., Orr, T., Antolik, L., Lee, L., and Kamibayashi, K., 2014, Continuous monitoring of Hawaiian volcanoes with thermal cameras: *Journal of Applied Volcanology*, v. 3, no. 1, p. 1–19, <https://doi.org/10.1186/2191-5040-3-1>.
- Patrick, M., Orr, T., Fisher, G., Trusdell, F., and Kauahikaua, J., 2017, Thermal mapping of a pāhoehoe lava flow, Kīlauea Volcano: *Journal of Volcanology and Geothermal Research*, v. 332, p. 71–87, <https://doi.org/10.1016/j.jvolgeores.2016.12.007>.
- Patrick, M.R., Younger, E.F., and Tollett, W., 2019, Lava level and crater geometry data during the 2018 lava lake draining at Kīlauea Volcano, Hawai'i: *U.S. Geological Survey data release*, <https://doi.org/10.5066/P9MJY24N>.
- Poland, M.P., 2014, Time-averaged discharge rate of subaerial lava at Kīlauea Volcano, Hawai'i, measured from TanDEM-X interferometry—Implications for magma supply and storage during 2011–2013: *Journal of Geophysical Research, Solid Earth*, v. 119, no. 7, p. 5464–5481, <https://doi.org/10.1002/2014JB011132>.
- Poland, M., Orr, T., Kauahikaua, J., Brantley, S., Babb, J., Patrick, M., Neal, C., Anderson, K., Antolik, L., Burgess, M., Elias, T., Fuke, S., Fukunaga, P., Johanson, I., Kagimoto, M., Kamibayashi, K., Lee, L., Miklius, A., Million, W., Moniz, C., Okubo, P., Sutton, A., Takahashi, T., Thelen, W., Tollett, W., and Trusdell, F., 2016, The 2014–2015 Pāhoehoe lava flow crisis at Kīlauea Volcano, Hawai'i—Disaster avoided and lessons learned: *GSA Today*, v. 26, no. 2, p. 4–10, <https://doi.org/10.1130/GSATG262A.1>.
- Ramsey, M., and Dehn, J., 2004, Spaceborne observations of the 2000 Bezymianny, Kamchatka eruption—The integration of high-resolution ASTER data into near real-time monitoring using AVHRR: *Journal of Volcanology and Geothermal Research*, v. 135, no. 1–2, p. 127–146, <https://doi.org/10.1016/j.jvolgeores.2003.12.014>.
- Reath, K., Pritchard, M., Poland, M., Delgado, F., Carn, S., Coppola, D., Andrews, B., Ebmeier, S.K., Rumpf, E., Henderson, S., Baker, S., Lundgren, P., Wright, R., Biggs, J., Lopez, T., Wauthier, C., Moruzzi, S., Alcott, A., Wessels, R., Griswold, J., Ogburn, S., Loughlin, S., Meyer, F., Vaughan, G., and Bagnardi, M., 2019, Thermal, deformation, and degassing remote sensing time series (CE 2000–2017) at the 47 most active volcanoes in Latin America—Implications for volcanic systems: *Journal of Geophysical Research, Solid Earth*, v. 124, no. 1, p. 195–218, <https://doi.org/10.1029/2018JB016199>.
- Schneider, D.J., Vallance, J.W., Wessels, R.L., Logan, M., and Ramsey, M.S., 2008, Use of thermal infrared imaging for monitoring renewed dome growth at Mount St. Helens, 2004—chap. 17 of Sherrod, D.R., Scott, W.E., and Stauffer, P.H., eds., 2008, *A volcano rekindled—The renewed eruption of Mount St. Helens, 2004–2006*: U.S. Geological Survey Professional Paper 1750–17, 13 p., <https://doi.org/10.3133/pp175017>.
- Taddeucci, J., Scarlato, P., Capponi, A., Del Bello, E., Cimarelli, C., Palladino, D.M., and Kueppers, U., 2012, High-speed imaging of Strombolian explosions—The ejection velocity of pyroclasts: *Geophysical Research Letters*, v. 39, no. 2, p. L02301, <https://doi.org/10.1029/2011GL050404>.
- Vanderkluysen, L., Harris, A.J.L., Kelfoun, K., Bonadonna, C., and Ripepe, M., 2012, Bombs behaving badly—Unexpected trajectories and cooling of volcanic projectiles: *Bulletin of Volcanology*, v. 74, no. 8, p. 1849–1858, <https://doi.org/10.1007/s00445-012-0635-8>.
- Vaughan, R.G., Hook, S.J., Ramsey, M.S., Realmuto, V.J., and Schneider, D.J., 2005, Monitoring eruptive activity at Mount St. Helens with TIR image data: *Geophysical Research Letters*, v. 32, no. 19, 4 p., <https://doi.org/10.1029/2005GL024112>.
- Vaughan, R.G., Hungerford, J.D.G., and Keller, W., 2020, A newly emerging thermal area in Yellowstone: *Frontiers in Earth Science*, v. 8, <https://doi.org/10.3389/feart.2020.00204>.

- Vaughan, R.G., Keszthelyi, L.P., Lowenstern, J.B., Jaworowski, C., and Heasler, H., 2012, Use of ASTER and MODIS thermal infrared data to quantify heat flow and hydrothermal change at Yellowstone National Park: *Journal of Volcanology and Geothermal Research*, v. 233–234, p. 72–89, <https://doi.org/10.1016/j.jvolgeores.2012.04.022>.
- Waythomas, C.F., Angeli, K., and Wessels, R.L., 2020, Evolution of the submarine-subaerial edifice of Bogoslof volcano, Alaska, during its 2016–2017 eruption based on analysis of satellite imagery: *Bulletin of Volcanology*, v. 82, no. 21, 26 p., <https://doi.org/10.1007/s00445-020-1363-0>.
- Wessels, R.L., Vaughan, R.G., Patrick, M.R., and Coombs, M.L., 2013, High-resolution satellite and airborne thermal infrared imaging of precursory unrest and 2009 eruption at Redoubt Volcano, Alaska: *Journal of Volcanology and Geothermal Research*, v. 259, p. 248–269, <https://doi.org/10.1016/j.jvolgeores.2012.04.014>.
- Wolfe, E.W., Neal, C.A., Banks, N.G., and Duggan, T.J., 1988, Geologic observations and chronology of eruptive events, chap. 1 of Wolfe, E.W., ed., *The Puu Oo eruption of Kilauea Volcano, Hawai‘i—Episodes 1 through 20, January 3, 1983, through June 8, 1984*: U.S. Geological Survey Professional Paper 1463, p. 1–97, <https://doi.org/10.3133/pp1463>.
- Wright, R., Flynn, L.P., Garbeil, H., Harris, A.J.L., and Pilger, E., 2002, Automated volcanic eruption detection using MODIS: *Remote Sensing of Environment*, v. 82, no. 1, p. 135–155, [https://doi.org/10.1016/S0034-4257\(02\)00030-5](https://doi.org/10.1016/S0034-4257(02)00030-5).
- Wright, R., Flynn, L.P., Garbeil, H., Harris, A.J.L., and Pilger, E., 2004, MODVOLC—Near-real-time thermal monitoring of global volcanism: *Journal of Volcanology and Geothermal Research*, v. 135, no. 1–2, p. 29–49, <https://doi.org/10.1016/j.jvolgeores.2003.12.008>.

Chapter H



Aerial photograph of a lahar originating from the crater of Mount St. Helens and flowing into Spirit Lake (left) and the North Fork Toutle River (right), Washington. Photograph taken from a helicopter by T. Casadevall, U.S. Geological Survey, March 20, 1982.

Chapter H

Monitoring Lahars

By Weston A. Thelen, John J. Lyons, Alexandra M. Iezzi, and Seth C. Moran

Introduction

Lahars, or debris flows that originate from a volcano (Pierson and Scott, 1985; Pierson, 1995), are among the most destructive, far-reaching, and persistent hazards on stratovolcanoes. Lahars may be triggered by syneruptive rapid melting of snow and ice, lake breakouts, or heavy rains in conjunction with large eruptive columns. Alternatively, lahars can follow eruptions, when clastic deposits are mobilized by heavy rainfall or lake breakouts, occurring sporadically for years to decades after large eruptions. Some lahars can travel many tens of kilometers in river drainages stemming from volcanoes, as during the 1980 eruption of Mount St. Helens (Washington) (for example, Janda and others, 1981), recent eruptions of Redoubt Volcano (Alaska) (fig. H1; Dorava and Meyer, 1994; Waythomas and others, 2013), and the 1991 eruption of Mount Pinatubo (Philippines) (Major and others, 1996; Pierson and others, 1996). Large lahars are less likely in the absence of eruptive activity, but still possible. The Electron Mudflow at Mount Rainier (approximately A.D. 1500), Wash., is an example of a potential noneruptive lahar, likely initiated by a spontaneous collapse of weak rock, that reached the Puget Lowland after it flowed dozens of kilometers without a recognized eruptive trigger (Sisson and Vallance, 2009).

The extreme hazard posed by lahars was demonstrated tragically by the 1985 Nevado del Ruiz (Colombia) catastrophe that claimed the lives of more than 20,000 people (Naranjo and others, 1986). The potential to provide warnings of minutes to hours in advance of lahar arrival in a populated area (for example, Voight, 1990) is a strong reason to provide special monitoring attention to the hazard. Populated river valleys are located downstream from many very high threat and high threat volcanoes, and these areas could be affected by lahars (for example, Hoblitt and others, 1998). The volume and mobility of lahars are two characteristics that can influence the extent of downstream effects (for example, George and others, 2022). The flows that reach the farthest downstream are mobile and voluminous. Additionally, entrainment of material as a lahar travels downstream may increase the volume, and a lahar that starts small may grow to a destructive size under certain conditions.

Increasingly, stratovolcanoes host recreational enthusiasts who could be affected by relatively localized geologic hazards, such as rainfall-induced debris flows, glacial outburst floods, rockfalls, and avalanches. These types of events can be common on many volcanoes, occurring seasonally in the case of debris flows and several times per year in the case of avalanches and rockfalls (for example, Allstadt and others, 2018). Many very high threat stratovolcanoes, especially within the contiguous

Figure H1. Photograph of the lahar associated with an eruption at Redoubt Volcano, Alaska, within the Drift River valley on April 4, 2009. The proximal deposits are a combination of pyroclastic flows and ash, but the distal lahar flowed in the valley almost 48 kilometers (30 miles) from the summit of the volcano to Cook Inlet. Photograph by R.G. McGimsey, U.S. Geological Survey, 2009.



United States, have low eruption frequencies (less than once per century), such that monitoring networks could be used more often for detection and characterization of small surface flows than for identification of volcanic unrest. Such information can be used to validate avalanche forecasts, inform rescue efforts, or notify other agencies of potentially damaged infrastructure (for example, roads, powerlines, or trails). Note that although many of these smaller surface flows create seismic and infrasound waves, the signals are typically highly distorted by the complex volcanic topography and geology. In general, the smaller the flow, the weaker the geophysical signals that it generates, and thus a denser geophysical network is required to study smaller flows (for example, Allstadt and others, 2018).

Lahar detection may not be an appropriate or necessary monitoring capability for all volcanoes. Some very high threat volcanoes, like Kilauea and Mauna Loa, have no lahar hazards currently, and thus no detection, tracking, and characterization capabilities for lahars are needed. At other very high threat volcanoes, such as Pavlof Volcano, Alaska, lahars might be common but pose minimal threat because the volcano is so remote. Ideally, the local observatory would understand the combination of hazard and risk associated with surface flows and assign monitoring and detection capabilities appropriately. Several volcano monitoring techniques (for example, Real-Time Seismic Amplitude Measurement [RSAM], amplitude-based locations, and infrasound array processing) can be adapted to also detect, characterize, and track debris flows, lahars, and other surface flows, so instrumentation installed for detecting volcanic unrest and eruptions can have multiple purposes. The utility of instrumentation for the purpose of monitoring unrest and lahars further justifies the importance and utility of a dense network of monitoring stations, even if the volcano remains quiescent.

Recommended Capability

Detect and Characterize the Onset, Size, and Flow Front Migration of Lahars

For lahars, required capabilities include detecting the onset, characterizing the volume, and locating the fronts of surface flows. An effective monitoring strategy is to be able to detect those lahars that may affect or approach downstream communities to account for uncertainties in the estimates of volume, speed, and previous modeling. Especially in the case of lahars, early detection is required for timely warnings to be issued to downstream communities. Paired with modeling, characterizing the potentially evolving volume of a lahar can provide information on the likely inundation extent and locating flow fronts and calculating flow velocities provide important information for emergency managers who may be coordinating evacuations of populated areas downstream.

Detection systems should be tailored to the volcano because some volcanoes, like Mount Rainier, have the potential for destructive and far-reaching lahars originating as large landslides as well as by eruptions. In such cases, detection systems are most effective if established in the drainages most likely to be affected by such events, as determined by geological studies of the volcano.

Another critical element in lahar monitoring is pre-event assessment of lahar hazards and risks for individual drainages. The planimetric area of lahar inundation can be estimated using models such as LAHARZ (Iverson and others, 1998; Schilling, 1998) or D-Claw (George and Iverson, 2014; George and others, 2022); however, the accuracy of such assessments partly depends on the accuracy of digital elevation models (DEMs) and the accuracy of the flow volume estimate. Therefore, acquisition of DEMs through aerial photography, satellite imagery, or light detection and ranging (lidar) surveys is also critical, particularly at high threat level volcanoes with at-risk population centers and (or) infrastructure (see chapter G of this volume [Orr and others, 2024] for more information).

Reliably detecting the initiation and downstream advance of surface flows on volcanoes has been a long-standing monitoring challenge (Allstadt and others, 2018). Debris flows and rockfalls have been detected using seismic and infrasound data (for example, Lavigne and others, 2000; Deparis and others, 2008; Burtin and others, 2009; Zobin and others, 2009; Dammeier and others, 2011). Lahars and debris flows have been coarsely located using seismic amplitudes at Volcán Cotopaxi, Ecuador (Kumagai and others, 2009; Ogiso and Yomogida, 2015), and at Illgraben, Switzerland (Walter and others, 2017), and using infrasound array processing at both Volcán Villarrica, Chile (Johnson and Palma, 2015), and Volcán de Fuego, Guatemala (Bosa and others, 2021; Johnson and others, 2023). Seismic-amplitude-based methods have been found, in the best case, to have errors of at least 1 kilometer (km) and commonly much more depending on the seismic network (Walsh and others, 2017). Infrasound is susceptible to both wind noise and topographic shielding and, thus, infrasound detections of lahars may be confined to instruments within the affected drainage during periods of low winds (for example, Johnson and Palma, 2015). Flows interacting with natural and anthropogenic hydrologic features (waterfalls and check dams) can dominate the signals in seismic and infrasound datasets, especially for stations close to the drainage (Johnson and Palma, 2015; Marchetti and others, 2019), making the tracking of flow fronts more difficult. Tilt has also been used to detect a passing lahar, where the magnitude of tilt is most correlated to the flow thickness (Wenner and others, 2022). Recent modeling of two end-member flows at Mount Rainier has shown that for a given flow mobility and no entrainment, the velocity of the flow may be a proxy for the volume of the flow (George and others, 2022). If correct, then characterizing the speed with a combination of seismic-based locations and infrasound-based back azimuths may be critical to understanding the potential downstream effects of the flow in real time.

Instrumentation

U.S. Geological Survey lahar monitoring systems deployed in the 1990s were dominantly composed of tripwires and acoustic flow monitors (AFMs), for example, at Redoubt Volcano (Dorava and Meyer, 1994), Mount St. Helens (Hadley and LaHusen, 1995), Mount Rainier (Lockhart and Murray, 2003), and several international volcanoes (Marcial and others, 1996; Lavigne and others, 2000). A next-generation system deployed at Mount Rainier in the late 2010s and early 2020s emphasized a more diverse suite of instrumentation, combining broadband seismic, infrasound, web cameras, and Global Navigation Satellite Systems (GNSS) to detect surface-flow events (fig. H2; Kramer and others, 2024). Coupling seismic and infrasound data allows for unique detection of surface flows, which produce both seismic and acoustic energy, reducing detection uncertainty and decreasing the potential for false alarms. Data are telemetered in real time, which reduces delays in detection and warning time that were a part of the previous generation of systems.

Broadband seismometers can be used to detect, localize, and track flows using various methods. A staple of volcano monitoring includes using RSAM analysis and alarming for the initial detection of a large event, including energetic surface-flow onsets. Amplitude-based seismic locations are commonly used to track surface flows and can use the same network already in place for monitoring volcano seismicity. However, high-hazard drainages or slopes may or may not lie in a sufficiently dense part of the seismic network, resulting in unacceptable errors in location; for that reason, additional seismic instrumentation may be needed to adequately monitor specific drainages. Even without a well-constrained location, changes in amplitude at a single downstream station or group of downstream stations may be sufficient to track the head of a surface flow. A subset of seismic sites may also be placed in areas that could be affected by large and infrequent lahars. Any data outage after a large-amplitude seismic signal may

be evidence of station destruction and could provide a constraint on the volume, as determined by pre-event modeling.

Broadband seismometers are preferred over short-period seismometers or AFMs for lahar monitoring because they can record low-frequency waves associated with large landslides (Allstadt and others, 2018), can record tilt signals if sufficiently close to the drainage (Wenner and others, 2022), and have broader scientific use for monitoring unrest and seismic imaging. Sample rates from 50 to 200 hertz (Hz) are encouraged, depending on telemetry constraints. Higher sampling rates enable recording of higher frequencies, which may be advantageous for stations within a few hundred meters of a drainage where high-frequency energy may be diagnostic of a passing lahar (Lai and others, 2018). If higher sampling rates cannot be telemetered in real time, onboard storage and processing is encouraged to enable post-event analysis.

Infrasound arrays have shown promise for detecting and tracking lahars (Johnson and Palma, 2015; Johnson and others, 2023), debris flows (Marchetti and others, 2019), and snow avalanches (Ulivieri and others, 2011; Marchetti and others, 2015; Watson and others, 2021). Infrasound arrays have the benefit over single instruments of providing a direction (back azimuth) and relative velocity of the coherent infrasound wavefield. The back azimuth is a useful parameter to separate a moving source, such as a lahar, from a stationary source, such as Strombolian activity, vigorous fumaroles, or anthropogenic noise. Furthermore, with knowledge of drainage geometry, changes in back azimuth associated with a lahar can be used to measure flow velocity. Unlike other methods, such as tripwires, radar, or laser rangefinders, infrasound arrays can be located several hundred meters from active channels in safer, more accessible locations and still provide low-latency detection and monitoring capability. The frequency content of infrasound from surface flows varies widely; lahars from Volcán Villarrica produced primarily high-frequency energy greater than 10 Hz (Johnson and Palma, 2015), whereas energy from nonvolcanic



Figure H2. Photograph of monitoring site Copper Mountain at Mount Rainier, Washington. This site is part of the Rainier Lahar Detection Network and has seismic, geodetic, and infrasound equipment installed. An infrasound wind filter is on the far right. Sunset Amphitheater, the source area of the Electron Mudflow, is in the background. Photograph by Liz Westby, U.S. Geological Survey, 2022.

debris flows in an alpine setting peaked between 3 and 5 Hz (Marchetti and others, 2019). Infrasound arrays designed with four or more elements can detect a wide range of frequencies and are useful for monitoring a wide variety of flows. An ideal array configuration features irregular spacing with some closely spaced elements (about 20 meters [m]) to avoid aliasing of high-frequency signals as well as some with a wide aperture (about 100 m or more) to resolve low-frequency signals. Suggested sample rates for volcano monitoring (100–400 Hz; see chapter C of this volume [Lyons and others, 2024] on infrasound for details) are suitable for detecting and studying large surface flows; however, bandwidth considerations may reduce the sample rate to 50 Hz. As with seismic data, we suggest onboard storage and processing of higher sampling rates if bandwidth is limited to enable post-event analysis. To detect a signal and obtain a velocity and back azimuth with acceptable errors, the recommended minimum number of array elements is four, but five or more is preferred. In places that have multiple arrays in the same vicinity, or because of land-use or telemetry bandwidth restrictions, three-element arrays may be acceptable. Three-element arrays can provide velocity and back azimuth capabilities but have higher uncertainty, limited frequency range, and lack of redundancy to sensor failure. Installation of additional three-element arrays within the same drainage can provide redundancy and better constrain flow characteristics and migration.

The location of infrasound array installation is critically important to its effectiveness in lahar detection. Placing infrasound arrays several hundred meters from a drainage and siting them to provide the largest possible change in back azimuth allows downstream tracking of flows (Johnson and others, 2023). Topographic shielding can affect infrasound signals; the most useful are those that have line of sight to flows. Infrasonic waveforms from surface flows are commonly emergent and low amplitude, so instruments with low noise floors are essential, particularly at higher frequencies (>5 Hz). Wind noise has the potential to obscure infrasound signals from any surface flow. Minimizing wind-noise exposure, either through siting sensors in vegetated areas or by placing a wind-noise filter over individual sensors, can improve signal quality.

Web cameras may be a valuable tool for verifying the occurrence of a surface flow if the view is correct, the visibility good, and the light sufficient for a quality image. Many of these factors may occur sporadically, especially in winter, and streaming video is commonly too demanding for limited-bandwidth, real-time telemetry. For these reasons, web cameras require careful thought regarding use and placement. Web cameras provide a complementary multidisciplinary observation tool that can augment other monitoring techniques; however, they are not a primary monitoring technique.

Other instrumentation, such as radar sensors, extensometers, and laser rangefinders, have been installed in lahar-prone drainages (Iezzi and others, 2024). However, every drainage is unique in terms of its vegetation, siting opportunities, and land-use restrictions. Hence, installation of these types of monitoring instruments requires case-by-case determination.

Recommendations

Levels 1 and 2.—No monitoring recommended.

Level 3.—Capability to detect infrequent, large surface-flow events that are associated with eruptive activity in drainages that have substantial potential for lahars.

- At least one four- to six-element infrasound array that is sensitive to multiple drainages; arrays are sited to minimize topographic barriers to potentially active drainages and provide azimuthal separation between drainages.
- Two seismometers in or near each drainage of interest, with one in the potential source area and the other in a downstream location but upstream from any at-risk population centers or infrastructure. The infrasound array could be co-located with one of the seismic stations if conditions are acceptable.

Level 4.—Capability to detect, characterize, and track surface-flow events of varying sizes, including those that are not associated with eruptions but that could affect population centers or infrastructure.

- Three or more three- to six-element infrasound arrays along each potential flow channel that has high lahar hazard. Include at least one array that has four to six elements that are sensitive to multiple drainages to minimize topographic shielding and provide azimuthal separation between drainages.
- At least one seismometer in the source area of each drainage, with additional sensors along each drainage at 1- to 5-km intervals. Some of these stations may already exist as part of a volcano monitoring network.
- Web cameras, where possible, to verify surface-flow occurrence.

References Cited

- Allstadt, K.E., Matoza, R.S., Lockhart, A.B., Moran, S.C., Caplan-Auerbach, J., Haney, M.M., Thelen, W.A., and Malone, S.D., 2018, Seismic and acoustic signatures of surficial mass movements at volcanoes: *Journal of Volcanology and Geothermal Research*, v. 364, p. 76–106, <https://doi.org/10.1016/j.jvolgeores.2018.09.007>.
- Bosa, A., Johnson, J.B., De Angelis, S., Lyons, J., Roca, A., Anderson, J., and Pineda, A., 2021, Tracking secondary lahar flow paths and characterizing pulses and surges using infrasound array networks at Volcán de Fuego, Guatemala: *Volcanica*, v. 4, no. 2, p. 239–256, <https://doi.org/10.30909/vol.04.02.239256>.

- Burtin, A., Bollinger, L., Cattin, R., Vergne, J., and Nábělek, J.L., 2009, Spatiotemporal sequence of Himalayan debris flow from analysis of high-frequency seismic noise: *Journal of Geophysical Research, Earth Surface*, v. 114, no. F4, <https://doi.org/10.1029/2008JF001198>.
- Dammeier, F., Moore, J.R., Haslinger, F., and Loew, S., 2011, Characterization of alpine rockslides using statistical analysis of seismic signals: *Journal of Geophysical Research, Earth Surface*, v. 116, no. F4, <https://doi.org/10.1029/2011JF002037>.
- Deparis, J., Jongmans, D., Cotton, F., Baillet, L., Thouvenot, F., and Hantz, D., 2008, Analysis of rock-fall and rock-fall avalanche seismograms in the French Alps: *Bulletin of the Seismological Society of America*, v. 98, no. 4, p. 1781–1796, <https://doi.org/10.1785/0120070082>.
- Dorava, J.M., and Meyer, D.F., 1994, Hydrologic hazards in the lower Drift River basin associated with the 1989–1990 eruptions of Redoubt Volcano, Alaska: *Journal of Volcanology and Geothermal Research*, v. 62, no. 1, p. 387–407, [https://doi.org/10.1016/0377-0273\(94\)90044-2](https://doi.org/10.1016/0377-0273(94)90044-2).
- George, D.L., and Iverson, R.M., 2014, A depth-averaged debris-flow model that includes the effects of evolving dilatancy. II. Numerical predictions and experimental tests: *Proceedings of the Royal Society A*, v. 470, no. 2170, <https://doi.org/10.1098/rspa.2013.0820>.
- George, D.L., Iverson, R.M., and Cannon, C.M., 2022, Modeling the dynamics of lahars that originate as landslides on the west side of Mount Rainier, Washington: U.S. Geological Survey Open-File Report 2021–1118, 66 p., <https://doi.org/10.3133/ofr20211118>.
- Hadley, K.C., and LaHusen, R.G., 1995, Technical manual for the experimental acoustic flow monitor: U.S. Geological Survey Open-File Report 95–114, 26 p., <https://doi.org/10.3133/ofr95114>.
- Hoblitt, R.P., Walder, J.S., Driedger, C.L., Scott, K.M., Pringle, P.T., and Vallance, J.W., 1998, Volcano hazards from Mount Rainier, Washington (revised 1998): U.S. Geological Survey Open-File Report 98–428, 11 p., 2 plates, <https://doi.org/10.3133/ofr98428>.
- Iezzi, A., Thelen, W.A., Bryant, E., Gabrielson, C., Moran, S.C., Obryk, M.K., Patrick, M., and Younger, F., 2024, Characterization of a debris flow at Mount Rainier via seismoacoustics and a novel usage of a laser rangefinder [abs.]: *Seismological Research Letters*, v. 95, no. 2B, p. 1262.
- Iverson, R.M., Schilling, S.P., and Vallance, J.W., 1998, Objective delineation of lahar-inundation hazard zones: *Geological Society of America Bulletin*, v. 110, no. 8, p. 972–984, [https://doi.org/10.1130/0016-7606\(1998\)110<0972:ODOLIH>2.3.CO;2](https://doi.org/10.1130/0016-7606(1998)110<0972:ODOLIH>2.3.CO;2).
- Janda, R.J., Scott, K.M., Nolan, K.M., and Martinson, H.A., 1981, Lahar movement, effects, and deposits, *in* Lipman, P.W., and Mullineaux, D.R., eds., *The 1980 eruptions of Mount St. Helens*: U.S. Geological Survey Professional Paper 1250, p. 461–478, <https://doi.org/10.3133/pp1250>.
- Johnson, J.B., and Palma, J.L., 2015, Lahar infrasound associated with Volcán Villarrica's 3 March 2015 eruption: *Geophysical Research Letters*, v. 42, no. 15, p. 6324–6331, <https://doi.org/10.1002/2015GL065024>.
- Johnson, J.B., Roca, A., Pineda, A., Mérida, R., Escobar-Wolf, R., Anderson, J.F., Mock, J., Bosa, A., Bejar, G., and Waite, G., 2023, Infrasound detection of approaching lahars: *Scientific Reports*, v. 13, no. 6476, <https://doi.org/10.1038/s41598-023-32109-2>.
- Kramer, R.L., Thelen, W.A., Iezzi, A.M., Moran, S.C., and Pauk, B.A., 2024, Recent expansion of the Cascades Volcano Observatory geophysical network at Mount Rainier for improved volcano and lahar monitoring: *Seismological Research Letters*, 15 p., <https://doi.org/10.1785/0220240112>.
- Kumagai, H., Palacios, P., Maeda, T., Castillo, D.B., and Nakano, M., 2009, Seismic tracking of lahars using tremor signals: *Journal of Volcanology and Geothermal Research*, v. 183, no. 1–2, p. 112–121, <https://doi.org/10.1016/j.jvolgeores.2009.03.010>.
- Lai, V.H., Tsai, V.C., Lamb, M.P., Ulizio, T.P., and Beer, A.R., 2018, The seismic signature of debris flows—Flow mechanics and early warning at Montecito, California: *Geophysical Research Letters*, v. 45, no. 11, p. 5528–5535, <https://doi.org/10.1029/2018GL077683>.
- Lavigne, F., Thouret, J.-C., Voight, B., Young, K., LaHusen, R., Marso, J., Suwa, H., Sumaryono, A., Sayudi, D.S., and Dejean, M., 2000, Instrumental lahar monitoring at Merapi Volcano, Central Java, Indonesia: *Journal of Volcanology and Geothermal Research*, v. 100, no. 1–4, p. 457–478, [https://doi.org/10.1016/S0377-0273\(00\)00151-7](https://doi.org/10.1016/S0377-0273(00)00151-7).
- Lockhart, A.B., and Murray, T.L., 2003, The Mount Rainier lahar detection system [abs.]: *Eos, Transactions, American Geophysical Union*, v. 84, no. 47, no. V51F-0343.
- Lyons, J.J., Fee, D., Thelen, W.A., Iezzi, A.M., and Wech, A.G., 2024, Infrasound for volcano monitoring, chap. C *of* Flinders, A.F., Lowenstern, J.B., Coombs, M.L., and Poland, M.P., eds., *Recommended capabilities and instrumentation for volcano monitoring in the United States*: U.S. Geological Survey Scientific Investigations Report 2024–5062–C, 11 p., <https://doi.org/10.3133/sir20245062C>.
- Major, J.J., Janda, R.J., and Daag, A.S., 1996, Watershed disturbance and lahars on the east side of Mount Pinatubo during the mid-June 1991 eruptions, *in* Newhall, C.S., and Punongbayan, S., eds., *Fire and mud—Eruptions and lahars of Mount Pinatubo*, Philippines: Seattle, University of Washington Press, p. 895–919.

- Marchetti, E., Ripepe, M., Olivieri, G., and Kogelnig, A., 2015, Infrasound array criteria for automatic detection and front velocity estimation of snow avalanches—Towards a real-time early-warning system: *Natural Hazards and Earth System Sciences*, v. 15, no. 11, p. 2545–2555, <https://doi.org/10.5194/nhess-15-2545-2015>.
- Marchetti, E., Walter, F., Barfucci, G., Genco, R., Wenner, M., Ripepe, M., McARDell, B., and Price, C., 2019, Infrasound array analysis of debris flow activity and implication for early warning: *Journal of Geophysical Research, Earth Surface*, v. 124, no. 2, p. 567–587, <https://doi.org/10.1029/2018JF004785>.
- Marcial, S., Melosantos, A.A., Hadley, K.C., LaHusen, R.G., and Marso, J.N., 1996, Instrumental lahar monitoring at Mount Pinatubo in Newhall, C.G., and Punongbayan, R.S., eds., *Fire and mud—Eruptions and lahars of Mount Pinatubo*, Philippines: Seattle, University of Washington Press, p. 1015–1022.
- Naranjo, J.L., Sigurdsson, H., Carey, S.N., and Fritz, W., 1986, Eruption of the Nevado del Ruiz Volcano, Colombia, on 13 November 1985: Tephra Fall and Lahars: *Science*, v. 233, p. 961–963, <https://doi.org/10.1126/science.233.4767.961>.
- Ogiso, M., and Yomogida, K., 2015, Estimation of locations and migration of debris flows on Izu-Oshima Island, Japan, on 16 October 2013 by the distribution of high frequency seismic amplitudes: *Journal of Geophysical Research, Solid Earth*, v. 298, p. 15–26, <https://doi.org/10.1016/j.jvolgeores.2015.03.015>.
- Orr, T.R., Dietterich, H.R., and Poland, M.P., 2024, Tracking surface changes caused by volcanic activity, chap. G of Flinders, A.F., Lowenstern, J.B., Coombs, M.L., and Poland, M.P., eds., *Recommended capabilities and instrumentation for volcano monitoring in the United States*: U.S. Geological Survey Scientific Investigations Report 2024–5062–G, 11 p., <https://doi.org/10.3133/sir20245062G>.
- Pierson, T.C., 1995, Flow characteristics of large eruption-triggered debris flows at snow-clad volcanoes—Constraints for debris-flow models: *Journal of Volcanology and Geothermal Research*, v. 66, no. 1–4, p. 283–294, [https://doi.org/10.1016/0377-0273\(94\)00070-W](https://doi.org/10.1016/0377-0273(94)00070-W).
- Pierson, T.C., Daag, A.S., Reyes, P.J.D., Regalado, M.T.M., Solidum, R.U., and Tubianosa, B.S., 1996, Flow and deposition of posteruption hot lahars on the east side of Mount Pinatubo, July–October 1991, in Newhall, C.S., and Punongbayan, S., eds., *Fire and mud—Eruptions and lahars of Mount Pinatubo*, Philippines: Seattle, University of Washington Press, p. 921–950.
- Pierson, T.C., and Scott, K.M., 1985, Downstream dilution of a lahar—Transition from debris flow to hyperconcentrated streamflow: *Water Resources Research*, v. 21, no. 10, p. 1511–1524, <https://doi.org/10.1029/WR021i010p01511>.
- Schilling, S.P., 1998, LAHARZ—GIS programs for automated mapping of lahar-inundation hazard zones: U.S. Geological Survey Open-File Report 98-638, 85 p., <https://doi.org/10.3133/ofr98638>.
- Sisson, T.W., and Vallance, J.W., 2009, Frequent eruptions of Mount Rainier over the last ~2,600 years: *Bulletin of Volcanology*, v. 72, no. 6, p. 595–618, <https://doi.org/10.1007/s00445-008-0245-7>.
- Olivieri, G., Marchetti, E., Ripepe, M., Chiambretti, I., De Rosa, G., and Segor, V., 2011, Monitoring snow avalanches in Northwestern Italian Alps using an infrasound array: *Cold Regions Science and Technology*, v. 69, no. 2–3, p. 177–183, <https://doi.org/10.1016/j.coldregions.2011.09.006>.
- Voight, B., 1990, The 1985 Nevado del Ruiz volcano catastrophe—Anatomy and retrospection: *Journal of Volcanology and Geothermal Research*, v. 42, nos. 1–2, p. 151–188, [https://doi.org/10.1016/0377-0273\(90\)90075-Q](https://doi.org/10.1016/0377-0273(90)90075-Q).
- Walsh, B., Jolly, A.D., and Procter, J., 2017, Calibrating the amplitude source location (ASL) method by using active seismic sources—An example from Te Maari Volcano, Tongariro National Park, New Zealand: *Geophysical Research Letters*, v. 44, no. 8, p. 3591–3599, <https://doi.org/10.1002/2017GL073000>.
- Walter, F., Burtin, A., McARDell, B.W., Hovius, N., Weder, B., and Turowski, J.M., 2017, Testing seismic amplitude source location for fast debris-flow detection at Illgraben, Switzerland: *Natural Hazards and Earth System Sciences*, v. 17, no. 6, p. 939–955, <https://doi.org/10.5194/nhess-17-939-2017>.
- Watson, L.M., Carpenter, B., Thompson, K., and Johnson, J.B., 2021, Using local infrasound arrays to detect plunging snow avalanches along the Milford Road, New Zealand (Aotearoa): *Natural Hazards*, v. 111, p. 949–972, <https://doi.org/10.1007/s11069-021-05086-w>.
- Waythomas, C.F., Pierson, T.C., Major, J.J., and Scott, W.E., 2013, Voluminous ice-rich and water-rich lahars generated during the 2009 eruption of Redoubt Volcano, Alaska: *Journal of Volcanology and Geothermal Research*, v. 259, p. 389–413, <https://doi.org/10.1016/j.jvolgeores.2012.05.012>.
- Wenner, M., Allstadt, K., Thelen, W., Lockhart, A., Hirschberg, J., McARDell, B.W., and Walter, F., 2022, Seismometer records of ground tilt induced by debris flows: *Bulletin of the Seismological Society of America*, v. 112, no. 5, p. 2376–2395, <https://doi.org/10.1785/0120210271>.
- Zobin, V.M., Reyes, G.A., Guevara, E., and Bretón, M., 2009, Scaling relationship for Vulcanian explosions derived from broadband seismic signals: *Journal of Geophysical Research*, v. 114, no. B03203, <https://doi.org/10.1029/2008JB005983>.

Chapter I



U.S. Geological Survey Alaska Volcano Observatory scientist J. Lyons prepares to deploy hydrophones (underwater acoustic sensors) in the Bering Sea near Bogoslof Island, Alaska. These instruments were deployed in response to the shallow submarine eruption of 2016–2017. Photograph by A. Van Eaton, U.S. Geological Survey, May 21, 2017.

Chapter I

Monitoring Marine Eruptions

By Gabrielle Tepp¹

Introduction

Submarine volcanoes produce much of the same seismicity and eruptive activity as subaerial volcanoes and can pose hazards to society. Although they can be monitored with similar techniques and methods as described in other chapters of this volume, their submerged location brings unique challenges. This chapter addresses these challenges and provides recommendations for monitoring volcanoes fully or partly in marine environments to meet the capabilities described in other chapters of this volume.

The United States and its territories host dozens of submarine volcanoes with most (around 60) in the Commonwealth of the Northern Mariana Islands. Approximately 20 of the Northern Mariana Islands submarine volcanoes are known to be hydrothermally active, and 10 have confirmed eruptions since the 1950s (for example, Baker and others, 2008; Tepp and others, 2019a). Nine of those volcanoes were considered by the National Volcanic Threat Assessment (Ewert and others, 2018) to have a combination of eruptive type and summit depth that poses a higher risk of hazardous eruptions, although only one was listed as a moderate (level 3) threat. Other notable submarine volcanoes of interest to the United States that have historically erupted are Axial Seamount off the Washington State coast, Kama‘ehuakanaloa in Hawai‘i, and Vailulu‘u seamount in American Samoa. All of these, however, have a low risk of hazards because of their depth (greater than 600 meters below sea level) and eruptive type and so are not included in the National Volcanic Threat Assessment. In addition to submarine volcanoes, the submerged flanks of island volcanoes can also be a source of hazardous submarine eruptions—for example, the 1877 eruption of Mauna Loa, Hawai‘i, in Kealakekua Bay (Wanless and others, 2006).

The most notable submarine eruption in recent times was the 2022 eruption of Hunga Tonga–Hunga Ha‘apai in Tonga, which was one of the largest eruptions on Earth in the past 100 years. It created a massive volcanic plume, unprecedented shock waves, and far-reaching tsunami (Lynett and others, 2022). Other recent submarine eruptions in the Pacific Ocean Basin have produced subaerial plumes that reached aircraft heights (Carey and others, 2014) and large pumice rafts that can affect marine traffic and harbors (for example, Jutzeler and others, 2014; Kornei, 2019). These examples illustrate the potential hazards of major submarine eruptions. Yet, submarine volcanoes are largely unmonitored, and

many eruptions occur that are unnoticed or only identified hours or days afterward.

Within U.S. territory, submarine volcanoes in the Northern Mariana Islands have been known to produce eruptive activity that can affect society. Reports from fishermen and other marine vessels in the Northern Mariana Islands have noted underwater explosions, sea-surface discoloration, and bubbling water, all of which are known to be signs of submarine volcanic activity. South Sarigan seamount, located about 160 kilometers (km) north of Saipan, erupted in 2010 from greater than 150 meters below the sea surface, resulting in a gas and ash plume that reached more than 11.9 km into the atmosphere (for example, Searcy, 2013; Embley and others, 2014), high enough to affect international air traffic. Precursory and co-eruptive seismicity was detected on the regional Northern Mariana Islands seismic network (Searcy, 2013) and on global monitoring instruments (Green and others, 2013).

Monitoring of submarine volcanoes is best accomplished with marine-based instrumentation, which is also useful for monitoring small island volcanoes that may not have the land area necessary for comprehensive subaerial monitoring. The primary marine-based instrumentation used for submarine volcanoes includes ocean-bottom pressure sensors to assess sea-floor deformation, ocean-bottom seismometers (OBSs) to detect seismicity, and both moored and ocean-bottom hydrophones to detect submarine explosions. Other sensors offer important monitoring data, such as turbidity, temperature, and chemistry of hydrothermal emissions. Marine-based instruments are typically deployed in campaign-style networks with no real-time telemetry owing to cost considerations and technical limitations. However, when necessary, marine instruments can be operated in real time using cables to transmit data to land-based facilities; other technologies for this purpose are in use or in development, such as acoustic transmission from the instrument to a moored buoy (Matsumoto and others, 2016) and a winch-based system with a satellite antenna that is part of the instrument mooring (Matsumoto and others, 2019). Emerging technologies for marine-based monitoring may be considered as part of a future monitoring plan. These technologies include ocean gliders and floats with on-board hydrophones that have been used to record earthquakes and submarine eruptions (for example, Matsumoto and others, 2013; Sukhovich and others, 2015) and fiber-optic cables that have been used as strainmeters to detect earthquakes (for example, Marra and others, 2018; Lindsey and others, 2019). Land-based instruments and satellites can also provide some capability for monitoring submarine volcanoes, but they provide more limited observations than marine-based instrumentation.

¹Now at California Institute of Technology.

Recommended Capabilities

Regional-Scale Monitoring of Submarine Eruptions

To provide for public safety from submarine volcanoes, it is important to monitor for submarine volcanic unrest and to detect eruptions, even at volcanoes far from monitoring instrumentation. Remote monitoring of submarine volcanic activity is best accomplished with hydroacoustic and seismic signals, although infrasonic and atmospheric acoustic signals are sometimes detected from submarine eruptions that breach the sea surface (for example, Tepp and Dziak, 2021). Hydroacoustic signals (hereinafter referred to as T-phases) can be produced directly in the water column by explosions, or they can be generated by the conversion of a seismic signal at the seafloor (for example, Talandier and Okal, 1998). Importantly, T-phases can propagate much farther than seismic signals owing to the comparatively low attenuation of sound in water and the deep-ocean waveguide known as the Sound Fixing and Ranging (SOFAR) channel. T-phases from volcanic activity have been detected at distances exceeding 15,000 km and even from different ocean basins (for example, Johnson and others, 1963; Metz and others, 2016).

Beginning in the 1950s, hydrophone arrays operated by the Department of Defense recorded at least a dozen submarine eruptions (for example, Dietz and Sheehy, 1954; Dziak and Fox, 2002). Currently, the Comprehensive Test Ban Treaty Organization operates several cabled hydrophone arrays around the world as part of its International Monitoring System (IMS) that monitors for nuclear explosions. These arrays transmit data in real time, and some have data publicly available for volcano monitoring purposes, such as the Wake Island (U.S.) arrays. Hydrophone arrays (fig. 11) operate similarly to infrasound arrays and can be used for finding bearings to volcanic activity at regional distances. IMS data have also been used in numerous

research studies of submarine volcanoes (for example, Green and others, 2013; Metz and others, 2016; Tepp and others, 2019b), which demonstrates the potential benefit of such systems to monitoring.

Land-based instruments have also been used for real-time monitoring of submarine volcanoes. The longest operating and most successful network in this regard is the Polynesian Seismic Network (RSP; for example, Talandier and Kuster, 1976; Talandier, 2004), which was specifically designed to optimize T-phase detection. The seismic-station recording parameters and locations are based on T-phase characteristics and propagation physics. The RSP has detected volcanic activity throughout the Pacific Ocean Basin, including activity of submarine volcanoes in the Northern Mariana Islands. The IMS hydroacoustic network also contains some land-based seismic stations that have been optimized for T-phase detection in the same way as the RSP (for example, Okal, 2001). Non-optimized land-based seismic networks can also detect submarine volcanic activity, including typical seismic phases and T-phases. For example, the Northern Mariana Islands seismic network recorded precursory seismicity and eruptive activity from South Sarigan seamount in 2010 (Searcy, 2013); an earthquake swarm, major eruption, and large landslide at NW Rota-1 Seamount in 2009; and explosive eruptions from Ahyi seamount in 2014 (Tepp and others, 2019b). Typically, land-based seismic monitoring is most successful when sensors are located within 30 km of the submarine activity, which allows for the detection of most seismic phases. More distant seismometers may only detect strong seismic phases or some T-phases.

Satellite and aerial imagery can also be important for detecting submarine volcanic activity that has resulted in discolored water, pumice rafts, subaerial plumes, or other surficial activity. These monitoring methods provide little to no ability for monitoring preeruptive unrest of submarine volcanoes but are useful for identifying and characterizing eruptions that are active or very recently ended.

Figure 11. Photograph from the June 2017 Northern Mariana Islands hydrophone deployment. Four hydrophone moorings, arranged in a diamond-shaped array, were deployed about 110 kilometers northwest of Saipan in about 4,000 meters of water. The large orange spheres are floats that hold the moorings vertical in the water column and allow for instrument retrieval. Old train wheels are used as anchors and the spools of cord connect all parts of the mooring. Deployment operations were done off the motor vessel (M/V) *Peregrine* (Pacific Marine Enterprises) in collaboration with the National Oceanic and Atmospheric Administration (NOAA) and with assistance from the Commonwealth of the Northern Mariana Islands Office of Homeland Security and Emergency Management. The hydrophones recorded signals from submarine volcanoes, earthquakes, and other natural and man-made sources for approximately 1 year (Tepp and others, 2021). Photograph by G. Tepp, U.S. Geological Survey.



Instrumentation

Small-aperture hydrophone arrays are typically deployed with either three or four instruments spaced about 2 km apart (for example, Hanson and others, 2001; Bohnenstiehl and others, 2013). Additional instruments can help refine detection parameters and provide redundancy in case of instrument failure. Each instrument is deployed on a mooring that holds the hydrophone within the SOFAR channel to achieve the best long-range detection capability. These moorings can be self-contained and powered by batteries, with data available only after instrument recovery. To provide real-time monitoring, they must be cabled to a land-based receiving facility or have a telemetry component (for example, satellite buoy); as such, they are costly to operate. Global and regional small-aperture hydrophone arrays, such as those in the IMS, typically have sampling rates of 250 samples per second. This covers the expected dominant frequency range for most volcanic signals; however, some types of signals (for example, mass flows or venting) may contain frequencies as high as several hundred hertz, so higher sampling rates are recommended when possible and desired for the expected activity.

Regional-scale (that is, large-aperture) networks cover a large area with wide spacing (several to hundreds of kilometers) between instruments. Although hydrophones and OBSs have been deployed in such network configurations (for example, Dziak and others, 2005), it is costly and difficult to operate in real time with current technology because every individual station may need to be cabled to shore or have another method of telemetry. Thus, only land-based regional-scale networks are recommended for real-time monitoring. To best use land-based seismic networks for submarine monitoring, T-phase-optimized seismic stations, as discussed for the RSP above, should be incorporated into the regular regional network.

Recommendations

The following recommendations would ideally be applied to regions with at least one submarine volcano at or above the given threat level. For regions with submarine volcanoes that have not been assigned a threat level, the levels 1 and 2 minimums are recommended.

Levels 1 and 2.—Detect major submarine eruptions and large earthquakes (magnitude >3) that may indicate significant volcanic unrest, constrain source location or back-azimuth of volcanic signals, and characterize submarine eruption activity to identify potential hazards.

- Minimum of one to three land-based seismic stations optimized for T-phase detection; distribution determined by the number and location of submarine volcanoes.
- Short-term (6–12 month) deployments of two to three non-real-time hydrophones for regions with higher risk, more volcanoes, and (or) sparser or more distant land-based networks.

- Weekly to daily regional satellite monitoring for signs of volcanic activity dependent on risk in region.

Levels 3 and 4.—Characterize baseline seismic and submarine volcanic activity, identify long-term changes in activity, and detect low-level activity in real time.

- One to two cabled small-aperture hydrophone arrays that have four moorings.
- Additional optimized T-phase stations and short-term hydrophone deployments, dependent on regional situation and activity levels.
- Additional monitoring via satellite and other methods as needed for understanding eruption hazards.

Local-Scale Monitoring of Submarine Volcanoes

Local instrument networks are required to provide adequate event detection at high-risk submarine volcanoes. These networks should be largely equivalent to those at subaerial volcanoes. For example, at least four local OBSs or hydrophones would be needed to accurately locate earthquakes at a submarine volcano. Local networks can detect weaker activity than regional instruments, allowing for a more complete characterization of volcanic activity and the possibility of forecasting eruptions.

Cabled networks and instrument arrays are currently in real-time operation at some locations around the world—for example, the Ocean Observatories Initiative network at Axial Seamount (Kelley and others, 2014). Nooner and Chadwick (2016) described a successful forecast of the 2015 eruption of Axial Seamount based on deformation data from the Ocean Observatories Initiative network. OBSs in the network recorded seismicity before, during, and after the 2015 eruption, and earthquakes as small as magnitude 0 were located (Wilcock and others, 2016). Hydroacoustic data were critical for identifying events from the eruption that initiated at the water-seafloor interface rather than below ground, including impulsive signals generated by seawater interacting with lava flows that could provide time and location constraints for effusive events (for example, Caplan-Auerbach and others, 2017; Le Saout and others, 2020). A more limited local cabled observatory (the Hawai‘i Undersea Geo-Observatory) was deployed at Kama‘ehuakanaloa from October 1997 to April 1998 (Duennebiele and others, 2002) and detected seismicity at Kama‘ehuakanaloa (Caplan-Auerbach and Duennebiele, 2001) as well as landslides from lava-delta collapses at Kilauea (Caplan-Auerbach and others, 2001).

Although remote sensing techniques such as interferometric synthetic aperture radar do not work underwater, submarine volcanoes can be mapped with sonar techniques. The resulting bathymetric maps allow for better understanding of changes in the edifice from volcanic activity. For example, comparisons of bathymetric maps produced years apart have identified landslides on Ahihi seamount (Tepp and others, 2019b) and tracked lava cone growth within the summit crater of Vailulu‘u seamount (Tepp and others, 2019a).

Instrumentation

All local networks should include OBSs and hydrophones, as well as sensors for hydrothermal activity (turbidity, temperature, and chemistry) and surface deformation. Currently, the best option for transmitting data in real time from marine-based instrument networks is by cables, although other less expensive methods have been tested (for example, Matsumoto and others, 2016, 2019). Short-term (less than about 6 months), non-real-time instruments may be more cost effective for monitoring long-term unrest and lower risk activity. Where possible, local networks may make use of land-based instruments on nearby islands that are close enough (within about 20 km) to detect low-level activity at the submarine volcano.

The Axial Seamount network provides a template for an optimal local submarine volcano network that can inform the design of networks at other volcanoes. It is composed of real-time broadband and short-period seismometers, hydrophones, bottom-pressure sensors, tilt instruments, and various instruments for measuring chemistry and hydrothermal activity (Kelley and others, 2014). The cabled instruments are supplemented by non-cabled instruments for more detailed scientific investigation (Wilcock and others, 2018).

Recommendations

Level 1.—Detect major eruptions and locate large earthquakes (magnitude >4) that could indicate significant unrest that is highly likely to lead to a major eruption.

- No local monitoring recommended; regional marine-based and land-based monitoring is adequate.

Level 2.—Detect and characterize major local eruptions or activity that could indicate significant unrest that could potentially lead to a major eruption.

- One to two land-based seismic stations optimized for T-phases on the nearest island (may be part of regional network).
- Use regional marine-based and land-based monitoring.
- Non-real-time, marine-based instruments deployed during periods of unrest as needed.
- Bathymetric mapping when possible.

Level 3.—Detect and monitor signs of volcanic unrest, including increases in local seismicity and low-level eruptions.

- At least one real-time, marine-based instrument site with a broadband seismometer, hydrophone, and other sensors.
- Additional non-real-time, marine-based instruments deployed during prolonged periods of unrest.
- One to two land-based seismic stations optimized for T-phases on the nearest islands (may be part of regional network).

- Use regional monitoring to supplement local instruments.
- Bathymetric mapping every 5–10 years and after periods of volcanic activity.

Level 4.—Locate local earthquakes, detect signs of volcanic unrest and low-level eruptions, and potentially forecast major eruptions.

- At least four real-time, marine-based instrument sites with a broad-band seismometer, hydrophone, and other sensors.
- Additional non-real-time, marine-based instruments deployed during prolonged periods of unrest.
- One to two land-based seismic stations optimized for T-phases on nearest islands (may be part of regional network).
- One to two infrasound sensors or arrays on nearest islands (may be part of another network), if volcano is shallow enough to produce acoustic waves.
- Use regional monitoring to supplement local instruments.
- Bathymetric mapping every 1–5 years and after periods of volcanic activity.

Marine Monitoring for Small Island Volcanoes

Some island volcanoes in the United States have edifices that are largely submerged even though their summits are above the sea surface. Their small sizes limit the ability to install land-based instruments; thus, monitoring of small island volcanoes can benefit from similar techniques used for submarine volcanoes. One example is Bogoslof Island, Alaska, which erupted in 2016–17 (Coombs and others, 2019). Even though the volcano has a large submarine edifice, the small Bogoslof Island had an area of only 0.3 square kilometer (km²) before the 2016–17 eruption and has maintained an area of approximately 1.5 km² to date (2022). This volcano had no local instrumentation during the 2016–17 eruption, and monitoring and understanding of the eruption was improved by the use of submarine monitoring techniques, including a local hydrophone deployed as a rapid-response instrument, the use of regional seismometers and infrasound arrays, and the detection of T-phases (for example, Tepp and others, 2019c). Of note, the local hydrophone recorded mass-flow events that followed a few of the eruptions and that were not recorded seismically, demonstrating one benefit of using hydrophones. Anatahan Island, in the Northern Mariana Islands, is a subaerial volcanic island large enough to host a few local monitoring instruments and provides an example of how marine-based instruments can supplement land-based monitoring for small island volcanoes. During Anatahan Island's 2003 eruption, seismicity was recorded on regional hydrophones, allowing for additional characterization of the seismicity (Dziak and others, 2005).

Non-real-time OBSs have been used for continuous monitoring of Nishinoshima, a small island volcano in Japan, by switching out the instruments and retrieving data every 6 months (Shinohara and others, 2017). Although this approach does not provide data in real time, it provides a baseline of activity and could be used to detect long-term changes that may reveal an increase or decrease in volcanic activity.

Instrumentation

For small island volcanoes, monitoring networks would ideally rely on land-based instruments, with marine-based instruments used as needed to upgrade networks to the recommended monitoring capabilities outlined in other chapters of this volume. Marine-based monitoring should focus on OBSs but may include other geophysical, hydrothermal, or geochemical sensors. Marine-based instruments may also be deployed on a short-term basis to improve characterization of baseline activity.

Recommendations

Level 1.—Detect major eruptions or activity that could indicate significant unrest.

- Use local land-based and regional monitoring.

Level 2.—Detect moderate eruptions or activity that could indicate major unrest.

- Use local land-based and regional monitoring.

Level 3.—Locate local earthquakes; detect signs of volcanic unrest and low-level eruptions.

- Use local land-based and regional monitoring.
- Deploy short-term (3–12 month), marine-based instruments to improve characterization of baseline activity and to monitor long-term changes, particularly during periods of unrest.

Level 4.—Locate local earthquakes, detect signs of volcanic unrest and low-level eruptions, and forecast major eruptions when possible.

- Use local land-based and regional monitoring.
- Deploy additional marine-based, real-time instruments as needed to complete a network with a level-4-monitoring capability as outlined in other chapters of this volume.

Summary and Other Considerations

This chapter provides recommendations for marine-based monitoring of submarine and small island volcanoes at every threat level. The National Volcanic Threat Assessment (Ewert and others, 2018) lists only one submarine volcano in the United States as a moderate (level 3) threat and a few small island volcanoes as level 3 or 4 threats. Given the relatively poor understanding of

submarine volcanic systems, the threat rankings may change in the future as more information about their potential for hazardous eruptions becomes available. Similarly, volcanoes outside U.S. territory may be deemed higher threats and benefit from the recommended monitoring described here.

For marine-based monitoring, special consideration needs to be given to logistics and cost. The recommendations in this chapter aim to balance the high cost of marine-based instruments with the potential societal benefit. Thus, land-based and regional monitoring that requires as few marine instruments as possible are recommended for most cases. The deployment and maintenance of marine-based instruments requires ships with specific capacities, which may present added costs and extra planning time. Scientific research vessels are able to deploy instruments, but usage time may need to be booked years in advance. Developing partnerships with other agencies that operate capable ships (for example, U.S. Coast Guard or U.S. Fish and Wildlife Service) is highly recommended and may allow for reduced costs and more flexibility. Private contractors may also be an option in some cases.

References Cited

- Baker, E.T., Embley, R.W., Walker, S.L., Resing, J.A., Lupton, J.E., Nakamura, K.I., de Ronde, C.E.J., and Massoth, G.J., 2008, Hydrothermal activity and volcano distribution along the Mariana arc: *Journal of Geophysical Research, Solid Earth*, v. 113, no. B8, <https://doi.org/10.1029/2007JB005423>.
- Bohnenstiehl, D.R., Dziak, R.P., Matsumoto, H., and Lau, T.-K.A., 2013, Underwater acoustic records from the March 2009 eruption of Hunga Ha'apai-Hunga Tonga volcano in the Kingdom of Tonga: *Journal of Volcanology and Geothermal Research*, v. 249, p. 12–24. <https://doi.org/10.1016/j.jvolgeores.2012.08.014>.
- Caplan-Auerbach, J., and Duennebie, F., 2001, Seismic and acoustic signals detected at Lo'ihi Seamount by the Hawai'i Undersea Geo-Observatory: *Geochemistry, Geophysics, Geosystems*, v. 2, no. 5, <https://doi.org/10.1029/2000GC000113>.
- Caplan-Auerbach, J., Dziak, R.P., Haxel, J., Bohnenstiehl, D.R., and Garcia, C., 2017, Explosive processes during the 2015 eruption of Axial Seamount, as recorded by seafloor hydrophones: *Geochemistry, Geophysics, Geosystems*, v. 18, no. 4, p. 1761–1774, <https://doi.org/10.1002/2016GC006734>.
- Caplan-Auerbach, J., Fox, C.G., and Duennebie, F.K., 2001, Hydroacoustic detection of submarine landslides on Kilauea volcano: *Geophysical Research Letters*, v. 28, no. 9, p. 1811–1813, <https://doi.org/10.1029/2000GL012545>.
- Carey, R.J., Wysoczanski, R., Wunderman, R., and Jutzeler, M., 2014, Discovery of the largest historic silicic submarine eruption: *Eos, Transactions, American Geophysical Union*, v. 95, no. 19, p. 157–159, <https://doi.org/10.1002/2014EO190001>.

- Coombs, M.L., Wallace, K., Cameron, C., Lyons, J., Wech, A., Angeli, K., and Cervelli, P., 2019, Overview, chronology, and impacts of the 2016–2017 eruption of Bogoslof volcano, Alaska: *Bulletin of Volcanology*, v. 81, no. 62, 23 p., <https://doi.org/10.1007/s00445-019-1322-9>.
- Dietz, R.S., and Sheehy, M.J., 1954, Transpacific detection of Myojin volcanic explosions by underwater sound: *Geological Society of America Bulletin*, v. 65, no. 10, p. 941–956, [https://doi.org/10.1130/0016-7606\(1954\)65%5b941:TDOMVE%5d2.0.CO;2](https://doi.org/10.1130/0016-7606(1954)65%5b941:TDOMVE%5d2.0.CO;2).
- Duennebie, F.K., Harris, D.W., Jolly, J., Caplan-Auerbach, J., Jordan, R., Copson, D., Stiffel, K., Babinec, J., and Bosel, J., 2002, HUGO—The Hawai‘i Undersea Geo-Observatory: *Institute of Electrical and Electronics Engineers Journal of Oceanic Engineering*, v. 27, no. 2, p. 218–227, <https://doi.org/10.1109/JOE.2002.1002476>.
- Dziak, R.P., and Fox, C.G., 2002, Evidence of harmonic tremor from a submarine volcano detected across the Pacific Ocean basin: *Journal of Geophysical Research, Solid Earth*, v. 107, no. B5, p. ESE 1–1 to ESE 1–11, <https://doi.org/10.1029/2001JB000177>.
- Dziak, R.P., Park, M., Matsumoto, H., and Byun, S.-K., 2005, Hydroacoustic records and a numerical model of the source mechanism from the first historical eruption of Anatahan Volcano, Mariana Islands: *Journal of Volcanology and Geothermal Research*, v. 146, no. 1–3, p. 86–101, <https://doi.org/10.1016/j.jvolgeores.2004.12.009>.
- Embley, R.W., Tamura, Y., Merle, S.G., Sato, T., Ishizuka, O., Chadwick, W.W., Jr., Wiens, D.A., Shore, P., and Stern, R.J., 2014, Eruption of South Sarigan Seamount, Northern Mariana Islands—Insights into hazards from submarine volcanic eruptions: *Oceanography*, v. 27, no. 2, p. 24–31, <https://doi.org/10.5670/oceanog.2014.37>.
- Ewert, J.W., Diefenbach, A.K., and Ramsey, D.W., 2018, 2018 update to the U.S. Geological Survey national volcanic threat assessment: U.S. Geological Survey Scientific Investigations Report 2018–5140, 40 p., <https://doi.org/10.3133/sir20185140>.
- Green, D.N., Evers, L.G., Fee, D., Matoza, R.S., Snellen, M., Smets, P., and Simons, D., 2013, Hydroacoustic, infrasonic and seismic monitoring of the submarine eruptive activity and sub-aerial plume generation at South Sarigan, May 2010: *Journal of Volcanology and Geothermal Research*, v. 257, p. 31–43, <https://doi.org/10.1016/j.jvolgeores.2013.03.006>.
- Hanson, J., Le Bras, R., Dysart, P., Brumbaugh, D., Gault, A., and Guern, J., 2001, Operational processing of hydroacoustics at the Prototype International Data Center: *Pure and Applied Geophysics*, v. 158, p. 425–456, <https://doi.org/10.1007/PL00001190>.
- Johnson, R.H., Northrop, J., and Eppley, R., 1963, Sources of Pacific *T* phases: *Journal of Geophysical Research*, v. 68, no. 14, p. 4251–4260, <https://doi.org/10.1029/JZ068i014p04251>.
- Jutzeler, M., Marsh, R., Carey, R.J., White, J.D., Talling, P.J., and Karlstrom, L., 2014, On the fate of pumice rafts formed during the 2012 Havre submarine eruption: *Nature Communications*, v. 5, no. 3660, <https://doi.org/10.1038/ncomms4660>.
- Kelley, D.S., Delaney, J.R., and Juniper, S.K., 2014, Establishing a new era of submarine volcanic observatories—Cabling Axial Seamount and the Endeavour Segment of the Juan de Fuca Ridge: *Marine Geology*, v. 352, p. 426–450, <https://doi.org/10.1016/j.margeo.2014.03.010>.
- Kornei, K., 2019, Volcanic eruption creates temporary islands of pumice: *Eos, Transactions, American Geophysical Union*, v. 100, <https://doi.org/10.1029/2019EO132451>.
- Le Saout, M., Bohnenstiehl, D.R., Paduan, J.B., and Clague, D.A., 2020, Quantification of eruption dynamics on the north rift at Axial Seamount, Juan de Fuca Ridge: *Geochemistry, Geophysics, Geosystems*, v. 21, no. 9, <https://doi.org/10.1029/2020GC009136>.
- Lindsey, N.J., Dawe, T.C., and Ajo-Franklin, J.B., 2019, Illuminating seafloor faults and ocean dynamics with dark fiber distributed acoustic sensing: *Science*, v. 366, no. 6469, p. 1103–1107, <https://doi.org/10.1126/science.aay5881>.
- Lynett, P., McCann, M., Zhou, Z., Renteria, W., Borrero, J., Greer, D., and others, 2022, Diverse tsunamigenesis triggered by the Hunga Tonga-Hunga Ha‘apai eruption: *Nature*, v. 609, no. 7928, p. 728–733, <https://doi.org/10.1038/s41586-022-05170-6>.
- Marra, G., Clivati, C., Luckett, R., Tampellini, A., Kronjäger, J., Wright, L., Mura, A., Levi, F., Robinson, S., Xuereb, A., Baptie, B., and Calónico, D., 2018, Ultraprecise laser interferometry for earthquake detection with terrestrial and submarine cables: *Science*, v. 361, no. 6401, p. 486–490, <https://doi.org/10.1126/science.aat4458>.
- Matsumoto, H., Haxel, J., Khan, B., Roche, L., Dziak, R.P., Turpin, A., Childress, J., Sexton, K., Klinck, H., and Nakamura, T., 2019, Field testing and performance evaluation of the Long-term Acoustic Real-Time Sensor for Polar Areas (LARA) [abs.]: *OCEANS 2019 Marine Technology Society and Institute of Electrical and Electronics Engineers Conference*, 7 p., <https://doi.org/10.23919/OCEANS40490.2019.8962602>.
- Matsumoto, H., Jones, C., Klinck, H., Mellinger, D.K., Dziak, R.P., and Meinig, C., 2013, Tracking beaked whales with a passive acoustic profiler float: *The Journal of the Acoustical Society of America*, v. 133, no. 2, p. 731–740, <https://doi.org/10.1121/1.4773260>.

- Matsumoto, H., Turpin, A., Haxel, J., Meinig, C., Craig, M., Tagawa, D., Klinck, H., and Hanson, B., 2016, A Real-time Acoustic Observing System (RAOS) for killer whales [abs.]: OCEANS 2016 Marine Technology Society and Institute of Electrical and Electronics Engineers Conference, 6 p., <https://doi.org/10.1109/OCEANS.2016.7761032>.
- Metz, D., Watts, A.B., Grevemeyer, I., Rodgers, M., and Paulatto, M., 2016, Ultra-long-range hydroacoustic observations of submarine volcanic activity at Monowai, Kermadec Arc: *Geophysical Research Letters*, v. 43, no. 4, p. 1529–1536, <https://doi.org/10.1002/2015GL067259>.
- Nooner, S.L., and Chadwick, W.W., Jr., 2016, Inflation-predictable behavior and co-eruption deformation at Axial Seamount: *Science*, v. 354, no. 6318, p. 1399–1403, <https://doi.org/10.1126/science.aah4666>.
- Okal, E.A., 2001, T-phase stations for the International Monitoring System of the Comprehensive Nuclear-Test Ban Treaty—A global perspective: *Seismological Research Letters*, v. 72, no. 2, p. 186–196, <https://doi.org/10.1785/gssrl.72.2.186>.
- Searcy, C., 2013, Seismicity associated with the May 2010 eruption of South Sarigan Seamount, Northern Mariana Islands: *Seismological Research Letters*, v. 84, no. 6, p. 1055–1061, <https://doi.org/10.1785/0220120168>.
- Shinohara, M., Ichihara, M., Sakai, S., Yamada, T., Takeo, M., Sugioka, H., Nagaoka, Y., Takagi, A., Morishita, T., Ono, T., and Nishizawa, A., 2017, Continuous seismic monitoring of Nishinoshima volcano, Izu-Ogasawara, by using long-term ocean bottom seismometers: *Earth, Planets, and Space*, v. 69, no. 159, p. 159, <https://doi.org/10.1186/s40623-017-0747-7>.
- Sukhovich, A., Bonniex, S., Hello, Y., Irison, J.O., Simons, F.J., and Nolet, G., 2015, Seismic monitoring in the oceans by autonomous floats: *Nature Communications*, v. 6, article no. 8027, <https://doi.org/10.1038/ncomms9027>.
- Talandier, J., 2004, Seismicity of the Society and Austral Hotspots in the South Pacific—Seismic detection, monitoring and interpretation of underwater volcanism, in Hekinian, R., Cheminée, J.L., and Stoffers, P., eds., *Oceanic Hotspots*: Berlin, Heidelberg, Springer, p. 29–71, https://doi.org/10.1007/978-3-642-18782-7_3.
- Talandier, J., and Kuster, G.T., 1976, Seismicity and submarine volcanic activity in French Polynesia: *Journal of Geophysical Research, Solid Earth and Planets*, v. 81, no. 5, p. 936–948, <https://doi.org/10.1029/JB081i005p00936>.
- Talandier, J., and Okal, E.A., 1998, On the mechanism of conversion of seismic waves to and from T waves in the vicinity of island shores: *Bulletin of the Seismological Society of America*, v. 88, no. 2, p. 621–632, <https://doi.org/10.1785/BSSA0880020621>.
- Tepp, G., Chadwick, W.W., Haney, M.M., Lyons, J.J., Dziak, R.P., Merle, S.G., Butterfield, D.A., and Young, C.W., III, 2019b, Hydroacoustic, seismic, and bathymetric observations of the 2014 submarine eruption at Ahi Seamount, Mariana Arc: *Geochemistry, Geophysics, Geosystems*, v. 20, no. 7, p. 3608–3627, <https://doi.org/10.1029/2019GC008311>.
- Tepp, G., and Dziak, R.P., 2021, The seismo-acoustics of submarine volcanic eruptions: *Journal of Geophysical Research, Solid Earth*, v. 126, no. 4, <https://doi.org/10.1029/2020JB020912>.
- Tepp, G., Dziak, R., Haney, M.M., Lyons, J.J., Searcy, C., Matsumoto, H., and Haxel, J., 2019c, Seismic and hydroacoustic observations of the 2016–17 Bogoslof eruption: *Bulletin of Volcanology*, v. 82, no. 4, <https://doi.org/10.1007/s00445-019-1344-3>.
- Tepp, G., Dziak, R.P., Haney, M.M., Roche, L., and Matsumoto, H., 2021, A year-long hydroacoustic survey of the Mariana Islands region: OCEANS 2021, Institute of Electrical and Electronics Engineers Conference, San Diego, California, 5 p., <https://doi.org/10.23919/OCEANS44145.2021.9705805>.
- Tepp, G., Shiro, B., and Chadwick, W.W., 2019a, Volcanic hazards in the Pacific U.S. Territories: U.S. Geological Survey Fact Sheet 2019–3036, 6 p., <https://doi.org/10.3133/fs20193036>.
- Wanless, V.D., Garcia, M.O., Trusdell, F.A., Rhodes, J.M., Norman, M.D., Weis, D., Fornari, D.J., Kurz, M.D., and Guillou, H., 2006, Submarine radial vents on Mauna Loa Volcano, Hawai‘i: *Geochemistry, Geophysics, Geosystems*, v. 7, no. 5, <https://doi.org/10.1029/2005GC001086>.
- Wilcock, W.S., Dziak, R.P., Tolstoy, M., Chadwick, W.W., Jr., Noon, S.L., Bohnenstiehl, D.R., Caplan-Auerbach, J., Waldhauser, F., Arnulf, A.F., Baillard, C., Lau, T.-K., Haxel, J.H., Tan, Y.J., Garcia, C., Levy, S., and Mann, M.E., 2018, The recent volcanic history of Axial Seamount—Geophysical insights into past eruption dynamics with an eye toward enhanced observations of future eruptions: *Oceanography*, v. 31, no. 1, p. 114–123, <https://doi.org/10.5670/oceanog.2018.117>.
- Wilcock, W.S.D., Tolstoy, M., Waldhauser, F., Garcia, C., Tan, Y.J., Bohnenstiehl, D.R., Caplan-Auerbach, J., Dziak, R.P., Arnulf, A.F., and Mann, M.E., 2016, Seismic constraints on caldera dynamics from the 2015 Axial Seamount eruption: *Science*, v. 354, no. 6318, p. 1395–1399, <https://doi.org/10.1126/science.aah5563>.

Chapter J



Aerial photograph looking to the northeast of the March 28, 2016, eruption of Pavlof Volcano, Alaska. Many eruptive processes can be observed, including the formation of hot granular flows of rock material, formation of lahar deposits, white steam plumes associated with the interaction of hot eruptive material and snow and ice, and a vertical ash column and drifting ash cloud. Pavlof Volcano is just outside of Emmons Lake caldera, one of the largest caldera structures in the Aleutian Arc. Also shown are several of the young post-caldera volcanoes inside the caldera. The photograph was taken at 20,000 feet elevation aboard U.S. Coast Guard 1713 aircraft based at U.S. Coast Guard Air Station Kodiak, Alaska. Photography by U.S. Coast Guard.

Chapter J

Special Topic—Eruption Plumes and Clouds

By David J. Schneider and Alexa R. Van Eaton

Introduction

Explosive eruptions create plumes of volcanic ash and gas that can rise more than 30,000 feet (9.1 kilometers [km]) above sea level within minutes of eruption onset. The resulting clouds disperse under prevailing winds and may cause hazardous conditions hundreds to thousands of kilometers from the volcano, including in international airspace. Rapid detection and characterization of explosive activity is vital to mitigate the wide-ranging effects of volcanic ash. Ashfall thicknesses as small as a millimeter or so on the ground can affect infrastructure, agriculture, and air quality, requiring extensive clean-up procedures (Schuster, 1981; Warrick and others, 1981, U.S. Geological Survey, 2022). Volcanic clouds also pose substantial threats to aircraft. Since 1953, 88 encounters between airplanes and ash clouds have been documented worldwide (International Civil Aviation Organization, 2015, appendix F), resulting in aircraft damage and, in 9 cases, engine failure (Guffanti and others, 2010). In 1982, two large passenger planes suffered complete engine failure owing to eruptions in Indonesia (Global Volcanism Program, 1982) and a similar incident occurred over Alaska in 1989 (Casadevall, 1994). In all three cases, they were able to restart some engine capability and land safely once they emerged from the ash clouds, although with substantial damage (Guffanti and others, 2010).

The clear threat to aviation has led to establishment of nine Volcanic Ash Advisory Centers (VAAC) around the world to monitor and rapidly disseminate information about volcanic eruptions to the aviation community. U.S. Geological Survey (USGS) volcano observatories issue the Volcano Observatory Notice for Aviation that informs of preeruptive unrest or eruptive activity. When ash-producing eruptions do occur, volcano observatories work closely with their regional VAAC to ensure consistency and accuracy in eruption onset time, cloud altitude, ash production, and duration as reported in Volcanic Ash Advisories. Explosive volcanism in the United States and Commonwealth of the Northern Mariana Islands prompts 50–100 such advisories in any given year (table J1). This collaborative effort is greatly aided by USGS detection and monitoring of eruption clouds to ensure a timely and coordinated response.

To support these efforts to provide guidance on ash transport and fallout, the USGS developed the Ash3d volcanic ash dispersion model (<https://vsc-ash.wr.usgs.gov/ash3d-gui>) (Schwaiger and others, 2012). Automated simulations are run daily by the USGS for volcanoes that are in elevated states of unrest, and in response mode when eruptions occur. During eruptions, the model output is provided to local National Weather Service Weather Forecast Offices to guide them in the issuance of their information products (such as special weather statements, ashfall advisories, or ashfall warnings), as well as to State and

Table J1. Number of Volcanic Ash Advisories (VAAs) issued for ash-producing events in the United States and Commonwealth of the Northern Mariana Islands during the 10-year period from January 1, 2009, to January 1, 2019, from Engwell and others (2021).

[For this analysis, eruptive event is defined as a phase of ash-producing explosive activity that prompted a near-continuous sequence of VAAs]

Volcano	Region	Volcano threat level	Network level	VAAs	Eruptive events
Pavlof Volcano	Alaska	High	4	192	13
Kīlauea	Hawai‘i	Very high	4	153	33
Redoubt Volcano	Alaska	Very high	4	136	15
Bogoslof Island	Alaska	Moderate	3	132	49
Mount Veniaminof	Alaska	High	4	115	20
Pagan	Mariana Islands	High	4	41	17
Mount Cleveland	Alaska	High	4	33	16
Shishaldin Volcano	Alaska	High	4	9	4
Sarigan	Mariana Islands	Moderate	3	7	1
Semisopochnoi Island	Alaska	High	4	4	1
Total				822	169

local governments and the public. Characterization of the eruption source is needed to estimate the parameters used to initialize the Ash3d model, and by the Anchorage and Washington VAACs to initialize other dispersion models that inform forecasts for the airborne volcanic cloud. The source parameters that can be provided by observation during an eruption include eruption start time, eruption cloud height over time, and eruption duration. Other, nonobservable source parameters, such as mass eruption rate and grain-size distribution, are based on empirical correlations and study of historical deposits. The goal is to provide a time series of cloud heights, mass eruption rates, and particle-size distributions that accurately reflects current conditions. When feasible, the USGS also provides guidance on the nature of ongoing eruptions and forecasts future activity using petrologic monitoring of collected tephra samples.

The aims of providing accurate observable parameters are achieved through analysis of (1) near-real-time meteorological satellite data, (2) ground-based cameras (see chapter G, this volume; Orr and others, 2024), (3) weather radar, (4) volcanic lightning detection, and (5) ground-based ash sensors and sampling. Explosive eruptions can be detected by a variety of geophysical monitoring, including infrasound (see chapter C, this volume; Lyons and others, 2024) and seismicity (see chapter B, this volume; Thelen and others, 2024). However, those methods cannot quantify the altitude, ash content, and dispersal dynamics of resulting volcanic clouds. Ideally, all available sources of monitoring data are synthesized to develop a coherent understanding of eruptive activity. The guidance summarized here provides a framework for characterizing volcanic clouds in the atmosphere and tracking the evolution of explosive eruption dynamics.

Instrumentation

Satellite Remote Sensing

Many of the volcanoes in the United States that erupt explosively are in remote regions (such as Alaska and the Northern Mariana Islands) where direct observation is difficult or impossible (table J1). Telemetered cameras are valuable for characterizing explosive activity, as described in chapter G of this volume (Orr and others, 2024). However, visual observations can be obscured at night or during poor weather. In these cases, the primary method for detecting and characterizing volcanic eruption clouds is near-real-time satellite remote sensing using meteorological satellites. Meteorological satellite data can observe volcanic clouds at multiple wavelengths (ultraviolet, visible, mid-infrared, and thermal infrared), which can provide information about cloud composition and provide repeat, synoptic views of volcanic clouds during all stages of their eruption and transport in the atmosphere. These data are critical for determining whether ash emissions are occurring, to estimate cloud height, and to determine eruption duration. Multispectral image products can provide information about the ash, sulfur dioxide, and water content of volcanic clouds, their transport, dispersion, and removal.

In the United States, geostationary (Geostationary Operational Environmental Satellites [GOES]) and polar-orbiting (Polar Operational Environmental Satellite [POES]) meteorological satellites are operated by the National Oceanic and Atmospheric Administration (NOAA) National Environmental Satellite, Data, and Information Service as part of the worldwide operational system of observations. Sensors onboard these satellites image the Earth at visible through thermal infrared wavelengths in 16 channels for GOES Advanced Baseline Imager and at 22 channels for the POES Visible Infrared Imaging Radiometer Suite, at spatial resolutions that range from 375 meters to 2 km. The POES satellites also contain the Ozone Mapping and Profiler Suite that is used to detect and quantify sulfur dioxide emissions using ultraviolet absorption.

NOAA currently operates two GOES satellites, which are stationed over the equator in an east (75° W.) and a west (137° W.) position (fig. J1), and three POES satellites (Suomi National Polar-Orbiting Operational Environment Satellite System Preparatory Project [SNPP], NOAA-20, and NOAA-21). The data from the POES sensors complement the GOES data, especially at high latitudes where the GOES data have a severe oblique view. Full-disk GOES images are typically available every 10 minutes (fig. J1) but can be tasked at 1-minute resolution for smaller regions to assess severe weather or eruptions. For volcanoes in the western Aleutian Islands, the Northern Mariana Islands, and American Samoa, Himawari geostationary data (0° N. and 141° E.) provided by the Japanese Meteorological Agency provides additional geographic coverage for areas outside of the view of GOES-West (fig. J1A).

There are several satellite-based methodologies to detect and characterize eruption clouds. For volcanoes that are monitored by seismic and (or) local infrasound instruments, the appearance of a developing plume or cloud in conjunction with geophysical signals (that is, seismic tremor and [or] infrasound pressure waves) is a prime indication that an explosive eruption has occurred. Eruption clouds quickly cool as they rise, and for clouds in the troposphere, an estimate of the cloud altitude can be made by comparing the thermal infrared derived cloud temperature to the vertical temperature profile of the atmosphere (fig. J2).

For volcanoes that are not instrumented, USGS uses alerts generated by the Volcanic Cloud Analysis Toolkit (VOLCAT) developed by the NOAA Cooperative Institute for Meteorological Satellite Studies (<https://volcano.ssec.wisc.edu>). This system ingests and processes global satellite data and generates alerts when volcanic unrest or an eruption is detected (Pavolonis and others, 2015a, b, 2018). Several techniques are used to detect volcanic ash, including analysis of multispectral thermal infrared data (Prata, 1989; Watson and others, 2004; Pavolonis and others, 2015b) and Cloud Growth Anomaly (Pavolonis and others, 2018). The USGS and regional VAACs that receive these alerts check their own satellite sources to confirm whether an eruption has occurred and begin tracking changes over time.

The multispectral technique uses characteristic absorption of upwelling thermal radiance by volcanic ash and sulfur dioxide gas as infrared radiation passes through the volcanic cloud from the underlying surface (that is, land, water, or cloud). The

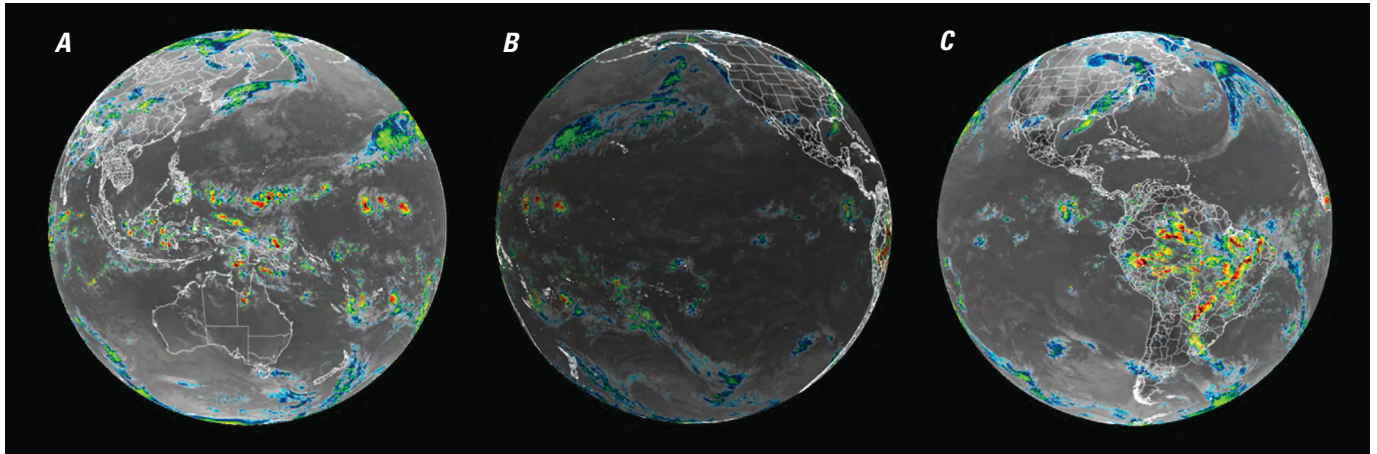


Figure J1. Satellite images showing the full-disk field of view from geostationary satellites (A) Himawari, (B) GOES-West, and (C) GOES-East. GOES, Geostationary Operational Environmental Satellites.

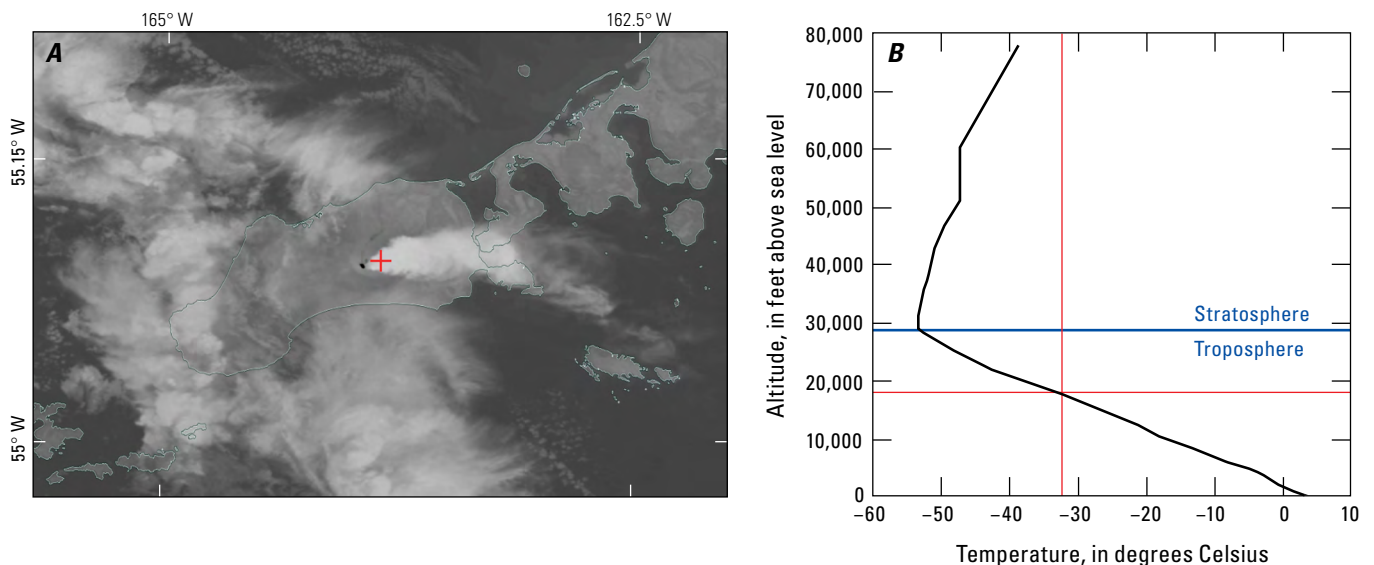


Figure J2. Thermal infrared satellite image of the January 20, 2020, eruption of Shishaldin Volcano in Alaska (left) and the Global Forecast System model temperature profile of the atmosphere (right) at the location of the crosshair in the satellite image. The temperature of the eruption cloud at the crosshair was -32 degrees Celsius, which corresponds to an altitude of 17,500 feet above sea level.

absorption properties vary with wavelength. For example, ash typically absorbs more infrared radiation at wavelengths of 11 micrometers (μm) than at 12 μm , whereas the opposite is true for meteorological cloud particles. Thus, a pixel from an ash cloud in a 12 μm infrared image will have a slightly higher brightness temperature than the same pixel in an 11 μm infrared image. The sulfur dioxide component of the volcanic cloud is detected in a similar manner, using data at 8.5 and 11 μm .

Multispectral images can be combined into a false-color composite image, which produces an image that contains information about both volcanic cloud constituents. False-color images are like true-color images but show data outside the visible spectra. For volcanic cloud images, the wavelengths that are used depend on the particular satellite sensor but typically use a brightness temperature difference (BTD) at 12–11 μm (sensitive

to volcanic ash) in the red image component, a BTD at 11–8.5 μm (sensitive to sulfur dioxide) in the green image component, and a brightness temperature at 11 μm in the blue image component. An example of a false-color volcanic cloud image from the 2020 eruption of Shishaldin Volcano is shown in figure J3. These images are routinely produced in near real time during eruptions by NOAA's VOLCAT.

The false-color composite image shown in figure J3 utilizes differences in thermal infrared brightness temperatures at three wavelengths to determine the extent of the volcanic cloud object (as shown by the polygons in each image). In this example, the volcanic cloud is ash-rich and is a red color. If the cloud had also contained abundant sulfur dioxide gas along with the ash, it would have had a yellow color. A cloud composed primarily of sulfur dioxide gas with little ash would be a green color.

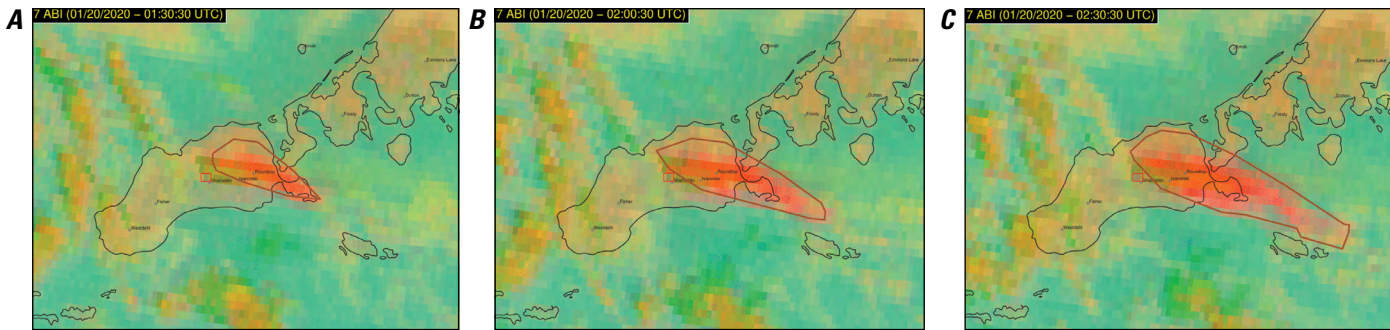


Figure J3. Multispectral false-color composite images of the January 2020 eruption of Shishaldin Volcano, Alaska, from the Geostationary Operational Environmental Satellites (GOES) Advanced Baseline Imager. These images were produced by the National Oceanic and Atmospheric Administration Cooperative Institute for Meteorological Satellite Studies Volcanic Cloud Analysis Tool (VOLCAT) system showing the automated volcanic cloud object detection as outlined by a dark red polygon. For these red-green-blue composite images, the 12 and 11 micrometer (μm) brightness temperature difference (BTD) is in the red channel, the 11 and 8.5 μm BTD (sensitive to SO_2 gas) is in the green channel, and the 11 μm brightness temperature is in the blue channel. The red pixels in the image are indicative of ash. If significant SO_2 was also present, the volcanic cloud would be yellow. Data were collected at 10-minute increments, and the images shown are representative of those produced during the eruptive activity on January 20, 2020. *A*, Image from 01:30 coordinated universal time (UTC). *B*, Image from 02:00 UTC. *C*, Image from 02:30 UTC.

Despite its utility, the multispectral technique shown in figure J3 is less successful at detecting volcanic clouds in the early stages of an eruption or eruptions that have high amounts of water in them (Schneider and others, 2020). The multispectral technique relies on upwelling radiance passing through the cloud and being differentially absorbed (as a function of wavelength) by the cloud constituents (ash, sulfur dioxide, and water). So-called “young” volcanic clouds are opaque in part because of the presence of water droplets and (or) ice particles. Opaque clouds emit thermal radiance from the cloud top only, and the multispectral technique is not able to detect the cloud as being volcanic in origin.

In these cases, the Cloud Growth Anomaly technique has been used to autonomously detect eruption clouds (Pavolonis and others, 2018). The technique utilizes geostationary satellite data to identify cloud objects near volcanoes that are rapidly growing vertically relative to clouds that form through meteorological processes. The alerts are only generated using geostationary satellite data because frequent observations are required to deduce rapid cooling. This technique is especially useful for detecting larger and more energetic explosive eruptions that generate umbrella clouds, like those shown in figure J4 from the 2008 eruption of Mount Okmok, Alaska. This cloud was not detectable using the multispectral technique because it was opaque and contained abundant ice but is observable in the visible wavelength image sequence in figure J4. Retrospective analysis of this sequence by Pavolonis and others (2018) showed that it would have been detected based on vertical cloud growth, which was greater than 17 standard deviations greater than that of meteorological clouds.

The presence of water in eruption clouds is a major factor that influences ashfall, satellite detection and tracking of drifting volcanic clouds, and ash transport and dispersion. Abundant water can enhance near-source ashfall through the growth of ash aggregates, bound by water, that prematurely removes very-fine-grained volcanic ash particles (Brown and others, 2012; Van Eaton and others, 2015). The removal of these particles in turn makes multispectral detection of volcanic ash more challenging, and the

presence of water can lead to ice-coated grains, masking the spectral properties of the ash. Ash transport and dispersion modeling, which form the basis of forecasts of ash cloud movement by the VAACs, does not explicitly account for water-enhanced aggregation processes that can reduce the lifetime of ash in the atmosphere (Mastin and others, 2016; Beckett and others, 2022). During daylight hours, visible wavelength (fig. J4) and color composite (fig. J5) satellite data can be used to qualitatively judge whether water is present in large amounts or if the cloud is primarily ash rich.

Meteorological Radar

Mobile, ground-based radar systems have been deployed at several volcanic systems to rapidly detect and measure ash eruptions (Rose and others, 1995; Lacasse and others, 2004; Arason and others, 2011; Schneider and Hoblitt, 2013). These systems have much lower latency than typical satellite products—on the order of minutes versus 10 minutes or more from standard satellites. Radar can promptly detect explosive volcanic eruptions irrespective of darkness and inclement weather and be used to anticipate areas that will be subjected to volcanic ashfall. The next-generation radar (NEXRAD) network that is operated by the National Weather Service provides adequate coverage of many volcanoes within the continental United States, Alaskan volcanoes near Cook Inlet and the Katmai group of volcanoes, Kilauea and Mauna Loa in Hawai‘i, and marginal coverage of the southernmost volcanoes in the Northern Mariana Islands. These NEXRAD systems have been recently upgraded with dual polarization capabilities that could provide information on the relative abundance of water and volcanic ash in eruption columns and clouds (Marzano and others, 2013; Crouch and others, 2014; Cahalan and others, 2023). These types of near-real-time observations are critical for the initialization of ash fallout and cloud transport models that are used as guidance for local communities and aviation. Figure J6 shows a comparison between a satellite view of a volcanic plume at Kilauea and a corresponding NEXRAD image from approximately the same time. Weather radar

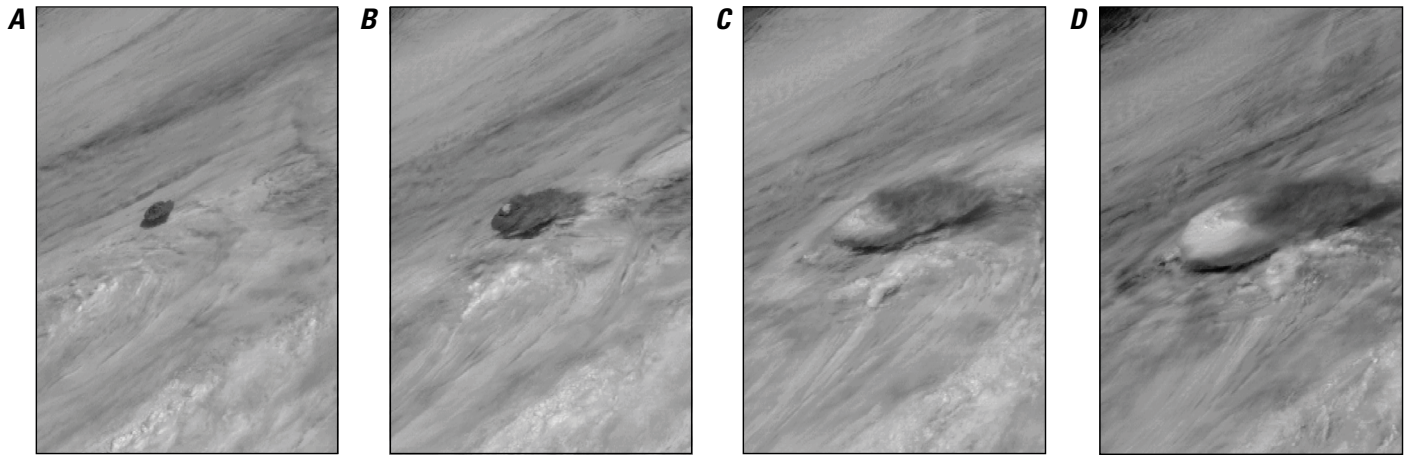


Figure J4. Visible wavelength satellite images of the July 12, 2008, eruption of Mount Okmok, Alaska, from the Geostationary Operational Environmental Satellites (GOES). Images were collected at 15-minute increments and hourly images are shown here. *A*, Image from 20:00 coordinated universal time (UTC) showing a dark-colored, ash-rich umbrella cloud. *B*, Image from 21:00 UTC showing further expansion of the eruption cloud. Ice development in the cloud is seen as a white circular feature in the center of the overshooting cloud top. *C*, Image from 22:00 UTC and, *D*, from 23:00 UTC, showing continued ice development and lateral expansion. Images from the National Oceanic Atmospheric Administration Cooperative Institute for Meteorological Satellite Studies.

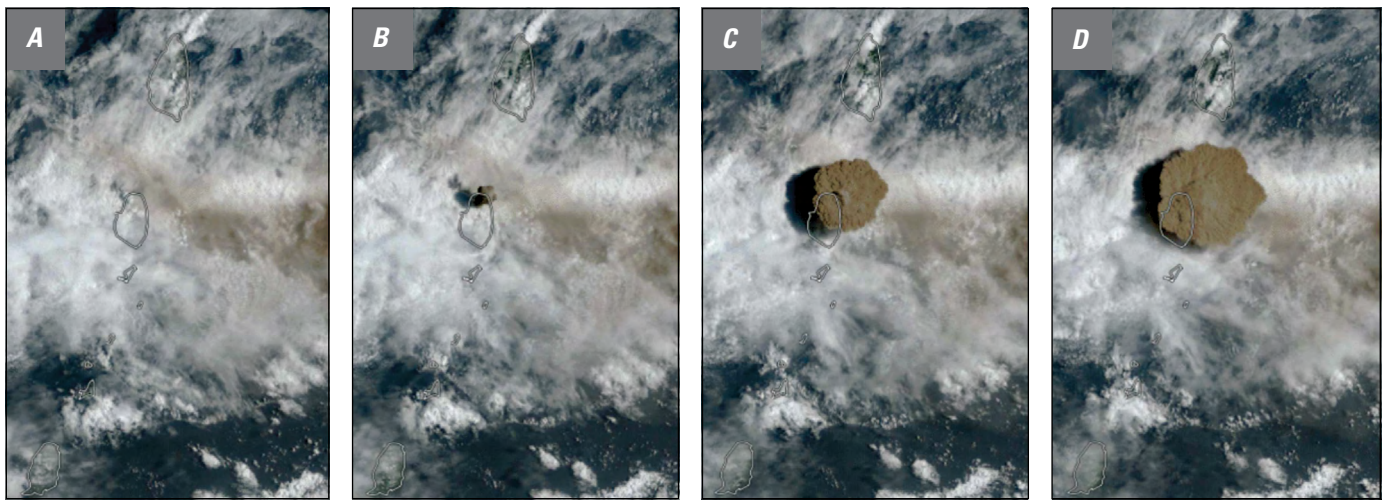


Figure J5. True color satellite images of the April 9, 2021, eruption of La Soufrière, Saint Vincent, from the Geostationary Operational Environmental Satellites (GOES) Advanced Baseline Imager. These images were collected at 10-minute increments and show the rapid rise and expansion of the brown, ash-rich eruption cloud. Diffuse ash from prior activity is visible to the east of the eruption cloud as a brown layer over the white meteorological clouds. *A*, Image from 13:20 coordinated universal time (UTC). *B*, Image from 13:30 UTC. *C*, Image from 13:40 UTC. *D*, Image from 13:50 UTC. Images from the National Oceanic Atmospheric Administration Cooperative Institute for Meteorological Satellite Studies.

was used throughout the response efforts to Kīlauea eruptions in 2018 (Neal and others, 2019) and 2020 to observe ash emissions and was especially useful during periods of darkness and during inclement weather that hampered visual observations.

Although meteorological radar systems are notable for providing the three-dimensional structure of volcanic plumes (fig. J6), their spatial coverage is limited. Radar systems located more than 100 km from a volcano may lead to uncertainties of several kilometers on plume height estimates, which limits the usable range of existing, stationary radar like the NEXRAD

systems. In addition, using some scanning strategies, the NEXRAD system may take as many as 10 minutes to complete a full 360° volume scan. Schneider and Hoblitt (2013) tested the utility of a relatively low-power transportable Doppler C-band radar during the 2009 eruption of Redoubt Volcano, Alaska. Using a scanning strategy limited to a 90° sector that was centered on the direction of the volcano, they imaged numerous explosive events at temporal resolution of 90–150 seconds. They were able to provide rapid estimates of cloud height (fig. J7) and document ash-ice aggregation processes that quickly removed fine-grained

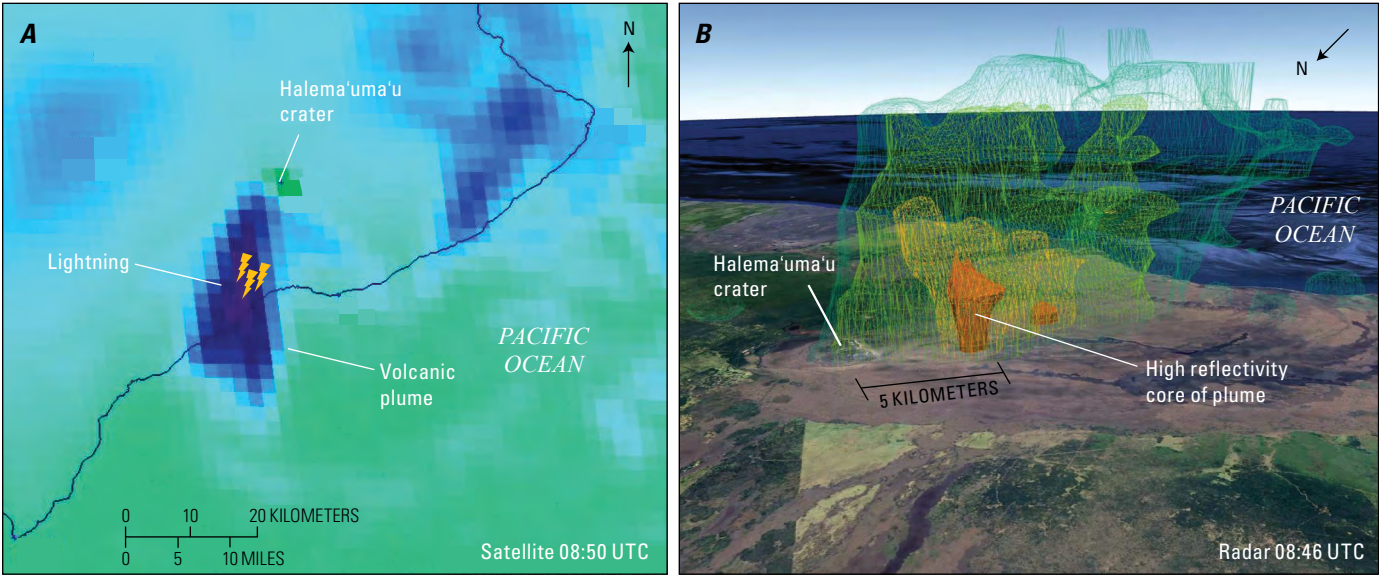


Figure J6. Images showing satellite, lightning, and radar perspectives into volcanic plume development from Kilauea, Hawai'i, on December 21, 2020. *A*, Satellite image showing infrared brightness temperatures at 08:50 coordinated universal time (UTC) and lightning detected by the optical Global Lightning Mapper on board GOES-17 from 08:44 to 08:45 UTC. Lightning locations from Calahan and others (2023). *B*, Next-generation radar (NEXRAD) reflectivity from 08:46 UTC, interpolated and contoured showing the three-dimensional structure of the plume in Google Earth (copyright 2023). Isosurfaces give radar reflectivity from 47 (orange) to 18 (teal) decibels relative to radar reflectivity factor Z (dBz). Radar reflectivity depends on particle size, concentration, and composition. In this case, Cahalan and others (2023) interpreted the high-reflectivity core as a region of large particles—likely water droplets—descending from the volcanic cloud.

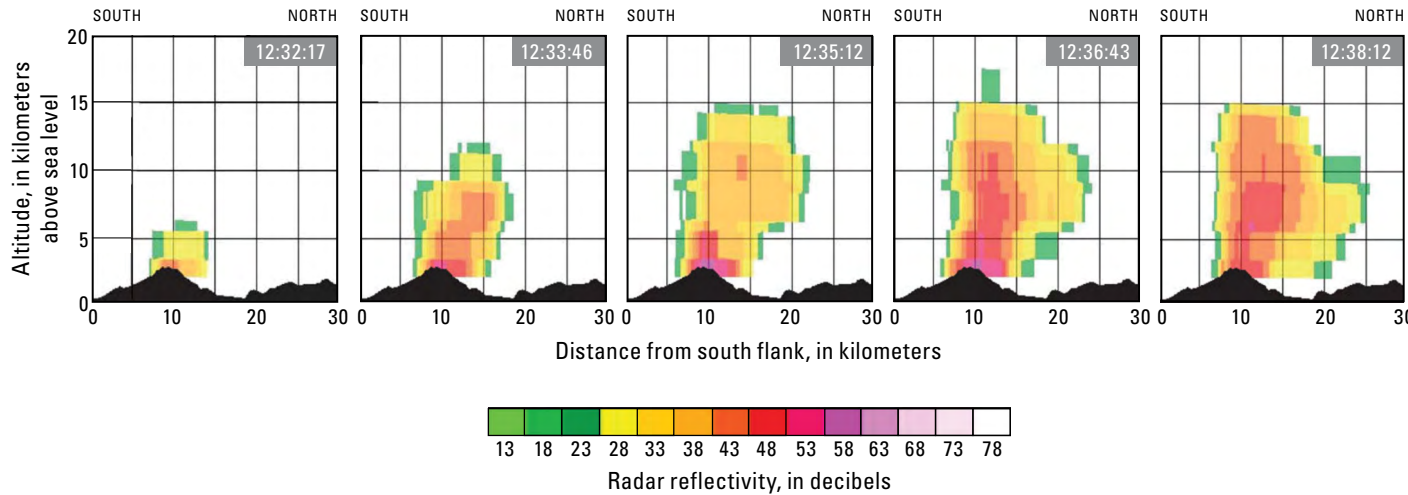


Figure J7. Radar cross sections of the eruption plume on March 23, 2009, at Redoubt Volcano, Alaska. The cross sections were generated from three-dimensional scans of the cloud that were collected approximately every 90 seconds. The time of each radar image is given in coordinated universal time (UTC), and the topography is shown along the bottom of the 30-kilometer-long cross sections. Radar reflectivity is highly dependent on the size of particles, as well as the amount of particles, in the cloud. Note the rapid ascent to 15 kilometers (about 50,000 feet) above sea level within 5 minutes of the eruption that began at 12:30:21 UTC.

ash from the atmosphere. Where possible (and where justified by the threat posed), deployment of transportable radar systems such as the USGS C-band system, or those operated by the National Weather Service National Severe Storms Laboratory, would greatly improve the capability to rapidly detect and characterize volcanic ash emissions.

Volcanic Lightning

Volcanic plumes commonly produce strong electric fields that lead to lightning (fig. J8). Lightning emits electromagnetic energy that travels at the speed of light through the atmosphere, providing a rapid source of information about volcanic plume behavior (Behnke and others, in press). During the eruption of Bogoslof Island, Alaska, in 2016–17, lightning-based alarms were received by USGS within 3 minutes of flash onset (Coombs and others, 2019) and, in some cases, provided the earliest indication of an explosive eruptive event (Van Eaton and others, 2020). Lightning detection provides a useful way to characterize explosive eruption plumes in near real time in three specific ways. First, volcanic plumes only produce abundant, globally detectable lightning once the plume rises above freezing altitudes of the atmosphere (approximately -20 degrees Celsius)—these heights tend to be in close range of aircraft cruising flight levels and provide a useful indication of potentially hazardous plume heights (Van Eaton and others, 2020). Second, the lightning rate tends to increase with increasing plume height and, therefore, with mass eruption rate (Hargie and others, 2019; Van Eaton and others, 2022, 2023), providing a means to track changes in emission through time. And third, the spatial trajectory of lightning locations follows the expansion of an umbrella cloud, if present, and parts of the downwind ash plume (Van Eaton and others, 2016; Smith and others, 2018). Each of these aspects is potentially valuable for identifying the onset, intensity, and spatial evolution of explosive volcanic hazards (Behnke and others, in press).

Optical sensors on satellite platforms can detect lightning flashes from space—for example, the Global Lightning Mapper (fig. J6) on GOES satellites has good coverage over the continental United States, and moderate coverage over the most volcanically active regions in Alaska, Hawai‘i, and the Northern Mariana Islands. The most robust approach to lightning detection uses a lightning mapping array—a near-field configuration of very high frequency (VHF) antennas configured within 200 km of the volcano. Such arrays have only been deployed at a handful of volcanoes during temporary campaigns, but the results provide a high-resolution, three-dimensional map of all electrical discharges taking place, including a special class known as vent discharges, which may provide the earliest warning of ash-rich emissions. Vent discharges emit continual radio frequency

impulses that are only detectable within about 200 km of the volcano. These vent discharges are smaller than lightning flashes and tend to initiate precisely at the onset of a high-speed, impulsive eruptive jet. For example, Behnke and others (2018) detected vent discharges before the plume even rose above the crater walls at Sakurajima in Japan. These signals are more challenging to detect, requiring at least one VHF radio antenna near the volcano, but they offer a powerful tool for early warning of ash-rich explosions. When an explosive eruption is too small or weak to create lightning, perturbations in the static electric field can still be detected with a field mill (Büttner and others, 2000; Miura and others, 2002). At present, VHF sensors have relatively high power (about 10 watts) and data transfer requirements and are most appropriate for non-telemetered campaigns. However, real-time data processing is currently in use for atmospheric studies (Nadler and others, 2009) and could be adapted for remote volcano monitoring.

If VHF sensors are not practical, the next best option is a longer range network of radio antennas tuned to the low and (or) very low frequency bands. Stations may be located several hundred to thousands of kilometers apart. The past 10–15 years have seen a major increase in this type of long-range lightning network coverage, maintained by private organizations, some of which offer subscription services. These include Vaisala’s Global Lightning Detection Network and National Lightning Detection Network, Earth Network’s Total Lightning Network, and the University of Washington’s World Wide Lightning and Location Network. The drawback of long-range networks is that only the most energetic lightning can be detected, generally comprising 10–70 percent of the total lightning produced. They also cannot detect vent discharges. Despite these shortcomings, recent studies have shown that global networks excel at detecting lightning from sustained, ash-rich eruption plumes that rise high enough to freeze (generally greater than 6–10 km above sea level).



Figure J8. Volcanic lightning formed in an ash-rich eruption plume during the 2010 eruption of Eyjafjallajökull, Iceland. Copyrighted photograph by Sigurður Stefnisson, April 17, 2010; used with permission.

Examples include the eruption of Pavlof Volcano in 2016 (Fee and others, 2017) and Bogoslof Island in 2016–17 (Van Eaton and others, 2020) in Alaska. The small- to moderate-sized eruptions (for example, the eruptions at Kīlauea’s summit, Hawai‘i, on May 17, 2018, and Mount Cleveland, Alaska, in July 2017) are generally missed, but it is plausible that their weaker electrical activity would have been measurable with short-range VHF or static electric field sensors. Strategic improvements can increase the sensitivity of long-range networks by adding new sensors to reduce gaps in coverage and developing algorithms to obtain lightning counts from two sensors rather than the standard three or more (coined the “two-sensor solution” by Lapierre and others, 2018).

Ground-Based Ash Sensors and Sampling

A key goal of the USGS volcano observatories is to provide timely assessment of ash-related hazards from explosive volcanism. In some cases, it is possible to send personnel directly into the downwind area of a recent eruption to measure the deposit thickness and sample material for petrologic analysis. This manual process is time consuming and, in many cases, not feasible because of the hazards from ongoing eruptive activity and extreme terrain. However, the past decade has seen promising developments in ground-based sensors that could provide the following capabilities: (1) remote measurement of suspended ash concentrations or particle-size distributions near the ground and (2) automated collection of time-varying samples of volcanic ashfall. The ultimate capability would be time-series measurements of ash concentration, grain-size distribution, and sampling that includes deposit mass per unit area. USGS has deployed instruments measuring particulate concentrations for resuspended ash from the Katmai region of Alaska, and more advanced instrumentation is in development to measure both ash concentrations and particle-size distributions (for example, Kaur and Kelly, 2023). In addition to timely information on ground-level concentrations and grain size of volcanic ash affecting air quality and infrastructure, it is also

possible to deploy automated ashfall sampling stations in targeted locations. Previous work has shown that rapid petrological analysis of recently erupted volcanic ash samples can help determine when fresh magma reached the surface (Cashman and Hoblitt, 2004; Benet and others, 2021), whether a hydrothermal system is involved (Gaunt and others, 2016), and if the eruption has tapped deep, gas-rich reservoirs (Gansecki and others, 2019; Halldórsson and others, 2022). These crucial pieces of information can inform forecasts of the eruption rate, style, and duration of ongoing activity (Sigmarsson and others, 2011; Gansecki and others 2019; Halldórsson and others, 2022). Ash collection systems currently in place at some observatories (for example, in Ecuador, Japan, and Mexico) use an automated, rotating table of vials (fig. J9) that can be set on hourly to monthly sampling schedules and activated remotely as appropriate (for example, Shimano and others, 2013), as reviewed in recent best practice recommendations for petrologic monitoring of active volcanoes (Re and others, 2021). The modest power draw of such systems (about 0.3 amperes) makes them feasible for installation alongside remote monitoring stations.

Recommended Capabilities

Detect and Characterize Ash-Producing Eruptions

The methodology described in this report to monitor volcanoes at a level that is commensurate with their threat level does not directly apply to the required capability to detect and characterize ash-producing eruptions. All ash-producing eruptions are potentially hazardous and need to be reacted to as soon as possible regardless of their preeruption threat level. In addition to the satellite, lightning, and radar techniques described in this chapter, the other key components to achieve this requirement are seismic (chapter B, this volume; Thelen and others, 2024) and infrasound (chapter C, this volume; Lyons and

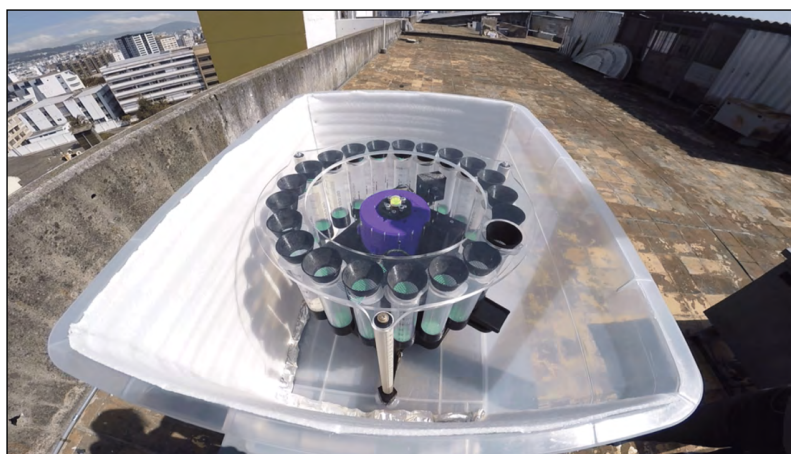


Figure J9. Photographs of two examples of automated ash collection systems at Instituto Geofísico, Ecuador. *A*, Photograph by Francisco Mejia, Instituto Geofísico Ecuador, September 15, 2022; used with permission. *B*, Photograph by Liz Gaunt, University College London, December 3, 2021; used with permission.

others, 2024) monitoring, as well as web cameras (chapter G, this volume; Orr and others, 2024). Integration of these various data sources provides the most timely and comprehensive analysis of eruptive activity.

Within the USGS volcano observatories, alerts are received regarding possible volcanic activity from seismic and infrasound networks and from satellite and lightning sources. The seismic alerts are typically local to a specific region, whereas infrasound can be local or regional, and satellite and lightning alerts are to date global in nature. These alerts need to be evaluated by an observatory scientist to determine their validity (because there are false positives) and to respond accordingly. Ideally, a 24/7 on-duty scientist would evaluate all alerts regardless of source within minutes of reception. For volcanoes that are not instrumented, lightning alerts have, in some cases (for example, Bogoslof Island, 2016–17; Shiveluch, 2023), been the first indication that an eruption has occurred. Satellite data are typically used to evaluate lightning alerts, but geostationary data currently have a latency of several tens of minutes at USGS observatories. For instrumented volcanoes, eruption onset may be observable quickly, but satellite latency can delay the interpretation if data from another source (such as a web camera) are not available or are obscured. Radar data can greatly aid the analysis of geophysical data streams with minimal latency, but coverage is limited.

The overarching recommendations for achieving the required capability to detect and characterize volcanic plumes and clouds are listed below. We note that satellite coverage and global lightning sensor data streams can be acquired for all U.S. volcanoes, whereas deployment of near-field sensors (for example, VHF lighting, radar, and ash sampling) would require evaluation of additional criteria such as a volcano's exposure ranking (that is, is it close to major population centers), expected duration of activity (a volcano that produced long-lived episodes of dome growth and collapse versus one expected to have a single short-lived eruption), and logistical considerations.

- Low-latency access to geostationary satellite image products from the GOES and Himawari platforms. Ideally, 5 minutes or less from image collection to USGS availability.
- Access to polar-orbiting satellite image products from NOAA platforms. Ideally, a latency of 30 minutes or less from image collection to USGS availability.
- Real-time data subscriptions and alarms from commercial and academic long-range lightning detection networks. Volcanoes in Alaska, Hawai'i, and the Commonwealth of the Northern Mariana Islands are covered by the Global Lightning Detection Network, Earth Networks Total Lightning Network, and World Wide Lightning Location Network, with moderate coverage from GOES Global Lightning Mapper. The contiguous U.S. volcanoes are additionally covered by the National Lightning Detection Network.
- Deployment of a telemetered, short-range electrical sensor (VHF sensor, field mill, or similar) to capture small-scale vent discharges associated with the earliest stages of volcanic plume development.
- Collaboration with National Weather Service and academic partners at the National Severe Storms Laboratory on volcanic cloud product development for the NEXRAD system and for portable radar systems.
- Deployment of a radar system for rapid evaluation of eruptions with potential for ashfall on populated areas and substantial effects on infrastructure.
- Deployment of ash sensor and collection systems in targeted areas near an erupting volcano (within approximately 10–100 km depending on eruption dynamics and wind field).
- Appropriate geophysical instrumentation and web cameras, as noted elsewhere in this volume.
- Integration of alerts from all sources and a 24/7 capability for an observatory duty scientist to evaluate and act upon them as needed.

References Cited

- Arason, P., Petersen, G.N., and Bjornsson, H., 2011, Observations of the altitude of the volcanic plume during the eruption of Eyjafjallajökull, April–May 2010: *Earth System Science Data*, v. 3, no. 1, p. 9–17, <https://doi.org/10.5194/essd-3-9-2011>.
- Beckett, F., Rossi, E., Devenish, B., Witham, C., and Bonadonna, C., 2022, Modelling the size distribution of aggregated volcanic ash and implications for operational atmospheric dispersion modelling: *Atmospheric Chemistry and Physics*, v. 22, no. 5, p. 3409–3431, <https://doi.org/10.5194/acp-22-3409-2022>.
- Behnke, S.A., Edens, H.E., Thomas, R.J., Smith, C.M., McNutt, S.R., Van Eaton, A.R., Cimarelli, C., and Cigala, V., 2018, Investigating the origin of continual radio frequency impulses during explosive eruptions: *Journal of Geophysical Research—Atmospheres*, v. 123, no. 8, p. 4157–4174.
- Behnke, S.A., Van Eaton, A.R., and Schultz, C.J., in press, Monitoring lightning and electrification in volcanic plumes, *in* Spica, Z. and Caudron, C. eds., *Modern volcano monitoring: International Association of Volcanology and Chemistry of the Earth's Interior Series*.
- Benet, D., Costa, F., Pedreros, G., and Cardona, C., 2021, The volcanic ash record of shallow magma intrusion and dome emplacement at Nevados de Chillán Volcanic complex, Chile: *Journal of Volcanology and Geothermal Research*, v. 417, article no. 107308, <https://doi.org/10.1016/j.jvolgeores.2021.107308>.

- Brown, R.J., Bonadonna, C., and Durant, A.J., 2012, A review of volcanic ash aggregation: Physics and Chemistry of the Earth, Parts A/B/C, v. 45–46, p. 65–78, <https://doi.org/10.1016/j.pce.2011.11.001>.
- Büttner, R., Zimanowski, B., and Röder, H., 2000, Short-time electrical effects during volcanic eruption—Experiments and field measurements: *Journal of Geophysical Research*, v. 105, no. B2, p. 2819–2827, <https://doi.org/10.1029/1999JB900370>.
- Cahalan, R.C., Mastin, L.G., Van Eaton, A.R., Hurwitz, S., Smith, A.B., Dufek, J., Solovitz, S.A., Patrick, M., Schmith, J., and Parcheta, C., Thelen, W.A., and Downs, D.T., 2023, Dynamics of the December 2020 ash-poor plume formed by lava-water interaction at the summit of Kīlauea Volcano, Hawai‘i: *Geochemistry, Geophysics, Geosystems*, v. 24, no. 3, <https://doi.org/10.1029/2022GC010718>.
- Casadevall, T.J., 1994, 1989–90 eruption of Redoubt Volcano, Alaska—Impacts on aircraft operations: *Journal of Volcanology and Geothermal Research*, v. 62, nos. 1–4, p. 301–316, [https://doi.org/10.1016/0377-0273\(94\)90038-8](https://doi.org/10.1016/0377-0273(94)90038-8).
- Cashman, K.V., and Hoblitt, R.P., 2004, Magmatic precursors to the 18 May 1980 eruption of Mount St. Helens, USA: *Geology*, v. 32, no. 2, p. 141–144, <https://doi.org/10.1130/G20078.1>.
- Coombs, M., Wallace, K., Cameron, C., Lyons, J., Wech, A., Angeli, K., and Cervelli, P., 2019, Overview, chronology, and impacts of the 2016–2017 eruption of Bogoslof Volcano, Alaska: *Bulletin of Volcanology*, v. 81, no. 62, <https://doi.org/10.1007/s00445-019-1322-9>.
- Crouch, J.F., Pardo, N., and Miller, C.A., 2014, Dual polarisation C-band weather radar imagery of the 6 August 2012 Te Maari Eruption, Mount Tongariro, New Zealand: *Journal of Volcanology and Geothermal Research*, v. 286, p. 415–436, <https://doi.org/10.1016/j.jvolgeores.2014.05.003>.
- Engwell, S., Mastin, L., Tupper, A., Kibler, J., Acethorp, P., Lord, G., and Filgueira, R., 2021, Near-real-time volcanic cloud monitoring: insights into global explosive volcanic eruptive activity through analysis of Volcanic Ash Advisories: *Bulletin of Volcanology*, v. 83, no. 9, <https://doi.org/10.1007/s00445-020-01419-y>.
- Fee, D., Haney, M.M., Matoza, R.S., Van Eaton, A.R., Cervelli, P., Schneider, D.J., and Iezzi, A.M., 2017, Volcanic tremor and plume height hysteresis from Pavlof Volcano, Alaska: *Science*, v. 355, no. 6320, p. 45–48, <https://doi.org/10.1126/science.aah6108>.
- Ganseccki, C., Lee, R.L., Shea, T., Lundblad, S.P., Hon, K., and Parcheta, C., 2019, The tangled tale of Kīlauea’s 2018 eruption as told by geochemical monitoring: *Science*, v. 366, no. 6470, <https://doi.org/10.1126/science.aaz0147>.
- Gaunt, H.E., Bernard, B., Hidalgo, S., Proaño, A., Wright, H., Mothes, P., Criollo, E., and Kueppers, U., 2016, Juvenile magma recognition and eruptive dynamics inferred from the analysis of ash time series—The 2015 reawakening of Cotopaxi Volcano: *Journal of Volcanology and Geothermal Research*, v. 328, p. 134–146, <https://doi.org/10.1016/j.jvolgeores.2016.10.013>.
- Global Volcanism Program, 1982, Report on Galunggung (Indonesia) (McClelland, L., ed.): Smithsonian Institution Scientific Event Alert Network Bulletin, v. 7, no. 6, <https://doi.org/10.5479/si.GVP.SEAN198206-263140>.
- Guffanti, M., Casadevall, T.J., and Budding, K., 2010, Encounters of aircraft with volcanic ash clouds—A compilation of known incidents, 1953–2009: U.S. Geological Survey Data Series 545, v. 1.0, 12 p., plus 4 appendixes including the compilation database, <https://pubs.usgs.gov/ds/545>.
- Halldórsson, S.A., Marshall, E.W., Caracciolo, A., Matthews, S., Bali, E., Rasmussen, M.B., Ranta, E., Robin, J.G., Guðfinnsson, G.H., Sigmarsson, O., MacLennan, J., Jackson, M.G., Whitehouse, M.J., Heejin Jeon, van der Meer, Q.H.A., Mibei, G.K., Kalliokoski, M.H., Repczynska, M.M., Rúnarsdóttir, R.H., Sigurðsson, G., Pfeffer, M.A., Scott, S.W., Kjartansdóttir, R., Kleine, B.E., Oppenheimer, C., Aiuppa, A., Ilyinskaya, E., Bitetto, M., Giudice, G., and Stefánsson, A., 2022, Rapid shifting of a deep magmatic source at Fagradalsfjall volcano, Iceland: *Nature*, v. 609, no. 7927, p. 529–534, <https://doi.org/10.1038/s41586-022-04981-x>.
- Hargie, K.A., Van Eaton, A.R., Mastin, L.G., Holzworth, R.H., Ewert, J.W., and Pavolonis, M., 2019, Globally detected volcanic lightning and umbrella dynamics during the 2014 eruption of Kelud, Indonesia: *Journal of Volcanology and Geothermal Research*, v. 382, p. 81–91, <https://doi.org/10.1016/j.jvolgeores.2018.10.016>.
- International Civil Aviation Organization, 2015, Manual on volcanic ash, radioactive material, and toxic chemical clouds (3d ed.): International Civil Aviation Organization document 9691, 194 p.
- Kaur, K., and Kelly, K.E., 2023, Laboratory evaluation of the Alphasense OPC-N3, and the Plantower PMS5003 and PMS6003 sensors: *Journal of Aerosol Science*, v. 171, article no. 106181, <https://doi.org/10.1016/j.jaerosci.2023.106181>.
- Lacasse, C., Karlsdóttir, S., Larsen, G., Soosalu, H., Rose, W.I., and Ernst, G.G.J., 2004, Weather radar observations of the Hekla 2000 eruption cloud, Iceland: *Bulletin of Volcanology*, v. 66, no. 5, p. 457–473, <http://doi.org/10.1007/s00445-003-0329-3>.
- Lapierre, J.L., Van Eaton, A.R., Stock, M., Haney, M.M., and Lyons, J.J., 2018, Remote measurements of volcanic plume electrification using a sparse network technique [abs.]: American Geophysical Union, Fall Meeting 2018, no. V43B-08.

- Lyons, J.J., Fee, D., Thelen, W.A., Iezzi, A.M., and Wech, A.G., 2024, Infrasound for volcano monitoring, chap. C of Flinders, A.F., Lowenstern, J.B., Coombs, M.L., and Poland, M.P., eds., Recommended capabilities and instrumentation for volcano monitoring in the United States: U.S. Geological Survey Scientific Investigations Report 2024–5062–C, 11 p., <https://doi.org/10.3133/sir20245062C>.
- Marzano, F.S., Picciotti, E., Montopoli, M., and Vulpiani, G., 2013, Inside volcanic clouds— Remote sensing of ash plumes using microwave weather radars: Bulletin of the American Meteorological Society, v. 94, no. 10, p. 1567–1586, <https://doi.org/10.1175/BAMS-D-11-00160.1>.
- Mastin, L.G., Van Eaton, A.R., and Durant, A.J., 2016, Adjusting particle-size distributions to account for aggregation in tephra-deposit model forecasts: Atmospheric Chemistry and Physics, v. 16, no. 14, p. 9399–9420, <https://doi.org/10.5194/acp-16-9399-2016>.
- Miura, T., Koyaguchi, T., and Tanaka, Y., 2002, Measurements of electric charge distribution in volcanic plumes at Sakurajima Volcano, Japan: Bulletin of Volcanology, v. 64, no. 2, p. 75–93, <https://doi.org/10.1007/s00445-001-0182-1>.
- Nadler, D., Darden, C., Stano, G., and Buechler, D., 2009, An operational perspective of total lightning information [abs.], in 4th Conference on the Meteorological Applications of Lightning Data: American Meteorological Society, Phoenix, Arizona, January 11–15, 2009.
- Neal, C.A., Brantley, S.R., Antolik, L., Babb, J.L., Burgess, M., Calles, K., Cappos, M., Chang, J.C., Conway, S., Desmither, L., Dotray, P., Elias, T., Fukunaga, P., Fuke, S., Johanson, I.A., Kamibayashi, K., Kauahikaua, J., Lee, R.L., Pekalib, S., Miklius, A., Million, W., Moniz, C.J., Nadeau, P.A., Okubo, P., Parcheta, C., Patrick, M.R., Shiro, B., Swanson, D., Tollett, W., Trusdell, F., Zoeller, M.H., Montgomery-Brown, E.K., Anderson, K.R., Poland, M.P., Ball, J.L., Bard, J.A., Coombs, M., Dietterich, H.R., Kern, C., Thelen, W.A., Cervelli, P.F., Orr, T., Houghton, B.F., Gansecki, C., Hazlett, R., Lundgren, P., Diefenbach, A.K., Lerner, A., Waite, G., Kelly, P.J., Clor, L., Werner, C., Burgess, M., Mulliken, K., Fisher, G., and Damby, D., 2019, The 2018 rift eruption and summit collapse of Kīlauea Volcano: Science, v. 363, no. 6425, p. 367–374, <https://doi.org/10.1126/science.aav7046>.
- Orr, T.R., Dietterich, H.R., and Poland, M.P., 2024, Tracking surface changes caused by volcanic activity, chap. G of Flinders, A.F., Lowenstern, J.B., Coombs, M.L., and Poland, M.P., eds., Recommended capabilities and instrumentation for volcano monitoring in the United States: U.S. Geological Survey Scientific Investigations Report 2024–5062–G, 11 p., <https://doi.org/10.3133/sir20245062G>.
- Pavolonis, M.J., Sieglaff, J., and Cintineo, J., 2015a, Spectrally enhanced cloud objects—A generalized framework for automated detection of volcanic ash and dust clouds using passive satellite measurements—1. Multispectral analysis: Journal of Geophysical Research—Atmospheres, v. 120, no. 15, p. 7813–7841, <https://doi.org/10.1002/2014JD022968>.
- Pavolonis, M.J., Sieglaff, J., and Cintineo, J., 2015b, Spectrally enhanced cloud objects—A generalized framework for automated detection of volcanic ash and dust clouds using passive satellite measurements—2. Cloud object analysis and global application: Journal of Geophysical Research—Atmospheres, v. 120, no. 15, p. 7842–7870, <https://doi.org/10.1002/2014JD022969>.
- Pavolonis, M.J., Sieglaff, J., and Cintineo, J., 2018, Automated detection of explosive volcanic eruptions using satellite-derived cloud vertical growth rates: Earth and Space Science, v. 5, no. 12, p. 903–928, <https://doi.org/10.1029/2018EA000410>.
- Prata, A.J., 1989, Infrared radiative transfer calculations for volcanic ash clouds: Geophysical Research Letters, v. 16, no. 11, p. 1293–1296, <https://doi.org/10.1029/GL016i011p01293>.
- Re, G., Corsaro, R.A., D’Orlando, C., and Pompilio, M., 2021, Petrological monitoring of active volcanoes—A review of existing procedures to achieve best practices and operative protocols during eruptions: Journal of Volcanology and Geothermal Research, v. 419, article no. 107365, <https://doi.org/10.1016/j.jvolgeores.2021.107365>.
- Rose, W., Kostinski, A., and Kelley, L., 1995, Real-time C-band radar observations of 1992 eruption clouds from Crater Peak, Mount Spurr Volcano, Alaska, in Keith, T.E.G., ed., The 1992 eruptions of Crater Peak vent, Mount Spurr Volcano, Alaska: U.S. Geological Survey Bulletin 2139, p. 19–26, <https://doi.org/10.3133/b2139>.
- Schneider, D.J., and Hoblitt, R.P., 2013, Doppler weather radar observations of the 2009 eruption of Redoubt Volcano, Alaska: Journal of Volcanology and Geothermal Research, v. 259, p. 133–144, <https://doi.org/10.1016/j.jvolgeores.2012.11.004>.
- Schneider, D.J., Van Eaton, A.R., and Wallace, K.L., 2020, Satellite observations of the 2016–2017 eruption of Bogoslof Volcano—Aviation and ash fallout hazard implications from a water-rich eruption: Bulletin of Volcanology, v. 82, no. 29, <https://doi.org/10.1007/s00445-020-1361-2>.
- Schuster, R.L., 1981, Effects of the eruptions on civil works and operations in the Pacific Northwest, in Lipman, P.W., and Mullineaux, D.R., eds., The 1980 eruptions of Mount St. Helens, Washington: U.S. Geological Survey Professional Paper 1250, p. 701–718.

- Schwaiger, H.F., Denlinger, R.P., and Mastin, L.G., 2012, Ash3d—A finite-volume, conservative numerical model for ash transport and tephra deposition: *Journal of Geophysical Research*, v. 117, no. B4, <https://doi.org/10.1029/2011JB008968>.
- Shimano, T., Nishimura, T., Chiga, N., Shibasaki, Y., Iguchi, M., Miki, D., and Yokoo, A., 2013, Development of an automatic volcanic ash sampling apparatus for active volcanoes: *Bulletin of Volcanology*, v. 75, no. 773, 7 p., <https://doi.org/10.1007/s00445-013-0773-7>.
- Sigmarrsson, O., Vlastelic, I., Andreassen, R., Bindeman, I., Devidal, J.L., Moune, S., Keiding, J.K., Larsen, G., Höskuldsson, A., and Thordarson, T., 2011, Remobilization of silicic intrusion by mafic magmas during the 2010 Eyjafjallajökull eruption: *Journal of Geophysical Research, Solid Earth*, v. 2, no. 2, p. 271–281, <https://doi.org/10.5194/se-2-271-2011>.
- Smith, C., Van Eaton, A., Said, R., and Holzworth, R., 2018, Volcanic lightning as a monitoring tool during the 2016–2017 eruption of Bogoslof Volcano, AK [abs.]: 25th International Lightning Detect Conference and 7th International Lightning Meteorology Conference, March 2018, Ft. Lauderdale, Florida, p. 5.
- Thelen, W.A., Lyons, J.J., Wech, A.G., Moran, S.C., Haney, M.M., and Flinders, A.F., 2024, Seismic techniques and suggested instrumentation to monitor volcanoes, chap. B of Flinders, A.F., Lowenstern, J.B., Coombs, M.L., and Poland, M.P., eds., *Recommended capabilities and instrumentation for volcano monitoring in the United States*: U.S. Geological Survey Scientific Investigations Report 2024–5062–B, 9 p., <https://doi.org/10.3133/sir20245062B>.
- U.S. Geological Survey, 2022, Volcanic ash and gas impacts and mitigation: U.S. Geological Survey website, accessed May 18, 2024, at https://volcanoes.usgs.gov/volcanic_ash.
- Van Eaton, A.R., Amigo, Á., Bertin, D., Mastin, L.G., Giacosa, R.E., González, J., Valderrama, O., Fontijn, K., and Behnke, S.A., 2016, Volcanic lightning and plume behavior reveal evolving hazards during the April 2015 eruption of Calbuco Volcano, Chile: *Geophysical Research Letters*, v. 43, no. 7, p. 3563–3571, <https://doi.org/10.1002/2016GL068076>.
- Van Eaton, A.R., Lapierre, J., Behnke, S.A., Vagasky, C., Schultz, C.J., Pavolonis, M., Bedka, K., and Khlopenkov, K., 2023, Lightning rings and gravity waves—Insights into the giant eruption plume from Tonga’s Hunga Volcano on 15 January 2022: *Geophysical Research Letters*, v. 50, no. 12, <https://doi.org/10.1029/2022GL102341>.
- Van Eaton, A.R., Mastin, L.G., Herzog, M., Schwaiger, H.F., Schneider, D.J., Wallace, K.L., and Clarke, A.B., 2015, Hail formation triggers rapid ash aggregation in volcanic plumes: *Nature Communications*, v. 6, article no. 7860, <https://doi.org/10.1038/ncomms8860>.
- Van Eaton, A.R., Schneider, D.J., Smith, C.M., Haney, M.M., Lyons, J.J., Said, R., Fee, D., Holzworth, R.H., and Mastin, L.G., 2020, Did ice-charging generate volcanic lightning during the 2016–2017 eruption of Bogoslof Volcano, Alaska?: *Bulletin of Volcanology*, v. 82, no. 3, <https://doi.org/10.1007/s00445-019-1350-5>.
- Van Eaton, A.R., Smith, C.M., Pavolonis, M., and Said, R., 2022, Eruption dynamics leading to a volcanic thunderstorm—The January 2020 eruption of Taal volcano, Philippines: v. 50, no. 4, p. 491–495, <https://doi.org/10.1130/G49490.1>.
- Warrick, R.A., Anderson, J., Lyons, J., Ressler, J., Mary, W., and Warrick, T., 1981, *Four communities under ash after Mount St. Helens*: Boulder, University of Colorado, Institute of Behavioral Science Program on Technology, Environment, and Man Monograph 34, 143 p.
- Watson, I.M., Realmuto, V.J., Rose, W.I., Prata, A.J., Bluth, G.J.S., Gu, Y., Bader, C.E., and Yu, T., 2004, Thermal infrared remote sensing of volcanic emissions using the moderate resolution imaging spectroradiometer: *Journal of Volcanology and Geothermal Research*, v. 135, no. 1–2, p. 75–89, <https://doi.org/10.1016/j.jvolgeores.2003.12.017>.

Chapter K



U.S. Geological Survey scientists D. Swanson and S. Hurwitz measure the depth to the water table at the 1,262 meter-deep National Science Foundation borehole (commonly referred to as the "Keller Well") within the summit caldera of Kilauea, Hawai'i. Campaign measurements of water-table depth following the 2018 summit caldera collapse and Lower East Rift Zone eruption enabled scientists to better understand the mechanisms for explosive summit eruptions and summit recharge. Photograph by S. Peek, U.S. Geological Survey, December 18, 2018.

Chapter K

Special Topic—Boreholes

By Shaul Hurwitz and Jacob B. Lowenstern

Introduction

Installation of instrument packages in deep (several hundred to several thousand meters) boreholes near volcanoes is relatively expensive (a few million to tens of millions of U.S. dollars), but can provide a low-noise, high-quality source of geophysical (seismic, strain, tilt, and pore pressure), physical (temperature and water level), and geochemical data. Observations from instruments at depth have the potential to provide insights into processes associated with magma intrusion, unrest, and eruption that would not otherwise be possible (Lowenstern and others, 2017; Eichelberger, 2020). Examples of instrumented boreholes in volcanic areas include the 3-kilometer (km)-deep Long Valley Exploratory Well (LVEW) in California (for example, Priest and others, 1998; Prejean and Ellsworth, 2001; Fischer and others, 2003; Roeloffs and others, 2003; Sorey and others, 2003), the 1,262 meter-deep NSF Well (commonly referred to as the “Keller Well”) within the summit caldera of Kīlauea, Hawai‘i (Keller and others, 1979; Myren and others, 2006), and the Caribbean Andesite Lava Island-volcano Precision Seismo-geodetic Observatory (CALIPSO) project at Soufrière Hills, Montserrat, which includes a series of four 200-meter (m)-deep holes (for example, Mattioli and others, 2004; Voight and others, 2006). The Plate Boundary Observatory (PBO) of the National Science Foundation’s Earthscope project placed seismometers, tiltmeters, strainmeters, and pore-pressure sensors at depths of 100 to 250 m in more than 100 boreholes scattered in western North America, including at Mount St. Helens, Washington, and Yellowstone Caldera, Wyoming. The total cost for an instrumented PBO borehole ranged from \$250,000 to \$270,000 U.S. dollars (USD) and a few thousand USD are required annually for maintenance (David Mencin, UNAVCO, written commun., October 2020).

Capabilities Provided

High-Quality Seismic and Geodetic Recordings

When deployed within boreholes, seismometers, strainmeters, and tiltmeters are insulated from the noise created at the surface by wind, rain, rivers, animals, machinery, and general temperature and pressure variations. These factors commonly degrade the quality of data obtained from surface-based instruments. For example, seismometers at high-altitude

and (or) high-latitude sites on the flanks of volcanoes are particularly susceptible to noise associated with strong storm systems. Borehole seismometers have demonstrably higher signal-to-noise ratios of seismic and strain recordings than surface-based instruments (for example, Prejean and Ellsworth, 2001). Thus, from a practical perspective, the consistently high signal-to-noise ratio of borehole seismometers provides a reliable record of seismicity regardless of surface noise levels. Likewise, strainmeters offer the most sensitive means of monitoring deformation associated with magmatic activity. In Iceland, strainmeter records provided the only detected transient deformation immediately prior (by tens of minutes) to the 1991 and 2000 eruptions of Hekla (Linde and others, 1993). Luttrell and others (2013) used strain signals from seiche waves in Yellowstone Lake as input for modeling the depth and extent of partially molten magma in the upper crust beneath Yellowstone Caldera.

An indirect source of noise on seismic records is the uppermost several tens to hundreds of meters of the crust, which generally is highly fractured and, thus, highly attenuative and subject to fluctuations in surface temperatures. Comparison of earthquakes recorded by surface seismometers near Long Valley Caldera and LVEW borehole seismometers indicates that borehole records contain more impulsive P- and S-wave arrivals and much higher frequency content (Prejean and Ellsworth, 2001). The records from the borehole seismometer were also less affected by scattering and attenuation. Because a primary goal of volcano seismology is to determine the nature of a seismic source, it is ideal to avoid scattering and attenuation as much as possible (Prevedel and others, 2015). Thus, borehole seismometers would likely increase a network’s ability to detect changes in seismic sources (see chapter B of this volume; Thelen and others, 2024), as well as to determine the processes that generate various types of seismicity. Indeed, Shelly and others (2013) and Shelly and Hardebeck (2019) relied on PBO borehole data for use in relocating hypocenters in Yellowstone earthquake swarms.

Direct and Indirect Measurements of Subsurface Geology and Hydrology

Boreholes provide a window into subsurface geologic, hydrologic, and thermal regimes that are largely hidden from instrumental measurements at the ground surface. Core samples from the LVEW borehole, for example, provided a continuous stratigraphic section to a depth of 2.3 km below Long Valley Caldera’s resurgent dome. Samples from this core led to the

discovery of numerous rhyolitic dikes and sills that intruded the Bishop Tuff (McConnell and others, 1995), providing direct evidence for post-caldera intrusions in the area of the resurgent dome. Several drilling programs have unexpectedly intersected molten magma bodies, for example, in Hawai‘i, Kenya, and Iceland, providing important insights about the geometry of the magmatic system as well as a direct test of the geophysical models that guided the drilling programs (Larsen and others, 1979; Teplow and others, 2009; Elders and others, 2011; Rooyakkers and others, 2021). Borehole instruments have also yielded important insights into the hydrothermal systems associated with volcanic areas (Pribnow and others, 2003; Hurwitz and others, 2010; Brown and others, 2013; Hurwitz and Anderson, 2019). For example, Roeloffs and others (2003) used borehole-pressure-transducer recordings from the LVEW and four other boreholes in Long Valley Caldera to investigate earthquake-induced, groundwater-level changes that persisted for days to weeks. They inferred that such changes are caused by accelerated inflation of Long Valley Caldera’s resurgent dome—inflation too small to be detected by surface-based deformation monitoring.

Boreholes on steep stratovolcanoes are rare but could provide crucial information on time-dependent water saturation and rock alteration within the edifice. These parameters are particularly important to measure because hydrothermal alteration can result in elevated pore-fluid pressures and strength reduction of rocks within a volcanic edifice, which can in turn lead to edifice flank collapse and lahar formation (Finn and others, 2001; Hurwitz and others, 2003; Reid, 2004; Ball and others, 2018). Among Cascade Range stratovolcanoes, Mount Hood, Oregon, is relatively rich in drill-hole information owing to geothermal reconnaissance in the 1970s and early 1980s. However, even at Mount Hood, all the drill holes are at least 5 km laterally away from the summit, and the highest wellhead is nearly 2 km vertically below the summit.

The Pucci drill hole, completed in 1980, reached a depth of 1,130 m from an elevation of 1,628 m (1,800 m below the summit) and revealed that the standing water level was 573 m below the land surface and the bottom-hole temperature was 76 degrees Celsius (°C) (Robison and others, 1981). These data suggest that the water table beneath the volcano is relatively deep or that the vertical fluid-potential gradient is near unity—information that could not be recovered from any other type of measurement.

An example of the utility of water-level measurements, water chemistry and water isotopic composition is provided by samples from and measurements within the NSF Well (“Keller Well”) at Kīlauea (fig. K1). A 6-centimeter, water-level (pressure) decrease in May 2001 was coincident with a rapid and large increase in compressional strain, recorded by the strainmeter that was installed in the well, and indicated that surface deformation at Kīlauea is not triggered by pressurization of the hydrothermal system (Hurwitz and Johnston, 2003). Analysis of water samples collected between 2003 and 2011 showed that the chemical and stable isotope compositions of groundwater were modified by magmatic gas condensation. Temporal variations of dissolved sulfate and chloride in the water coincided with changes in volcanic activity and indicate that magmatic gases were being absorbed (scrubbed) by groundwater, thus leading to underestimates of gas released from magma and magma volumes (Hurwitz and Anderson, 2019). The water level in the well measured a few months before the 2018 Kīlauea eruption (Hurwitz and others, 2019) guided interpretations of possible explosive magma-water interactions and hazards assessment during the 2018 eruption, when magma was draining from the summit lava lake (Hsieh and Ingebritsen, 2019; Cahalan and others, 2023).

Temperature sensors installed in boreholes enable continuous thermal profiling of the crust, for example, in Well CH-10B in Long Valley Caldera (Clor and others, 2018).

Figure K1. Photograph showing U.S. Geological Survey Hawaiian Volcano Observatory staff measuring water-table depth and collecting water samples for analysis from the 1,262-meter-deep NSF Well in the summit caldera of Kīlauea, Hawai‘i. Photograph by F. Younger, U.S. Geological Survey, March 22, 2022.



Temperature-depth data from shallow boreholes document conditions in hydrothermal systems, where phreatic eruptions might originate. Temperature data in deeper boreholes place constraints both on the position of the brittle-ductile transition (an important control on earthquake occurrence) and on the potential location of magma. For example, temperatures at a depth of 3 km in the LVEW borehole were unexpectedly low (about 100 °C) (Hurwitz and others, 2010), calling into question the previous assumption that a magma reservoir hotter than 800 °C resided at 4- to 5-km depths (Rundle and others, 1986).

General Recommendations and Considerations

Despite clear advantages for producing noise-free geophysical data close to magma and direct samples of geologic and hydrologic conditions at depth, boreholes are rarely a part of routine volcano monitoring, primarily because they are expensive to drill and maintain (for example, Mattioli and others, 2004). However, in some situations—for example, at a particularly active and hazardous volcano located in an area where the logistics of installation and maintenance are feasible—boreholes could be considered. These boreholes should (1) be at least 200 to 300 m deep, (2) include core recovery to better characterize the volcano's subsurface structure and eruptive history, and (3) be equipped with appropriate instrumentation. Instrumentation could include some combination of seismometers, tiltmeters, strainmeters, pore-pressure sensors, temperature sensors, and geochemical sensors. The data acquired from geologic and hydrologic sampling and geophysical instrument packages should be made available to the research community to maximize their utility. Drilling deeper boreholes (for example, more than 1 km) in active volcanoes and installing instrumentation is substantially more expensive and therefore may require partnerships with other academic and government agencies, which, in the United States, might include the Department of Energy or National Science Foundation.

References Cited

- Ball, J.L., Taron, J., Reid, M.E., Hurwitz, S., Finn, C., and Bedrosian, P., 2018, Combining multiphase groundwater flow and slope stability models to assess stratovolcano flank collapse in the Cascade Range: *Journal of Geophysical Research*, v. 123, no. 4, p. 2787–2805, <https://doi.org/10.1002/2017JB015156>.
- Brown, S.T., Kennedy, B.M., DePaolo, D.J., Hurwitz, S., and Evans, W.C., 2013, Ca, Sr, O and D isotope approach to defining the chemical evolution of hydrothermal fluids—Example from Long Valley, CA, USA: *Geochimica et Cosmochimica Acta*, v. 122, p. 209–225, <https://doi.org/10.1016/j.gca.2013.08.011>.
- Cahalan, R.C., Mastin, L.G., Van Eaton, A.R., Hurwitz, S., Smith, A.B., Dufek, J., Solovitz, S.A., Patrick, M., Schmith, J., Parcheta, C., and Thelen, W.A., 2023, Dynamics of the December 2020 ash-poor plume formed by lava-water interaction at the summit of Kīlauea Volcano, Hawai'i: *Geochemistry, Geophysics, Geosystems*, v. 24, no. 3, article no. e2022GC010718, <https://doi.org/10.1029/2022GC010718>.
- Clor, L., Hurwitz, S., Murphy, F., Howle, J., and Peek, S., 2018, Groundwater levels and temperatures in well CH-10b near Hot Creek, Long Valley Caldera, eastern California (ver. 2.0, May 2020): U.S. Geological Survey data release, accessed March 27, 2024, at <https://doi.org/10.5066/P96SHLT6>.
- Eichelberger, J., 2020, Distribution and transport of thermal energy within magma-hydrothermal systems: *Geosciences*, v. 10, no. 6, article no. 212, <https://doi.org/10.3390/geosciences10060212>.
- Elders, W.A., Friðleifsson, G.Ó., Zierenberg, R.A., Pope, E.C., Mortensen, A.K., Guðmundsson, Á., Lowenstern, J.B., Marks, N.E., Owens, L., Bird, D.K., Reed, M., Olsen, N.J., and Schiffman, P., 2011, Origin of a rhyolite that intruded a geothermal well while drilling at Krafla volcano, Iceland: *Geology*, v. 39, no. 3, p. 231–234, <https://doi.org/doi:10.1130/G31393.1>.
- Finn, C.A., Sisson, T.W., and Deszcz-Pan, M., 2001, Aerogeophysical measurements of collapse-prone hydrothermally altered zones at Mount Rainier volcano: *Nature*, v. 409, p. 600–603, <https://doi.org/10.1038/35054533>.
- Fischer, M., Röller, K., Küster, M., Stöckert, B., and McConnell, V.S., 2003, Open fissure mineralization at 2600 m depth in Long Valley Exploratory Well (California)—Insight into the history of the hydrothermal system: *Journal of Volcanology and Geothermal Research*, v. 127, no. 3–4, p. 347–363, [https://doi.org/10.1016/S0377-0273\(03\)00176-8](https://doi.org/10.1016/S0377-0273(03)00176-8).
- Hsieh, P.A., and Ingebritsen, S.E., 2019, Groundwater inflow toward a preheated volcanic conduit—Application to the 2018 eruption at Kīlauea Volcano, Hawai'i: *Journal of Geophysical Research, Solid Earth*, v. 124, no. 2, p. 1498–1506, <https://doi.org/10.1029/2018JB017133>.
- Hurwitz, S., and Anderson, K.R., 2019, Temporal variations in scrubbing of magmatic gases at the summit of Kīlauea Volcano, Hawai'i: *Geophysical Research Letters*, v. 46, no. 24, p. 14469–14476, <https://doi.org/10.1029/2019GL085904>.
- Hurwitz, S., Farrar, C.D., and Williams, C.F., 2010, The thermal regime in the resurgent dome of Long Valley Caldera, California—Inferences from precision temperature logs in deep wells: *Journal of Volcanology and Geothermal Research*, v. 198, nos. 1–2, p. 233–240, <https://doi.org/10.1016/j.jvolgeores.2010.08.023>.

- Hurwitz, S., and Johnston, M.J.S., 2003, Groundwater level changes in a deep well in response to a magma intrusion event on Kīlauea Volcano, Hawai'i: *Geophysical Research Letters*, v. 30, no. 22, 4 p., <https://doi.org/10.1029/2003GL018676>.
- Hurwitz, S., Kipp, K.L., Ingebritsen, S.E., and Reid, M.E., 2003, Groundwater flow, heat transport, and water table position within volcanic edifices—Implications for volcanic processes in the Cascade Range: *Journal of Geophysical Research, Solid Earth*, v. 108, no. B12, <https://doi.org/10.1029/2003JB002565>.
- Hurwitz, S., Peek, S., Younger, E.F., and Lee, R.L., 2019, Water level, temperature and chemistry in a deep well on the summit of Kīlauea Volcano, Hawai'i: U.S. Geological Survey data release, accessed March 27, 2024, at <https://doi.org/10.5066/P9UCGT2F>.
- Keller, G.V., Grose, L.T., Murray, J.C., and Skokan, C.K., 1979, Results of an experimental drill hole at the summit of Kīlauea volcano, Hawaii: *Journal of Volcanology and Geothermal Research*, v. 5, no. 3–4, p. 345–385, [https://doi.org/10.1016/0377-0273\(79\)90024-6](https://doi.org/10.1016/0377-0273(79)90024-6).
- Larsen, G., Grönvold, K., and Thorarinsson, S., 1979, Volcanic eruption through a geothermal borehole at Námafjall, Iceland: *Nature*, v. 278, p. 707–710, <https://doi.org/10.1038/278707a0>.
- Linde, A.T., Agustsson, K., Sacks, I.S., and Stefansson, R., 1993, Mechanism of the 1991 eruption of Hekla from continuous borehole strain monitoring: *Nature*, v. 365, p. 737–740, <https://doi.org/10.1038/365737a0>.
- Lowenstern, J.B., Sisson, T.W., and Hurwitz, S., 2017, Probing magma reservoirs to improve volcano forecasts: *Eos*, v. 98, <https://doi.org/10.1029/2017EO085189>.
- Luttrell, K., Mencin, D., Francis, O., and Hurwitz, S., 2013, Constraints on the upper crustal magma reservoir beneath Yellowstone Caldera inferred from lake-seiche induced strain observations: *Geophysical Research Letters*, v. 40, p. 501–506, <https://doi.org/10.1002/grl.50155>.
- Mattioli, G.S., Young, S.R., Voight, B., Steven, R., Sparks, J., Shalev, E., Sacks, S., Malin, P., Linde, A., Johnston, W., Hidayat, D., Elsworth, D., Dunkley, P., Herd, R., Neuberg, J., Norton, G., and Widiwijayanti, C., 2004, Prototype PBO instrumentation of CALIPSO project captures world-record lava dome collapse on Montserrat Volcano: *Eos*, v. 85, no. 34, p. 317–325, <https://doi.org/10.1029/2004EO340001>.
- McConnell, V.S., Shearer, C.K., Eichelberger, J.C., Keskinen, M.J., Layer, P.W., and Papike, J.J., 1995, Rhyolitic intrusions in the intracaldera Bishop Tuff, Long Valley, California: *Journal of Volcanology and Geothermal Research*, v. 67, no. 1–3, p. 41–60, [https://doi.org/10.1016/0377-0273\(94\)00099-3](https://doi.org/10.1016/0377-0273(94)00099-3).
- Myren, G.D., Johnston, M.J., and Mueller, R.J., 2006, Borehole dilatometer installation, operation, and maintenance at sites in Hawaii: U.S. Geological Survey Open-File Report 2006-1103, 81 p., <https://doi.org/10.3133/ofr20061103>.
- Prejean, S.G., and Ellsworth, W.L., 2001, Observations of earthquake source parameters at 2 km depth in the Long Valley Caldera, eastern California: *Bulletin of the Seismological Society of America*, v. 81, p. 165–177, <https://doi.org/10.1785/0120000079>.
- Prevedel, B., Bulut, F., Bohnhoff, M., Raub, C., Kartal, R.F., Alver, F., and Maln, P.E., 2015, Downhole geophysical observatories—Best installation practices and a case history from Turkey: *International Journal of Earth Science*, v. 104, p. 1537–1547, <https://doi.org/10.1007/s00531-015-1147-5>.
- Priest, S.S., Sass, J.H., Ellsworth, B., Farrar, C.D., Sorey, M.L., Hill, D.P., Bailey, R.A., Jacobson, R.D., Finger, J.T., McConnell, V.S., and Zoback, M., 1998, Scientific drilling in Long Valley, California—What will we learn?: U.S. Geological Survey Fact Sheet 077–98, 2 p., <https://pubs.usgs.gov/fs/old/1998/fs077-98>.
- Pribnow, D.F.C., Schütze, C., Hurter, S.J., Flechsig, C., and Sass, J.H., 2003, Fluid flow in the resurgent dome of Long Valley Caldera—Implications from thermal data and deep electrical sounding: *Journal of Volcanology and Geothermal Research*, v. 127, no. 3–4, p. 329–345, [https://doi.org/10.1016/S0377-0273\(03\)00175-6](https://doi.org/10.1016/S0377-0273(03)00175-6).
- Reid, M.E., 2004, Massive collapse of volcano edifices triggered by hydrothermal pressurization: *Geology*, v. 32, no. 5, p. 373–376, <https://doi.org/10.1130/G20300.1>.
- Robison, J.H., Forcella, L.S., and Gannett, M.W., 1981, Data from geothermal test wells near Mount Hood, Oregon: U.S. Geological Survey Open-File Report 81–1002, 26 p., <https://doi.org/10.3133/ofr811002>.
- Roeloffs, E., Sneed, M., Galloway, D.L., Sorey, M.L., Farrar, C.D., Howle, J.F., and Hughes, J., 2003, Water-level changes induced by local and distant earthquakes at Long Valley caldera, California: *Journal of Volcanology and Geothermal Research*, v. 127, no. 3–4, p. 269–303, [https://doi.org/10.1016/S0377-0273\(03\)00173-2](https://doi.org/10.1016/S0377-0273(03)00173-2).
- Rooyakkers, S.M., Stix, J., Berlo, K., Petrelli, M., and Sigmundsson, F., 2021, Eruption risks from covert silicic magma bodies: *Geology*, v. 49, p. 921–925, <https://doi.org/10.1130/G48697.1>.
- Rundle, J.B., Carrigan, C.R., Hardee, H.C., and Luth, W.C., 1986, Deep drilling to the magmatic environment in Long Valley caldera: *Eos*, v. 67, no. 21, p. 490–491, <https://doi.org/10.1029/EO067i021p00490>.

- Shelly, D.R., and Hardebeck, J.L., 2019, Illuminating faulting complexity of the 2017 Yellowstone Maple Creek earthquake swarm: *Geophysical Research Letters*, v. 46, no. 5, p. 2544–2552, <https://doi.org/10.1029/2018GL081607>.
- Shelly, D.R., Hill, D.P., Massin, F., Farrell, J., Smith, R.B., and Taira, T., 2013, A fluid-driven earthquake swarm on the margin of the Yellowstone caldera: *Journal of Geophysical Research Solid Earth*, v. 118, no. 9, p. 4872–4886, <https://doi.org/10.1002/jgrb.50362>.
- Sorey, M.L., McConnell, V.S., and Roeloffs, E., 2003, Summary of recent research in Long Valley Caldera, California: *Journal of Volcanology and Geothermal research*, v. 127, p. 165–173, [https://doi.org/10.1016/S0377-0273\(03\)00168-9](https://doi.org/10.1016/S0377-0273(03)00168-9).
- Teplov, W., Marsh, B., Hulen, J., Spielman, P., Kaleikini, M., Fitch, D., and Rickard, W., 2009, Dacite melt at the Puna geothermal venture wellfield, Big Island of Hawaii: *Geothermal Resources Council Transactions*, v. 33, p. 989–994.
- Thelen, W.A., Lyons, J.J., Wech, A.G., Moran, S.C., Haney, M., and Flinders, A.F., 2024, Seismic techniques and suggested instrumentation to monitor volcanoes, chap. B of Flinders, A.F., Lowenstern, J.B., Coombs, M.L., and Poland, M.P., eds., *Recommended capabilities and instrumentation for volcano monitoring in the United States: U.S. Geological Survey Scientific Investigations Report 2024–5062–B*, 9 p., <https://doi.org/10.3133/sir20245062B>.
- Voight, B., Linde, A.T., Sacks, I.S., Mattioli, G.S., Sparks, R.S.J., Elsworth, D., Hidayat, D., Malin, P.E., Shalev, E., Widiwijayanti, C., Young, S.R., Bass, V., Clarke, A., Dunkley, P., Johnson, W., McWhorter, N., Neuberg, J., and Williams, P., 2006, Unprecedented pressure increase in deep magma reservoir triggered by lava-dome collapse: *Geophysical Research Letters*, *Solid Earth*, v. 33, no 3, <https://doi.org/10.1029/2005GL024870>.

Chapter L



U.S. Geological Survey scientists L. Clor and A. Diefenbach prepare for a volcanic gas survey of the 2004–2008 lava dome of Mount St. Helens, Washington, using unoccupied aircraft systems. Photograph by P. Kelly, U.S. Geological Survey, September 25, 2018.

Chapter K

Special Topic—Unoccupied Aircraft Systems

By Angela K. Diefenbach

Introduction

Unoccupied aircraft systems (UAS) increasingly support volcano monitoring and eruption response activities in the United States and abroad (James and others, 2020). Advances in UAS platforms and miniaturization of sensors over the past decade have expanded the use of this technology for a wide range of applications within volcanology (Jordan, 2019; James and others, 2020). UAS can greatly enhance existing ground-, aerial-, and satellite-based observation and in situ monitoring networks at volcanoes by providing new avenues for data collection in terms of access, resolution, and timing. UAS can collect data in difficult and hazardous environments, reducing risk to occupied aircraft and (or) ground crews; support the generation of dense time series of data through frequent, low-cost, high-resolution surveys; and provide real-time, on-demand measurements at volcanic systems for indicators such as gas, thermal output, and topographic change without the need to wait for contracted aerial flight services or satellite orbit intervals.

During the 2018 response to the Kīlauea eruption on the Island of Hawai‘i, UAS were used extensively and successfully to monitor, track, investigate, and (or) warn of ongoing volcanic activity (fig. L1; Neal and others, 2019). Throughout the eruption, the UAS team was able to provide data products rapidly to emergency managers for situational awareness and to scientists for quantitative hazard assessment (Diefenbach and others, 2018). Over the course of 4 months, more than 1,200 UAS missions were flown and yielded critical data that included (1) live video to emergency operations centers in Hilo and Honolulu for situational awareness; (2) gas emission rates, compositions, and concentrations; (3) repeat nadir videos over sections of the lava channel to support measurements of lava effusion rate; (4) oblique videos for hazards assessment and outreach; and (5) photogrammetry surveys to create very high-resolution topographic models and orthophoto mosaics (Diefenbach and others, 2018). In coming years, the U.S. Geological Survey (USGS) Volcano Hazards Program (VHP) plans to expand its fleet of UAS, associated sensors, and remote pilots to enhance volcano monitoring and response capabilities.

Currently (2023), USGS operational capabilities are restricted to small class UAS (sUAS; less than [\leq] 55 pounds) that are limited in range, payload capacity, and flight duration. Additionally, USGS-piloted platforms are restricted to the U.S. Department of the Interior Office of Aviation Services approved fleet, which includes a limited number of small and medium

multi-rotor aircraft and vertical take-off and landing fixed-wing aircraft (<https://www.doi.gov/aviation/uas/fleet>). Each type of platform has advantages and disadvantages. Small rotor-wing quadcopters are fast to deploy, can be carried in a backpack, and are highly maneuverable, but are typically only equipped with a small camera and have a minimal flight range. Medium rotor-wing hexacopters can carry larger payloads (< 20 kilograms [kg]) and varied sensors, but, with the drawback of minimal flight time (< 30 minutes), they typically have similar range capabilities to their smaller counterparts and are not as easily deployable. Fixed-wing platforms provide relatively long endurance (< 60 minutes) and range and, with the vertical take-off and landing capabilities, can launch and land in relatively small spaces; however, they have less maneuverability and hovering capability than the rotor-wing platforms. Although the 2018 Kīlauea response showed the benefit of the current UAS fleet, all platforms have limited range [< 10 kilometers (km)], such that operators must be stationed relatively close to the region of interest. To expand UAS monitoring capabilities, VHP staff have been working closely with industry partners and the National Aeronautics and Space Administration to develop a next-generation UAS for volcano monitoring (Kern and others, 2020). This ruggedized, mid-range (> 20 km), multiparametric (gas and photogrammetry) UAS has been developed to meet volcano monitoring needs, particularly at less accessible, more dangerous stratovolcanoes. It is expected in the coming years that additional UAS platforms with new and smaller sensors will expand our capabilities to meet the Nation’s volcano monitoring objectives.

Capabilities Provided

Imagery (Including Thermal Infrared)

UAS provide a relatively new platform for near-field remote sensing with enhanced capability of resolution, timing, and access compared to other observation platforms. The most common application of UAS in volcano monitoring is collection of imagery, including both video and photography. UAS can be equipped with various camera sensors that have visible wavelength, thermal, and multispectral capabilities and range in size and sensor resolution from small-compact, lightweight cameras to large digital single-lens reflex cameras. Real-time telemetered video feeds offer situational awareness not only to the remote pilot and crew during

operations, but they can be transmitted to remote offices, such as emergency operations centers or volcano observatories, for on-demand situational awareness during an evolving volcanic event (for example, the 2018 eruption of Kīlauea).

UAS can capture extraordinarily stable video using onboard Global Positioning System (GPS), which proves useful for particle image velocimetry (PIV) analysis to support eruption rate measurements over lava channels (Dietterich and others, 2021) as well as surface-flow velocity measurements of streams, glaciers, or landslides on volcanoes that may support hazards assessment.

Additionally, UAS equipped with thermal cameras can assist in identifying, measuring, and tracking thermal anomalies to aid in forecasting. Thermal cameras onboard UAS can provide substantially higher resolution imagery than traditional airborne surveys, enhancing identification of thermal features and enabling detailed analysis of thermal structures and heat loss.

High-Resolution Mapping

Cameras aboard UAS are primarily used for photogrammetry surveys to create high-resolution [centimeter-scale] digital elevation models (DEMs) and orthophotograph mosaics. Accurate, precise, high-resolution topographic data are fundamental to understanding volcanic hazards—whether it be for modeling hazardous lava flows, geologic or hazard mapping, morphometric studies, or assisting with instrumentation and telemetry path planning. DEMs and orthophotograph mosaics derived from UAS surveys can be as many as two orders of magnitude higher resolution than what can be acquired by commercial satellite-based imagery (James and others, 2020). Repeat topographic modeling for change detection provides critical metrics such as (1) lava dome growth (for example, the two-dimensional displacement field, strain components, extrusion rate, and apparent lava viscosity; Zorn and others, 2020); (2) lava-flow advancement, volumes, and rates of extrusion (for example, Turner and others, 2017; Dietterich and others, 2021); and (3) the dynamics of caldera collapse (Diefenbach, 2018). Additionally, these very high-resolution DEMs support lahar modeling and measuring channel migration and the depths and volumes of lava and water lakes. Photogrammetry and ground-penetrating radar surveys can provide stream-bottom bathymetry measurements, and when flown over glaciers and ice fields, they can support an improved understanding of water budgets on ice-clad volcanoes. High-resolution DEMs can also be acquired by UAS equipped with miniaturized light detection and ranging (lidar) sensors; however, the mapping extent is commonly reduced compared to UAS photogrammetry surveys owing to the slow speed and close range required by current UAS-based lidar sensors. Rotor-wing UAS provide unprecedented access to vertical or overhanging surfaces (such as crater walls or cliffs) to create high-resolution three-dimensional models of these environments for mapping or quantifying change over time in ways that conventional aircraft or field crews cannot achieve. UAS aeromagnetic surveys allow for very detailed three-dimensional mapping of obscured deposits and subsurface structures (for example, Kaneko and others, 2011).

The ease with which UAS can be used to conduct repeat surveys allows UAS-based aeromagnetic monitoring to detect critical changes at a volcano, such as the movement of magma through time-series evaluation.

Direct Sampling and Airborne Measurements

Aside from the use of UAS for collecting imagery and photogrammetry, they also provide the potential for direct sampling of volcanic and geothermal gas, particles, and even sampling of waters from remote locations. Miniaturized multicomponent gas analyzer systems and differential optical absorption spectroscopy sensors can be placed on UAS to measure gas ratios and sulfur discharge in volcanic plumes (for example, D’Arcy and others, 2018; Syahbana and others, 2019; Liu and others, 2020). Various sampling devices are being developed to collect plume particulates (for example, Mandon and others, 2019). Nadeau and others (2020) described how UAS were used to sample the water lake at the summit of Kīlauea, which existed in the deep and inaccessible crater of Halema‘uma‘u between the lava eruptions in 2018 and 2020. Additional discussion on these topics is provided in chapter E on gas (this volume; Lewicki and others, 2024) and chapter F on water (this volume; Ingebritsen and Hurwitz, 2024), as is the promise of direct measurements of stream discharge through automated PIV analysis (Lewis and others, 2018) and radar techniques, such as the USGS’s Qcam (Fulton and others, 2020). Additionally, thermal cameras and temperature probes with data loggers onboard UAS can provide near-field remote and direct measurements of water temperatures, respectively, and repeat surveys can be flown to detect changes in temperature.

General Recommendations and Considerations

UAS-based volcano monitoring is relatively new, and expansion of its routine use is still in the development phase. UAS-based volcano monitoring strategies and recommendations will vary greatly depending on factors such as volcano accessibility and remoteness, eruption style, and landowner permissions. In addition, limiting factors imposed by the current USGS UAS fleet include flight altitude, distance, and duration. Therefore, we provide herein generalized recommendations for UAS-based volcano monitoring that take these factors into account along with identifying ways to fill critical data gaps identified at each volcano—specifically for levels 3 and 4 volcanoes. At all U.S. volcanoes, we recommend that UAS-based monitoring take an opportunistic approach. For example, if ground-based installations are taking place at a volcano that will involve helicopter support to deploy crews, a UAS component would ideally be involved if it serves to fill a specific monitoring gap or serves as a bridge between ongoing ground, air, and satellite observations.

One of the biggest advantages that UAS technology brings to volcano monitoring programs is its rapid deployment capability for eruption response work (for example, Kīlauea, 2018; Mauna Loa, 2022) that can fill critical data gaps, enhance and augment existing monitoring techniques, and most importantly reduce risk to personnel. Furthermore, UAS provide response teams with operational control of an aircraft that can be flown on-demand, day and night, to collect multiple types of data and observations. The suite of UAS platforms and sensors housed at each observatory would ideally be used as a cache for rapid response (see chapter M, this volume; Flinders, 2024) to a volcano under the purview of any one of the five U.S. volcano observatories. In addition to equipment, a cadre of pilots would ideally be available to operate the aircraft, collect and process the data, and support monitoring and emergency operations. Other groundwork needs to be laid to have an effective UAS emergency response, which includes having permits and permissions in place ahead of time, pre-coordination among agencies and institutions, UAS contracts made available, training and pilot proficiency established, data-management plans worked out, and plans made for effective and rapid integration of UAS operations into restricted and complicated national airspace.

UAS technology and sensor development are rapidly evolving and capabilities in this realm of technology are ever increasing. The limits seem nearly boundless for the use of UAS

in volcano monitoring as small UAS platforms are developing into more capable aircraft in terms of operational range, flight duration, and payload capacity. The miniaturization of various sensors along with new sensor and payload development will further expand volcano monitoring capabilities. In the coming years, development of deployable seismometers, Global Navigation Satellite System (GNSS) sensors, lightning detection sensors, and direct lava and rock sampling are expected. Developments in artificial intelligence to support enhanced autonomous flight, terrain following, obstacle avoidance, and real-time data processing will further capabilities. In summary, UAS have considerable potential to expand volcano monitoring capabilities and improve understanding of volcanic systems by bridging the unique spatial and temporal divides that limit current monitoring strategies.

Ideally, there would be at least two accredited UAS remote pilots at each volcano observatory; the success of UAS-based volcano monitoring relies heavily on having trained remote pilots to design and fly missions to collect critical data to enhance monitoring capabilities. In addition to remote pilots, each observatory would ideally have a fleet of sUAS platforms and sensors capable of a broad array of volcano monitoring techniques. Long-term investment by the VHP would allow expansion of its UAS monitoring capabilities, including remote pilot training, UAS procurement, development of platforms and sensors, and field campaign support.



Figure L1. Photograph showing a U.S. Geological Survey hexacopter unoccupied aircraft system mapping the lava flow field during the 2018 lower East Rift Zone eruption of Kīlauea, Hawai'i.

References Cited

- D'Arcy, F., Stix, J., de Moor, J., Rüdiger, J., Diaz, J., Alan, A., and Corrales, E., 2018, Drones swoop in to measure gas belched from volcanoes: *Eos*, v. 99, <https://doi.org/10.1029/2018eo102329>.
- Diefenbach, A.K., 2018, The use of UAS to monitor topographic change at the summit and lower east rift zone during the 2018 Kīlauea eruption response [abs.]: American Geophysical Union, 2018 Fall Meeting, Washington D.C., abstract G13A-05.
- Diefenbach, A.K., Adams, J., Burton, T., Koeckeritz, B., Sloan, J., and Stroud, S., 2018, The 2018 U.S. Geological Survey-Department of Interior UAS Kīlauea eruption response [abs.]: American Geophysical Union, 2018 Fall Meeting, Washington D.C., abstract V23D-0107.
- Dietterich, H.R., Diefenbach, A.K., Soule, S.A., Zoeller, M.H., Patrick, M.P., Major, J.J., and Lundgren, P.R., 2021, Lava effusion rate evolution and erupted volume during the 2018 Kīlauea lower East Rift Zone eruption: *Bulletin of Volcanology*, v. 83, no. 25, 18 p., <https://doi.org/10.1007/s00445-021-01443-6>.
- Flinders, A.F., 2024, Special topic—Rapid-response instrumentation, chap. M of Flinders, A.F., Lowenstern, J.B., Coombs, M.L., and Poland, M.P., eds., Recommended capabilities and instrumentation for volcano monitoring in the United States: U.S. Geological Survey Scientific Investigations Report 2024–5062–M, 4 p., <https://doi.org/10.3133/sir20245062M>.
- Fulton, J.W., Anderson, I.E., Chiu, C.-L., Sommer, W., Adams, J.D., Moramarco, T., Bjerklie, D.M., Fulford, J.M., Sloan, J.L., Best, H.R., Conaway, J.S., Kang, M.J., Kohn, M.S., Nicotra, M.J., and Pulli, J.J., 2020, QCam—sUAS-based Doppler radar for measuring river discharge: *Remote Sensing*, v. 12, no. 20, <https://doi.org/10.3390/rs12203317>.
- Ingebritsen, S.E., and Hurwitz, S., 2024, Streams, springs, and volcanic lakes for volcano monitoring, chap. F of Flinders, A.F., Lowenstern, J.B., Coombs, M.L., and Poland, M.P., eds., Recommended capabilities and instrumentation for volcano monitoring in the United States: U.S. Geological Survey Scientific Investigations Report 2024–5062–F, 9 p., <https://doi.org/10.3133/sir20245062F>.
- James, M.R., Carr, B.B., D'Arcy, F., Diefenbach, A.K., Dietterich, H.R., Fornaciai, A., Lev, E., Liu, E.J., Pieri, D.C., Rodgers, M., Smets, B., Terada, A., von Aulock, F.W., Walter, T.R., Wood, K.T., and Zorn, E.U., 2020, Volcanological applications of unoccupied aircraft systems (UAS)—Developments, strategies, and future challenges: *Volcanica*, v. 3, no. 1, p. 67–114, <https://doi.org/10.30909/vol.03.01.67114>.
- Jordan, B.R., 2019, Collecting field data in volcanic landscapes using small UAS (sUAS)/drones: *Journal of Volcanology and Geothermal Research*, v. 385, p. 231–241, <https://doi.org/10.1016/j.jvolgeores.2019.07.006>.
- Kaneko, T., Koyama, T., Yasuda, A., Takeo, M., Yanagisawa, T., Kajiwar, K., and Honda, Y., 2011, Low-altitude remote sensing of volcanoes using an unmanned autonomous helicopter—An example of aeromagnetic observation at Izu-Oshima volcano, Japan: *International Journal of Remote Sensing*, v. 32, no. 5, p. 1491–1504, <https://doi.org/10.1080/01431160903559770>.
- Kern, C., Diefenbach, A., Elston, J., Stachura, M., Dietrick, A., Kelly, P., Fladland, M., Stock, J., 2020, Developing a next generation UAS volcano observation platform: American Geophysical Union, 2020 Fall Meeting, abstract NH028-0001.
- Lewicki, J.L., Kern, C., Kelly, P.J., Nadeau, P.A., Elias, T., and Clor, L.E., 2024, Volcanic gas monitoring, chap. E of Flinders, A.F., Lowenstern, J.B., Coombs, M.L., and Poland, M.P., eds., Recommended capabilities and instrumentation for volcano monitoring in the United States: U.S. Geological Survey Scientific Investigations Report 2024–5062–E, 11 p., <https://doi.org/10.3133/sir20245062E>.
- Lewis, Q.W., Lindroth, E.M., and Rhoads, B.L., 2018, Integrating unmanned aerial systems and LSPIV for rapid, cost-effective stream gauging: *Journal of Hydrology*, v. 560, p. 230–246, <https://doi.org/10.1016/j.jhydrol.2018.03.008>.
- Liu, E.J., Aiuppa, A., Alan, A., Arellano, S., Bitetto, M., Bobrowski, N., Carn, S., Clarke, R., Corrales, E., de Moor, J.M., Diaz, J.A., Edmonds, M., Fischer, T.P., Freer, J., Fricke, G.M., Galle, B., Gerdes, G., Giudice, G., Gutmann, A., Hayer, C., Itikarai, I., Jones, J., Mason, E., McCormick Kilbride, B.T., Mulina, K., Nowicki, S., Rahilly, K., Richardson, T., Rüdiger, J., Schipper, C.I., Watson, I.M., and Wood, K., 2020, Aerial strategies advance volcanic gas measurements at inaccessible, strongly degassing volcanoes: *Science Advances*, v. 6, no. 44, <https://doi.org/10.1126/sciadv.abb9103>.
- Mandon, C.L., Christenson, B.W., Schipper, C.I., Seward, T.M., and Garaebiti, E., 2019, Metal transport in volcanic plumes—A case study at White Island and Yasur volcanoes: *Journal of Volcanology and Geothermal Research*, v. 369, p. 155–171, <https://doi.org/10.1016/j.jvolgeores.2018.11.024>.
- Nadeau, P.A., Diefenbach, A.K., Hurwitz, S., and Swanson, D.A., 2020, From lava to water—A new era at Kīlauea: *Eos*, v. 101, <https://doi.org/10.1029/2020EO149557>.
- Neal, C.A., Brantley, S.R., Antolik, L., Babb, J.L., Burgess, M., Calles, K., Capps, M., Chang, J.C., Conway, S., Desmither, L., Dotray, P., Elias, T., Fukunaga, P., Fuke, S., Johanson, I.A., Kamibayashi, K., Kauahikaua, J., Lee, R.L., Pekalib, S., Miklius, A., Million, W., Moniz, C.J., Nadeau, P.A., Okubo, P., Parcheta, C., Patrick, M.R., Shiro, B., Swanson, D., Tollett, W., Trusdell, F., Zoeller, M.H., Montgomery-Brown, E.K., Anderson, K.R., Poland, M.P., Ball, J.L., Bard, J.A., Coombs, M., Dietterich, H.R., Kern, C., Thelen, W.A., Cervelli, P.F., Orr, T., Houghton, B.F., Gansecki, C., Hazlett, R., Lundgren, P., Diefenbach, A.K., Lerner, A., Waite, G., Kelly, P.J., Clor, L., Werner, C., Burgess, M., Mulliken, K., Fisher, G., and Damby, D., 2019, The 2018 rift eruption and summit collapse of Kīlauea Volcano: *Science*, v. 363, no. 6425, p. 367–374, <https://doi.org/10.1126/science.aav7046>.

- Syahbana, D.K., Kasbani, K., Suantika, G., Prambada, O., Andreas, A.S., Saing, U.B., Kunrat, S.L., Andreastuti, S., Martanto, M., Kriswati, E., Suparman, Y., Humaida, H., Ogburn, S., Kelly, P.J., Wellik, J., Wright, H.M.N., Pesicek, J.D., Wessels, R., Kern C., Lisowski, M., Diefenbach, A., Poland, M., Beauducel, F., Pallister, J., Vaughan, R.G., and Lowenstern, J.B., 2019, The 2017–19 activity at Mount Agung in Bali (Indonesia)—Intense unrest, monitoring, crisis response, evacuation, and eruption: *Scientific Reports*, v. 9, no. 8848, <https://doi.org/10.1038/s41598-019-45295-9>.
- Turner, N.R., Perroy, R.L., and Hon, K., 2017, Lava flow hazard prediction and monitoring with UAS—A case study from the 2014–2015 Pāhoā lava flow crisis, Hawai‘i: *Journal of Applied Volcanology*, v. 6, article no. 17, <https://doi.org/10.1186/s13617-017-0068-3>.
- Zorn, E.U., Walter, T.R., Johnson, J.B., and Mania, R., 2020, UAS-based tracking of the Santiaguito Lava Dome, Guatemala: *Scientific Reports*, v. 10, article no. 8644, <https://doi.org/10.1038/s41598-020-65386-2>.

Chapter M



U.S. Geological Survey Hawaiian Volcano Observatory lead field engineer K. Kamibayashi conducts maintenance on a volcano-monitoring station located on Tutuila Island in American Samoa. This station was installed as part of a rapid-response effort for escalating volcanic seismicity in August 2022. Photograph by J. Chang, U.S. Geological Survey, December 2023.

Chapter M

Special Topic—Rapid-Response Instrumentation

By Ashton F. Flinders

Introduction

Based on the reports of Ewert and others (2005, 2018) and Moran and others (2008), most U.S. volcanoes are currently under-monitored and are likely to remain so until the goals of the National Volcano Early Warning System are fulfilled. In addition, volcanoes determined to have low to moderate threat levels (Ewert and others 2005, 2018) could awaken suddenly and, as a result, may need to have instrumentation installed rapidly. For these reasons, equipment caches would ideally be readily available for rapid response in the event of unrest at under-monitored volcanoes or during a volcanic crisis. Given that volcanoes in Alaska and Hawai‘i are frequently active, it is likely that several U.S. volcanoes could experience unrest simultaneously, as happened in 2018, 2019, and 2020, when unrest or eruptions occurred at Great Sitkin Volcano, Alaska; Mauna Loa, Hawai‘i; Mount Cleveland, Alaska; Semisopochnoi Island, Alaska; Shishaldin Volcano, Alaska; Mount Veniaminof, Alaska, as well as the most destructive documented eruption of Kīlauea, Hawai‘i. Therefore, we recommend that sufficient numbers of seismometers, infrasound sensors, Global Navigation Satellite System (GNSS) receivers, remote cameras, gas-monitoring instruments, and airborne and ground-based remote-sensing systems be made available and placed in a state of readiness at each observatory with the capability of bringing a level-2 monitoring network to near level-4 readiness. These rapid-response caches would ideally include sufficient equipment to provide real-time data telemetry, including satellite telemetry, where available, applicable, and appropriate. Rapid-response caches would be maintained in a state of readiness so that instruments can be deployed within several hours to days. Although the primary focus of the caches would be to enable rapid increases to a volcano observatory’s real-time monitoring capabilities, not all scenarios of volcanic unrest are conducive to rapid deployment of real-time data telemetry. Non-telemetered, campaign instruments, particularly seismometers and GNSS stations, can also be deployed to aid in detection of early signs of volcanic unrest given the data can be recovered in a timely fashion.

Given the geographic separation of the U.S. Geological Survey Volcano Science Center’s (VSC) four volcano observatory offices, the logistical difficulties in shipping equipment rapidly between them in response to unrest, the possible scenario that a volcano could reawaken with just hours or days of precursory unrest, and the difference in operating environments (for example,

tropical Hawai‘i compared to subarctic Alaska), we recommend three rapid-response instrument caches—for Hawai‘i, Alaska, and the lower 48 States. For the lower 48 States, a single cache shared among the Cascades Volcano Observatory, Yellowstone Volcano Observatory, and the California Volcano Observatory could be warehoused in California or Washington. Although these rapid-response caches would be located at one of the observatories, they would ideally be owned and maintained by VSC, and together form a flexible VSC-wide instrument pool. To maintain continuity of monitoring capabilities, this rapid-response cache could also serve to replace instruments destroyed during an on-going eruption. However, to retain eruption-response readiness, we recommend instruments in the rapid-response cache not be permanently reallocated to an observatory’s monitoring network unless they are replaced.

Recommended Instrumentation

For seismic, infrasound, and ground deformation capabilities, based on the maximum instrument numbers for a level-4 network, we recommend each volcano observatory’s rapid-response instrument cache include at least 12 broadband seismometers (Thelen and others, 2024b); 12 infrasound sensors and 2 four-element infrasound arrays (Lyons and others, 2024); and 12 GNSS stations (Montgomery-Brown and others, 2024). Unlike Moran and others’ (2008) previous recommendation, we no longer recommend tiltmeters for rapid response, given the logistical challenges involved in deploying them during a volcanic crisis. Similarly, for lahar monitoring, we no longer recommended acoustic flow monitors (Moran and others, 2008). Where appropriate, each cache could contain an additional eight broadband seismometers and two four-element infrasound arrays (Thelen and others, 2024a) for rapidly monitoring as many as four potential lahar drainages.

To ensure that data are recorded as quickly as possible, as well as provide monitoring network flexibility during ongoing unrest and eruption, the rapid-response instrument cache would ideally include non-telemetered, campaign, seismic and ground deformation instrumentation. Recently available, low-cost, low-power, wireless, three-component, short-period seismometers (nodes) provide for increases in seismic response capabilities (for example, improved earthquake locations, event-type characterization [volcano-tectonic versus long-period events], high-resolution tomography, and interferometry) and could

augment the broadband instruments recommended above. Although nodal seismometers are available through the Incorporated Research Institutions for Seismology (IRIS) Portable Array Seismic Studies of the Continental Lithosphere (PASSCAL) Instrument Center, to facilitate rapid deployment and ensure availability, we recommend that each cache contain 50 to 100 node-type stations (fig. M1). The recommended 12 GNSS stations could be designed to provide real-time and campaign capabilities.

For ground-based gas monitoring, increasing volcanic unrest may limit access to fumaroles near an active crater and direct sampling may not be practical or safe. We recommend sufficient instrumentation in a rapid-response instrument cache to enable rapid installation of autonomous, telemetered stations for tracking gas-emission rates and compositions. This instrumentation would ideally include three scanning spectrometer systems, one SO_2 camera, and one multicomponent gas analyzer system (multi-GAS) station. As periodic field surveys may also be required, we also recommend including one mobile differential optical absorption spectroscopy (DOAS) system, one portable SO_2 camera, one portable multi-GAS system, one field Fourier-transform infrared (FTIR) spectrometer (fig. M2), one portable soil- CO_2 fluxmeter, and, as safety allows, equipment for direct sampling of fumaroles and springs. As field-survey instrumentation is directly user operated (not installed at a fixed location), this instrumentation could be used for both rapid response, baseline monitoring, and research as needed (Lewicki and others, 2024).

For airborne gas monitoring, the rapid-response cache would ideally contain instrumentation to make gas measurements using traditional fixed-wing aircraft and helicopters, as well as small- to medium-sized unoccupied aircraft systems (UAS). For fixed-wing and helicopter-borne missions, the cache would ideally include one highly sensitive, temperature-stabilized, DOAS system and dedicated in situ instruments with the capability to measure CO_2 (at less than 1 part per million accuracy and precision) and major sulfur gases (SO_2 and H_2S at less than 5 parts per billion accuracy and precision at a 1 hertz sampling rate). In addition, one UAS equipped with multi-GAS and DOAS systems would ideally be available.

To track surface changes caused by volcanic activity, each rapid-response instrument cache would ideally include a minimum of four telemetered cameras with zoom (two with low-light capabilities). Each observatory would ideally assess their operational and rapid response need for including a forward-looking infrared camera, usable both on the ground and (or) from an airborne platform. Similarly, observatories would ideally assess their need for a ground-based Doppler radar system for monitoring explosive activity. For lightning detection, observatories can rely on global lightning detection networks, such as the University of Washington's World Wide Lightning and Location Network, and others. Where appropriate, observatories would work toward incorporating one or more short-range lightning sensors (very high frequency or broadband) or field mill (for detecting perturbations in the static electricity from small explosions) into their rapid-response cache (Schneider and Van Eaton, 2024).



Figure M1. Photograph showing U.S. Geological Survey Hawaiian Volcano Observatory geophysicist P. Dotray deploying a 5-second geophone in Halema'uma'u as part of a rapid response to the December 20, 2020, eruption of Kīlauea, Hawai'i. These instruments were made available through the Incorporated Research Institutions for Seismology (IRIS) Portable Array Seismic Studies of the Continental Lithosphere (PASSCAL) Instrument Center. Photograph by J. Chang, U.S. Geological Survey, January 3, 2021.



Figure M2. Photograph showing U.S. Geological Survey Hawaiian Volcano Observatory gas scientist M. Cappos using a field-portable Fourier-transform infrared (FTIR) spectrometer on the rim of Halema'uma'u to measure gas composition during the June 7, 2023, eruption of Kīlauea, Hawai'i. The FTIR measures the composition of emitted gases by measuring how the volcanic plume absorbs infrared energy. The plume generated by the summit eruption was sulfur-dioxide (SO_2) rich, but also contained water vapor, carbon dioxide, and halogen gases, such as HCl and HF. Photograph by P. Nadeau, U.S. Geological Survey, June 7, 2023.

Additional Considerations

In addition to specific instrumentation (table M1), the rapid-response instrument caches would ideally include all associated station infrastructure and equipment to provide power and telemetry, including batteries, solar panels, radios, cabling, housing, and mounting equipment, as well as radio repeaters and (or) satellite uplinks to ensure continuous data streams for stations that are installed in remote areas. To maintain operational readiness, some instrumentation (for example, seismometers, GNSS stations, and multi-GAS) could be used on a limited basis to support campaign monitoring or targeted scientific investigations during times of no significant unrest. Additionally, instruments could be rotated out of the cache and permanently deployed as part of the observatory's routine network maintenance and construction, and the cache resupplied with newer instruments. This practice would facilitate monitoring network repairs and keep the rapid-response cache instrumentation modern and up to date.

Instrumentation not currently recommended for rapid-response caches, for example, gravimeters, magnetometers, distributed acoustic sensing, rotational seismometers, and others, should be evaluated periodically to assess their value in responding to unrest at under-monitored volcanoes or to aid in monitoring during a volcanic crisis.

Marine Eruptions

To leverage capabilities and foster collaboration, observatories responsible for monitoring volcanoes in marine environments (Aleutian Islands, Hawai'i, Northern Mariana Islands, and American Samoa) could pursue partnerships with internal and (or) external partners (for example, U.S. Geological Survey Pacific Coastal and Marine Science Center, National Oceanic and Atmospheric Administration, and others) to develop a marine rapid-response instrument cache. Ideally, this cache would include ocean-bottom seismometers, hydrophones, bottom-pressure recorders, and other sensors of opportunity. A minimum of four marine instrument packages that include a seismometer is necessary for determining reliable earthquake locations. Similarly, three to four hydrophone moorings deployed as a network or small-aperture array could detect submarine explosions and T-phases from earthquakes (Tepp, 2024). Telemetry and real-time data would ideally be available for at least one or two instruments, with at least one option that can be quickly deployed (for example, a buoy system). As a vessel of opportunity would be required to deploy marine instruments, those instruments that can be easily and safely deployed from smaller vessels, such as large fishing vessels, would increase operational flexibility and response timeliness. When

Table M1. Recommended rapid-response instrument cache for volcano monitoring in the United States.

[In addition to the instrumentation listed below, the caches would ideally include all associated station infrastructure and equipment to provide power and telemetry for ground-based instruments, including batteries, solar panels, radios, cabling, housing, and mounting equipment, as well as radio repeaters and (or) satellite uplinks to ensure continuous data streams for stations installed in remote areas. DOAS, differential optical absorption spectroscopy; FLIR, forward-looking infrared; FTIR, Fourier-transform infrared spectroscopy; GNSS, Global Navigation Satellite System; Hz, hertz; NOAA, National Oceanic and Atmospheric Administration; ppb, part per billion; ppm, part per million; UAS, unoccupied aircraft system; USGS, U.S. Geological Survey]

Monitoring category	Instrumentation
Seismic	Twelve broadband seismometers; 50–100 node-type seismometers
Infrasound	Twelve infrasound sensors and two four-element infrasound arrays
Ground deformation and gravity	Twelve GNSS receivers
Gas	Three scanning spectrometer systems, one SO ₂ camera, and one multicomponent gas analyzer system (multi-GAS) station. Instrumentation for performing periodic field surveys, including one mobile DOAS system, one portable SO ₂ camera, one portable multi-GAS system, one field FTIR system, one portable soil-CO ₂ fluxmeter, and equipment for direct sampling of fumaroles and springs. For airborne gas monitoring from fixed-wing and helicopter-borne missions, the cache would ideally include one highly sensitive, temperature-stabilized DOAS spectrometer and dedicated in situ instruments that have the capability to measure CO ₂ at <1 ppm accuracy and precision and major sulfur gases (SO ₂ and H ₂ S) at <5 ppb accuracy and precision at a 1 Hz sampling rate. In addition, one UAS equipped with multi-GAS and DOAS systems would ideally be available
Springs, streams, and volcanic lakes	No specific instrument recommendations
Tracking surface changes caused by volcanic activity	If deemed appropriate by the observatory; one handheld FLIR camera and (or) one airborne (gimble mount) FLIR. Four telemetered cameras with zoom (two with low-light capabilities)
Eruption plumes and clouds	If deemed appropriate by the observatory; one ground-based Doppler radar system and one or more short range very high-frequency sensors (or broadband) or field mill
Lahars	Eight broadband seismometers and two four-element infrasound arrays
Marine eruptions	Observatories responsible for monitoring volcanoes in marine environments (Aleutian Islands, Northern Mariana Islands, and American Samoa) could pursue partnerships with internal and (or) external partners (for example, USGS Pacific Coastal and Marine Science Center, NOAA, and others), for developing a marine rapid-response instrument cache. Ideally, this cache would include ocean-bottom seismometers, hydrophones, bottom-pressure recorders, and other sensors of opportunity. When possible and appropriate, rapidly deploying multiple land-based seismometers optimized for T-phases on the nearest islands could supplement ocean-bottom seismometers and hydrophones

possible and appropriate, rapidly deploying multiple land-based seismometers optimized for T-phases on the nearest islands could supplement ocean-bottom seismometers and hydrophones (Tepp, 2024). Although broadband and three-component seismometers are preferable, a more important consideration is portability and ease of deployment. For example, during the 2022 earthquake swarm offshore Ta‘ū Island, American Samoa, rapidly deployed low-cost single-board computer-based seismometers proved critical in providing early situational awareness (earthquakes counts and relative magnitudes and epicentral distances).

References Cited

- Ewert, J.W., Diefenbach, A.K., and Ramsey, D.W., 2018, 2018 update to the U.S. Geological Survey national volcanic threat assessment: U.S. Geological Survey Scientific Investigations Report 2018–5140, 40 p., <https://doi.org/10.3133/sir20185140>.
- Ewert, J.W., Guffanti, M., and Murray, T.L., 2005, An assessment of volcanic threat and monitoring capabilities in the United States—Framework for a National Volcano Early Warning System: U.S. Geological Survey Open-File Report 2005–1164, 62 p., <https://doi.org/10.3133/ofr20051164>.
- Lewicki, J.L., Kern, C., Kelly, P.J., Nadeau, P.A., Elias, T., and Clor, L.E., 2024, Volcanic gas monitoring, chap. E of Flinders, A.F., Lowenstern, J.B., Coombs, M.L., and Poland, M.P., eds., Recommended capabilities and instrumentation for volcano monitoring in the United States: U.S. Geological Survey Scientific Investigations Report 2024–5062–E, 11 p., <https://doi.org/10.3133/sir20245062E>.
- Lyons, J.J., Fee, D., Thelen, W.A., Iezzi, A.M., and Wech, A.G., 2024, Infrasound for volcano monitoring, chap. C of Flinders, A.F., Lowenstern, J.B., Coombs, M.L., and Poland, M.P., eds., Recommended capabilities and instrumentation for volcano monitoring in the United States: U.S. Geological Survey Scientific Investigations Report 2024–5062–C, 11 p., <https://doi.org/10.3133/sir20245062C>.
- Montgomery-Brown, E.K., Anderson, K.R., Johanson, I.A., Poland, M.P., and Flinders, A.F., 2024, Ground deformation and gravity for volcano monitoring, chap. D of Flinders, A.F., Lowenstern, J.B., Coombs, M.L., and Poland, M.P., eds., Recommended capabilities and instrumentation for volcano monitoring in the United States: U.S. Geological Survey Scientific Investigations Report 2024–5062–D, 11 p., <https://doi.org/10.3133/sir20245062D>.
- Moran, S.C., Freymueller, J.T., LaHusen, R.G., McGee, K.A., Poland, M.P., Power, J.A., Schmidt, D.A., Schneider, D.J., Stephens, G., Werner, C.A., and White, R.A., 2008, Instrumentation recommendations for volcano monitoring at U.S. volcanoes under the National Volcano Early Warning System: U.S. Geological Survey Scientific Investigations Report 2008–5114, 47 p., <https://doi.org/10.3133/sir20085114>.
- Schneider, D.J., and Van Eaton, A.R., 2024, Special topic—Eruption plumes and clouds, chap. J of Flinders, A.F., Lowenstern, J.B., Coombs, M.L., and Poland, M.P., eds., Recommended capabilities and instrumentation for volcano monitoring in the United States: U.S. Geological Survey Scientific Investigations Report 2024–5062–J, 12 p., <https://doi.org/10.3133/sir20245062J>.
- Tepp, G., 2024, Monitoring marine eruptions, chap. I of Flinders, A.F., Lowenstern, J.B., Coombs, M.L., and Poland, M.P., eds., Recommended capabilities and instrumentation for volcano monitoring in the United States: U.S. Geological Survey Scientific Investigations Report 2024–5062–I, 7 p., <https://doi.org/10.3133/sir20245062I>.
- Thelen, W.A., Lyons, J.J., Iezzi, A.M., and Moran, S.C., 2024a, Monitoring lahars and debris flows, chap. H of Flinders, A.F., Lowenstern, J.B., Coombs, M.L., and Poland, M.P., eds., Recommended capabilities and instrumentation for volcano monitoring in the United States: U.S. Geological Survey Scientific Investigations Report 2024–5062–H, 6 p., <https://doi.org/10.3133/sir20245062H>.
- Thelen, W.A., Lyons, J.J., Wech, A.G., Moran, S.C., Haney, M.M., and Flinders, A.F., 2024b, Seismic techniques and suggested instrumentation to monitor volcanoes, chap. B of Flinders, A.F., Lowenstern, J.B., Coombs, M.L., and Poland, M.P., eds., Recommended capabilities and instrumentation for volcano monitoring in the United States: U.S. Geological Survey Scientific Investigations Report 2024–5062–B, 9 p., <https://doi.org/10.3133/sir20245062B>.



I S B N 978-1-4113-4586-7



ISSN 2328-031X (print)
ISSN 2328-0328 (online)
<https://doi.org/10.3133/sir20245062>